SYNTHESIS AND PROPERTIES OF ANODICALLY OXIDISED FILMS ON METAL TITANIUM SUBSTRATE FOR PHOTOCATALYTIC APPLICATIONS

Živa Marinko

Doctoral Dissertation
Jožef Stefan International Postgraduate School
Ljubljana, Slovenia

Supervisor: Prof. Dr. Miran Čeh, Jožef Stefan International Postgraduate School and Jožef Stefan Institute, Ljubljana, Slovenia

Evaluation Board:
Prof. Dr. Srečo Davor Škapin, Chair, Jožef Stefan International Postgraduate School and Jožef Stefan Institute, Ljubljana, Slovenia
Prof. Dr. Urška Lavrenčič Štangar, Member, Faculty of Chemistry and Chemical Technology, University of Ljubljana, Slovenia
Prof. Dr. Andreja Gajović, Member, Ruđer Bošković Institute, Zagreb, Croatia

MEDNARODNA PODIPLOMSKA ŠOLA JOŽEFA STEFANA
JOŽEF STEFAN INTERNATIONAL POSTGRADUATE SCHOOL

Živa Marinko

SYNTHESIS AND PROPERTIES OF ANODICALLY OXIDISED FILMS ON METAL TITANIUM SUBSTRATE FOR PHOTOCATALYTIC APPLICATIONS

Doctoral Dissertation

SINTEZA IN LASTNOSTI ANODNO OKSIDIRANIH PLASTI NA TITANOVI PODLAGI ZA UPORABO V FOTOKATALIZI

Doktorska disertacija

Supervisor: Prof. Dr. Miran Čeh

Ljubljana, Slovenia, August 2022

"On the arid lands there will spring up industrial colonies without smoke and without smokestacks; forests of glass tubes will extend over the plains and glass buildings will rise everywhere; inside of these will take place the photochemical processes that hitherto have been the guarded secret of the plants, but that will have been mastered by human industry which will know how to make them bear even more abundant fruit than nature, for nature is not in a hurry and mankind is. And if in a distant future the supply of coal becomes completely exhausted, civilization will not be checked by that, for life and civilization will continue as long as the sun shines!"

Giacomo Ciamician in The photochemistry of the future (1912)

Acknowledgements

First and foremost, I would like to thank Prof. Dr. Miran Čeh, my supervisor, for his support and understanding. His office door was always open for discussion. At the same time, he consistently allowed the research to be my work, a result of my imagination, and for the thesis to be my own endeavour. Secondly, my gratitude goes to Dr. Luka Suhadolnik, my laboratory guide. His research assistance and dedicated involvement in every step gently steered me in the right direction, whenever or not I thought I needed it. During our many and often long talks, they both led me into the world of catalysis. Thus, they opened many doors of imagination that were previously closed. I am thankful for their openness and willingness to discuss my ideas; moreover, for our communication to be a two-way street, with as many left and right turns as possible.

For the financial support, I gratefully acknowledge the Slovenian Research Agency (ARRS) and the research programmes L2-2614, P1-0034, P1-0045, P1-0192, P2-0056, P2-0082, and P2-0084, and the European Union's Horizon 2020 research and innovation programme under grant agreement No. 823717-ESTEEM3.

Next, I would like to thank my evaluation board, including Prof. Dr. Miran Čeh, Prof. Dr. Srečo Davor Škapin, Prof. Dr. Urška Lavrenčič Štangar, and Prof. Dr. Andreja Gajović for their objective views and comments about the written work.

The unknown territory of various analytical techniques and getting all the experimental work done required more academic support. And for that, I can hardly imagine a better environment than that offered by the Jožef Stefan Institute, Jožef Stefan International Postgraduate School and the nearby Institute of Metals and Technology and the National Institute of Chemistry. The assistance provided by the following researchers (in alphabetical order) is greatly appreciated.

— Dr. Barbara Šetina Batič for performed EBSD analyses and discussions over coffee.
— Barbara Ljubec and Dr. Belisa Alcantara Marinho for bringing "fresh air" into the catalysis group and for representing strong women in science.
— Prof. Dr. Boris Majaron for his sincere and valuable guidance on photoluminescence and statistical analysis.
— Damjan Vengust for his guidance and lectures on Raman analysis.
— Dr. Gregor Filipič for his discussion and out-of-the-box ideas regarding plasma treatments.
— Dr. Janez Kovač for his time, understanding, and kind approach to my many questions, and for performing the XPS and ToF-SIMS analyses.
— Dr. Kristian Radan for clarifying XRD pattern and the instructions for ATR-FTIR, together with Dr. Aleksander Matavž.
— Asst. Prof. Dr. Miha Čekada for imparting his knowledge about thin films and the titanium foil nitridation.
— Dr. Nataša Hojnik and Lea Vukanovič for the endless source of sarcastic optimism, support and constructive criticism, no matter the hour.

— Dr. Maja Ponikvar-Svet for her time and discussion regarding the fluoride species.
— Monika Koren for technical support with the photoluminescence measurements.
— Dr. Sandra Drev and Maja Koblar for unselfishly taking time when I needed them and for sharing their knowledge on electron microscopy and sample preparation.
— Silvo Drnovšek for his kind words and help whenever I was in the K5 department.
— Dr. Tilen Koklič for his enthusiasm and tutoring on the EPR machine.
— The team of the ULTRACOOL lab (Director's Fund 2017) from the Jožef Stefan Institute for their support on working with Dektak Profilometry.
— Dr. Vid Simon Šelih for his kind guidance with Zygo optical profilometry and performing the ICP-OES analyses.
— Dr. Zoran Samardžija for his expertise on scanning electron microscopy.

Moreover, the administrative work was relentless and never-ending. In that field, my gratitude goes to the administrative staff at the Jožef Stefan International Postgraduate School and the K7 Department for Nanostructured Materials.

My special thanks goes to the entire K7 Department at the Jožef Stefan Institute for making me feel welcome and keeping up the science spirit. I take this opportunity to express gratitude to the "lunch club" on the terrace, especially to Dr. Špela Trafela and Matej Kocen for their laughs and chit-chats. However, my special thank you goes to my office mates (in alphabetical order); Anja Korent, Dr. Luka Kelhar, Dr. Luka Suhadolnik, Dr. Matic Korent, Monika Kušter and Dr. Vanja Jordan. Time spent with you was most instructive.

Additionally, the organization of conferences and the established communication between the management of the school and the students offered many opportunities for personal and career growth. In this aspect, I will never forget the input and talks we exchanged with Patricia Jovičević Klug. I learned a lot as a representative of the Jožef Stefan International Postgraduate School Student Council.

Nevertheless, the optimism that drove me at the beginning turned into a series of quarantines and a "never-ending" lockdown in the middle of my doctoral studies. While observing the world of self-destruction, I surprisingly found a place of calm and common sense in science, which too often seems chaotic and messy. As for science, my appreciation also goes to nature, for her resistance against human stupidity and never-ending inspiration.

An enormous thank you goes to video communication platforms and our "card club" for making each lockdown indescribably easier. Lastly, thank you, Gandalf and Dumbledore, for keeping the Star Wars gang company and making late-night writings less lonely.

Getting this thesis written required more than just academic support. Loyalty, honesty and kindness from my old friends are much appreciated. My deepest and warmest appreciation goes to my family, their supportive environment, and their love. But the sweetest gratitude goes to my love - you make the future look bright.

Thank you all for your support throughout the process; this thesis would have never been realized in the present form without you.

Abstract

The link between TiO_2 and photocatalysis was recognized a long time ago. However, there was originally no scientific knowledge relating to the process of photocatalysis. Given this, it is impressive that the most significant advances in the properties of TiO_2 in photocatalytic processes have been made since the first reports of the so-called Honda-Fujishima effect, roughly 50 years ago.

Fast-developing technological progress over the last two hundred years is taking a heavy toll in many areas, including in environmental pollution issues. Although the problem of pollution is very complex and requires a comprehensive and unified approach, the use of TiO_2 can partly contribute to the solution. The most favourable properties of TiO_2 are its non-toxicity, inertness, and high availability. It also has very interesting optical properties under UV illumination, which enable the use of TiO_2 in photocatalytically based processes, such as the decomposition of persistent organic pollutants in wastewater and air. The final products of the process are mostly CO_2 and H_2O in the case of complete mineralization.

When TiO_2 is illuminated by UV light, electron-hole pairs are formed, which are consequently present in the formation of reactive oxygen species. However, there may be up to 90% loss of these pairs due to their rapid recombination. This recombination yield is lower in one-dimensional structures of TiO_2, such as in TiO_2 nanotubes. These can be produced by various synthesis methods. However, electrochemical oxidation or anodic oxidation is the most promising process. Anodic oxidation is a highly controllable process influenced by the composition of the electrolyte, its age, the applied voltage, the time of the process and the choice of the initial substrate. In this process, rigidly attached TiO_2 nanotubes are formed on the titanium metal substrate. Titanium of various shapes and purities can be used for the substrate.

The present thesis discusses three aspects of TiO_2 nanotubes: their synthesis, their optical properties under UV and their photocatalytic efficiency in the degradation of a model organic compound. Each chapter of the thesis is dedicated to one of the above-stated aspects. First, it is shown that the roughness of the titanium surface significantly impacts on the final surface area of photocatalytically active TiO_2 nanotube layers. Namely, we showed that titanium substrate pre-treatment, such as electropolishing, influences the TiO_2 nanotubes' growth and photocatalytic activity. Next, by studying the influence of the titanium substrate's thickness from 30 to 600 µm, we successfully determined which thickness resulted in nanotube layers that are rigidly attached and can thus be bent without risk of losing the material. And finally, we also focused on investigating repetitive anodization and change in electrolyte composition. In this aspect, it was concluded that fresh electrolyte results in uniform nanotube morphology and consequently better photocatalytic activity.

Systematic investigations of the relevant parameters were performed to gain knowledge about the material's preparation, the importance of understanding the behaviour of nanotube growth and to determine the properties of an ideal photocatalyst in the remediation of organic pollutants. The knowledge described in those sections can also be easily applied at the practical industry level.

Povzetek

Doktorska disertacija se osredotoča na sintezo in lastnosti anodno oksidiranih plasti na titanovi podlagi za uporabo v fotokatalizi. Povezava med TiO_2 in fotokatalizo je bila prepoznana že relativno zgodaj v zgodovini človeštva, vendar o procesu fotokatalize ni bilo nobenih znanstvenih spoznanj. Glede na to je impresivno, da so bile najpomembnejše lastnosti materiala TiO_2 v fotokatalitskih procesih prepoznane v zadnjih petdesetih letih, od prelomne točke tako imenovanega učinka Honda-Fujishima.

Hitro razvijajoči se tehnološki napredek v zadnjih dveh stoletjih terja visok davek na številnih področjih življenja. Pri tem je potrebno izpostaviti problem onesnaževanja, ki je kompleksen in zahteva celovit in enoten pristop. Del rešitve pri tem predstavlja uporaba TiO_2 pri razgradnji onesnaževal. Najbolj ugodne lastnosti TiO_2 so njegova nestrupenost, inertnost in visoka razpoložljivost. Ima tudi zelo zanimive optične lastnosti pod UV-osvetlitvijo, ki omogočajo uporabo TiO_2 v fotokatalitsko zasnovanih procesih, kot je razgradnja obstojnih organskih onesnaževal v odpadni vodi in zraku. Končna produkta procesa sta v primeru popolne mineralizacije večinoma CO_2 in H_2O.

Ko TiO_2 osvetlimo z UV-svetlobo, nastanejo pari elektron-luknja, ki so posledično prisotni pri tvorbi reaktivnih kisikovih spojin. Vendar pa lahko zaradi njihove hitre rekombinacije pride do 90-% izgube teh parov. Ta rekombinacijski izkoristek je nižji v enodimenzionalnih strukturah, kot so nanocevke TiO_2. Te je mogoče proizvesti z različnimi metodami sinteze. Optimalen postopek je elektrokemična oksidacija ali anodna oksidacija, ki je visoko obvladljiv proces, na katerega vplivajo sestava elektrolita, njegova starost, uporabljena napetost, čas procesa in izbira začetnega substrata. V tem procesu se na kovinskem substratu iz titana oblikujejo togo pritrjene nanocevke TiO_2. Za podlago lahko uporabimo titan različnih oblik in čistosti.

Pričujoče doktorsko delo obravnava tri vidike TiO_2 nanocevk: njihovo sintezo, njihove optične lastnosti pod UV-žarki in njihovo fotokatalitično učinkovitost pri razgradnji modelne organske spojine. Vsako poglavje doktorske naloge je posvečeno enemu od zgoraj navedenih vidikov. Prikazano je, da hrapavost površine titana pomembno vpliva na končno površino fotokatalitsko aktivnih plasti nanocevk TiO_2. Pokazali smo namreč, da predobdelava titanovega substrata, kot je elektropoliranje, vpliva na rast in fotokatalitično aktivnost TiO_2 nanocevk. Nato smo s preučevanjem vpliva debeline titanovega substrata od 30 do 600 µm uspešno ugotovili, katera debelina je povzročila plasti nanocevk, ki so togo pritrjene in jih je tako mogoče upogniti brez tveganja izgube materiala. Osredotočili pa smo se tudi na raziskovanje ponavljajoče se anodizacije in spremembe v sestavi elektrolita. S tega vidika je bilo ugotovljeno, da sveži elektroliti povzročijo enotno morfologijo nanocevk in posledično boljšo fotokatalitično aktivnost.

Izvedena je bila sistematična raziskava relevantnih parametrov, da bi pridobili znanje o pripravi materiala in pomenu razumevanja obnašanja rasti nanocevk ter določili lastnosti idealnega fotokatalizatorja pri sanaciji organskih onesnaževal. Znanje, opisano v teh razdelkih, je mogoče zlahka uporabiti tudi na praktični ravni industrije.

Contents

List of Figures

List of Tables

Abbreviations

3D	... Three-Dimensional
AFM	... Atomic Force Microscopy
ASTM	... American Society for Testing and Materials
CB	... Conduction Band
DC	... Direct Current
DEPMPO	... 5-(Diethylphosphono)-5-methyl-1-pyrroline N-Oxide
DMSO	... Dimethyl Sulfoxide
DSSC	... Dye Sensitized Solar Cell
EBSD	... Electron Backscatter Diffraction
EDXS/EDS	... Energy-Dispersive X-Ray Spectroscopy
EM spectrum	... Electromagnetic Spectrum
EP	... Electropolished
EPR	... Electron Paramagnetic Spectrometry
FEG-SEM/FSEM	... Field Emission Scanning Electron Microscopy
FWHM	... Full Width at Half Maximum
hcp	... Hexagonal Close-Packed
HRTEM	... High-Resolution Transmission Electron Microscopy
HPLC	... High-Performance Liquid Chromatography
ICP-OES	... Inductively Coupled Plasma Optical Emission Spectrometry
IPF	... Inverse Pole Figure
IPS	... Jožef Stefan International Postgraduate School
JSI	... Jožef Stefan Institute
LH	... Langmuir–Hinshelwood
NT(s)	... Nanotube(s)
OM	... Optical Microscopy
PBR	... Pilling-Bedworth Ratio
PL	... Photoluminescence
ROS	... Reactive Oxygen Species
SEM	... Scanning Electron Microscopy
SIMS	... Secondary Ion Mass Spectrometry
ToF-SIMS	... Time-of-Flight Secondary Ion Mass Spectrometry
UT	... Untreated
UV	... Ultraviolet
UVA	... Ultraviolet A
UVB	... Ultraviolet B
UV-Vis-IR	... Ultraviolet-Visible-Infrared
VB	... Valence Band
XPS	... X-Ray Photoelectron Spectroscopy
XRD	... X-Ray Diffraction

Symbols

ΔG	... Excitation Energy
Å	... angstrom
%	... Percentage
ζ	... Photonic Efficiency
λ	... Wavelength
λ_s	... Short Cutoff
λ_c	... Long Cutoff
μm	... Micrometre
Φ	... Quantum yield
$a.u.$	... Arbitrary Unit
Al^+	... Short-lived Aluminium(I) Ion
C	... Reactant Concentration
c	... Speed of Light
C_0	... Starting Concentration
Ca^+	... Short-lived Calcium(I) Ion
Cl^-	... Chloride Ion
cm^3	... Cubic Centimetre
$C_6H_8O_7$	... Citric Acid
CO_2	... Carbon Dioxide
Cs^+	... Caesium Ion
C_t	... Concentration at Time [t]
e^-	... Electron
e^-/h^+	... Electron-Hole Pair
e^-_{CB}	... Electron in the Conduction Band
E_G	... Bandgap Energy
eV	... Electron Volt
E_{x-y}	... Activation Energies
F^-	... Fluoride Ion
$F+$	... F-Centre
F_2	... Fluorine

Fe^+	... Short-lived Iron(I) Ion
g	... Gram
h	... Planck Constant
h^+	... Hole
$h\nu$	... The Energy of the Single Photon
H^+	... Hydrogen Ion
h^+_{VB}	... Valence Band Hole
HCl	... Hydrochloric Acid
$HClO_4$	... Perchloric Acid
HF	... Hydrofluoric acid
H_2	... Hydrogen
H_2O	... Water
H_2O_2	... Hydrogen Peroxide
H_2SO_4	... Sulfuric Acid
I	... Light Intensity
I_a	... Absorbed Photon Flux
I_0	... Incident Photon Flux
K	... Adsorption Coefficient of the Reactant
k/k_0	... Reaction Rate Constant
K^+	... Potassium Ion
KF	... Potassium Fluoride
Li^+	... Lithium Ion
Mg^+	... Short-lived Magnesium(I) Ion
$mL\ L^{-1}$	... Millilitre per Litre
mol	... Mole
N	... Nitrogen
N_A	... Avogadro Constant
Na^+	... Sodium Ion
NaF	... Sodium Fluoride
$NaOH$	... Sodium Hydroxide
$NaHSO_4$	... Sodium Hydrogen Sulphate
NH_3	... Ammonia
NH_4F	... Ammonium Fluoride
NH_4^+	... Ammonium Ion
$(NH_4)_2TiF_6$	... Hexafluorotitanate(IV) Ammonium
nm	... Nanometre
O	... Atomic Oxygen
$^1O_2$	... Singlet Oxygen

O_2	... Oxygen
O^{2-}	... Oxygen Ion
$O^{\bullet -}$	... Oxygen Anion Radical
O_2^-	... Superoxide
$O_2^{\bullet -}$	... Superoxide Radical
O_2^{2-}	... Peroxide
OH	... Hydroxyl Groups
OH^-	... Hydroxide Anion
$OH^\bullet$	... Hydroxy Radical
ps	... Picosecond
R_a	... Average Arithmetical Roughness
R_i	... Initial Reaction Rate
R_t	... Peak-to-Valley Roughness
R_q	... Root-Mean-Square Roughness
Si^+	... Short-lived Silicon(I) Cation
t	... Time
T	... Temperature
Ti	... Titanium
Ti^+	... Short-lived Titanium(I) Ion
Ti^{3+}	... Titanium(III) Ion
Ti^{4+}	... Titanium(IV) Ion
$Ti6Al4V$	... Alpha-beta Titanium Alloy
Ti_xF_y	... Fluorotitanium Compounds (TiF_2, TiF_3, *etc.*)
$[TiF_6]^{2-}$	... Titanium Hexafluoride
TiO_2	... Titanium Dioxide
TiO^+	... Titanium Oxide Ion
$TiOF$	... Oxofluorotitanate
$TiOF_2$	... Titanium Oxyfluoride
$wt\%$	... Weight Percent
ZnO	... Zinc Oxide

Chapter 1

Introduction

The world of materials is a unique and spectacular marvel, complementing biodiversity and making things run smoothly. It is dazzling in its variety and richness, and in these billions of pieces, titanium dioxide (TiO_2) is only a minor feature, yet so interesting for exploration.

History has provided us with a basic understanding of TiO_2's behaviour, its nanoparticulate forms, and the vast range of research applications, such as photocatalysis. Nevertheless, so many aspects need deeper investigation. There is still a long way to fully understand all the TiO_2 nanotube (NT) growth mechanisms and the parameters contributing to photocatalysis' actual conditions. And although our research covered only a small proportion of TiO_2's uniqueness, it is nonetheless a significant contribution, since it integrated both basic and applied science to understand and improve the photocatalytic properties of TiO_2 nanotube (NT) arrays obtained by anodic oxidation.

This thesis investigates the influence of titanium's surface properties on the growth of photocatalytically active TiO_2 NTs. A systematic investigation of the relevant parameters, such as chemical composition, surface roughness, grain size and crystal orientation, foil thickness, electrolyte age, and photocatalytic activity, would allow us to control the active area of rigidly attached NTs. Using different shapes and sizes of the catalyst would extend its use as an ideal photocatalyst in pollutant remediation.

The study's main outcome was to gain knowledge about the material's preparation by tuning the properties and the importance of understanding the behaviour of NTs' growth that can be used in practical photocatalytic applications.

The thesis comprises several chapters that provide an overview of TiO_2 nanotubular layers. The insight will begin with the historical background to TiO_2 research in Section 1.1. The introduction will then continue with the fundamental concepts of TiO_2 NTs, the growth mechanism of anodic oxidation, and the principles of photocatalytic degradation for organic compounds in Section 1.2. Following this, Section 1.3 will focus on our research motivation and the objectives of the thesis. The chapter will then close with a general outline and the methods used in the study.

The thesis is designed as a three-layered paper, meaning that the common backgrounds of TiO_2 NTs are interconnected throughout. However, three major tipping points of efficient catalysts are presented as individual chapters. Chapter 2 is dedicated to the influence of the surface treatment of metal titanium (Ti) foil on the photocatalytic properties of TiO_2 nanotubular layers grown with anodic oxidation. Highlighted are the results from the published manuscript and additional unpublished results that contributed to the choice of the material and its preparation for the work in Chapter 3, where the investigation led towards a flexible and efficient TiO_2 photocatalyst. Several thicknesses of titanium-foil substrate were chosen in this experimental setup. Lastly, the third point will

focus on the joint research in Chapter 4, where the influence of the anodisation electrolyte and its ageing on the photocatalytic activity of TiO_2 nanotubular layers will be discussed. The presented work will finish with conclusions and dissemination, and with a future exploitation chapter.

1.1 Starting Point

Titanium dioxide (TiO_2), also called Ti(IV) oxide or titania was discovered as a natural compound in 1791 by William Gregor. However, it was not until 100 years later that it was first produced commercially [1]. At the time, its popularity escalated, and it was mainly used as a pigment since it has many unique characteristics (e.g., non-toxicity and high refractive index). Moreover, it can be found in abundance [2]. The use of TiO_2 further revealed additional beneficial features. Durability and chemical stability paved the way in other industrial areas, from plastics, paper, ceramics, cosmetics, and pharmaceuticals to the food industry [1]. The most important milestones in the history of TiO_2 are presented in Figure 1.1a and b.

The sun's energy is among the most abundant and underexploited natural sources. The received energy has a direct impact and is responsible for numerous processes such as photosynthesis, the generation of fossil fuels and various technologies that exploit solar energy and convert it into heat, light, and electricity. The sun's power is immense – in an hour, the Earth's atmosphere receives enough sunlight to power the population's electricity needs for a year [3]. Exploring this solar body began in the 17th century [4]. Over the following years, scientists like Descartes, Newton, Huygens, Young, and Maxwell studied the concept of light. Finally, in the 19th century, an important milestone was set. A consensus on the wave-particle duality of light was published [5], which is still used nowadays to explain light's behaviour.

After that, different scientific directions took place, like the discovery of the photovoltaic effect by Becquerel [6] or the first description of the process of photocatalysis in the late 1910s [7]. In an excellent perspective written by Serpone et al. [8], the essential concepts and origins of photocatalysis were presented between 1910 and the 1980s. However, key events are presented below to understand the complexity of TiO_2 better.

At the beginning of the 20th century, there were two significant concepts defined. The first defined solar energy as the "fuel of the future" and set the foundation of photo/green chemistry. The movements' founder was Giacomo Ciamician, shown in Figure 1.1c in the middle of the experiment with his colleague Paul Silber. And the second concept determined the photoactivity of TiO_2, which is (even nowadays) a crucial characteristic of a TiO_2 catalyst, previously called photosensitiser [9].

A definition by Goodeve and Kitchener [10] states that "*Photosensitisers are generally considered to be substances which absorb light and cause a photochemical change, but appear more or less unchanged at the end of the reaction… Of the mechanisms proposed to account for the action of photosensitisers only two have wide application. In some cases the absorption of a light quantum by a molecule leaves this molecule with an electron in an excited state, the energy subsequently being transferred on collision to a second molecule by some physical process. In other cases the photosensitiser, on absorption of a quantum, is dissociated into atoms or free radicals, which act as catalysts or chain carriers for the main reaction, later recombining to form the photosensitiser. The energy transfer in both of these types of process is a result of molecular diffusion*". Goodeve and Kitchener were among the first to try TiO_2 as a bleaching agent in the 1930s. The reaction occurred due to the presence of oxygen and ultraviolet (UV) absorption that combined to produce reactive oxygen species (ROS) [11]. Other reports from the scientific community from that

time include basic research [12]–[26] of the degradation/oxidation/synthesis mechanisms [27]–[40], new materials, hydrogen reactions, water splitting, and oxygen transfer. Although the material resulted in promising findings, the scientific interest was limited, and the progress was slow. By typing keywords like "TiO_2 *photosensitiser*", "TiO_2 *photocatalyst*", and "TiO_2 *catalyst*", we get only a fraction of today's hits.

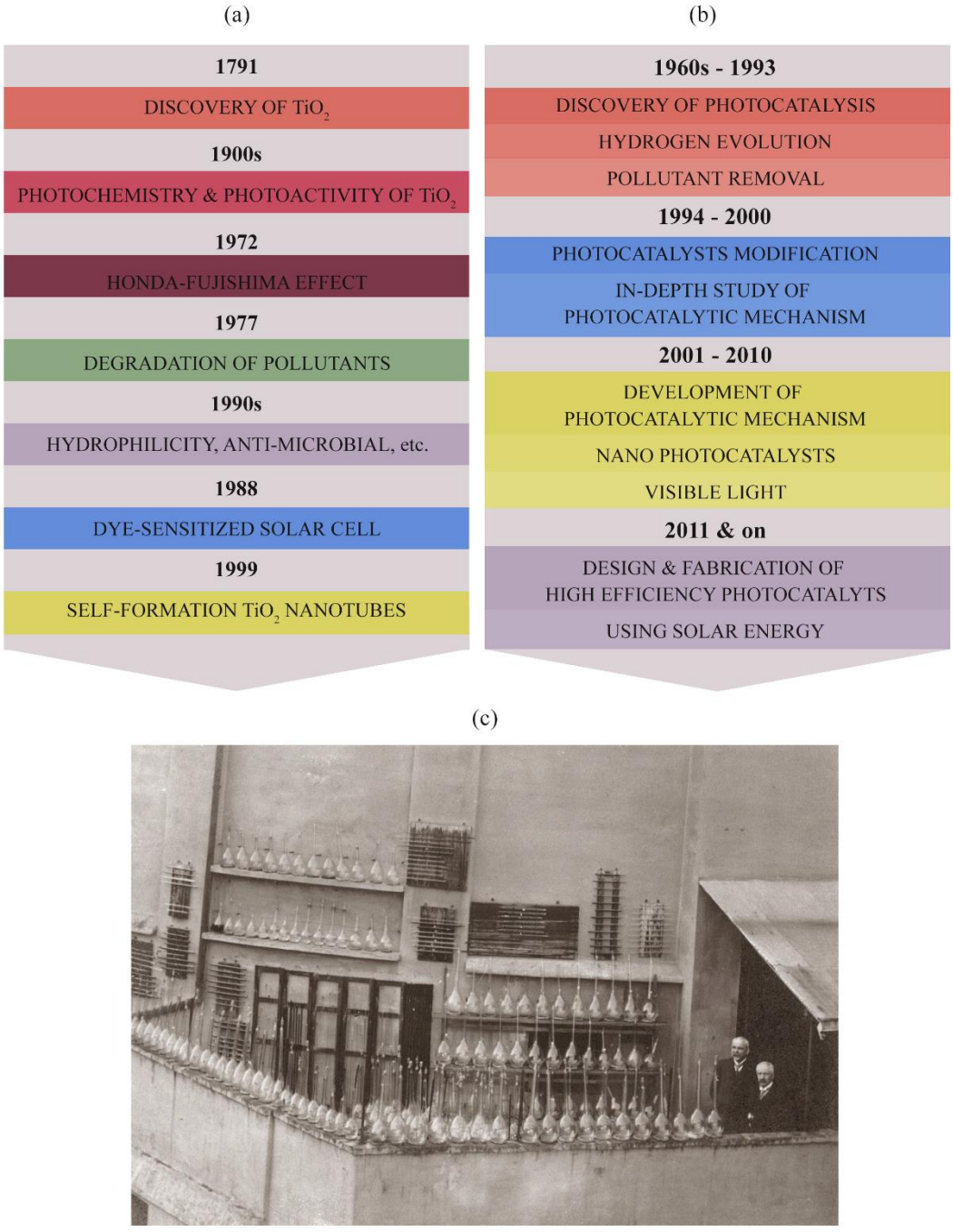

Figure 1.1: (a) Significant milestones in the history of the TiO_2 and (b) the development of photocatalysis, adapted from [41], [42]. (c) The founder of photochemistry (sun radiation) exploration, Giacomo Ciamician, with his colleague Paul Silber in the middle

of an experiment on the roof of the university. Courtesy of Department of Chemistry "Giacomo Ciamician" – Alma Mater Studiorum - Università di Bologna.

However, the band theory of semiconductors did not appear until the 1960s. The event coincided with an economic crisis, so the scientific interest in the possibilities and solutions offered by TiO_2 greatly increased. The most important milestone that put photocatalysis on the scientific map was in 1972, with the discovery by Honda and Fujishima, marking the start of modern photocatalysis. They published a breakthrough study [43] describing water (H_2O) photolysis, light-induced H_2O splitting into hydrogen (H_2) and oxygen (O_2) on TiO_2 surfaces. The phenomenon is now known as the "*Honda-Fujishima effect*".

Although many research studies were made on the purification of wastewater and polluted air, it took a few years to develop photocatalysis on an industrial level. In the beginning, the research focused only on powdered TiO_2 [44]. But slowly, in the late 1980s, immobilized TiO_2 was also introduced [9]. Unfortunately, UV light presents only a small fraction of visible light, leading to poor absorption. Therefore, the use of a TiO_2 catalyst for energy acquisition was pointless. However, in 1977, the oxidation power of TiO_2 for the degradation of pollutants was known [45]. In the following years, the topic gained popularity since it did not require any additional energy source and because both processes, oxidation and reduction, took place simultaneously. The issues they were facing during the scale-up were *(1)* low energy conversion [46]–[48], *(2)* inability to treat the vast amount of water/air [49]–[51], and *(3)* poor absorption of light on the catalyst [52], [53] – obstacles that are still present nowadays.

The evolution of laboratory equipment enabled detailed observations of photocatalysis and other processes on the TiO_2 surface. It was discovered that illuminated TiO_2 has self-cleaning properties [54], [55] and that its hydrophilic characteristic makes it an ideal candidate for anti-fogging applications [56] – a process that is effective only if the number of incident photons is greater than the number of molecules at the TiO_2 surface at a given time [57], [58].

Next, the 1990s brought knowledge of TiO_2's antibacterial characteristics [55], [59]–[61] when illuminated with UV light [62], [63]. As a consequence of the antimicrobial and biomedical properties, the TiO_2 material was introduced even in medicine [64]–[68].

Furthermore, the unique properties of the material were used in 1988 for the creation of a dye-sensitized solar cell (also known as a Grätzel cell), more commonly known as the DSSC solar cell [69], [70]. Although the system's configuration represents a simple photo-electro-chemical mechanism where a semiconductor is formed between the photo-sensitized anode and an electrolyte [71], it took the inventors several years to develop an efficient dye-sensitized solar cell [72].

Finally, intensive research took us to 1999, when Zwilling et al. reported the self-formation of TiO_2 NTs, grown with the electrochemical method of anodic oxidation [73]. Suddenly a new era of research began, and NTs became promising material for various applications. NT production was relatively cheap compared to other methods [74], and their morphology and properties were easily manipulated [75] – the details will be presented in the following sections of the thesis. The progress followed the so-called Zwilling's' first-generation NTs [73], [76] and continued with the second generation of larger NTs up to a few microns and with smooth walls [76]. Further research led to the third generation NTs [74], [77], [78] that elucidated a new understanding of the growth mechanism of TiO_2 NTs with improved optical and electrical characteristics. The focus of this work is set on these last TiO_2 NTs, used in the process of photocatalysis for the degradation of organic pollutants.

1.2 General Concepts

1.2.1 Titanium Dioxide Nanotubes

1.2.1.1 Why Nanotubes?

TiO_2 NTs possess many unique physical, optical, and electrical properties. Among those, non-toxicity, high resistance to corrosion, and biological/chemical inertness [79] have most significantly contributed to the increasing popularity of TiO_2 in recent years. In this chapter, the structural and morphological characteristics of NTs are presented in more detail.

For efficient catalytic reactions, the specific surface area of the catalyst must be maximized. Until the discovery of electrochemically self-organized TiO_2 NTs, the nanoparticulate form of TiO_2 was the most widely used. P25 Degussa [80], the gold standard in photocatalytic reactions, is still popular today. It is a mixture of anatase and rutile particles with different ratios (e.g., 70:30, 80:20, etc.) resulting in a large active surface area (35 - 65 m^2 g^{-1}) and high activity in photocatalytic reactions [80], [81]. Although their growth can be easily manipulated, nanoparticles tend to form agglomerates. The key to high photocatalytic activity is that the formed agglomerates break down and enable single anatase and rutile particles to contact the pollutant [81].

One-dimensional (1D) oxides are stable nanostructures with unique properties [82], [83]. Their growth and morphology can be easily controlled through many synthesis routes [84]. For example, NTs grown with anodic oxidation are rigidly attached structures. Therefore, they cannot be released into the environment during the process of pollutant removal as easily as the nanoparticulate TiO_2 [50]. This characteristic is essential for use in purification reactors where the stability and longevity of a catalyst are crucial. Other significant factors that contribute to NT efficiency are the control of the degradation process [85], optimized geometry for shorter carrier-diffusion paths, and a lower recombination rate [86], [87]. Another important characteristic is the generation of ROS and the presence of oxygen vacancies [89].

1.2.1.2 Crystalline Polymorphs TiO_2

The characteristics of TiO_2 nanostructures are directly connected to the material's crystallinity. Therefore, any changes directly impact the dangling bonds and the lattice structure, and thus influence the total surface area and status of the surface OH [88]. As synthesized NTs with anodic oxidation are, as a rule, amorphous, annealing under specific conditions changes them into one of the most stable polymorphs. For example, brookite could be transformed to rutile at elevated temperatures, directly or via anatase, depending on the crystallite size, size distribution, and contact area [89].

Zhu and Gao [90] investigated the formation and stability of different TiO_2 polymorphs formed under added pressure (e.g., rutile, anatase, brookite, columbite, baddeleyite, cotunnite, pyrite, and fluorite). Tetragonal rutile, anatase, and orthorhombic brookite [91] are the three most common TiO_2 crystalline forms. The choice of a suitable TiO_2 polymorph is critical for determining the application and its effectiveness. A basic TiO_2 structure represents a Ti^{4+} surrounded by the O^{2-} anions [88] and is mainly presented with TiO_6 octahedron building blocks, as shown in Figure 1.2.

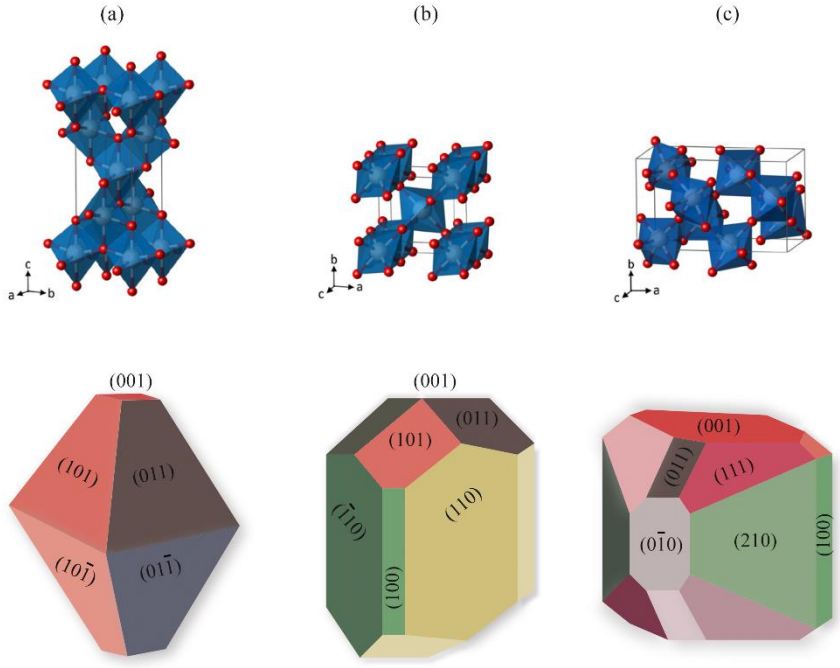

Figure 1.2: The crystal structures and crystallographic facets of the three most common TiO_2 crystalline polymorphs – (a) anatase, (b) rutile and (c) brookite. Adapted from [92] and [91], Journal of Physics: Condensed Matter, Landmann et al., The electronic structure and optical response of rutile, anatase and brookite TiO_2, 24, 19, 195503, 2012,

The transformation to anatase and rutile from an amorphous film is thermodynamically the most favourable. The concentration of lattice and surface defects, particle size, and synergetic activity between the reaction parameters (e.g., pressure lowers the temperature needed for the transformation) influence the conversion. Since both polymorphs are stable at room temperature, the transformation does not occur naturally but at higher temperatures or additional pressures [93].

Prasai et al. [94] studied the optical, electronic, and structural properties of an amorphous film. By combining the experimental results with modelling data, they concluded that the amorphous film is similar to the anatase phase in terms of electronic structure and optical properties. Although the rutile is the most stable polymorph [89], anatase is the most actively researched and used material. Compared to rutile, it has a slightly higher bandgap, by about 0.2 eV [95], a wider optical absorption gap, and higher mobility for the charge carriers [96].

The detailed crystal structure data of anatase, rutile, and brookite are presented in Table 1.1. The most significant difference in the electronic parameters can be seen in the bandgap values [97]. The bandgap of amorphous phase is 2.22 eV [94], but once crystallized, it is above 3 eV - rutile phase 3 eV, anatase 3.2 eV [95], and brookite up to 3.5 eV. Brookite is special since it has a broad absorption edge extending into visible light [98]. Overall, all three TiO_2 polymorphs are photoactive in the UV region of the electromagnetic light spectrum and usually transparent in visible light [57]. Because only this small percentage of the light spectrum is available, the appropriate illumination and the direction of the incoming photons significantly impact on photoactive applications [99]. Other key factors

in the photocatalytic activity are the crystallographic orientations and the NTs' layer thickness [96].

Table 1.1: Crystal structure data of TiO_2 [91], [93], [95], [97], [98], [100].

	Rutile	Anatase	Brookite
Lattice constraints (Å)	*a = 4.5936*	*a = 3.784*	*a = 9.184*
			b = 5.447
	c = 2.9587	*c = 9.515*	*c = 5.145*
Volume /Molecule ($Å^3$)	*31.2160*	*34.061*	*32.172*
Density (g/cm^3)	*4.13*	*3.79*	*3.99*
Ti–O bond length (Å)	*1.949 (4)*	*1.937 (4)*	*1.87 ~ 2.04*
	1.980 (2)	*1.965 (2)*	
O–Ti–O bond angle	*81.2°*	*77.7°*	*77.0°~ 105°*
	90.0°	*92.6°*	
Crystal structure	*tetragonal*	*tetragonal*	*orthorhombic*
Refractive index	*2.9*	*2.6*	*2.8*
Band gap	*3*	*3.2*	*~ 3.5*

1.2.2 Anodic Oxidation of Titanium

The electrochemical method of anodic oxidation is used to grow TiO_2 NTs in a specific set of conditions on a Ti metal substrate. The grown layer of NTs provides a highly defined and ordered geometry with a high surface area [101]. Although external conditions can guide the process, it is still self-organized, resulting in a homogenous distribution and a maximum density of grown NTs. The length of the NT is the result of the competition between the steady-state growth and the dissolution of the formed oxide. The dissolution is controlled by fluoride ions (F^-), which also influence the acidity of the NTs and the electrolyte. The NT morphology and optoelectrical properties are easily controlled by changing the anodisation parameters and substrate surface morphology [102]. Both affect the formation of the passive oxide layer, NT growth and final morphology. These parameters will be explained in more detail in the following subsections. Furthermore, the size and distribution of the grains may influence the uniformity of the grown NTs. The substrate surface must be free of impurities before the anodisation. Only a 1–10-nm-thin and dense oxide layer is always present on the air-exposed Ti substrate surface and acts as an anti-corrosive [103].

1.2.2.1 From Titanium Substrate to the Anatase TiO_2 Nanotubes

The anodic oxidation of Ti is based on the knowledge gained during the anodic oxidation of alumina. The most important outcomes include *(1)* the origin of a NT on the surface and the beneficial aspects of the two-step anodisation [104], *(2)* knowledge that anodisation is a spontaneous process controlled by anodisation parameters, *(3)* information that dimples act as the starting point for nanoporous growth [105], [106], and *(4)* documentation that the so-called flow mechanism of growth is responsible for additional lengthening of the NTs [107].

It was already mentioned that Zwilling et al. [108] started with the anodic oxidation of Ti and its alloys. Their research work covers the anodisation of pure Ti and Ti6Al4V in chromic acid with or without hydrofluoric acid (HF). They compared the morphological characteristics of both anodised layers. They showed that the overall size of the pores was smaller when pure titanium was used. Moreover, that a larger anodisation voltage resulted in more prominent pores and finally, that the incorporation of F^- into NTs from the electrolyte is possible. The research set a solid foundation for further investigation on the importance of forming NT starting pits, the choice of substrate, electrolyte composition, anodisation parameters, presence of a starting hydrolysed TiO_2 oxide, detection of fluorine and the presence of other elements.

Many NT growth theories evolved over the years, *(1) the viscous flow model, (2) the growth model of two currents, and (3) field-assisted dissolution.* The latter is also the most widely used in the scientific world [109]–[111] and is known as the self-organization of titania into TiO_2 NTs. *In fluoride-containing electrolytes, the NTs form as a result of the oxidation of Ti metal and the formation of oxide, following the dissolution of Ti metal ions in the electrolyte, and finally, the chemical dissolution of Ti and TiO_2 due to etching with F^- ions* [77].

Anodic oxidation usually occurs when a constant voltage is applied in an electrochemical cell between the anode and the cathode. The anodisation process is monitored by recording the current-vs-time since it directly indicates the applied voltage (or current if a constant current drives the process) with porous oxide formation. Using that information we can predict the final morphology of the TiO_2 NTs [112], as schematically presented in Figure 1.3a. Ti foil anodised in the fluoride-type of electrolyte always results in nanotubular oxide film [113]. The simplified step-by-step formation of NTs is shown in the SEM micrographs in Figure 1.3b. The NT growth steps are:

- *Local dissolution of Ti substrate creates small pits, which function as starting points for NT growth.*
- *The formation of a compact oxide as a chemical dissolution and electrochemical etching coincides, creating a thin barrier layer between the substrate and electrolyte.*
- *The continuation of the growth of pores is due to the electric field and their rearrangement.*
- *Etching of the oxide layer by F^- increases the current density. Chemical dissolution then removes the top shallow oxide surface layer, and NTs start to form.*
- *In the last step, the NTs are grown to the length where dissolution and etching are in equilibrium. At this point, a slight drop can be observed in current and the growth goes into steady state* [111], [114].

A constant voltage is needed for the reaction to begin. At this instant, the electrical field is perpendicular to the Ti metal surface. The NTs start to grow in this direction [115]. The value of anodic potential significantly impacts the NT diameters and lengths. For example, different impurities such as nitrogen (N) can be found in the commercial Ti foil. They often act as an additional protective barrier for the corrosion to overcome; therefore, higher starting anodisation potentials are necessary [116]. Seong et al. [117] suggested that the local electric field during the anodisation is critical for enhancing the degree of preferred orientation of the NTs because it affects the thickness of the oxide layer and the ribs' formation.

Macak et al. [118] observed a linear increase of layer thickness up to 20 V. Higher voltages resulted in continuous growth due to chemical dissolution and significant thinning

of the NT walls [119]. Interestingly, the chemical composition of NTs also changes with a lower or higher anodisation voltage. Lower voltages result in a smaller amount of oxygen than higher voltages (for example, 40.56 at. % of titanium and 59.44 at. % of oxygen at 20 V if compared to 30.86 at. % of titanium and 69.14 at. % of oxygen at 60 V). Looking at the elemental distribution and amounts in the TiO_2 NT structure at different voltages, Durdu et al. observed a homogeneous distribution of titanium and oxygen elements over the surface [120].

The final structure of the oxide is primarily defined by electrolyte composition. If the content of F^- is low, a compact oxide layer is formed, and if the F^- content is high, electropolishing (EP) or corrosion of the Ti occurs. Due to the titanium's high corrosion resistivity, F^- ions are added to the electrolyte, and they corrode through the amorphous oxide protective layer [109]. H_2O added to the electrolyte accelerates the dissolution of the NT layer compared to non-aqueous electrolytes. Chemical dissolution is slowed down if higher F^- concentrations are present and if the hydrolysis of the Ti ions increases. Slowing down the chemical dissolution prolongs the equilibrium state, which results in the formation of longer NTs. Consequently, Cai et al. [111] determined that the best pH for optimal NTs growth is between 3 and 5.

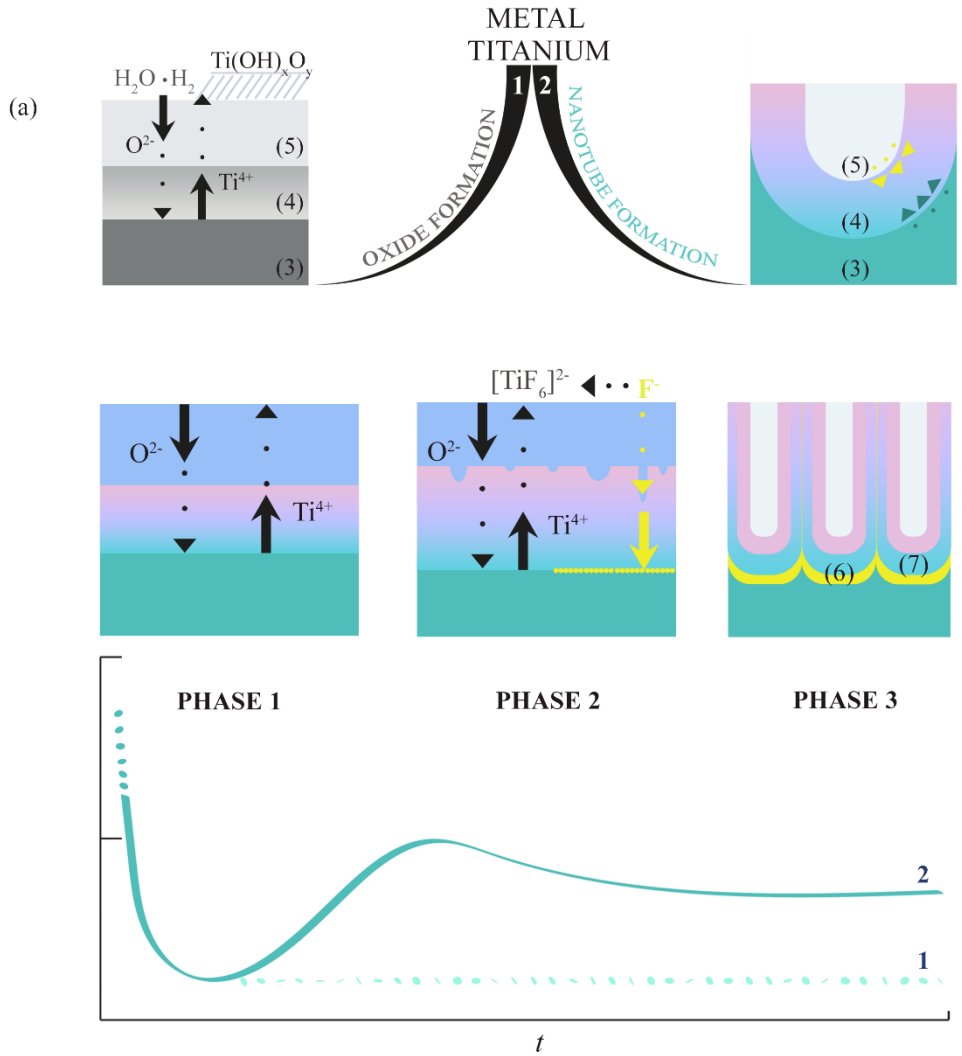

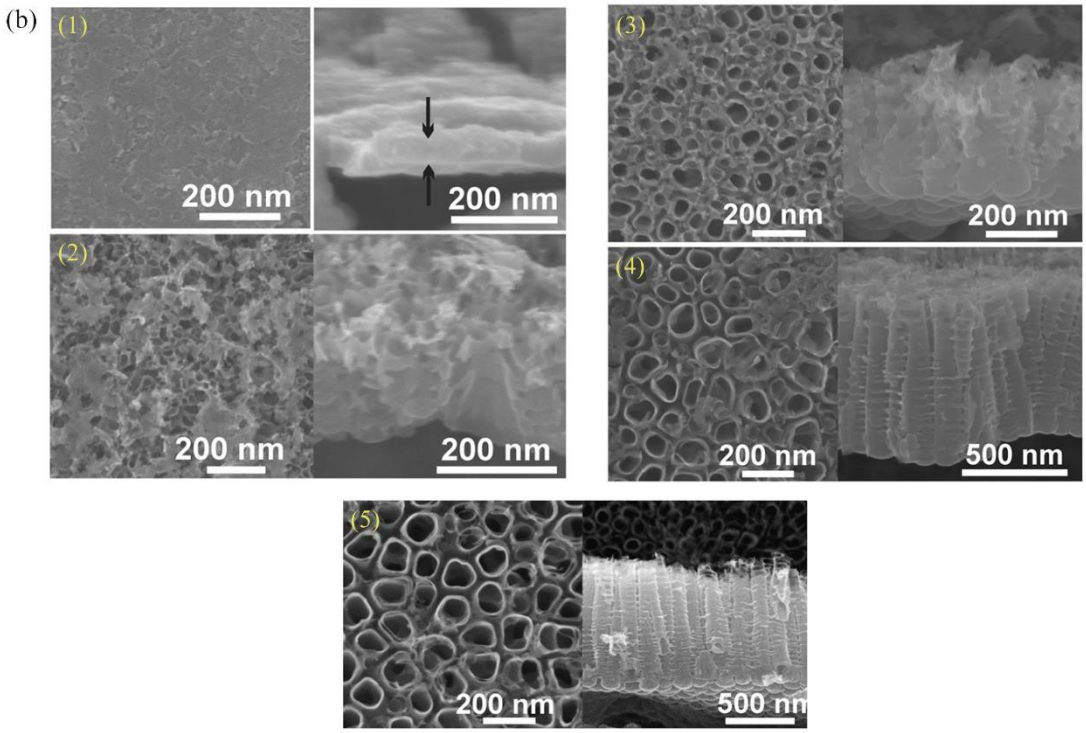

Figure 1.3: (a) Detailed presentation of NT formation by anodic oxidation of Ti substrate and the growth of NTs in the presence/absence of F^- ions. The formation of compact and nanotubular oxide layers can be monitored as current over time, with typical growth stages presented schematically. Adapted from [109], [110], [121]. (b) The step-by-step growth of NTs, top and cross-section view after *(1)* 0 min, *(2)* 3 min, *(3)* 10 min, *(4)* 30 min, and *(5)* 1 h. Reprinted from [118], Journal of Electroanalytical Chemistry, 621, Macak et al., Mechanistic aspects and growth of large diameter self-organized TiO_2 nanotubes, 254-266, Copyright (2008), with permission from Elsevier.

In the first step is formed a thicker compact oxide layer at the Ti substrate surface with the Ti dissolution into Ti^{4+} and the reaction with O^{2-} from H_2O in the electrolyte (Eq. 1.1 – 1.3). Simultaneously, a hydrogen-evolution reaction occurs at the cathode (Eq. 1.4). Due to the volume expansion in the oxide layer, internal energy increases, and stress needs to be reduced by increasing the surface area [109]. With the synergetic action of F^- etching, cracks start to appear, and the current starts to rise again. Cracks in the oxide layer present active sites for the development of corrosion pits, which grow upwards with time. F^- and oxygen ions compete in migration to reach the TiO_2 bottom oxide. Because they are smaller, F^- ions migrate at twice the rate. That leads to a tubular shape, showing an F^- rich layer between the substrate and the oxide. Unfortunately, the fluoride-rich layer also increases the probability of NT layer detachment from the substrate [122].

Fluorides can either react with Ti^{4+} at the oxide-electrolyte interface (Eq. 1.5) or with the formed oxide layer (Eq. 1.6). In both cases, the fluoride-water-soluble species $[TiF_6]^{2-}$ are created, which are important for the pore formation [123]. However, in our experiments $(NH_4)_2TiF_6$ were formed because of ammonium fluoride (NH_4F) that was a source of F^- ions (Eq. 1.7).

When the interpore begins to form, the chemical dissolution of Ti foil further enhances the growth of the NTs. The growth of NTs continues inwards into the substrate until the current reaches a steady state. At that point, the walls of the NTs come in close contact

and thus stop growing in the horizontal direction, as stated by Lu et al. [115]. Meanwhile, the reactions at the bottom of the NTs continue, and the NTs grow in the vertical direction. The conductivity of the electrolytes changes during the anodisation process. Therefore, caution with a longer anodisation time is needed as it can lead to undesired etching of the top of a nanotube [109].

Ti dissolution and oxide formation

$$Ti \rightarrow Ti^{4+} + 4e^- \tag{1.1}$$

$$2Ti + 4H_2O \rightarrow 2TiO_2 + 8H^+ + 8e^- \tag{1.2a}$$

$$Ti^{4+} + 4H_2O \rightarrow Ti(OH)_4 + 4H^+ \tag{1.3b}$$

$$2Ti(OH)_4 \rightarrow 2TiO_2 + 4H_2O \tag{1.3}$$

Hydrogen evolution reaction on a cathode

$$2H_2O + 2e^- \rightarrow H_2 \uparrow + 2OH^- \tag{1.4}$$

Presence of F^- ions

$$Ti^{4+} + 6F^- \rightarrow [TiF_6]^{2-} \tag{1.5}$$

$$TiO_2 + 6HF \rightarrow H_2[TiF_6] + 2H_2O \tag{1.6}$$

$$TiO_2 + 6NH_4F \rightarrow (NH_4)_2TiF_6 + 2H_2O + 4NH_3 \tag{1.7}$$

The oxide thickness can be measured *directly* in a cross-section view using scanning electron microscopy (SEM) or *indirectly* with several mathematical calculations. The first one states that the measured current is dropping while the oxide is growing. When the system enters the steady state, the field-effect is lost, and the thickness of such a layer can be measured via equation $d = f \times U$, where f is called the growth factor of the oxide [124], [125], [126]. For TiO_2, that factor is 2-2.5 nm/V [118]. The second equation takes into consideration that the NT diameter (d) and barrier layer thickness (t) are dependent on the applied voltage and can therefore be calculated as $d \approx 5 \times U$ and $t \approx 2.2 \times U$ [118]. And thirdly, the thickness of TiO_2 can be mathematically determined by calculating the Pilling-Bedworth ratio (PBR). The PBR represents the volume ratio of *metal oxide* and *metal* from which the oxide was grown. The importance of this balance was presented by Zhang et al. [127]. The group investigated the volume expansion by modifying the F^- concentrations and current densities and observing their effect on the mechanism of the TiO_2 NT growth. Surprisingly, they found that the volume of the NT array depended only on anodising current.

Adjustment of the dissolution rate of the oxide by the electrolyte composition is the key to the high ratio growth of the longer NTs. According to Fu and Mo [73], diffusion and pH affect the hydrolysis of the Ti ions, influencing the electrochemical etching and chemical dissolution. If the pH values go up, the hydrolysis rate increases and slows down

the dissolution, resulting in longer NTs. Sulka et al. [114] observed that a decrease in the pH at the bottoms of the pores accelerates the local dissolution of the oxide. As a result, the pH and layer thickness decrease, and the measured current increases. Because diffusion balances acidification of the electrolyte (and with that, the NTs), a more viscous electrolyte is better for easier process regulation. However, suppose the temperature of the electrolyte is too high. In that case, the viscosity decreases, and the acidification increases, resulting in an increased rate of oxide formation. Interestingly the change of rate growth is only observed at a specific temperature of approx. 20 °C [114], [128]. These processes are presented in Figure 1.4.

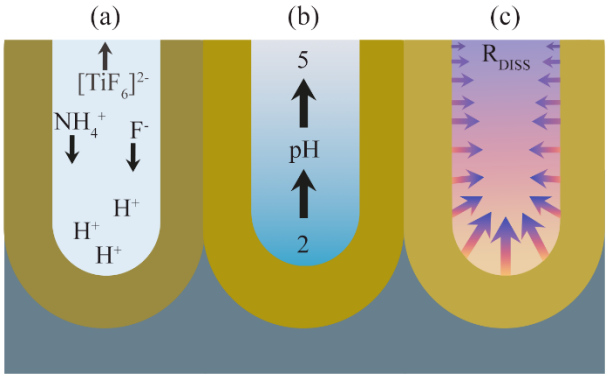

Figure 1.4: Electrochemical conditions along TiO_2 NT. (a) Dissolution reaction, oxidation and hydrolysis are among the main reasons for changes in pH profile, (b) pH at the bottom of the NT is around 2 and at the top around 5, (c) the dissolution rate profile is depending on the pH value. Adapted from [123].

It depends on the chosen electrolyte whether the grown nanotubes are single- or double-walled. Electrolytes based on dimethyl sulfoxide (DMSO) result in single-wall morphology (such NTs are composed of only the outer wall). Meanwhile, double-walled NTs are grown in electrolytes with ethylene glycol. Because the electrolyte in our experiments was based on ethylene glycol, further explanations will be based on a double-walled morphology. After the anodisation, such NTs consist of an outer and inner tube wall. The overall thicknesses of the two parts are changing along the tube wall. Furthermore, while the inner wall changes significantly from bottom to top, the outer wall remains more or less constant. All the structures are shown in Figure 1.5a.

Grown NTs are amorphous and, as such, not useful in photocatalytic reactions. The process of annealing is needed to transform them into crystalline polymorphs. With that, specific electrical, optical, and chemical properties are obtained. Ghikov et al. [129] reported that the transformation of amorphous TiO_2 to the anatase phase begins at 280 °C. Macak and his group [101] reported that after annealing at 450 °C for 3 hours, the NTs transform to smooth and round single-phase anatase NTs. HRTEM measurements and XRD pattern confirmed their findings. Moreover, a detailed analysis showed that the NTs are composed of randomly oriented TiO_2 crystallites below 50 nm and with a preferred (101) plane orientation. Albu et al. [130] studied the effect of annealing on the double-wall morphology. While a slower heating rate leads to double-walled structure morphology loss, a more rapid heating rate leads to fusion into a porous membrane. Therefore, the correct heating rate is necessary for keeping a stable double-walled morphology. Moreover, they identified a 15-nm-thick fluoride-rich layer (Figure 1.5a) at the NT bottom and Ti substrate interface. They also performed a complete chemical characterization across the TiO_2 nanotubes, as shown in Figure 1.5b. The NT is composed of different ratios of Ti and O species; however,

a significant amount of F^- and carbon (C) species can also be present and are attributed to the residuals from the electrolyte that are incorporated into the inner wall. A double-walled NT is usually thinner in the tube top due to prolonged etching and, therefore, fewer F^- and C species can be found there. The effect of annealing on the NTs' chemistry is presented in Figure 1.5c.

However, the annealing process does change the crystallinity and the morphology of the NTs. The change is drastic as the inner and outer layers are separated – the outer layer remains compact while the inner becomes porous. That happens due to the evaporation of high C and a reduction of F^- concentration by evaporation as HF or F_2 gas species (other detected gases can be TiF, TiF_2, TiF_3, TiOF, and $TiOF_2$ [103]). Fluorine species that could otherwise introduce undesired electronic states into the material [130], [131]. Finally, a subsequent heat treatment is necessary to "solidify" the flexible amorphous nanotubular layer [101]. Few reports can be found where leftover rutile was identified under or sometimes in between the anatase layer [132].

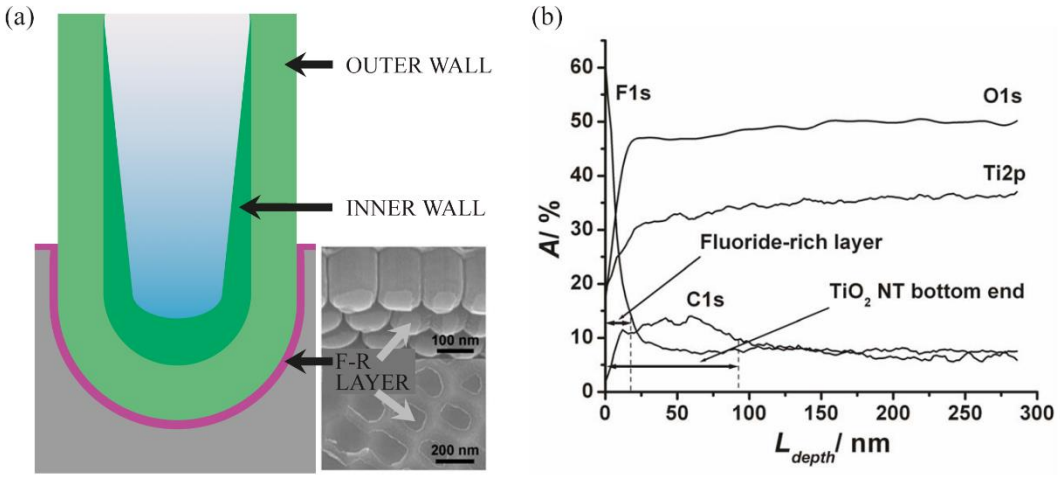

(c)

	Wt%	At%
C	3	6
O	35	55
F	9	12
Ti	54	29
C	5	10
O	37	56
F	5	7
Ti	54	28
C	5	10
O	38	57
F	6	7
Ti	51	26

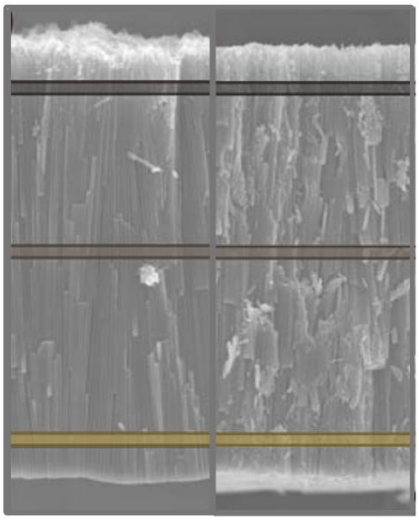

	Wt%	At%
C	2	3
O	38	63
F	<1	<1
Ti	60	33
C	2	4
O	38	63
F	<1	<1
Ti	60	33
C	2	4
O	39	64
F	<1	<1
Ti	59	32

Figure 1.5: (a) Schematic of a formed TiO_2 NT in an organic electrolyte, consisting of two regions: outer and inner shells. (b) X-Ray Photoelectron Spectroscopy (XPS) depth profile measurement and the differences in/outward migration rates of the anodic species

such as carbon, oxygen, fluorine and titanium species and (c) Energy-Dispersive X-Ray Spectroscopy (EDS) measurements over the bottom, middle, and top of NTs before/after annealing. Adapted and taken from [109], Copyright © 2011 WILEY-VCH Verlag GmbH & Co. KGaA, Weinheim and reproduced with permission from Ref. [130], Copyright © 2008 WILEY-VCH Verlag GmbH & Co. KGaA, Weinheim.

However, not all grown NTs have smooth walls. An observed rare phenomenon is the occurrence of ripples/ribs on the NT walls. They result from the competition between NT formation and dissolution. They can be seen on a graph monitoring current as periodic current fluctuations [114]. The formation of ribs is schematically presented in Figure 1.6. It results from several sequential steps where the dissolution of the outer wall F^- rich layer occurs faster than the field-assisted dissolution of the inner layer. This happens at higher H_2O contents and the high solubility of a fluoride-rich layer [117]. The physical cause of their formation is the high H_2O concentration in the electrolyte and the generation of oxygen at the anode during the anodisation process. Both parameters were investigated by Valota et al. [131]. They manipulated the H_2O concentrations and concluded that a H_2O content above 10 % resulted in significantly higher current densities, when compared with lower concentrations. The result was ribs, approximately 5 nm thick and separated by 5–30 nm. The after-effect of their formation was the reduced length of the NTs.

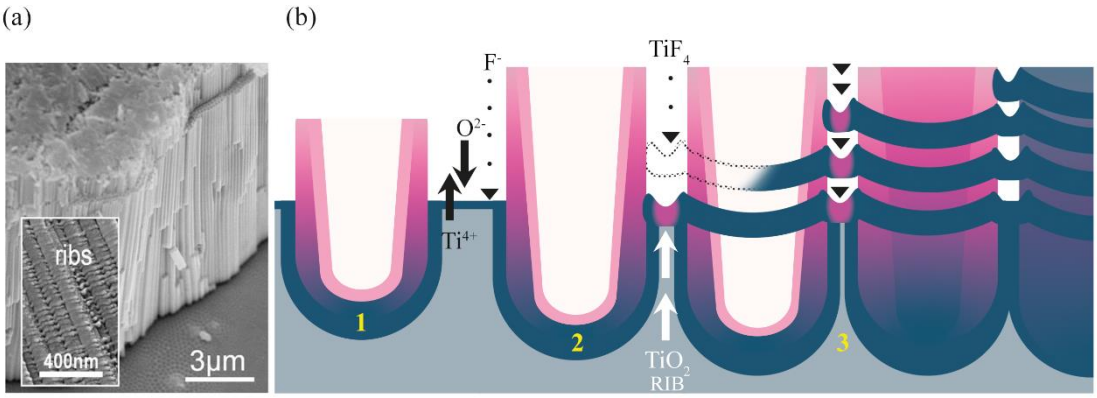

Figure 1.6: (a) SEM imaging of ribs' phenomena. Reused with permission from Ref. [133] under the License CC BY. (b) The schematic diagram of ribs' occurrence. Rib formation is a process in which cations and anions transverse during NT growth, following *(1)* dissolution of the F^- rich layer and the oxide while the main tube grows and *(2)* formation of a bridge from TiO_2 between two neighbouring NTs. The rib is formed because of excessive dissolution from the previous step and continuing oxide growth. Another rib is formed *(3)* when the electrolyte further dissolves the NT oxide. Adapted from [131].

On the other hand, Huang et al. [134] investigated the formation of split NTs and oxygen evolution during anodisation under breakdown conditions over a short period (15 min) of previously formed NTs with the conventional method. In principle, the approach "separates" the electronic and ionic current from the total current. When an electronic current reaches its minimum, it starts to increase continuously. That change accelerates the oxygen evolution and splits the NTs, similar to NT cleaving. Such growth cannot be explained with previously mentioned classical theories, but with the so-called *oxygen bubble mould theory* [134].

1.2.2.2 Choice of the Substrate

The choice of Ti substrate depends on the result the researcher wants to achieve for the TiO_2 NTs layers. To understand the effect of surface morphology of the starting Ti substrate on the TiO_2 NT formation, the properties of the substrate should be carefully considered since crystallographic defects and impurities are common and influence the physical, chemical, and electrochemical characteristics of titanium. The size and distribution of the grains may affect the uniformity of the grown NTs. However, the key advantage is that any form of Ti (e.g., sheet, foil, coil) can be treated with anodic oxidation.

This thesis is based on work with a commercially pure Ti foil. Such a foil is usually polycrystalline with a hexagonal close-packed (hcp) structure and grains of different crystallographic orientations and sizes, schematically presented in Figure 1.7a [135]. Properties of the hexagonal unit cell such as surface area, number of atoms per surface plane and atomic surface density are presented in Figure 1.7b. Commercial Ti is produced as a foil with the process of cold rolling. The most common crystallographic texture that results after the rolling is such that the [0 0 0 1] axis is perpendicular to the sheet plane [136]. Because of the nature of the generation of commercial Ti foil, the surfaces can be uneven. The relationship between the Ti substrate grain orientation and the electrochemical process of anodic oxidation was researched by several authors.

(a)

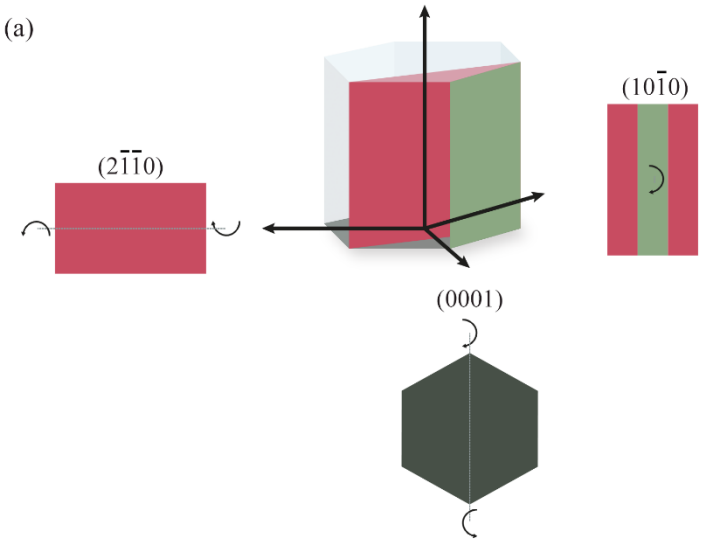

(b)

PLANE/ RELATION	SURFACE AREA [cm^2]	No. OF ATOMS/ SURFACE PLANE	ATOMIC SURFACE DENSITY x NUMBER OF ATOMS/cm^2
(0001)	2.3×10^{-15}	3	1.3×10^{15}
(01-10)	1.4×10^{-15}	1	7.2×10^{14}
(11-20)	2.4×10^{-15}	2	8.3×10^{14}
(0001)/(01-10)	1.6	3	1.8
(0001)/(11-20)	1	1.5	1.6
(01-10)/(11-20)	0.6	0.5	0.9

Figure 1.7: (a) Hexagonal unit cell for polycrystalline commercially pure Ti with indicated (0001), (10$\bar{1}$0) and (2$\bar{1}\bar{1}$0) planes and (b) properties of the hexagonal unit cell such as surface area, number of atoms per surface plane and atomic surface density. Adapted from [137], [138].

Lu et al. [115] linked surface curvature and electrical field – if the surface was curved, so was the electrical field. Consequently, the grown NTs are tilted across the Ti surface in the electrical field direction. Smaller NTs can be found underneath the convex surface, while prominent, more expanded NTs can be observed underneath the concave surface. Additional research included as-received Ti foil, chemically polished, mechanically polished and electropolished (EP) Ti foil. After anodisation, the NTs grown on the as-received substrate appeared non-uniform, compared with other polishing treatments.

Meanwhile, Seong et al. [117] focused on Ti surface roughness as a critical factor for controlling the degree of the preferred orientation of anatase NTs. They investigated 2-mm-thick Ti foil, untreated (UT) or mechanically polished. By calculating the root-mean-square roughness (R_q) of the Ti surface and comparing the data with the nanotube growth and their crystallinity, they concluded that lower roughness numbers resulted in a higher degree of preferred orientation. Moreover, the uniformity of the NTs improved if anodic oxidation was performed on flatter (less rough) surfaces, since the grain boundaries in polycrystalline structures can also function as charge-trapping centres. The effect of surface topography on the NT growth is presented in Figure 1.8a.

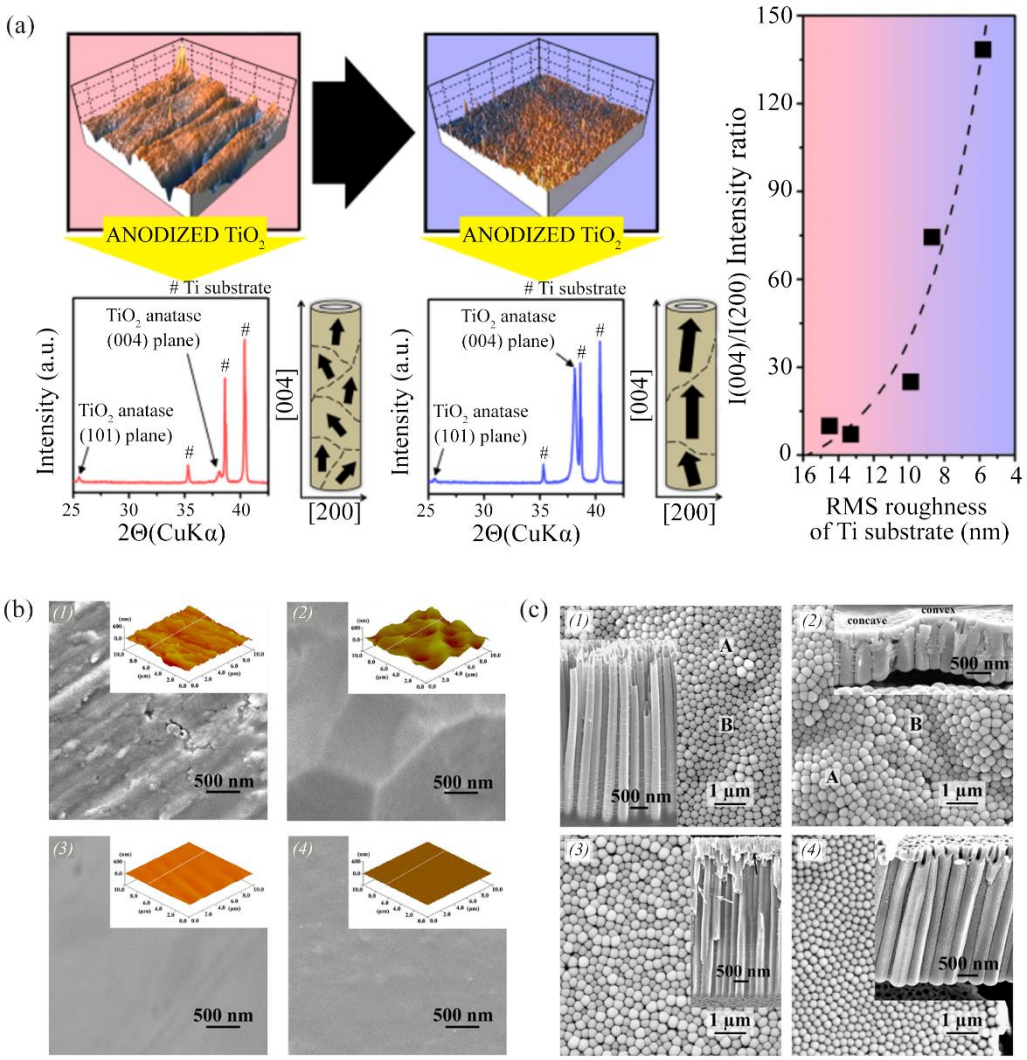

Figure 1.8: (a) Influence of substrate surface on NTs growth. Dependency of root-mean-square roughness values on the degree of preferred orientation to the (004) plane of the anatase [117]. Reprinted with permission from Journal of Physical Chemistry C, 19, 23,

Seong et al., Roughness of Ti substrates for control of the preferred orientation of TiO_2 nanotube arrays as a new orientation factor. Copyright (2015) American Chemical Society. (b) SEM and AFM images of UT *(1)*, chemically *(2)*, mechanically *(3)* polished and electropolished (EP), *(4)* Ti substrates and (c) their NTs [115]. Reprinted from Electrochimica Acta, 56 /17, Lu et al., Polishing effect on anodic titania nanotube formation, 7, Copyright (2011), with permission from Elsevier.

Among different polishing procedures (Figure 1.8b-c), EP significantly influences the electrochemistry. Therefore, it is not uncommon that the most homogenous layer of NTs results from EP Ti foil [115]. The process of EP is a three-step reaction in which Ti^{4+} cations diffuse in the electrolyte after the applied voltage between Ti anode and cathode (Eq. 1.8). At the same time, oxygen evolution occurs (Eq. 1.9), and active dissolution results in the polishing process [139].

$$Ti \rightarrow Ti^{4+} + 4e^- \tag{1.8}$$

$$4OH^- \rightarrow O_2 + 2H_2O + 4e^- \tag{1.9}$$

$$Ti + 4OH^- \rightarrow TiO_2 + 2H_2O + 4e^- \tag{1.10}$$

Consequently, the Ti surface becomes unstable, and a passive oxide film is formed (Eq. 1.10). If the voltage during the formation of the anodic film increases, pitting of the Ti surface occurs [140], [141]. The passive oxide film covering the Ti foil plays a vital role, because it limits the ions' migration towards the anode and thus prevents extensive or uneven surface etching [142]. The final surface topography can be tailored by controlling the EP parameters, such as the electrolyte's composition and temperature, the polishing time, and the applied voltage. The proper selection of EP parameters is crucial for controlled titanium-surface preparation. For example, high applied voltages result in the production of excess hydrogen gas. They can cause '*burned spots*' on the Ti surface. On the other hand, low voltages result in the absence of an oxide film during the polishing, which leads to greater roughness [139]. Furthermore, EP residues act as nucleation sites for NT growth, which could simultaneously lead to a poor arrangement if present in excess numbers [143].

Apart from the polishing, the surface roughness can be reduced by repetitive anodisation. Repetitive anodisation is a process when the NT layer from the first anodisation is removed from the substrate directly after anodic oxidation. What remains on the Ti surface are dimples (presented in Figure 1.9) that act as initiation sites for the NTs' growth through the hexagonal ordering from the previous NTs. After the removal, another anodisation follows, resulting in NTs with smaller diameters, more uniformity, and a smoother NT wall. This is important because the smoother the surface, the fewer defects are present, and NT layers form without cracks, variations in local thickness, etc. [144], [145]. Zhang et al. [146] performed various repeated anodisations. Afterwards, they suggested additional steps of *(1)* substrate annealing to release residual stress or *(2)* choosing a Ti substrate with larger grains before any anodisation to eliminate defects at the grain boundaries. Both options result in an ordered structure with enhanced photocatalytic activity (the ordered form is usually more active than the disordered tubular structure).

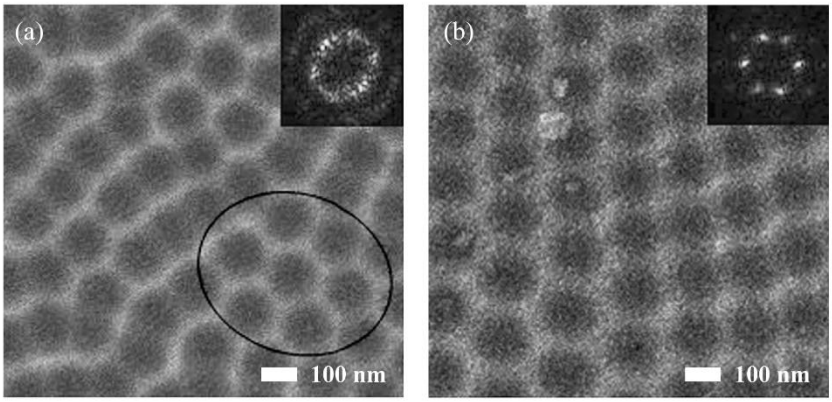

Figure 1.9: SEM images of Ti substrate dimples (a) after the first anodisation and (b) after the second [146]. Reprinted from Electrochemistry Communications, 9 /12, Zhang et al., Highly ordered nanoporous TiO_2 and its photocatalytic properties, 5, Copyright (2007), with permission from Elsevier.

While one direction of research was focused on investigating the effect of different Ti surfaces on the anodisation process and NT morphology, the other studied the substrate microstructure. For example, Macak et al. [147] observed the microstructure related to polished/untreated Ti substrates and their influence on the anodic growth of self-organized TiO_2 NT layers in ethylene glycol electrolytes. The preferred grain orientation for growth-promoting NT growth was when the [0001] axis was perpendicular to the surface of the polished samples. In contrast, no specific orientation was found to significantly promote or retard the NT growth in an unpolished Ti substrate. Furthermore, Davepon et al. [138], [148] suggested that the density of the surface atoms determines the formation of oxide films. The oxide growth is constant on the low packed planes and smaller for tightly packed planes (0001). Moreover, twins can have a much higher activity than grains in some cases. The (0001) plane ($\Phi = 0°$) has an atomic density of 1.8, and is 1.6 times larger than the plane $(2\bar{1}\bar{1}0)$ and $(10\bar{1}0)$ ($\Phi = 90°$). However, if $\varphi_2 = 0°/\ 30°$, the atomic densities are similar. Because (0001) has a higher atomic density, electron (e^-) transfer reactions like oxygen evolution are favoured over reactions like oxide growth and dissolution. Therefore, there is no breaking point for NT growth to occur [137].

The electrochemical reactivity depends on the thermodynamic properties of the substrate and the oxide film, ionic conductivity, and electronic properties. Further research on this topic [149], [150] includes electron-backscatter diffraction (EBSD) studies of starting Ti surface. The NTs start to form randomly and without order on the UT surface. However, the grown oxide showed interdependence on EP titanium to the grain structure and orientation. Leonardi et al. [150] investigated whether the NT length can be correlated with the crystallographic parameters of the Ti substrate. They confirmed the dependency on the atomic density of different planes. The growth rate increased with a decreasing planar atomic density of the substrate, as shown in Figure 1.10a. For further clarification on the topic, the electrochemical behaviour towards oxide formation is presented in Figure 1.10b.

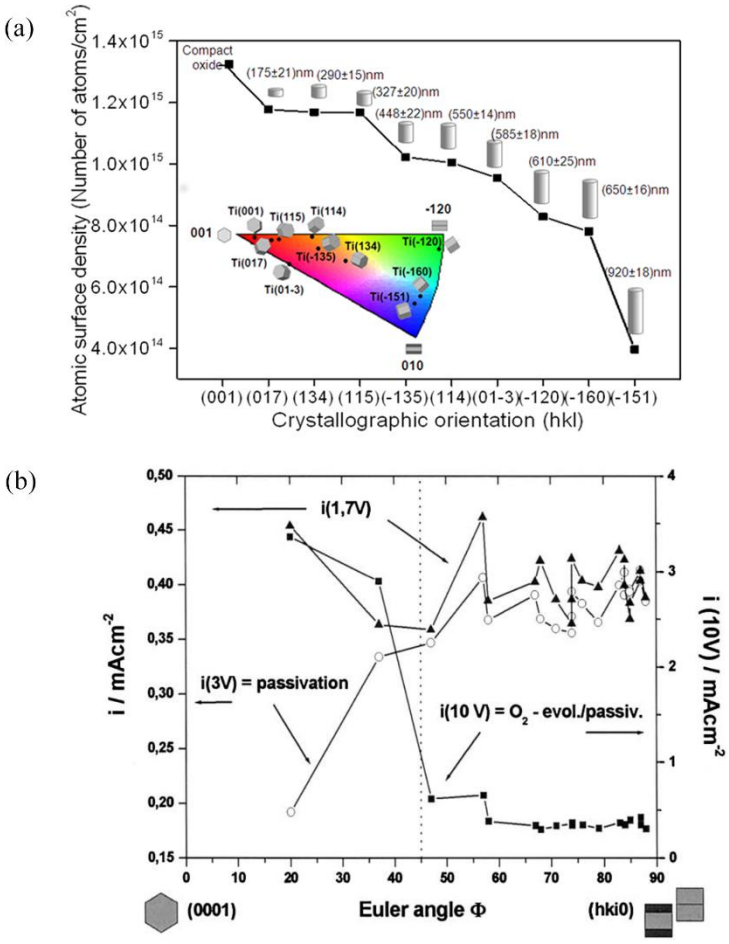

Figure 1.10: (a) Investigation of Ti microstructure and its influence on NT growth and electrochemical behaviour towards oxide formation. The length of grown NTs regarding the crystallographic orientation of Ti substrate [150]. Reprinted with permission from ACS Applied Materials and Interfaces, 7 /3, Leonardi et al., TiO_2 nanotubes: Interdependence of substrate grain orientation and growth rate, 1662–1668, Copyright 2015 American Chemical Society. (b) Electrochemical behaviour of current densities and relation to oxide formation on the specific Euler angle [138]. Reprinted from Electrochimica Acta, 47 /1-2, König and Davepon, Microstructure of polycrystalline Ti and its microelectrochemical properties by means of electron-backscattering diffraction (EBSD), 12, Copyright (2001), with permission from Elsevier.

1.2.2.3 Choice of the Electrolyte

At the beginning of TiO_2 NT research, it was established that ethylene glycol-based electrolytes need to be aged before their first use when preparing NTs that are ordered [108]. The chemical composition of the electrolytes naturally changes with each use since it reacts with the chosen Ti substrate. At the end of each anodisation cycle, the electrolyte is aged for one generation. Nowadays, most studies on electrolytes are based on freshly prepared electrolytes. However, the ageing of electrolytes is an important phenomenon influencing the NT morphology and photo-efficiency [109].

Sopha et al. [151] confirmed that the electrolyte's age significantly influences the NT length and diameter. When fresh electrolyte was used, the NTs with a high aspect ratio were grown and with a low aspect ratio when the electrolyte was aged. The most significant conclusion of their study was that the electrolyte could be used several times, without any

critical issues with regards to lowering the quality of the NTs. In contrast, Raja et al. [152] observed that ordered NT arrays are formed only after the third electrolyte use. They performed a series of anodisations with an electrolyte containing ethylene glycol, 0.2 wt% NH_4F and different amounts, i.e., 0–1.0 wt%, of H_2O. They concluded that a minimum quantity of 0.18 wt% of H_2O is needed to form ordered NT arrays.

Controlling the growth rate through F^- ion diffusion inwards and $[TiF_6]^{2-}$ diffusion outwards suggests that the anodic oxidation of NTs is a highly controllable process where electrolyte composition plays a crucial part [118], [153]. The review by Fu and Mo [73] identified that the electrolytes for NT anodisation were divided into the following generations that evolved over years of research according to their chemical composition:

- *HF-based aqueous electrolytes,*
- *buffered electrolytes,*
- *polar organic electrolytes and*
- *non-fluoride-based electrolytes.*

The first investigations were based on the anodisation of Ti substrates in aqueous electrolytes with HF. Such anodisation usually results in a high density and uniform TiO_2 areas [154], [155] where the NTs' diameter increases with the voltage [156].

Continuing with the new findings, the focus was on buffered electrolytes that were still based on F^- sources, such as sodium fluoride (NaF) and potassium fluoride (KF), as the prime factor for NT growth. During that time, the significance of pH during the anodisation process was determined [111]. By adjusting the pH level with sulfuric acid (H_2SO_4), sodium hydroxide (NaOH), sodium hydrogen sulphate ($NaHSO_4$) and citric acid ($C_6H_8O_7$) to approximately 4.5, Cai et al. [111] were able to grow longer NTs. The most significant conclusion from their work was that the alkaline electrolytes are not appropriate for NT growth, due to the unwanted debris on top of the NTs. In addition, Macak et al. [157] found that NT growth is limited when NTs reach a certain thickness.

Recently, most experimental work has involved using polar organic electrolytes where the primary sources of fluorides are NH_4F, KF, and/or NaF. The significant difference from previous studies is that H_2O is added in small quantities into different polar organic compounds, glycerol [76], [118], DMSO, formamide, N-methyl formamide [77], [158], [159], and ethylene glycol [78], [114] which was also used in our studies. In an aqueous solution, the electrochemical oxidation of ethylene glycol undergoes a reaction to carbon dioxide (CO_2) over glycol-aldehyde, glyoxal, glyoxylic acid, and oxalic acid. However, the number of anodisations is too small for the ethylene glycol to undergo a reaction to CO_2. The most crucial role of ethylene glycol is providing H^+ ions and oxygen in the NT growth [152], [160].

The common findings of extensive research on polar organic electrolytes with added NH_4F and H_2O are, *(1) grown NTs are ordered and homogeneous*, *(2) less H_2O content in the electrolyte results in longer NTs, (3) the cation choice (e.g., H^+, NH_4^+, Na^+) influences the NTs' growth rate and length so that the NTs' length increases with increasing cation size* [161], and *(4) oxide thickness increases when the temperature of the electrolyte increases* [77], [158], [159]. For instance, Lee et al. [162] extensively investigated the formation of TiO_2 NTs in fluoride-containing electrolytes, their crystallinity and chemical composition. They assumed that the HF-based electrolytes are not that successful because the NTs grow up to 500 nm due to the oxide's fast dissolution and slow formation. Another reason for using NH_4F instead of HF is the reduced acidity and the slower dissolution rate [161].

Due to the toxicity of the F^- ions and their loading in the environment [163], the future of research is heading into greener solutions, with the substitution of non-fluoride-based

electrolytes such as hydrochloric acid (HCl), hydrogen peroxide (H_2O_2), perchloric acid ($HClO_4$) solutions and their mixtures [73], [164], [165], [166], [167], [168].

Interestingly, the mechanism of growth in fluoride-free electrolytes is slightly different, as the NTs are grown with so-called rapid-breakdown anodisation [168]. Cheong et al. [168] defined rapid-breakdown anodisation as a process at which the anodisation voltage is high enough to create local breakdown on the Ti surface substrate. Those breakdown points then act as starting sites for NT growth to occur. Although the NTs were not uniform and organized, the photoconversion efficiencies could be easily compared with the efficiency of those in F^- electrolytes. The mechanism of rapid-breakdown anodisation is schematically presented in Figure 1.11. Macak et al. [110] observed that rapid-breakdown anodisation in electrolytes containing chloride leads to the formation of NTs bundles. Although the process is less homogeneous, chloride (Cl^-) ions were a good substitute for the F^- ions. The mechanism of growth is similar to the one when F^- ions are used [164], [165], [166]. The oxide layer is formed after the applied potential, Cl^- ions randomly attack and pits are formed. Cl^- and OH^- rush towards the Ti and OH^- are responsible for oxide and Cl^- for etching, as seen in Eq. (1.11) below. The entire process is not homogeneous. NTs are grown inside and along with those pits [164].

$$TiO_2 + 4H^+ + 6Cl^- \rightarrow TiCl_6^{2-} + 2H_2O \tag{1.11}$$

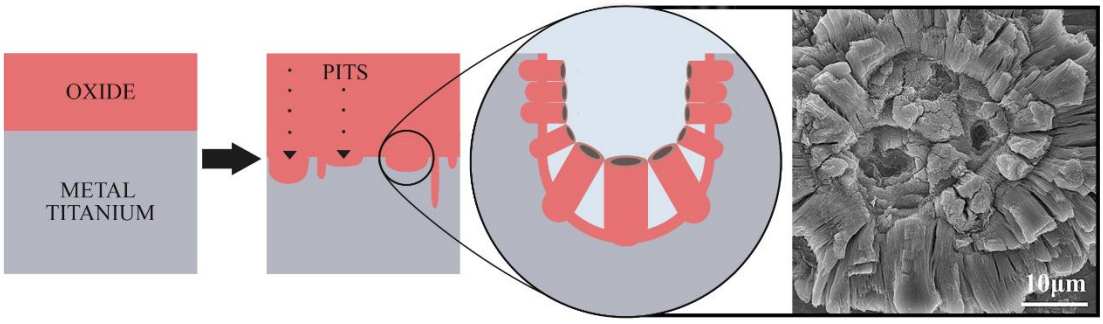

Figure 1.11: Formation of bundles via rapid-breakdown anodisation in chloride-containing electrolytes. Schematic of the process and SEM imaging of NTs bundles [168]. Adapted by permission from Springer, Journal of Porous Materials, Fabrication of titanium dioxide nanotubes in fluoride-free electrolyte via rapid breakdown anodization, Cheong et al., COPYRIGHT (2015).

1.2.3 The Process of Photocatalysis

The sun's energy is among the most promising energy sources since it is abundant, clean, and safe. Additionally, it is sustainable and economically available. The broad light spectrum can be used as an energy source for many photocatalytic reactions. It is also used to bridge the bandgap in TiO_2 catalysts to decompose unwanted organic compounds. However, a significant drawback of TiO_2 is its characteristic of being photoactive only in UV light, which represents a tiny fraction of the whole EM spectrum. However, there are other means (e.g., doping) to decrease the bandgap and make the photocatalyst active in visible light as well.

Photocatalysis emerged as a versatile technology from environmental remediation to energy harvesting in the last decade. In photocatalysis, irradiating a semiconductor that works as a catalyst accelerates the chemical reaction that is thermodynamically favourable, but otherwise kinetically slow. In environmental applications, the degradation of organic

compounds is targeted, and the pollutant is mineralised into CO_2 and H_2O. Meanwhile, the catalyst can be regenerated at the end of the degradation cycle and reused for another cycle.

1.2.3.1 Heterogeneous over Homogeneous Photocatalysis

The main difference between homogeneous and heterogeneous catalysis is in the photocatalyst phase and the reaction medium. Heterogeneous photocatalysis is a complex phenomenon that originates from photochemistry, catalysis, spectroscopy, and surface materials science [7]. It is based on a fundamental principle of oxidation, which derives from the transfer of one or more electrons from an electron donor to the electron acceptor. The transfer from the reductant to an oxidant is necessary for the reaction to occur [169]. Statistically, the most probable pathways for the degradation of organic pollutants are degradation with *(1)* the help of free radicals, *(2)* surface-bound radicals and *(3)* with direct hole (h^+) oxidation [170], [171].

Semiconductor photocatalysis deals with aerobic photooxidation reactions, i.e., with the degradation of pollutants present in the air and H_2O [171]. The process as such is fast (up to femtosecond) [172] and can be direct with a strong adsorption of the pollutant when free radicals are acting as surface-trapped holes (Eq. 1.11 and 1.12) or indirect with weak adsorption and oxidation at the surface or after deposition with the means of free radicals (Eq. 1.13 – 1.15). The process of photocatalysis usually occurs on the photocatalyst surface or in its proximity [173]. A simplified version of the reduction and oxidation power of electron-hole (e^-/h^+) pairs is presented in the following equations:

$$Photocatalyst \rightarrow e^-_{CB} + h^+_{VB} \tag{1.11}$$

$$h^+_{VB} + Pollutants \rightarrow \ Pollutants^{\bullet} \tag{1.12}$$

$$h^+_{VB} + OH_s \rightarrow \ OH_s{}^{\bullet} \tag{1.13}$$

$$OH_s + Pollutant \rightarrow Oxidation\ Products \tag{1.14}$$

$$OH_s{}^{\bullet} \Longrightarrow \ OH_f{}^{\bullet} + Pollutant \rightarrow Oxidation\ Products \tag{1.15}$$

TiO_2 is an n-type, indirect semiconductor and has narrower absorption coefficients than direct semiconductors (e.g., zinc oxide). The energy difference between the conduction band (CB) and the valence band (VB) is known as bandgap. It represents the minimum energy needed for the excitation. In anatase, the bandgap value is 3.2 eV, which means that only light wavelengths (λ) shorter than ~390 nm are absorbed and thus used for excitation. However, TiO_2 catalysts usually have surface states (localized electronic states) within the bandgap (occupied or unoccupied), originating from the solvent or absorbent at the TiO_2 surface [171]. Generated carriers undergo trapping, recombination, and interfacial transfer and slow down the degradation process [172].

The general scheme of the process of photocatalysis is presented in Figure 1.12 as a simplified version of a catalyst, a light-harvesting system in which nanoparticle play the role of sensitizer and the source of photoelectrons and holes [7]. The photocatalysis process starts with the absorption of light photons by the photocatalyst and finishes with chemical transformations of pollutants molecules. It is an inefficient process where up to 90% of the photogenerated e^-/h^+ pairs can recombine and are lost. According to Schneider [44] and

Henderson [88], the basic steps in the process are *(1)* absorption of photons, *(2)* formation of charge carriers, *(3)* e^-/h^+ trapping, *(4)* charge-carrier recombination, *(5)* adsorption of pollutants, and *(6)* oxidative and reductive reactions to yield mineralization products. Mineralization is a complete degradation of the organic material to the end products, CO_2, H_2O, and inorganic ions. Therefore, it is of great concern if the degradation is incomplete since different intermediates and by-products could be more toxic than the pollutant itself. Therefore, knowing the complete degradation pathway and intermediates concentrations is essential [169].

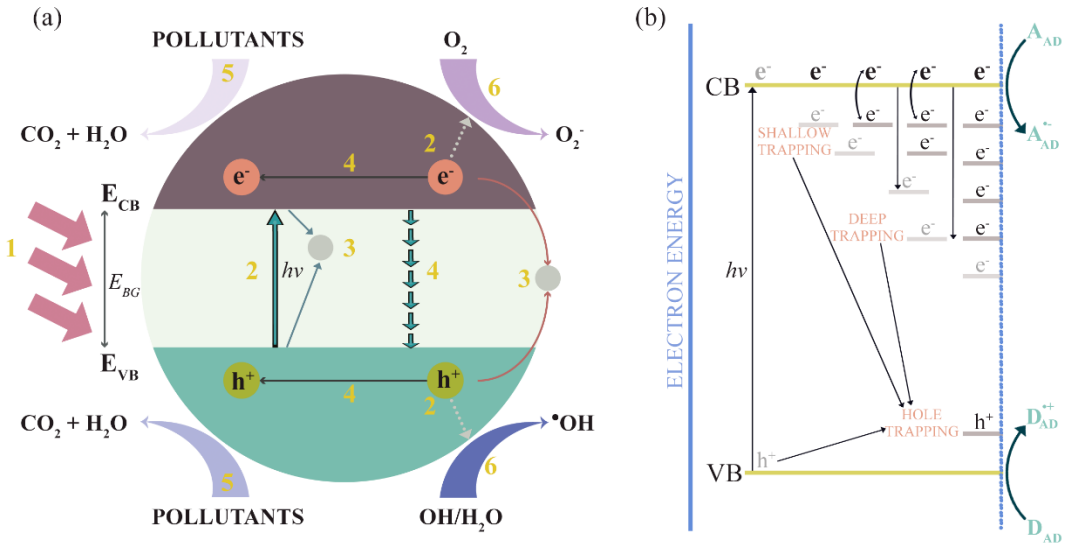

Figure 1.12: (a) Schematic of photocatalysis process in a semiconductor TiO_2. Basic steps of the process include *(1) absorption of photons, (2) formation of charge carriers, (3) e^-/h^+ trapping, (4) charge carrier recombination, (5) adsorption of pollutants, and (6) oxidative and reductive reactions.* (b) Next is presented photoinduced charge carriers' generation, their trapping, recombination and interfacial transfer reactions. Adapted from [44], [88], [170], [171], [170].

The process is activated when the photocatalyst is illuminated with the light of an appropriate energy, equal, or larger than, the material's bandgap (Eq. 1.16) [169]. Due to the nature of a photocatalyst, we must consider the absorption and scattering of the light [7]. The photon absorption is a subsurface rather than bulk process due to the differences in electronic structures between bulk and surface and the significance of the overall photon absorption capacity at the surface [88]. Absorption of light is the direct transfer of photon energy transformed into the energy of electronic excitations (e^-/h^+ pair generation, excitons generation). Quantities used to evaluate incident photons and photocatalytic activity are absorbance, reflectance, and transmittance. Among those, light's intrinsic and extrinsic absorption is the most important. While the intrinsic is caused by light absorption and electronic transitions between states, the extrinsic is caused by defect states. Intrinsic structural point defects are typical for metal-oxide specimens/cation-anion vacancies. Oxygen vacancies are also called F-type centres with one or two trapped electrons [7]. Oxygen vacancies can improve the photocatalysis by trapping e^- or h^+ and inhibiting recombination by changing the local atomic structure, electronic structure, intrinsic chemical and physical properties [174].

Absorption of photons and generation of charge carriers

$$h\nu_1 \geq E_G \tag{1.16}$$

$$TiO_2 + hv \rightarrow TiO_2(e^-_{CB} + h^+_{VB}) \text{ [172]} \tag{1.17}$$

$$e^-_{CB} + O_2 \rightarrow O^-_2 \tag{1.18}$$

$$O^-_2 + H^+ \rightarrow HO^\bullet_2 \tag{1.19}$$

$$h^+ + H_2O \rightarrow OH^\bullet + H^+ \tag{1.20}$$

$$h^+ + O^-_2 \rightarrow 2O^\bullet \tag{1.21}$$

Once the TiO_2 is photoactivated, the bandgap excitation should result in separated charge carriers, as shown in Eq. 1.17. Afterwards, the electrons migrate towards the bulk and holes to the surface [169]. Interestingly, the excitonic energy does not transfer to an adsorbate or supported material; instead, the energy is transferred across the TiO_2. Charge separation can be enhanced/promoted artificially by heterojunction (interfacial) with modifier (usually nanoparticles of Au, Ag, etc.) or by dopant (bulk) [88]. In some cases, the presence of defects in the TiO_2 lattice can cause interference in photon absorption and consequently generate excited defects in the form of bound or self-trapped excitons [169]. The critical factor that Fujishima et al. [9] pointed out is that the reduction (Eq. 1.18 and 1.19) and oxidation (Eq. 1.20 and 1.21) sites are located on the TiO_2 surface. More specifically, oxidizing holes and active oxygen species are formed, which both contribute to the decomposition reactions [9].

The trapping of electrons lowers their energy. After the excitation, the e^- and h^+ can be trapped either on the surface or in the bulk TiO_2 (Eq. 1.22 – 1.24), which leads to a negative outcome only if the trapping leads to recombination. It was shown that electron traps could be localized in the TiO_2 lattice as Ti^{3+} sites [88]. However, Ti^{3+} states, one of the primary intrinsic defects, also allow the transfer of electrons to adsorbed O_2 to form O_2^- and O_2^{2-} species. The superoxide form is less favourable and less energetically stable [175].

Charge carrier trapping

$$e^-_{CB} + > Ti^{IV}OH \rightarrow \{> Ti^{III}OH\}(shallow\ trapping) \text{ [172]} \tag{1.22}$$

$$e^-_{CB} + > Ti^{IV} \rightarrow > Ti^{III}\ (deep\ trapping) \text{ [168]} \tag{1.23}$$

$$h^+_{VB} + > Ti^{IV}OH \rightarrow \{> Ti^{IV}OH\}^+\ (h^+_{VB}) \text{ [168]} \tag{1.24}$$

Immediately after the illumination and e^-/h^+ pair generation, the generated free electrons can reach the surface; the rest are trapped in the bulk (shallow or deep traps) [176]. Bulk and subsurface trapping are favoured over surface trapping [44]. And because

both species of electrons are similar and close to the CB, they can migrate between the surface trap and shallow bulk trap site (500 ps period). Once they go too deep, the mobility is difficult and the recombination is slow [176]. Several authors [88], [177], [178] suggested that excited electrons are preferentially trapped at the surface hydroxyl (OH) groups that are present there due to UV irradiation. In contrast, trapped holes are localized at surface sites but delocalized over the surface region at room temperature. The holes are trapped at the bridging O^{2-} or are transferred to surface-bound OH^- anions which result in $O^{\bullet -}$ or/and $OH^\bullet$ centres [44].

Electron transfer is a process between a surface and an adsorbed species [88]. The most common outcome of the generation of e^-/h^+ pairs is recombination (Eq. 1.25 – 1.27), which can be direct (free electrons) or indirect (defects as recombination centres) [7]. Moreover, it can be radiative (e.g., photoluminescence, PL) or non-radiative (e.g., heat generation). The most common types of e^- transfer are from donor to the CB, h^+ transfer from VB to h^+ acceptor, e^- transfer from the CB to acceptor and h^+ transfer from donor to VB [88].

Charge carrier recombination

$$e^-_{CB} + Ti^{IV}OH \; + \rightarrow Ti^{IV}OH \text{ [168]} \tag{1.25}$$

$$h^+_{VB} + \{> Ti^{III}OH\} + \rightarrow Ti^{IV}OH \text{ [168]} \tag{1.26}$$

$$h^+_{VB} + Ti^{III} \; \rightarrow Ti^{IV} \text{ [168]} \tag{1.27}$$

The site that the pollutant uses for binding on a substrate is critical. The TiO_2 particle, in general, has a specific electronic characteristic and many adsorption sites for the pollutant (or its part) to adsorb onto [170]. The foremost important ROS species that contribute to the photocatalytic activity in TiO_2 NTs are superoxide radicals ($O_2^{\bullet -}$), H_2O_2, singlet oxygen ($^1O_2$) and most importantly, the hydroxy radical ($OH^\bullet$). They are generated from surrounding oxygen molecules, H_2O or OH groups that are attached to the TiO_2 surface [179]. It was already shown in the above equations that the oxidation of H_2O can produce the $OH^\bullet$ at the TiO_2 surface by photogenerated holes. The mechanism is also schematically presented in Figure 1.13. The OH group can be either terminal or bridge-like bound to the TiO_2 surface. Both groups are in equilibrium with the H^+ release at the aqueous interface. However, the terminal OH might be blocked due to the excess of the positive charge of the Ti atom, which prevents the hole from attacking the Ti-O bond. In contrast, the O in the bridge-like OH has a negative charge, which is more favourable for attacking the positive hole. Sometimes, surface-trapped holes can be regarded as adsorbed $OH^\bullet$ [180].

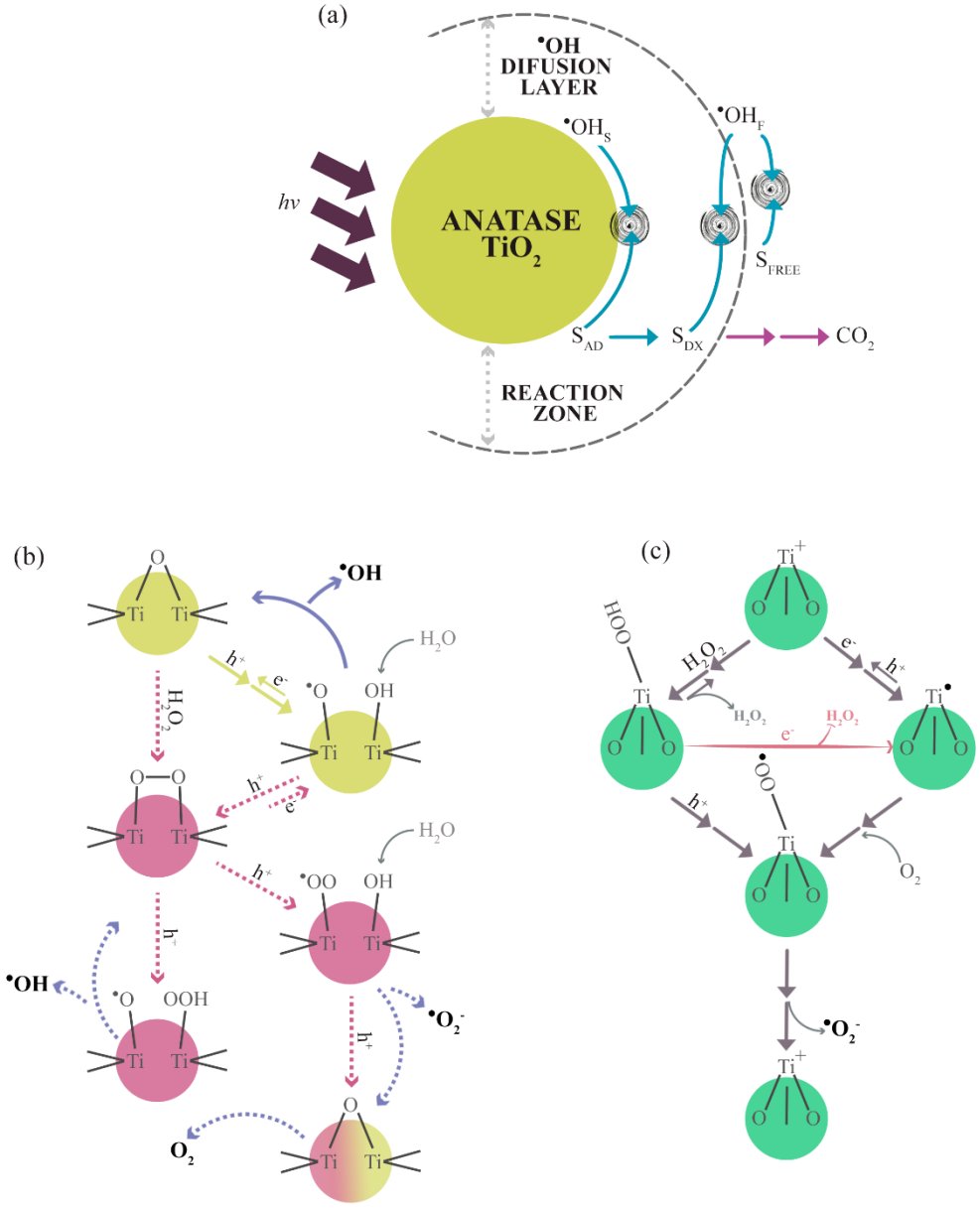

Figure 1.13: (a) Illustration of photocatalysis on anatase by $OH^{\bullet}$, $OH_s^{\bullet}$ meaning reaction on the surface and $OH_f^{\bullet}$ in liquid. Possible reaction pathways at the (b) bridge OH of anatase (solid) or rutile (dotted) TiO_2 and (c) terminal OH site of TiO_2. Adapted from [180].

Extensive structural and chemical characterization of the catalyst material is essential using different analysis techniques since impurities and contaminations in the material affect the process of photocatalysis [181]. Macak et al. [182] compared the photocatalytic properties of TiO_2 nanotubular layers with nanoparticulate P25 Degussa layers. To achieve the maximum decomposition efficiency, it is necessary for the catalysts to have a large catalyst area, appropriate band-edge positions, and rapid charge separation. Interestingly, the photocatalytic nature of the catalyst changes with its size, meaning that smaller particles (nanoparticles) can shift the absorption threshold.

Apart from size, the material's crystallinity is directly correlated with the photocatalytic activity. It was determined that the activity improves after annealing because annealing eliminates charge-trapping and/or recombination sites, as dangling

bonds and distorted lattice structures. However, the adverse effects of crystallinity are a loss of surface OH groups and a reduction in the total surface area [88]. An important fact is that the illuminated total surface area is not equal to the total of photocatalyst active centres. Meaning that the illumination reaches only a fraction of the exposed centres; the others remain inactive due to the specifics in catalyst morphology, which remain hidden for light activation [181]. Liu et al. [183] concluded that the enhanced photocatalytic response could be correlated with the presence of a more significant concentration of lattice defects and a lower degree of crystallinity near the NT surface. Additionally, they showed that annealing in an O_2 atmosphere reduces the local surface defects and enhances the local structure and crystallinity.

1.2.3.2 Kinetics of the Reactions

Any reaction's kinetics follows a series of consecutive steps where the overall reaction rate depends on the slowest, determining step. However, this general rule cannot be applied due to the nature of the generation of e^-/h^+ pairs in photocatalysis. The process is thus presented in parallel series (as is schematically illustrated in Figure 1.14a-b) rather than a series of consecutive steps. This assumption is needed to determine the overall reaction rate [184].

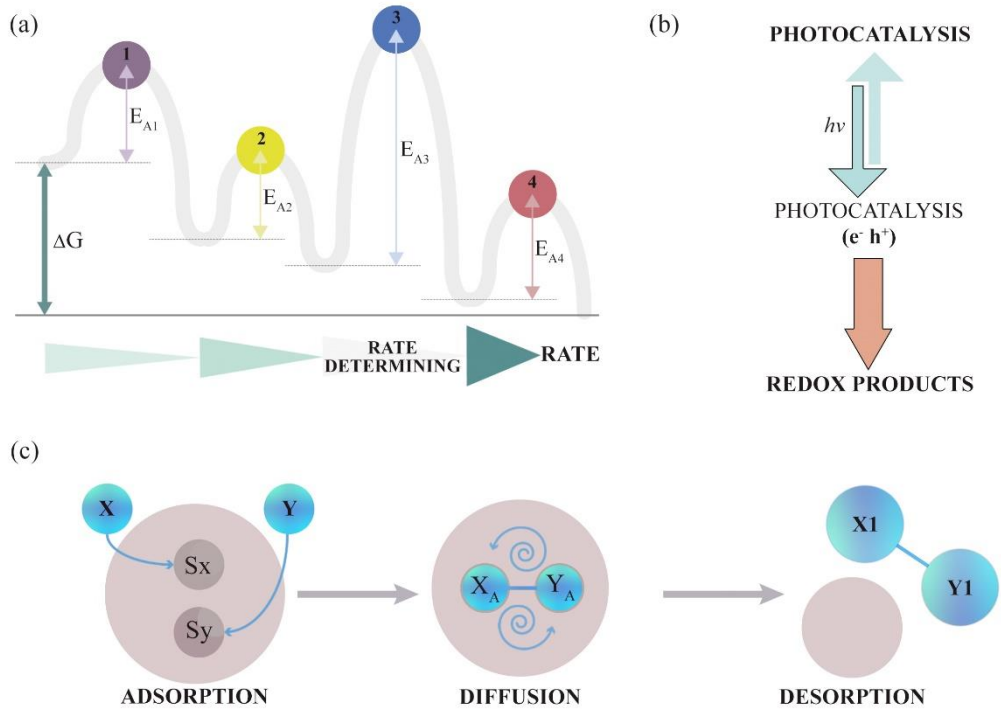

Figure 1.14: (a) Scheme of rate-determining step as a general model of reaction determination step where ΔG is the excitation energy and $E_{x\text{-}y}$ are the activation energies. (b) Reaction of photocatalysis is shown as a series of reactions. Adapted from [184]. (c) Schematic presentation of Langmuir-Hinshelwood reaction kinetics. Adapted from [169].

The reaction rate of photocatalysis can be measured with different analytical methods (e.g., photochemistry, photoluminescence) or can be calculated. The reaction rate is a product of the absorbed photon flux (I_a) and quantum yield (Φ). Although the photon flux depends on the light intensity, the quantum yield is independent and can be used to compare the efficiency of different reactions. For a more straightforward calculation, the

absorbed photon flux is replaced with the incident flux (I_0) because the photons arriving at the catalyst are more easily measured. For that reason, photonic efficiency is not used for a comparison because the light intensity, scattering and reflection have too large an impact on the measurements [171].

The Langmuir–Hinshelwood (LH) model is one of the main mechanisms of the surface chemical reaction and is presented in Figure 1.14c [169]. The mechanism assumes "*that the interaction takes place between pre-adsorbed reagent molecules and surface species* (either pre-adsorbed molecules or surface-active centres)" [7]. The LH-mechanism promotes surface chemical processes, where adsorbed molecules connect directly with the surface charge carriers and excitons. The exchange between the surface and the bulk happens by diffusion or drift. Adopted from (Eq. 1.28) Choo et al. [185], the LH-mechanism equation is:

$$r = \frac{dC}{dt} = - \frac{k_0 KC}{1 + KC} \tag{1.28}$$

where C is the reactant concentration, t is the reaction time, k_0 is the reaction-rate constant, and K is the adsorption coefficient of the reactant on the catalysts. The last two parameters can be estimated using lineralization and determination of the linear regression coefficient. Suppose the KC is smaller than 1 (when the adsorption coefficient and reactant concentration are small). In that case, the LH equation can be simplified to:

$$ln \frac{C_t}{C_0} = -k_1 t \tag{1.29}$$

where C_t and C_0 are the reactant concentrations at time t and 0 [185]. The reaction undergoes a pseudo-first-order reaction, which is typical for TiO_2 photocatalytic reactions in wastewater treatment [186].

1.3 Motivation and Thesis Objectives

TiO_2 NTs represent an attractive solution for environmental pollution. It is a widely used material due to its wide bandgap; it is not toxic, has a low price, is photostable and chemically inert [187]. The critical element for the degradation of pollutants is a photoactive catalyst with a high chemical reactivity, photoactive surface area, stability, and the ability to regenerate and produce reactive oxygen species, which later decompose organic compounds into H_2O and CO_2.

Although there are many synthesis routes to obtain TiO_2 NTs, the process of anodic oxidation is one of the most widely used methods. It yields NTs that are rigidly attached to the Ti substrate with a length in the micrometre range [188]. Anodically grown NTs show good mechanical strength [50], enable direct charge transfer and have a short electron diffusion path [109], [110]. In contrast to a TiO_2 nanoparticulate catalyst, the NTs are firmly attached to the substrate and not released into the environment during the photocatalytic reaction.

Parameters like electrolyte composition (e.g., F^- concentration, pH), the addition of H_2O, temperature, anodisation conditions (e.g., time, voltage, temperature) and choice of Ti substrate (e.g., shape, size, pre-treatment) affect the formation and properties of TiO_2 NT arrays [136], [147], [189]. Among these, the choice of the starting material is crucial because *(1)* surface topology [115], [190] influences the top surface of TiO_2 NTs [126], [136], and *(2)* an amorphous and chemically stable oxide layer with a thickness of approximately 10 nm protects the substrate from corrosion [191], *(3)* impurities present in the commercially available Ti substrate act as an additional layer for overcoming corrosion [116]. However, F^- ions in the electrolyte can overcome the protective barrier and help format a nanotubular layer [113].

Despite these results and extended studies on the topic, it is still unclear how the fundamental processes work and what happens at the atomic level for anodic oxidation, catalysis and photocatalysis. A systematic approach to the main categories (substrate, anodisation, photocatalysis) is needed to understand the complete system. At the moment, different research groups around the world focus on one aspect of the process. However, rarely are those aspects integrated with each other.

This thesis aims to overcome one aspect of the barrier, with a detailed investigation into the importance of the choice of the substrate. Especially if it is not the ideal laboratory sample but a commercially available Ti foil with different structural and chemical impurities. The focus of the work is on determining the ideal surface on which morphologically active photoactive NTs will grow, emphasizing the influence of the substrate surface. Parameters like roughness, chemical composition, grain size, orientation, twinning, foil thickness, electrolyte age and photocatalytic activity could answer the question of how to control the active area of anodic NTs.

The thesis is a **three-fold study** of the main factors, i.e., Ti foil, anodisation, and NTs, with the central aspect of the influence of starting material and electrolyte age on NTs growth and the photocatalytic activity.

One part of our research encompassed an investigation of Ti foil from two different suppliers that were used as UT or EP. A series of analyses were performed before and after anodisation to know the properties of the foil and the characteristics of the NTs. After the final determination of photocatalytic activity, we were able to choose the best photocatalytic activity sample and understand the path that leads towards it. In the next step, we purchased a series of foils of different thicknesses from the selected supplier. The foils were produced with cold rolling from the thickest foil, which hugely influenced their

crystallographic orientation and the size of grains. In this part of the thesis, our goal was to determine how the Ti foil thickness affects the NT growth and properties. Moreover, we aimed to finish the research with a flexible TiO_2 catalyst that would be photostable and have the possibility for $OH^{\bullet}$ production. In the last, and third, part of the study, we observed the effect of electrolyte age and its change of chemical composition on NT growth and photocatalytic activity.

To conclude, the thesis is based on a systematic study that integrates both basic and applied science and could be used on an industrial scale, keeping in mind that the focus on material preparation is crucial for understanding the behaviour and tuning to gain properties that make the material useful in photocatalytic applications. The main **objectives** are:

1. To investigate the relevant morphological and structural parameters of the starting Ti metal foil.

2. To study the effect of Ti foil thickness on TiO_2 NTs growth and the rigidity of their attachment.

3. To observe the influence of electrolyte ageing on TiO_2 NTs growth and photocatalytic activity.

Meanwhile, the central work **hypothesis** arises from a knowledge of fine-tuning and influencing the NT growth and final photocatalytic activity. We expect to show the difference in NT growth and photocatalytic activity by changing the Ti foil and the electrolyte's age parameters. Furthermore, we expect to show how to improve the intrinsic properties of the anode by modifying the surface of the Ti foil. The particular focus was set to the following points:

1. Substrate pre-treatment influences the TiO_2 NT growth and their photocatalytic activity.

2. Substrate surface roughness significantly impacts the final surface area of the photocatalytically active TiO_2 NT layers.

3. High NTs density, shorter NTs, and fewer cracks result in better adhesion of the TiO_2 NT layer to the Ti substrate.

4. Higher grain-boundary surface density represents more nucleation sites for the NT growth.

5. Higher surface roughness of the TiO_2 NTs equals larger active surface area and thus resulting in higher photocatalytic activity in the degradation test.

6. Repetitive anodisation changes the electrolyte's chemical composition, thus influencing the NT growth and final photocatalytic activity.

7. Anodisation of Ti foil with fresh electrolytes results in NTs with a uniform morphology.

1.4 Materials and Methods

1.4.1 Materials

The investigated material in this thesis is commercially available titanium foil purchased from two different suppliers. Titanium foil from the Chinese Baoji Lyne Metals Co., Ltd is in the experimental part denoted as *Supplier 1*. Meanwhile, the titanium foil from the English provider, Advent Research Materials Ltd, is denoted as *Supplier 2*. The chemical purity of the titanium foil from Supplier 1 is 99.9 %, and from Supplier 2, 99.7 %. As stated in Chapters 2-4, the foils were used in different modifications as a substrate for TiO_2 NTs growth. Characterisation and evaluation of the physio-chemical properties of the researched samples are summarised in the following subchapters.

1.4.2 Methods

Procedures for sample preparation and the methods used for their characterisation are presented in detail in Chapters 2-4. The methods used can be subdivided into the following subsections.

1.4.2.1 Ti foil sample preparation and microstructure characterization

Ti foils were prepared with a standard electropolishing procedure on LectroPol-5 (Struers, USA). In the next step, they were observed under the light stereomicroscope, Discovery V8 (Carl Zeiss Microscopy, Germany). Various electropolishing conditions (temperature, voltage, and time) were applied to reduce the surface roughness and achieve a mirror-like surface finish. Ti foils without visible scratches and damaged surfaces were selected for further analysis in the FSEM 7600 equipped with EDXS (JEOL, Japan).

To assess the texture, crystallographic orientation, grain size distribution, and misorientation angle of the Ti foils, EBSD (Hikari Super, EDAX) was used. The material's crystallographic structure and identification of the crystalline phases were determined using an X-ray diffractometer (XRD) with Cu-K α 1 radiation (X'Pert PRO, Malvern Panalytical Ltd., UK and D5000 Bruker AXS, US). The grain size distribution was additionally determined under light microscope, Axio Imager Z1-m (Carl Zeiss Microscopy, Germany), after the polished samples were etched with concentrated HCl and the grain boundaries were exposed. Further statistical analyses were performed with the ImageJ programme (1.53e, NIH).

1.4.2.2 Surface roughness measurements

The surface roughness of the polished and untreated titanium foils was mapped and determined with a stylus profiler with a 2-µm tip on the DektakXT apparatus (Bruker, USA). Parameters such as the average arithmetical roughness, root-mean-square roughness and peak-to-valley roughness were calculated.

1.4.2.3 Determination of Ti foil chemical composition

The chemical composition of the titanium foils was measured with inductively coupled plasma optical emission spectrometry (ICP-OES, Varian 715-ES) in a semiquantitative mode. Before the measurement, the foils were digested on a hot plate using concentrated HCl and slowly heated in a covered beaker for 5 h, three times over several days. Next, the commercial Ti foil's oxide layer and chemical impurities were analysed with the X-ray photoelectron spectroscopy (XPS, PHI–TFA, USA) equipped with an Al monochromatic

X-ray source. Additionally, XPS depth profile analyses were performed to follow depth distribution of elements in thin surface layer of thickness 10 nm. A removal of the material during XPS depth profiling was performed by ion sputtering with Ar^+ ions with 4-keV energy. The sputtering rate was about 1.5 nm/min. XPS method can provide data on chemical composition in at.%. The method is not sensitive for hydrogen detection.

1.4.2.4 Monitoring of anodic oxidation

Electrochemical oxidation of the Ti foil was performed for 3 h at 60 V, powered by a direct current (DC) power supply (Toellner Electronic Instrumente, Germany). The electrical current was measured with a data acquisition/logger (Agilent, USA).

The conductivity and pH of the electrolyte were measured with the conductivity meter (ProLine Plus M330) and pH meter (Mettler Toledo). Additionally, we determined the electrolyte chemical composition with potentiometric measurements of F^- (Metrohm model 906 Titrando and Thermo Orion, model 9609), ammonia (Iskra pH−meter MA 5740 and HACH DR/2010 spectrophotometer) and the H_2O content (Karl Fischer titration using a double platinum electrode by ISKRA HEP 0701).

1.4.2.5 TiO_2 NTs characterization

The grown TiO_2 NTs were first examined in FSEM-EDXS. The researched parameters were the TiO_2 NTs morphology, NTs' length, the porosity of the film, and the area of cracks in the NTs' thin film. Acquired imaging data were further analysed with the ImageJ programme. A three-dimensional (3D) interference optical profiler, ZeGage™ Pro HR (Zygo Corporation, USA), was used to evaluate the average surface roughness.

A cross-section of TiO_2 NTs on the substrate was also observed in the FSEM-EDXS. The samples were first embedded in resin. Grinding and polishing were performed on the metallographic specimen-preparation device LaboPol (Struers, USA).

The chemical composition of the TiO_2 NTs was determined with XPS measurements as described above for Ti foil. Additionally, time-of-flight secondary ion mass spectrometry (ToF-SIMS) was applied to analyses surface-composition and to perform depth-profile analyses for thicker layers, like 250 nm thick layer. Positive and negative secondary ions emitted from surface were measured with a SIMS spectrometer (model TOF-SIMS 5, ION TOF, Germany) using a Bi^+ ion beam of 30 keV for the secondary ion excitation and the Cs^+ ion beam at 2 keV for ion sputtering during the depth-profile analyses. Sputtering rate was about 0.2 nm/s. Unfortunately, the ToF-SIMS method is not quantitative, so only the relative comparison of the ion signals can be applied among the samples.

XRD measurements were performed on a diffractometer with Cu-Kα1 radiation between 2° and 100° 2θ (X'Celerator detector), using a mask diameter of 5 and 10 mm over the sample.

The adhesion of rigidly attached TiO_2 NTs was tested with a Scotch-tape test, following the ASTM D3359 standard. The area of NTs loss around the cut in the test was determined under an optical microscope, and a final statistical analysis was made with the ImageJ programme.

1.4.2.6 Photocatalytic activity

The photocatalytic activity was determined using electron paramagnetic resonance (EPR) for the concentration measurements of the $OH^\bullet$ radicals and identification of e^-/h^+ recombination by photoluminescence. The formed $OH^\bullet$ radicals' were measured under the illumination of TiO_2 NTs with 365-nm light. A drop of 0.5-M DEPMPO spin-trapper (5-(Diethoxyphosphoryl)-5-methyl-1-pyrroline-N-oxide) and 30 % ethanol was illuminated.

After 3 min, the solution was drawn into a 1-mm-wide capillary and inserted into a 5-mm-wide tube for measurement. An EPR spectrophotometer (ELEXSYS, Bruker) was used at room temperature, 1-Gauss modulation amplitude, 100-kHz modulation frequency, 1.28-ms time constant, 0.20-mW microwave power, and 100-G sweep width with the centre field positioned at 3320 G. In the meantime, photoluminescence measurements were performed with a photoluminescence spectrofluorometer (Quanta-Master 8000, Horiba-PTI) with a low-noise photomultiplier (Hamamatsu R2658). The analysis of e^-/h^+-pair recombination, oxygen vacancies and defects on the TiO_2 surface was identified for samples excited at 370 nm (with emission spectra between 400 and 750 nm).

For the photocatalytic activity measurements, the degradation of the organic pollutant was measured. Caffeine was used as a model compound, and its concentration was measured periodically over several hours using a UV-Vis-IR Spectrophotometer (Lambda 950, PerkinElmer Inc., USA). Samples were illuminated with different UV-light spectra (280 to 410 nm). Additionally, photocatalytic efficiency by measuring the caffeine degradation was also performed using high-performance liquid chromatography (HPLC, Agilent, HP1100).

1.5 Thesis Outline

The thesis was set as a three-fold study of *(1)* the starting Ti foil properties, *(2)* the anodic oxidation process, and *(3)* electrolyte age with the central aspect to determine the influence of starting Ti and electrolyte age on NTs' growth and their subsequent photocatalytic activity. Although all three topics are correlated, they are addressed in three published articles. The 1st article, with the title "*The Influence of a Surface Treatment of Metallic Titanium on the Photocatalytic Properties of TiO_2 NTs Grown by Anodic Oxidation*", is dedicated to the structural and chemical characterization of the starting Ti foil. From it, the key results emerged that enabled a more complex understanding of the anodisation process of flexible thin foils. These results were published in the 2nd article, entitled "*Toward a Flexible and Efficient TiO_2 Photocatalyst Immobilized on a Titanium Foil*". The importance of the thickness of the starting substrate and its influence on the photocatalytic activity is presented in detail. The thesis is rounded off with the study of electrolyte ageing in the 3rd manuscript with the title "*Influence of Anodization-Electrolyte Aging on the Photocatalytic Activity of TiO_2 Nanotube Arrays*", where changes in the electrolyte's composition and the influence on the NT growth are studied.

Chapter 2

The Influence of a Surface Treatment of Metallic Titanium on the Photocatalytic Properties of TiO_2 Nanotubes Grown by Anodic Oxidation

This chapter addresses the thesis **objective** to *investigate the relevant morphological and structural parameters of the starting Ti metal foil* with the following working **hypotheses**:

1. Substrate pre-treatment influences the TiO_2 NTs' growth and their photocatalytic activity.
2. Substrate surface roughness significantly impacts the final surface area of the photocatalytically active TiO_2 NT layers.

As such, the chapter presents a **paper** entitled "*The influence of a surface treatment of metallic titanium on the photocatalytic properties of TiO_2 NTs grown by anodic oxidation*", written by **Živa Marinko**, Luka Suhadolnik, Zoran Samardžija, Janez Kovač and Miran Čeh. The article appeared in the Catalysts journal, Vol. 10, No. 803 in 2020. The results from the work were also presented at several conferences. The list is given in the Bibliography section.

After the publication of the article, some new results that were not included in the article were obtained that additionally clarify the surface effect on the influence of Ti substrate surface on NT growth. Characterization results were used to define the best TiO_2 sample in terms of photocatalytic activity. Titanium foil from the chosen supplier was also used in the experimental work described in Chapters 3 and 4.

This chapter describes the experimental procedures to investigate the differences in the surface structure and chemical composition between two Ti foils provided by two different suppliers after the surface treatment. Different electropolishing conditions with varying temperatures (15, 20, 25 °C), time (5, 10, 20, 30, 60 s) and voltage (10, 30, 35, 40, 45 V) were determined and used for titanium foils from both suppliers. An additional surface treatment of Ti foils also included Ar^+ ion etching, thermal annealing and plasma treatment. Since these techniques have not significantly influenced the NTs' growth, this

chapter does not include these results. Among the assortment of prepared Ti substrates, we chose an untreated (UT) sample and a few electropolished (EP) samples with a minimum of scratches and other surface markings for further anodisation experiments. Preliminary testing of the EP samples was then reduced to just one sample per supplier. On selected specimens, surface characterization was performed using FSEM with backscatter imaging to determine the surface topology, followed by surface-roughness measurements with the stylus profilometry. Then, the surface of the Ti foils was etched with HCl to reveal the grains in the foil. Using a light microscope, a statistical analysis of the microstructures was performed to measure the grain size and size distribution for each supplier. In parallel, XRD and EBSD analyses were also performed. Since the EDS did not show any differences in the chemical composition between the samples, a more sensitive depth-profiling XPS method was used together with the ToF-SIMS analysis.

After the complete characterisation of the Ti foil and the designated differences, the Ti foils were anodised simultaneously under identical experimental conditions and electrolyte composition (ethylene glycol, H_2O and NH_4F) for 3 h at 60 V. The current was monitored from the start to the end of the anodisation. The samples were further annealed for 1 h at 450 °C to transform them from amorphous to the crystalline anatase phase. The formation of anatase was confirmed with the XRD patterns. TiO_2 NTs layers were then analysed in the SEM to observe the NT morphology, porosity, and the cracking area. The sample slabs were analysed for cross-section viewing of the NTs' length. A cross-section view was also used when the samples were side cut, polished and seen under the SEM. The chemical composition of the NTs was determined with XPS and ToF-SIMS.

The caffeine-degradation test showed that all anodised and annealed samples have the ability to degrade pollutants photocatalytically. Caffeine was chosen as a model compound because it is abundant as a pollutant in wastewaters. It is easy to handle and can be detected in UV-Vis spectrophotometry. The degradation of caffeine was monitored over several hours. The samples were periodically collected from the caffeine solution to determine the caffeine concentration.

After the manuscript was published, additional experiments were made on the previously investigated samples. The photocatalytic activity of each sample was tested under various illumination wavelengths, i.e., 365, 395, 405 nm, and under a wide range of UV-Vis wavelengths in the sterilizer.

Next, we performed a detailed chemical analysis of the Ti foil and TiO_2 NTs for both suppliers with the ToF-SIMS method. We were able to specify the thickness of the amorphous oxide, the purity of the Ti foil, and finally, the F^- distribution in the top few nm layers of the TiO_2 oxide. Finally, the texture and grain size distribution were investigated with an EBSD analysis.

Regarding my contribution: I performed the EP of the Ti foils and their characterization to choose the best samples. Further, my work included the chemical and microstructure characterization of the Ti foils (topography – surface roughness with stylus profiler, grain size distribution, optical microscopy). Next, I performed the anodisation of all the chosen samples and their annealing. Regarding the NTs' characterization, the work included SEM and light microscopy (OM) and a determination of the NTs' lengths, porosity, the area of cracks, and surface roughness of the TiO_2 NTs. Finally, I measured the photocatalytic activity of the anodised samples using caffeine as a model compound. I wrote the first draft of the manuscript and then completed it with my co-authors.

catalysts

MDPI

Article

The Influence of a Surface Treatment of Metallic Titanium on the Photocatalytic Properties of TiO_2 Nanotubes Grown by Anodic Oxidation

Živa Marinko [1,2,*], Luka Suhadolnik [1], Zoran Samardžija [1], Janez Kovač [3] and Miran Čeh [1]

[1] Department for Nanostructured Materials, Jožef Stefan Institute, Jamova 39, 1000 Ljubljana, Slovenia; luka.suhadolnik@ijs.si (L.S.); zoran.samardzija@ijs.si (Z.S.); miran.ceh@ijs.si (M.Č.)
[2] Jožef Stefan International Postgraduate School, Jamova 39, 1000 Ljubljana, Slovenia
[3] Department of Surface Engineering, Jožef Stefan Institute, Jamova 39, 1000 Ljubljana, Slovenia; janez.kovac@ijs.si
* Correspondence: ziva.marinko@ijs.si; Tel.: +386-1-4773-931

Received: 16 June 2020; Accepted: 16 July 2020; Published: 19 July 2020

Abstract: Titanium dioxide (TiO_2) nanotubes obtained by the anodic oxidation of titanium metal foils can be used for the photocatalytic degradation of organic pollutants. The aim of our study was to determine the influence of the titanium foil's surface treatment on the final morphology of the TiO_2 nanotubes and their photocatalytic activity. In our experiments, we used two different titanium foils that were electropolished or untreated prior to the anodic oxidation. The morphologies of the starting titanium foils and the resulting TiO_2 nanotube layers were investigated and the photocatalytic activities measured by the decomposition of caffeine under UV irradiation. Our results showed that electropolishing of the starting foils produced a more uniform and smoother TiO_2 nanotubes surface. In contrast, the TiO_2 nanotube surfaces from untreated titanium foils mimic the initial surface roughness of the titanium foil. A comparison of the photocatalytic properties of the TiO_2 nanotube layers obtained from the untreated and electropolished titanium foils showed that electropolishing does not necessarily improve the photocatalytic properties of the resulting TiO_2 nanotube layer. It was found that the determining factors influencing the photocatalytic activity are the chemical impurities (Ti-nitride) on the surface of the titanium foils and the surface roughness of the TiO_2 nanotube layer. The highest photocatalytic activity was achieved with the anodized untreated foil with the minimal presence of Ti-nitride and a relatively high roughness of the TiO_2 nanotubes.

Keywords: electropolishing; anodic oxidation; TiO_2 nanotubes; photocatalysis; metal titanium foil

1. Introduction

TiO_2 is a versatile, chemically inert, and low-cost photocatalyst that can decompose various organic pollutants with reactive oxygen species. The photocatalytic decomposition of the organic compounds starts with the absorption of photons with a suitable energy. It takes place in the presence of oxygen and consists of different chemical reactions, such as bond breakage and electron transfer/substitution. As a consequence, reactive oxygen species (ROS) are created [1,2]. The photocatalysis process takes place primarily at structural defect sites [3] or on the facets of the TiO_2 crystal with the highest surface energies [4–6].

TiO_2 anatase can be synthesized with a variety of approaches [7–11]. However, the anodic oxidation process is the most straightforward method for synthesizing TiO_2 nanotube arrays [12] due to the high degree of control over the nanotubes' morphology [7]. The driving force for the self-organized growth mechanism of the electrochemical oxidation process is the tendency to balance the formation of the oxide film and its dissolution in order to achieve the maximum nanotube density

on the titanium substrate [13]. The nanotubes formed during the anodization process are most often amorphous. In order to transform them into polycrystalline nanotubes, subsequent heat treatment at elevated temperatures is needed [14]. The obtained polycrystalline TiO_2 nanotubes are inherently intergrown into the metal substrate and thus represent a TiO_2 photocatalyst that can be directly used as a photocatalyst in immobilized photocatalytic or photoelectrocatalytic reactors [12,15]. Furthermore, an ingrown TiO_2 nanotube layer can provide a higher mechanical strength than a nanoparticulate film [16].

The formation and morphology of TiO_2 nanotubes are to some extent controlled by the titanium's surface topology, in particular by the surface roughness and the dislocation density [17,18]. These initial titanium surface artefacts influence the top surfaces of the TiO_2 nanotubes [19,20]. Additionally, a few-nm-thick oxide film forms spontaneously when the titanium foil is exposed to the air. The film is approximately 10 nm thick, amorphous, compact, chemically stable, and firmly adhered to the titanium foil [21]. It acts as a barrier and protects the titanium surface from corrosion.

The nanotubes' uniformity can be improved by (i) repeated anodization of the same substrate, after removing the anodized layer grown in the previous anodization [19] or (ii) with the polishing of the titanium surface, with mechanical, chemical or electropolishing techniques [17]. The process of electropolishing consists of three synergistic reactions: anodic dissolution, oxygen evolution, and the formation of a passive oxide film [22]. After applying a voltage between the titanium anode and the cathode, Ti^{4+} cations diffuse into the electrolyte. Active dissolution results in direct electropolishing of the titanium surface. Lee et al. [23] reported that the formation of electropolishing residues on the titanium surface have the ability to act as additional nucleation sites and at the same time lead to poor arrangements of the nanotubes due to the simultaneous activation.

In the present work, we studied the influence of the preparation of the titanium metal surface on the growth of TiO_2 nanotubes and their photocatalytic properties. Anodic oxidation of untreated and electropolished titanium foils from two different suppliers was performed to prepare photocatalytically active TiO_2 layers. The paper presents novel insights into the 'synthesis–properties–photocatalytic performance' relationships and reveals the main reason for the improvement or deterioration of TiO_2 photocatalytic properties with the titanium electropolishing procedure.

2. Results and Discussion

2.1. Characterization of the Titanium Metal Foils

Characterization of the titanium metal foils started with the grain size distribution analysis which influences the growth of TiO_2 nanotubes. In order to determine the grain size distribution of the starting titanium foils the electropolished foils were first chemically etched using hydrochloric acid and examined with optical microscope (see Supplementary Figure S1). Quantitative analysis of the grain size area revealed that the largest number of grains for the foil of Supplier 1 ranged between 10 and 30 μm^2, while for the foil of Supplier 2, the average grain area was around 100 μm^2. Smaller grains have a greater surface-to-volume ratio, which means more grain boundaries. Therefore, the titanium surface with a smaller grain size has a higher number of nucleation sites for the nanotube growth to occur [24]. The grain size analysis of untreated substrates could not be reliably conducted due to large surface roughness and present surface preferential deformations from cold rolling production. This is why the samples were electropolished and etched in order to reveal grain boundaries between different grains.

Observation of the titanium metal surfaces under field-emission gun scanning electron microscope (FSEM) revealed very different rolling patterns between the two suppliers: Supplier 1 showed straight and parallel lines, while the titanium foil of Supplier 2 exhibited random irregularities over the surface. In two studies, Zou and Wang [25,26] reported that the internal stress of a titanium foil influences the activity of local nucleation sites and therefore the nanotube growth. Baek et al. [27] additionally reported that deep valleys cause inhomogeneous deformation of the surface. These later lead to

various irregularities on top of nanotube oxide layer. The roughness factors, Ra (average arithmetical roughness), Rq (root-mean-square roughness), and Rt (peak-to-valley roughness), were measured on electropolished (190-µm-thick) and untreated (200-µm-thick) foils from both suppliers (see results in Supplementary Figure S2). Line scanning over an evaluation length of 4 mm of the sample was performed four times to determine the average value. Both untreated samples (Figure 1a,c) have a rough surface with cracks, pores, and scratches. Measurements showed that the average roughness is 0.161±0.02 µm for the sample of Supplier 1 and 0.168±0.02 µm for the sample of Supplier 2. Figure 1b,d shows the reduced surface roughnesses after the electropolishing, where the grain boundaries are also visible. The average arithmetical roughness decreased to 0.116±0.01 µm for the sample of Supplier 1 and to 0.123±0.02 µm for the sample of Supplier 2. It is interesting that the factor Rt is more prominent for the untreated sample from Supplier 2, which suggests that the specific analyzed surface area is larger than the untreated sample of Supplier 1. A closer look at the surface roughness of all the samples reveals that the specific surface area of the untreated titanium foils was higher than for the electropolished foils [24]. We also observed that electropolishing exposes the grain boundaries and causes the formation of pitting spots. They both influence the number of nucleation sites for nanotube formation, which affect the available active surface area for the photocatalytic reactions.

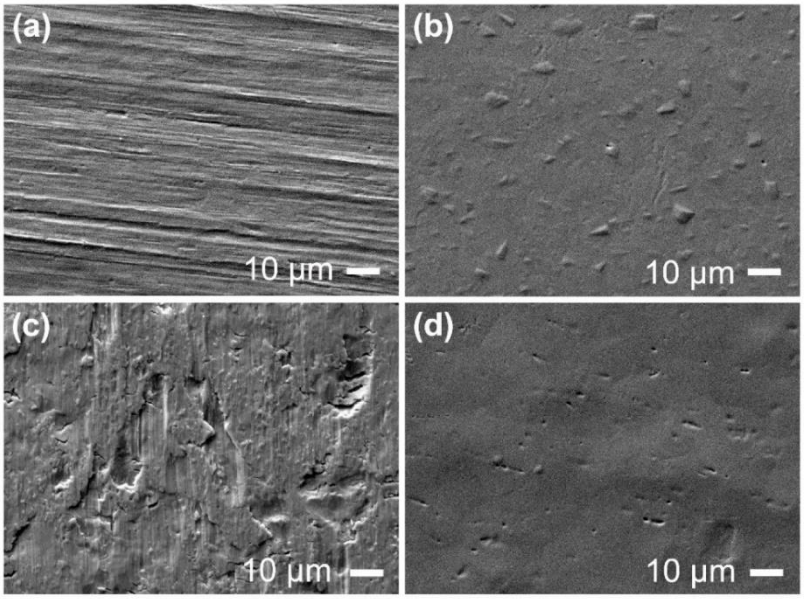

Figure 1. SEM images of metal titanium foil before and after electropolishing. (**a**) Untreated; (**b**) electropolished titanium foil from Supplier 1; (**c**) untreated and (**d**) electropolished titanium foil from Supplier 2.

Additionally, profilometry 3D mapping of a sample area of 1 × 1 mm^2 was recorded. Statistical analyses with a Gaussian regression filter with standard values for both short (λs) and long (λc) cutoffs were calculated according to ISO 4287. Figure 2a,d presents the selective topographic results from the 3D surface roughness mapping. Although the difference in the z-axis was much smaller on the electropolished samples, the surface defects and shaping from the factory rolling remained visible. We also noticed some residues and undulations in the foil surface after the electropolishing, observed also by Jarosc et al. [28]. While the untreated titanium foil of Supplier 1 had an even distribution of peaks and valleys, different phenomena were observed on the untreated titanium foil from Supplier 2 (marked area in Figure 2c). Pits up to 5 µm deep surrounded with a series of peaks with a height of 4 µm were found on the foil. In detail, they are presented in Figure 2e (top and cross-section view).

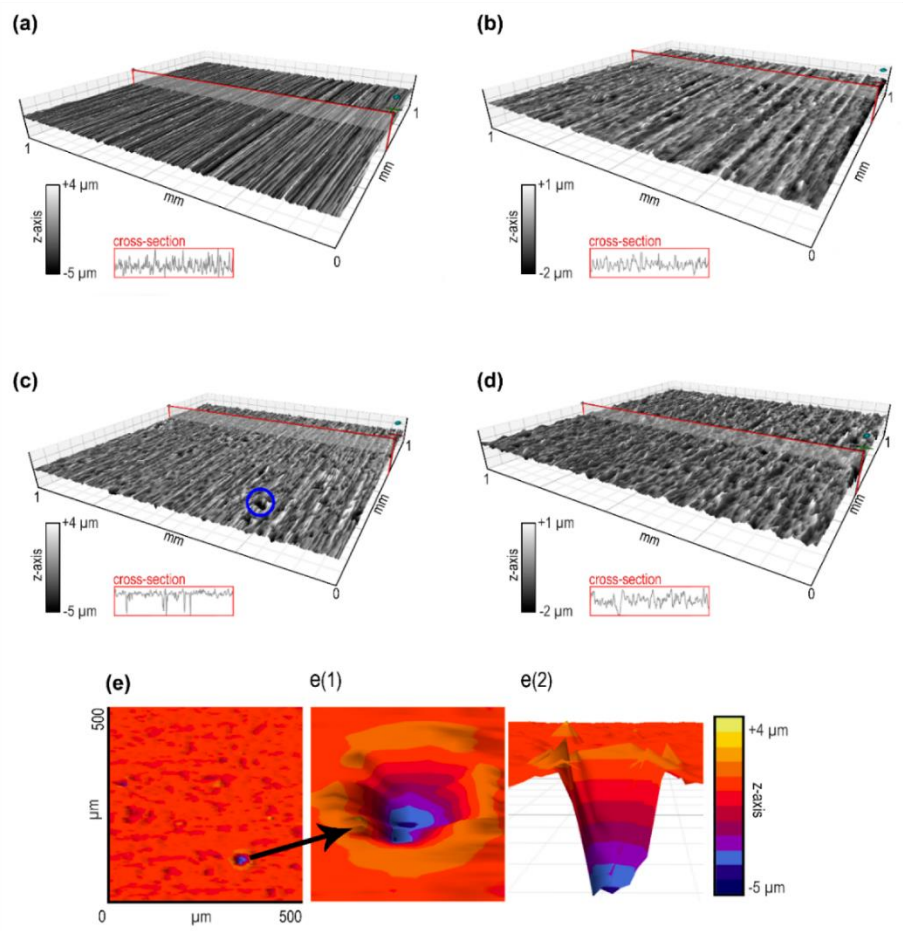

Figure 2. Profilometry 3D mapping of (**a**) untreated and (**b**) electropolished titanium metal foil from Supplier 1 and (**c**) untreated and (**d**) electropolished titanium metal foil from Supplier 2. The 3D mapping was measured on 1×1 mm^2 surface. Each inset is showing a cross-section of the roughness profile. (**e**) Deep pit in the surface of titanium foil from Supplier 2, (**e1**) magnified area and (**e2**) cross-section image of the pit with *z*-axis legend.

As can be seen from the titanium foil's X-ray diffraction (XRD) patterns from both suppliers (see Supplementary Figure S3), the peak locations of both titanium foils overlap, however their relative intensities differ. The XRD peaks correspond to the hexagonal titanium crystal planes (100), (002), (101), (102), (110), (103), (112), (201), (004), (202), and (104). The diffractograms of our samples show the strongest peak intensities for the (103) crystal plane for Supplier 1 and (002) crystal plane for Supplier 2. Davepon et al. [29] reported that the crystallographic orientation of the titanium foil can be correlated to the electrochemical behavior. However, a recent study performed by Macak et al. [24] showed that grain orientation of the titanium foil does not play a significant role in promoting or retarding the growth of TiO_2 nanotubes in ethylene glycol electrolytes.

The surface chemistry was investigated using the X-ray photoelectron spectroscopy (XPS) method. The presence of Ti and O was revealed on the surfaces by the Ti $2p_{3/2}$ peak at 458.6 eV and the O 1s peak at 530.0 eV, indicating the TiO_2-like surface oxide layer on all the samples [30]. In addition, surface contamination with carbon species (C 1s at 284.8 eV) was found. The subsurface region between 0 and 10 nm in depth on all the samples was analyzed by XPS depth profiling. The obtained XPS depth profiles are shown in Figure 3. The thickness of the oxide layer was estimated from the XPS depth profiles as a depth at which the concentration curve for oxygen dropped to the half of its maximum

value. This is a rough estimation of the oxide thickness due to the limited depth resolution during XPS depth profiling related to not flat surface. They show that the untreated Ti foils were covered by a thin Ti-oxide film with a thickness of about 6 nm, while after electropolishing the oxide film was slightly thicker (7–8 nm). The main difference between the untreated metallic foils and the polished foils was in the presence of Ti-nitrides and Ti-carbides in the subsurface region. They were identified by the XPS spectra of N 1s at 397.0 eV and C 1s spectra at 282.0 eV, related to the nitrides and carbides [30]. As can be seen from Figure 3a,c, Ti-carbide and Ti-nitrides are present in the subsurface of the untreated sample of Supplier 1 (about 15 at.% of carbon and 2 at.% of nitrogen at a depth of 5 nm). In the subsurface region of the untreated sample of Supplier 2 a lower Ti-carbide concentration was found (about 12 at.% of C), but more Ti-nitride was present (about 10 at. %).

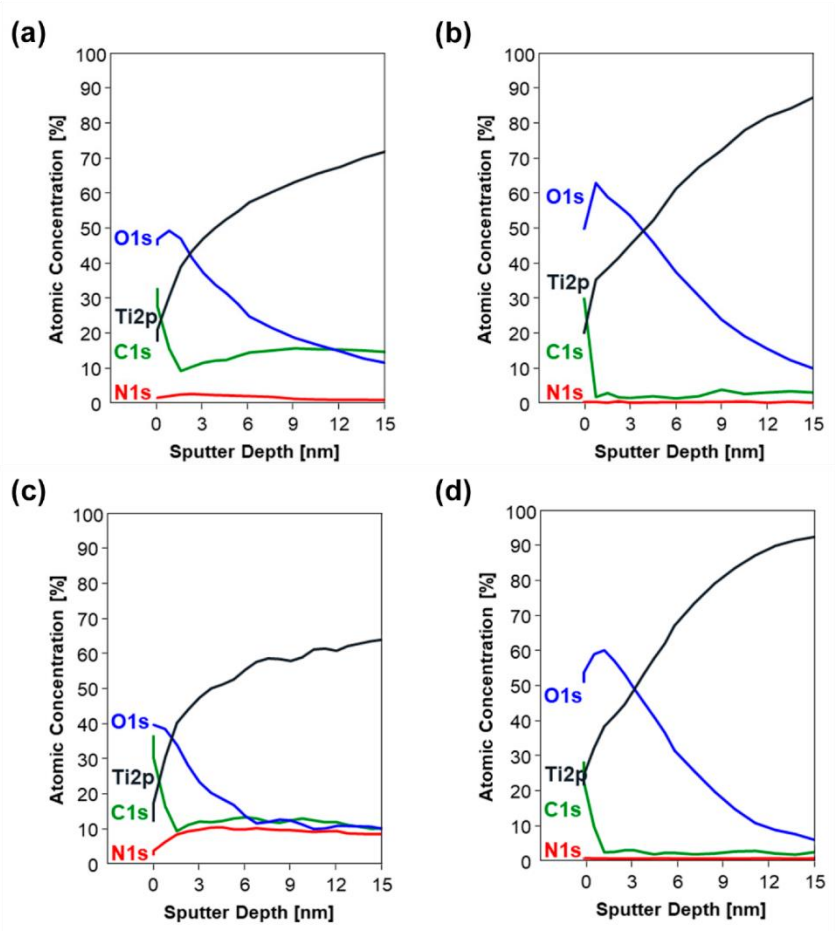

Figure 3. XPS depth profiling spectra for (**a**) untreated and (**b**) electropolished anodized samples from Supplier 1 and (**c**) untreated and (**d**) electropolished samples from Supplier 2. O 1s, Ti 2p, C 1s and N 1s peaks are marked.

2.2. Anodic Oxidation of the Titanium Foils

The current-time characteristics measured during the anodic oxidation of the differently treated titanium foils are presented in Figure 4. The magnified part shows the beginning of the anodization process, where the most significant differences appear. The current-time characteristics influences the morphological properties of grown TiO_2 nanotubes which are presented in Figure 5. For the purpose of clear presentation, all the observations from Figures 4 and 5 together with the reasons for the observed behaviours are described in Table 1.

Table 1. Observed behaviour during anodic oxidation for untreated and electropolished samples.

	Untreated Samples	Electropolished Samples
Shape of the anodization curve	• Flat current-time curves after the steady state was reached. • A small periodic current oscillation with more intensive bubble formation (the largest impact is seen for Supplier 2). • Foil from Supplier 2 needs longer time to reach the steady-state electrical current which delayed pore formation before the nanotube growth occurs.	A typical 3-step anodization curve corresponding to the 3 phases of the nanotube's formation process: compact oxide formation, initial porous structure formation, and nanotube growth.
	Explanation: electropolishing decreased the thickness of the starting compact oxide layer, which resulted in the faster formation of etching pits and nanotubes and an increase of current for EP samples can be seen. In case of the untreated titanium foil from Supplier 2 larger undulations and the deep pits present on the titanium foil's surface caused prolonged generation of the passive oxide layer and the formation of bubbles during the anodization which influenced the appearance of the anodized surface. The current oscillations are due to the repeated dissolution—formation of oxide layer. In contrast, the nanotubes that are grown on the electropolished titanium foil are round with smooth and thinner nanotube walls (Figure 5, Figures S4 and S5).	
Steady-state current	Less than 1 mA.	More than 1 mA.
	Explanation: a thicker oxide layer is formed at the beginning of the anodization of untreated samples with present impurities and surface defects. This thick oxide layer slows down the migration of the fluoride ions from the electrolyte, resulting in lower currents during the anodic oxidation. The smaller thickness of the compact oxide layer in EP samples caused a higher current density which promoted the growth of longer nanotubes.	
Nanotubes' shape	A hexagonal shape and ripples along the nanotube wall (Figure 5 and Figure S4).	Round with smooth and thinner nanotube walls (see Figure 5 and Figure S4).
	Explanation: ripples across the nanotube wall are due to the small periodic current oscillations during anodization.	
Nanotubes' length	Shorter (4 μm).	Longer (8 μm).
	Explanation: the growth of longer nanotubes was promoted by higher current density in case of electropolished samples. In case of untreated samples, a thinner layer of nanotubes formed under the thicker layer of the upper oxide.	

Observed behaviours are in accordance with results from the literature [22,31]. Different surface treatments of the starting titanium foils influence the amount of chemical impurities on the titanium surface and lead to a distinct electrochemical behaviour. Perillo and Rodriguez [32] performed experiments with air bubbling during the anodization process where the anodized nanotube layer showed a sponge-like porous structure with local areas of a dense, partially closed, top surface and an open tubular structure. Similar morphological characteristics were also achieved for the anodized, untreated sample from Supplier 2, as can be seen in Supplementary Figure S5. The nanotubes resulted in a dense and porous layer rather than a nanotubular layer which reduced the available active surface area for photocatalytic reaction.

Nanotubes grown on the untreated titanium foils exhibit a hexagonal shape and ripples along the nanotube wall. These are shown in Figure 5. The mentioned effect is more noticeable for the nanotubes grown by anodization of titanium from Supplier 2. In contrast, the nanotubes that are grown on the electropolished titanium foil are round with smooth and thinner nanotube walls (additional micrographs are shown in Supplementary Figure S4).

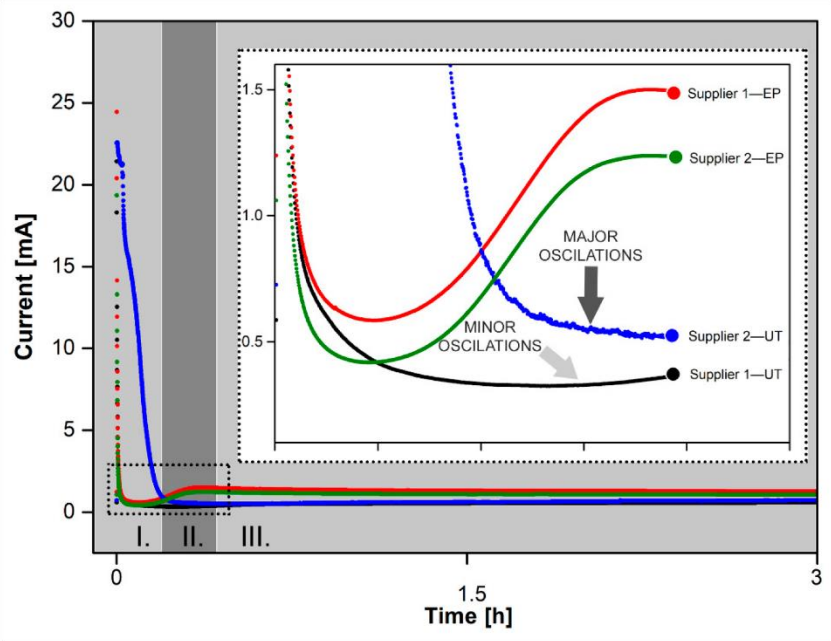

Figure 4. Current-time characteristics recorded during the anodic oxidation of the electropolished (EP) and untreated (UT) titanium foils from both suppliers. The inset shows the current at the beginning of the anodization process. Grey areas mark 3 stages of anodization curve for EP samples.

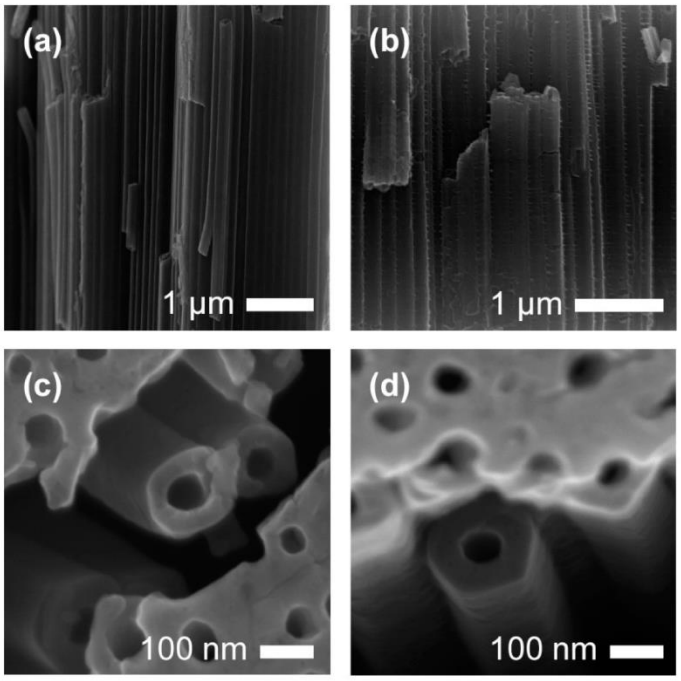

Figure 5. SEM micrographs of the anodized and annealed TiO_2 nanotubes: (**a**) anodized electropolished titanium with smooth nanotube wall, (**b**) anodized untreated titanium with ripples along the nanotube wall, (**c**) round-like shape grown on electropolished titanium foil and (**d**) hexagonal shape of TiO_2 nanotubes grown on untreated titanium foil. The same trend was observed for both suppliers.

2.3. Morphology of the TiO_2 Nanotube Arrays

Supplementary Figure S5 shows the anodized titanium foils after annealing. Considerable differences in the surface morphology can be observed between the untreated and the electropolished samples. It can be observed that the top surface of the TiO_2 nanotube layer mimics the initial surface roughness of the titanium foil and that more ordered and defect-free nanotube arrays are grown if the titanium foil is electropolished prior to the anodization. The imprints of the initial surface structural defects are more pronounced on the surface of the TiO_2 nanotube arrays of both untreated samples, where multiple steps and terraces can be seen. Supplementary Figure S8 shows topography results from 3D surface roughness mapping whereas the calculated values are shown in Table 2. Significant differences can be observed. The untreated sample from Supplier 2 exhibits the highest surface roughness of 0.632 µm, followed by the untreated sample from Supplier 1 with 0.187 µm, electropolished sample from Supplier 2 with 0.136 µm, and electropolished sample from Supplier 1 with 0.108 µm. On top of the nanotubes grown on the electropolished foils, a thinner and flatter top-oxide layer was formed. Its characteristics correspond to the appearance of the electropolished titanium foils including a thin oxide layer before anodization. Apart from that, the samples prepared with untreated foils have a higher fraction of closed nanotube tops. Cracks in the nanotube arrays can be observed for all the TiO_2 nanotube layers as a result of the annealing process in which the crystallization of the amorphous TiO_2 to the denser anatase phase occurs. The results are shown in Table 2 and the results of the nanotubular layer thicknesses and the nanotube wall thicknesses are presented in Figure 6. Those calculations were made by analyzing micrographs taken with the scanning electron microscope. Annealing of TiO_2 nanotube layers grown on the foil from Supplier 1 resulted in more dense and broader cracks in comparison to the small and curved cracks observed in the layers grown on the foil from Supplier 2. Campanelli et al. [33] attributed the cracking pattern to the existence of residual stresses during annealing. Hence, it can be assumed that the cracks appear at the locations of the grain boundaries in the titanium metal. This is also in agreement with the observations of Macak et al. [24], who observed that cracks are positioned over the grain boundaries in the titanium foil. If the cracks are wide enough for the organic molecules to traverse between them, then an additional catalytic surface area is available for the degradation reactions to occur. In our study, we noticed minor differences in the number and surface areas of the cracks between the nanotubular layers grown on the untreated and electropolished titanium foils.

Table 2. Measured and calculated pore density, cracked area and average surface roughness evaluated over the complete 3D surface of anodized untreated (UT) and electropolished (EP) titanium foils from both suppliers.

	Supplier 1—UT	Supplier 1—EP	Supplier 2—UT	Supplier 2—EP
Pore Density [%]	9.7 ± 0.6	12.7 ± 3.7	5.8 ± 2.9	10.9 ± 0.8
Cracked Area [%]	1.8 ± 0.2	4.6 ± 1.6	1.0 ± 0.3	2.5 ± 0.5
Average roughness [µm]	0.187	0.108	0.632	0.136

However, cross-sectioning of the nanotube layers showed that the nanotubes grown on the electropolished foil are more ordered, uniform, and two times longer (average length of 8 µm) than those grown on the untreated titanium foil (average length of approximately 4 µm). The nanotube arrays grown on the untreated foils show a waviness and should therefore exhibit a larger specific surface area when compared with the electropolished samples.

The nanotubes grown with anodic oxidation are amorphous and can be transformed into polycrystalline anatase nanotubes after annealing at 450 °C for 1 h. In all the samples, the characteristic peaks of tetragonal TiO_2 were detected, which correspond to the (101), (103), (004), (200), (105), (211), (204), (116), (220), and (215) anatase crystal planes (see Supplementary Figure S6). In the untreated foils, the signal from the titanium relative to the TiO_2 was higher due to the thinner TiO_2 nanotube

layer. From the relative peak-intensity values, the (101) peak appeared to be the preferred anatase crystal plane in all the samples.

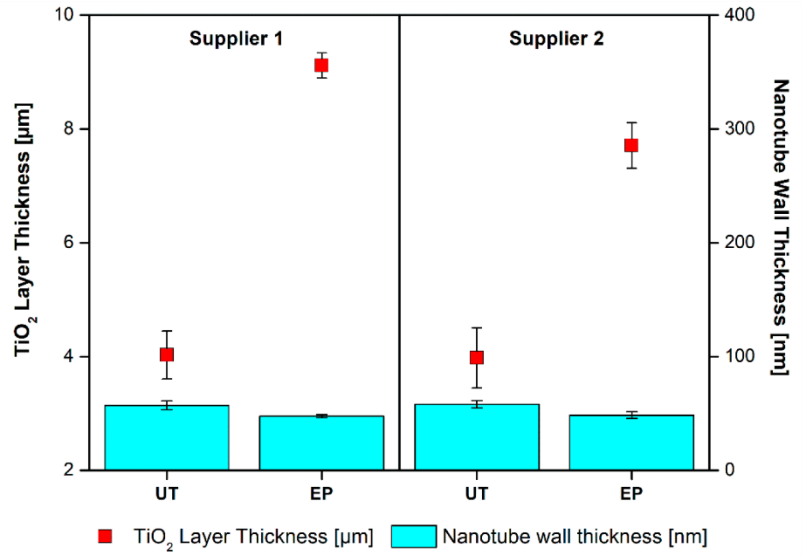

Figure 6. TiO_2 nanotube layer thickness, wall thickness and standard deviation of the results for the anodized untreated and electropolished titanium foils from both suppliers.

The TiO_2 surface composition was determined by the XPS, taking into account the relative sensitivity factors provided by the instrument manufacturer [30]. During data processing, the XPS spectra were aligned by setting the C 1s peak at 284.8 eV, characteristic for C-C/C-H bonds. On every sample, a survey spectrum over a wide energy range was acquired, as shown in Figure 7.

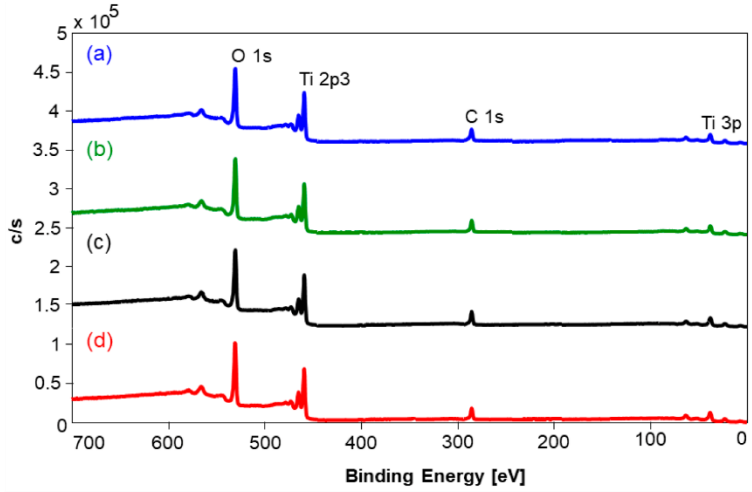

Figure 7. XPS survey spectra for (**a**) untreated and (**b**) electropolished anodized samples from Supplier 2 and (**c**) untreated and (**d**) electropolished samples from Supplier 1. The O 1s, Ti 2p3, C 1s and Ti 3p peaks are marked.

In order to get an insight into the chemical bonding of the surface atoms, we measured high-energy resolution XPS spectra on every sample. The elements C, Ti, and O were identified on the surfaces of

all the samples, together with some traces of nitrogen. The carbon atoms probably originated from the surface contamination. The spectra are very similar and contain the O 1s, Ti 2p, Ti 3p, O KLL, and C 1s peaks. From the intensities of the O 1s, Ti 2p, and C 1s peaks, the surface concentrations were calculated. On all the samples, the chemical composition was 25–29 at. % of C, 50–52 at. % of O, and 21–23 at. % of Ti.

The Ti 2p spectrum is presented in Supplementary Figure S7a. It is composed of a doublet consisting of a Ti $2p_{3/2}$ peak at 458.6 eV and a Ti $2p_{1/2}$ peak at 464.4 eV. All the Ti $2p_{3/2}$ peaks are very narrow, having a full width at half maximum (FWHM) of 1.1 eV, indicating a very ordered and defect-free TiO_2 nanotube phase. The binding energy of the Ti $2p_{3/2}$ peak at 458.6 eV means that the Ti atoms are in the Ti^{4+} oxidation state in the TiO_2 nanotube. The Ti^{3+} states that should appear as a peak at about 457.5 eV were not detected in the XPS spectra. The O 1s spectrum in all the samples is relatively similar, having the main peak at 529.8 eV (Figure S7b). This peak is usually assigned to O^{2-} ions in the TiO_2 oxide matrix. All the O 1s spectra also contain a small peak at 532.0 eV. This small peak may be related either to oxygen vacancies (defects) in the TiO_2 matrix or to adsorbed OH, H_2O, C-O groups at the surface. The untreated sample from Supplier 2 has the most substantial portion of O 1s sub-peak, relatively, at 532.0 eV, and the electropolished sample from Supplier 1 has, relatively, the smallest portion of O 1s sub-peak at 532.0 eV. This sub-peak in the O 1s spectra is often correlated with the photocatalytic activity of TiO_2 nanotubes. The carbon C 1s spectra were measured, and they are presented in Supplementary Figure S7c. The main peak is at 284.8 eV, representing C-C/C-H bonded carbon atoms, probably originating from surface contamination. There is also a peak at 286.2 eV in the C 1s spectra, probably related to the C−O/C−OH bonds and the peak at 288.9 eV related either to the O−C=O groups or the CO_3 species.

2.4. Photocatalytic Degradation of the Caffeine

The photocatalytic activities of TiO_2 nanotube layers grown on four distinct titanium foil surfaces were determined with the photocatalytic degradation of caffeine as a model degradation compound. Due to the hydrophobicity of the caffeine molecule, oxidation reactions with oxygen radicals are necessary for its degradation during photocatalytic reactions [34]. Under UV illumination, OH^- radicals are formed at the TiO_2 nanotube surface, which attack the C4=C8 double bond of the caffeine. After a series of hydroxylations and oxidations, caffeine degrades into 1,3,7-trimethyluric acid [35,36]. In the experiment, each anodized titanium foil was placed in a petri dish with 5 mL of the initial caffeine solution of 10 mg/L and illuminated with UV light intensity of 3.89 mW/cm^2 in a sterilizer (Kambič I-265 CK UV). The total reaction time was 350 min and the degradation was determined with a UV-Vis-IR spectrometer several times throughout the entire illumination period. The caffeine degradation results are shown in Figure 8.

The degradation performance of the anodized foils decreases in the order untreated foil from Supplier 1 (100% degradation in 5.5 h), electropolished foil of Supplier 1 (99 % degradation in 5.5 h), electropolished foil of Supplier 2 (91% degradation in 5.5 h), and untreated foil of Supplier 2 (83% degradation in 5.5 h). The best photocatalytic activity achieved with the anodized untreated foil from Supplier 1 corresponds to a photonic efficiency (ξ) of 0.9% and an initial reaction rate (Ri) of 0.005 (mol L-1s-1) x 106. The values were calculated using the equations described by Krivec et al. [37]. Whereas the results reported in the literature by different authors are difficult to compare, the comparison of the four samples tested in our study is straightforward. The differences observed can be explained with the results of the foils and the photocatalytic nanotube layers' characterization with X-ray diffraction, electron microscopy and X-ray photoelectron spectroscopy. The most noticeable difference is between the foils of different manufacturers. In the case of the foil from Supplier 1, electropolishing of the foil surface impairs the photocatalytic properties of the TiO_2 nanotube layer. The opposite is observed for the foil from Supplier 2, in which electropolishing greatly enhances the photocatalytic properties of the TiO_2 nanotube layer grown during anodic oxidation. The reason is the difference in the chemical composition of the starting titanium foils. The foil from Supplier 2 contains a higher concentration

of nitrogen present in the form of titanium nitride. The content of nitride is greatly reduced during electropolishing, which causes the growth of a higher-quality TiO_2 nanotubular layer during the anodic oxidation. Electropolishing the foil from Supplier 2 also greatly reduces the surface roughness and removes large peaks and valleys that affect the electrical current during anodization and result in the formation of a less photocatalytically active, uneven TiO_2 nanotube layer with areas of sponge-like structure. The deep valleys observed on the titanium foil of Supplier 2 impair the accessibility of these regions to fluoride ions during the anodization process, which further affects the slower dissolution of the initial oxide film present before the anodization of the foil and therefore the smaller surface area of the photocatalytically active top surface of the nanotubes. The foil from Supplier 1 contains much less nitride, and its percentage also decreases after electropolishing. In this case, it does not improve the photocatalytic properties of the grown TiO_2 nanotubular layer, since the surface roughness of the untreated foil from Supplier 1 was more suitable than that obtained after electropolishing. In addition to the roughness of the foil prior to anodizing, the photocatalytic activity of the TiO_2 nanotube layer is also affected by the nanotube wall's morphology, which is smooth in the case of the electropolished sample and bamboo-like in the case of the untreated sample. The latter has the effect of increasing the photocatalytic surface and thus the activity of the photocatalyst. In addition, the thickness of the TiO_2 nanotube layer and the smoothness of its top surface do not significantly affect its photocatalytic properties, as is often described in the literature. The TiO_2 nanotube layers that were grown on the electropolished foils are about twice as thick and have a much smoother surface, which does not necessarily mean better photocatalytic activity.

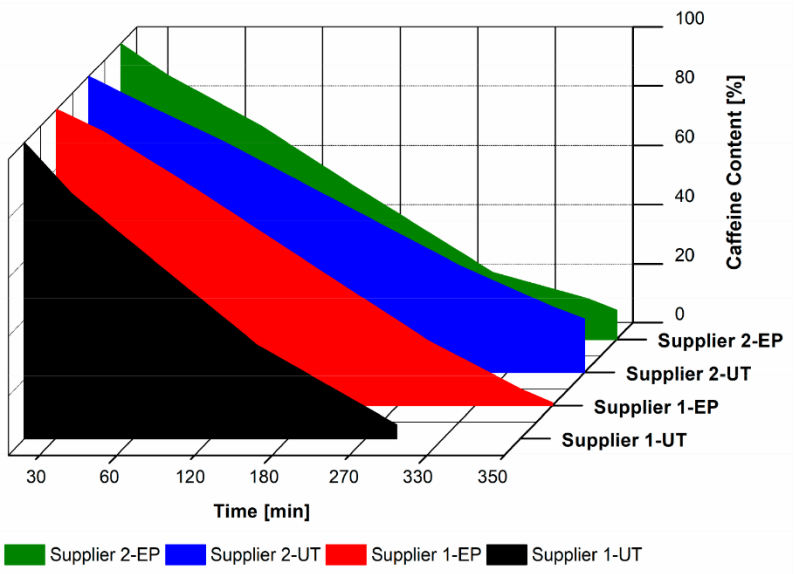

Figure 8. Photocatalytic degradation of caffeine by anodized untreated and electropolished titanium foils from both suppliers under UV irradiation. The degradation of the caffeine solution (10 ppm) was measured over a time period of 350 min. Samples were taken periodically, and the degradation was evaluated with a UV-Vis-IR spectrophotometer.

3. Materials and Methods

The study was divided into two parts. In the first part, we identified the optimum electropolishing conditions that would give a mirror-like finish on the titanium foil. In the second part, the untreated and electropolished titanium foils were anodized and their photocatalytic activity was determined. The most photocatalytically active TiO_2 nanotube arrays were then studied in detail to determine the

morphological and structural differences among them and the factors that contribute to the differences in their photocatalytic activity

3.1. Electropolishing of Titanium Foils

Titanium foils from two different suppliers, 200 µm thick, 99.9%, Baoji Lyne Metals Co., Ltd., Baoji, China (designated as Supplier 1) and 200 µm thick, 99.7%, Advent Research Materials Ltd., Oxford, UK (designated as Supplier 2) were cut into 15 × 15 mm^2 samples and ultrasonically cleaned to remove impurities. Table 3 shows the chemical composition of both titanium foils as received from the manufacturers. There are different amounts of impurities present in both titanium foils. The biggest difference is the iron content. There is 0.15% Fe in the foil from Supplier 2 and only 0.05% Fe in the foil from Supplier 1. This is followed by the nitrogen content, with 0.012% in the foil from Supplier 2 and 0.005% in the foil from Supplier 1. Before anodization, some titanium foils were electropolished and some were left untreated. Electropolishing was carried out on an electrolytic polishing machine (LectroPol-5, Struers, Cleveland, OH, USA) under various conditions: temperature (10, 15, and 20 °C), applied voltage (10, 30, 35, 40, and 45 V) and time of electropolishing (5, 10, 20, 30, and 60 s), using Struers A3 electrolyte (methanol, 2-butoxyethanol, and 60% perchloric acid). The same side of titanium foil was always electropolished.

Table 3. Declared chemical composition of starting titanium foils [1].

[wt %]	Ti	Fe	C	N	H	O
Supplier 1	99.850	0.05	0.012	0.005	0.003	0.08
Supplier 2	99.663	0.15	0.02	0.012	0.005	0.15

[1] EDS analysis did not show any significant differences between both suppliers and is therefore not presented.

3.2. Microstructure and Chemical Composition of the Metal Surfaces

Chemical and microstructure characterization of titanium foils was performed to determine their surface roughness, grain size distribution, crystal structure, and the surface and subsurface chemical composition. Altogether, 27 different polishing conditions were used to polish the titanium foils from each supplier. However, only the best five polishing conditions were used for the subsequent detailed investigations. These were selected according to the appearance of the polished foils under optical stereomicroscope (Discovery V8, Carl Zeiss Microscopy GmbH, Jena, Germany). The selected foils had no visible scratches or otherwise damaged surfaces. Polished and raw titanium foils were further characterized in a field-emission gun scanning electron microscope (FSEM JSM-7600F, JEOL Ltd., Tokyo, Japan). Additionally, the topography and the surface roughness of the electropolished and untreated titanium foils were determined with a stylus profiler with a 2-µm tip (DektakXT, Bruker, Billerica, MA, USA). For the determination of the grain size distribution, electropolished samples were etched for approximately 10 min with concentrated hydrochloric acid (37%, Carlo Erba Reagents SAS, Val de Reuil, France) and thoroughly rinsed with deionized water and ethanol. After that they were observed under an optical microscope (Axio Imager Z1-m, Carl Zeiss Microscopy GmbH, Jena, Germany). Electropolished samples were etched to expose grain boundaries and to improve their visibility under an optical microscope. Etched samples had clearly visible grains on which we were able to perform statistical analysis. A complete statistical analysis of the grain size distribution was performed with the Axio Vision program (AxioVs40 V 4.8.2.0, Carl Zeiss MicroImaging GmbH, Germany, 2006–2010). Diffraction patterns of both titanium foils were investigated by XRD (X'Pert PRO, Malvern Panalytical Ltd., Malvern, UK) analysis using a Cu-Kα source. The diffractograms were measured between 2° and 100° (X'Celerator detector) with a step of 0.034° 2θ over the area of 10 mm in diameter for 100 s. The phase identification was performed with the X'Pert HighScore Plus program (3.0e (3.0.5), PANalytical B.V., Almelo, The Netherlands, 30 January 2012) using the International Centre

for Diffraction Data (ICDD) PDF-4+ 2019 database. X-ray photoelectron spectroscopy (XPS) was used to characterize the surface and subsurface chemistry of the untreated and polished samples. The XPS analyses were performed on a PHI–TFA XPS spectrometer (Physical Electronics Inc., Eden Prairie, MN, USA) with an Al monochromatic X-ray source on a surface area of 0.4 mm in diameter. The analyzed depth of the XPS method is about 3–5 nm. The surface composition and the chemical bonding of the detected elements was deduced from the XPS spectra. In order to analyze the subsurface region, XPS depth profiling was performed, combining ion sputtering with Ar+ ions with 4-keV energy and XPS spectra acquisition. The sputtering rate was estimated to be 1.5 nm/min and a subsurface region to a depth of 10 nm was analyzed.

3.3. Anodic Oxidation of Titanium Foils

Prior to anodization, the foils were cleaned ultrasonically in acetone for 10 min, rinsed in ethanol and dried under a nitrogen stream. Electrolyte for the anodization was prepared with a mixture of 0.3 wt. % ammonium fluoride (Sigma-Aldrich, St. Louis, MO, USA) and 2 vol. % deionized water in ethylene glycol (99.99%, Sigma-Aldrich, St. Louis, MO, USA). All the experiments were carried out in a specially designed electrochemical cell (Figure 9), which was connected to a DC power supply.

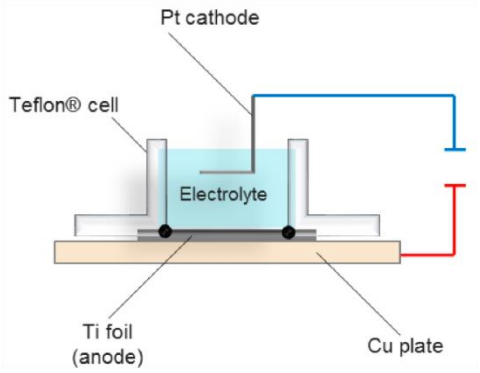

Figure 9. Electrochemical cell for anodic oxidation.

Electropolished and untreated titanium foils were anodized under a constant voltage of 60 V for 3 h using a DC power supply (TOELLNER Electronic Instrumente GmbH, Herdecke, Germany). The electrical current was monitored with a data acquisition/data logger (Agilent, Santa Clara, CA, USA). After the anodization, the titanium foils were rinsed with ethanol, dried under a nitrogen stream and annealed in air at 450 °C for 1 h (heating and cooling rates of 5 °C/min).

3.4. Characterization of the TiO_2 Nanotube Array

The morphology of the TiO_2 nanotubes was observed in a field-emission gun scanning electron microscope (FSEM JSM-7600F, JEOL Ltd., Tokyo, Japan). For the determination of the nanotubes' length, the samples were prepared by separating and crushing the nanotube layer from the titanium substrate. After placing these crushed particles on the carbon tape many situations revealed the slabs of TiO_2 nanotubes in cross-section view. The porosity and the area of the cracks in the TiO_2 nanotube array were estimated from plan-view images of the surface using the ImageJ program (ImageJ 1.52a, National Institutes of Health, United States, the program is in the public domain). Average roughness of the TiO_2 nanotube surface layers was measured with optical profiler (ZeGage™ Pro HR, Zygo Corporation, Middlefield, CT, USA) and evaluated over the complete 3D surface (Mx™ Software, Zygo Corporation, Middlefield, CT, USA). The nanotube crystallinity was investigated by XRD analysis of the immobilized annealed TiO_2 nanotube arrays, using an X'Pert PRO diffractometer (X'Pert PRO, Malvern Panalytical Ltd., Malvern, UK) with a Cu-Kα source. The 2θ angular regions between 20° and 80° were explored for 100 s (X'Celerator detector) with a step of 0.034° over an area

of 5 mm in diameter on annealed TiO_2 nanotube samples. The phase identification was performed with the X'Pert HighScore Plus program (3.0e (3.0.5), PANalytical B.V., Almelo, The Netherlands, 30 January 2012) using the International Centre for Diffraction Data (ICDD) PDF-4+ 2019 database. XPS was used to characterize the stoichiometry and oxidation states of the elements on the surfaces of the anodized TiO_2 nanotube arrays. The survey wide-energy spectrum was taken with the pass energy of the analyzer equal to 187 eV in order to identify and quantify the elements on the surface. The high-energy resolution spectrum was acquired with the energy analyzer operating at a resolution of about 0.6 eV and a pass energy of 29 eV.

3.5. Photocatalytic Degradation of the Caffeine

The photocatalytic degradation of the caffeine was measured on annealed anodized samples to determine their photocatalytic properties. Only the untreated and the most photocatalytically active electropolished (achieved with electropolishing conditions: 35 V, 30 s, 10 °C) samples from both suppliers were chosen for further testing. Titanium foils with an approximate anodized area of 0.79 ± 0.03 cm^2 were placed in a petri dish with 5 mL of the initial 10 ppm caffeine solution. The solution was stirred at 250 rpm and the samples were placed in a sterilizer (I-265 CK UV, Kambič d.o.o., Semič, Slovenia) and illuminated with UV light (Ultra-Vitalux, E27, 300W, OSRAM GmbH, Munich, Germany) with intensity of 3.89 mW/cm^2. The chosen lamp has two regions of illumination, namely UVA, from 315 to 400 nm, and UVB, from 280 to 315 nm (as provided by the supplier). After 30 min in the dark, 200 µL of caffeine solution was withdrawn and analyzed in a high-precision UV-Vis-IR spectrophotometer (Lambda 950, PerkinElmer Inc., Waltham, MA, USA). The next sample was withdrawn after the TiO_2 nanotube layer illumination for 30 min. Additional samples were later withdrawn periodically, six times over a 350-min time frame.

4. Conclusions

In summary, the anodic oxidation process was used to synthesize immobilized TiO_2 photocatalysts on untreated and electropolished titanium foils from two different suppliers. The as-purchased titanium foils varied in their chemical composition, surface roughness, and grain size distribution. These properties influenced the anodic oxidation process in which TiO_2 nanotubes with different morphology were grown. The annealed nanotube layers were characterized using FSEM, profilometry, XRD, and XPS and the photocatalytic activities for the degradation of caffeine were measured. The results presented in this paper show that the most important factor determining the photocatalytic activity is not surface morphology but, in our case, the presence of nitrides in one foil and the absence of nitrides in the other. That resulted in a significant difference because untreated titanium foil from one supplier and electropolished foil from the other supplier resulted in the best photocatalytically active samples.

Supplementary Materials: The following are available online at http://www.mdpi.com/2073-4344/10/7/803/s1, Figure S1: Optical microscope micrographs of chemically etched, electropolished titanium surfaces with the corresponding grain-area histogram for both titanium foil suppliers. (a) Titanium foil from Supplier 1 and (b) titanium foil from Supplier 2, Figure S2: Measured roughness factors for both titanium foil suppliers; Ra—average arithmetical roughness, Rq—root-mean-square roughness, Rt—peak-to-valley roughness, UT—untreated, EP—electropolished, Figure S3: XRD pattern for both untreated titanium foils, Figure S4: SEM micrographs of the anodized and annealed titanium foils showing (a) untreated and (b) electropolished titanium foil from Supplier 1. (c) Untreated and (d) electropolished titanium foil from Supplier 2, Figure S5: SEM images of the top surface of the annealed TiO_2 nanotube arrays. (a) Untreated and (b) electropolished titanium foil from Supplier 1. (c) Untreated and (d) electropolished titanium foil from Supplier 2, Figure S6: XRD patterns of annealed TiO_2 nanotubular layers for untreated and electropolished samples of both suppliers. Unmarked peaks correspond to the titanium foil, Figure S7: (A) Ti 2p, (B) O 1s and (C) C 1s spectrums from XPS measurement, Figure S8: Average roughness evaluated over the complete 3D surface roughness of TiO_2 nanotube layers. (a) Untreated and (b) electropolished sample from Supplier 1 and (c) untreated and (d) electropolished sample from Supplier 2 are shown. Each inset is showing a captured TiO_2 nanotube layer surface as seen through the camera on the optical profiler.

Author Contributions: Conceptualization, Ž.M. and L.S.; validation, Ž.M., L.S., Z.S., J.K., and M.Č.; investigation, Ž.M., Z.S., and J.K.; resources, Ž.M., L.S., Z.S., J.K., and M.Č.; writing—original draft preparation, Ž.M.; writing—review and editing, Ž.M., L.S., Z.S., J.K., and M.Č; visualization, Ž.M.; supervision, M.Č.; project administration, M.Č.; funding acquisition, M.Č. All authors have read and agreed to the published version of the manuscript.

Funding: The authors gratefully acknowledge the Slovenian Research Agency (ARRS) for financial support within the research program P2-0084. This project has also received funding from the European Union's Horizon 2020 research and innovation programme under grant agreement No. 823717-ESTEEM3.

Acknowledgments: The authors would also like to thank the ULTRACOOL lab financed by Director's fund 2017 from Jožef Stefan Institute, Ljubljana for their support on working with Dektak Profilometry, CEMM team from Jožef Stefan Institute, Ljubljana for sharing their knowledge on electron microscopy and Vid Simon Šelih for his kind guidance with Zygo optical profilometry.

Conflicts of Interest: The authors declare no conflict of interest. The funders had no role in the design of the study; in the collection, analyses, or interpretation of data; in the writing of the manuscript, or in the decision to publish the results.

References

1. Ibhadon, A.O.; Fitzpatrick, P. Heterogeneous photocatalysis: Recent advances and applications. *Catalysts* **2013**, *3*, 189–218. [CrossRef]
2. Hoffmann, M.R.; Martin, S.T.; Choi, W.; Bahnemann, D.W. Environmental applications of semiconductor photocatalysis. *Chem. Rev.* **1995**, *95*, 69–96. [CrossRef]
3. Kong, M.; Li, Y.; Chen, X.; Tian, T.; Fang, P.; Zheng, F.; Zhao, X. Tuning the relative concentration ratio of bulk defects to surface defects in TiO_2 nanocrystals leads to high photocatalytic efficiency. *J. Am. Chem. Soc.* **2011**, *133*, 16414–16417. [CrossRef] [PubMed]
4. Ge, M.; Li, Q.; Cao, C.; Huang, J.; Li, S.; Zhang, S.; Chen, Z.; Zhang, K.; Al-Deyab, S.S.; Lai, Y.; et al. One-dimensional TiO_2 nanotube photocatalysts for solar water splitting. *Adv. Sci.* **2017**, *4*, 1–31. [CrossRef]
5. Yu, J.; Low, J.; Xiao, W.; Zhou, P.; Jaroniec, M. Enhanced photocatalytic CO_2-Reduction activity of anatase TiO_2 by Coexposed {001} and {101} facets. *J. Am. Chem. Soc.* **2014**, *136*, 8839–8842. [CrossRef]
6. Bai, S.; Wang, L.; Li, Z.; Xiong, Y. Facet-engineered surface and interface design of photocatalytic materials. *Adv. Sci.* **2017**, *4*, 1–26. [CrossRef]
7. Roy, P.; Berger, S.; Schmuki, P. TiO_2 nanotubes: Synthesis and applications. *Angew. Chemi. Int. Ed.* **2011**, *50*, 2904–2939. [CrossRef]
8. Ou, H.H.; Lo, S.L. Review of titania nanotubes synthesized via the hydrothermal treatment: Fabrication, modification, and application. *Sep. Purif. Technol.* **2007**, *58*, 179–191. [CrossRef]
9. Zhang, J.; Xiao, X.; Nan, J. Hydrothermal-hydrolysis synthesis and photocatalytic properties of nano-TiO_2 with an adjustable crystalline structure. *J. Hazard. Mater.* **2010**, *176*, 617–622. [CrossRef]
10. Gong, D.; Grimes, C.A.; Varghese, O.K.; Hu, W.; Singh, R.S.; Chen, Z.; Dickey, E.C. Titanium oxide nanotube arrays prepared by anodic oxidation. *J. Mater. Res.* **2001**, *16*, 3331–3334. [CrossRef]
11. Maiyalagan, T.; Viswanathan, B.; Varadaraju, U.V. Fabrication and characterization of uniform TiO_2 nanotube arrays by sol-gel template method. *Bull. Mater. Sci.* **2006**, *29*, 705–708.
12. Zhou, X.; Liu, N.; Schmuki, P. Photocatalysis with TiO_2 nanotubes: "Colorful" Reactivity and designing site-specific photocatalytic centers into TiO_2 nanotubes. *ACS. Catal.* **2017**, *7*, 3210–3235. [CrossRef]
13. Tao, J.; Zhao, J.; Tang, C.; Kang, Y.; Li, Y. Mechanism study of self-organized TiO_2 nanotube arrays by anodization. *New J. Chem.* **2008**, *32*, 2164–2168. [CrossRef]
14. Zhou, X.; Nguyen, N.T.; Özkan, S.; Schmuki, P. Anodic TiO_2 nanotube layers: Why does self-organized growth occur—A mini review. *Electrochem. Commun.* **2014**, *46*, 157–162. [CrossRef]
15. Kowalski, D.; Kim, D.; Schmuki, P. TiO_2 nanotubes, nanochannels and mesosponge: Self-organized formation and applications. *Nano Today* **2013**, *8*, 235–264. [CrossRef]
16. Boyjoo, Y.; Sun, H.; Liu, J.; Pareek, V.K.; Wang, S. A review on photocatalysis for air treatment: From catalyst development to reactor design. *Chem. Eng. J.* **2017**, *310*, 537–559. [CrossRef]
17. Lu, K.; Tian, Z.; Geldmeier, J.A. Polishing effect on anodic titania nanotube formation. *Electrochim. Acta* **2011**, *56*, 6014–6020. [CrossRef]

18. Hu, N.; Gao, N.; Starink, M.J. The influence of surface roughness and high pressure torsion on the growth of anodic titania nanotubes on pure titanium. *Appl. Surf. Sci.* **2016**, *387*, 1010–1020. [CrossRef]
19. Sopha, H.; Jäger, A.; Knotek, P.; Tesař, K.; Jarosova, M.; Macak, J.M. Self-organized anodic TiO_2 nanotube layers: Influence of the Ti substrate on nanotube growth and dimensions. *Electrochim. Acta* **2016**, *190*, 744–752. [CrossRef]
20. Albu, S.P.; Schmuki, P. Influence of anodization parameters on the expansion factor of TiO_2 nanotubes. *Electrochim. Acta* **2013**, *91*, 90–95. [CrossRef]
21. Pouilleau, J.; Devilliers, D.; Garrido, F.; Durand-Vidal, S.; Mahé, E. Structure and composition of passive titanium oxide films. *Mater. Sci. Eng. B* **1997**, *47*, 235–243. [CrossRef]
22. Asgari, V.; Noormohammadi, M.; Ramazani, A.; Kashi, M.A. A new approach to electropolishing of pure Ti foil in acidic solution at room temperature for the formation of ordered and long TiO_2 nanotube arrays. *Corros. Sci.* **2018**, *136*, 38–46. [CrossRef]
23. Lee, B.G.; Hong, S.Y.; Yoo, J.E.; Choi, J. Electropolishing for the formation of anodic nanotubular TiO_2 with uniform length and density. *Appl. Surf. Sci.* **2011**, *257*, 7190–7194. [CrossRef]
24. Macak, J.M.; Jarosova, M.; Jäger, A.; Sopha, H.; Klementová, M. Influence of the Ti microstructure on anodic self-organized TiO_2 nanotube layers produced in ethylene glycol electrolytes. *Appl. Surf. Sci.* **2016**, *371*, 607–612. [CrossRef]
25. Zou, J.P.; Wang, R.Z. Debonding phenomenon of TiO_2 nanotube film. *Trans. Nonferrous Met. Soc. China* **2012**, *22*, 2691–2699. [CrossRef]
26. Zou, J.P.; Wang, R.Z. Crack initiation, propagation and saturation of TiO_2 nanotube film. *Trans. Nonferrous Met. Soc. China* **2012**, *22*, 627–633. [CrossRef]
27. Baek, S.M.; Polyakov, A.V.; Moon, J.H.; Semenova, I.P.; Valiev, R.Z.; Kim, H.S. Effect of surface etching on the tensile behavior of coarse- and ultrafine-grained pure titanium. *Mater. Sci. Eng. A* **2017**, *707*, 337–343. [CrossRef]
28. Jarosz, M.; Kapusta-Kołodziej, J.; Jaskuła, M.; Sulka, G.D. Effect of different polishing methods on anodic titanium dioxide formation. *J. Nanomater.* **2015**, 1–10. [CrossRef]
29. Konig, U.; Davepon, B. Microstructure of polycrystalline Ti and its microelectrochemical properties by means of electron-backscattering diffraction (EBSD). *Electrochim. Acta* **2001**, *47*, 149–160. [CrossRef]
30. Moulder, J.F.; Stickle, W.F.; Sobol, P.E.; Bomben, K.D. *Handbook of X-ray Photoelectron Spectroscopy*; Chastain, J., Ed.; Physical Electronics (Perkin-Elmer Corporation): Eden Prairie, MN, USA, 1992; p. 261.
31. Xie, Z.B.; Blackwood, D.J. Effects of anodization parameters on the formation of titania nanotubes in ethylene glycol. *Electrochim. Acta* **2010**, *56*, 905–912. [CrossRef]
32. Perillo, P.M.; Rodriguez, D.F. Growth control of TiO_2 nanotubes in different physical environments. *Nanosci. Methods* **2012**, *1*, 194–200. [CrossRef]
33. Contri Campanelli, L.; Sergio Carvalho Pereira da Silva, P.; Camarinho Oliveira, N.T.; Bolfarini, C. Effect of the modification by titanium dioxide nanotubes with different structures on the fatigue response of Ti grade 2. *Mater. Res.* **2017**, *20*, 120–124. [CrossRef]
34. Tavagnacco, L.; Schnupf, U.; Mason, P.E.; Saboungi, M.-L.; Cesàro, A.; Brady, J.W. Molecular dynamics simulation studies of caffeine aggregation in aqueous solution. *J. Phys. Chem. B* **2011**, *115*, 10957–10966. [CrossRef] [PubMed]
35. Dalmázio, I.; Santos, L.S.; Lopes, R.P.; Eberlin, M.N.; Augusti, R. Advanced oxidation of caffeine in water: On-line and real-time monitoring by electrospray ionization mass spectrometry. *Environ. Sci. Technol.* **2005**, *39*, 5982–5988. [CrossRef]
36. Telo, J.P.; Vieira, A.J.S.C. Mechanism of free radical oxidation of caffeine in aqueous solution. *J. Chem. Soc. Perkin. Trans.* **1997**, *2*, 1755–1757. [CrossRef]
37. Krivec, M.; Žagar, K.; Suhadolnik, L.; Čeh, M.; Dražić, G. Highly efficient TiO_2-based microreactor for photocatalytic applications. *ACS. Appl. Mater. Interfaces* **2013**, *5*, 9088–9094. [CrossRef]

catalysts

MDPI

Article

The Influence of a Surface Treatment of Metallic Titanium on the Photocatalytic Properties of TiO_2 Nanotubes Grown by Anodic Oxidation

Živa Marinko [1,2,*], Luka Suhadolnik [1], Zoran Samardžija [1], Janez Kovač [3] and Miran Čeh [1]

[1] Department for Nanostructured Materials, Jožef Stefan Institute, Jamova 39, 1000 Ljubljana, Slovenia; luka.suhadolnik@ijs.si (L.S.); zoran.samardzija@ijs.si (Z.S.); miran.ceh@ijs.si (M.Č.)
[2] Jožef Stefan International Postgraduate School, Jamova 39, 1000 Ljubljana, Slovenia
[3] Department of Surface Engineering, Jožef Stefan Institute, Jamova 39, 1000 Ljubljana, Slovenia; janez.kovac@ijs.si (J.K.)
* Correspondence: ziva.marinko@ijs.si (Ž.M.); Tel.: 00386 1 4773 931

Received: 16 June 2020; Accepted: 16 July 2020; Published: date

Supporting information

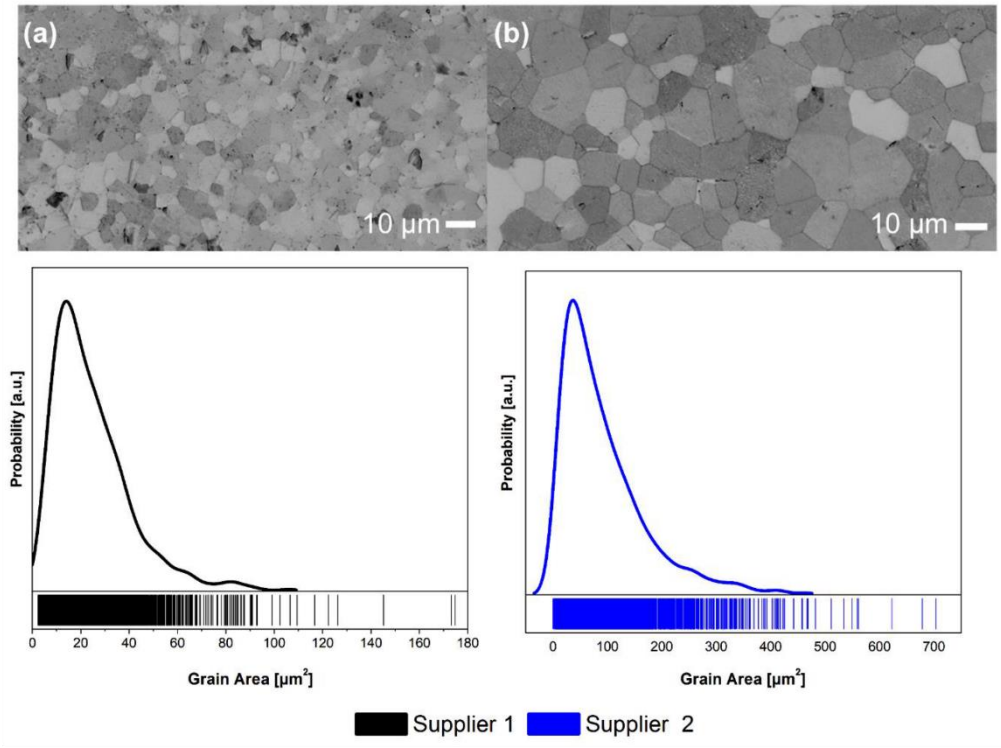

Figure S1. Optical microscope micrographs of chemically etched, electropolished titanium surfaces with the corresponding grain-area histogram for both titanium foil suppliers. (a) Titanium foil from Supplier 1 and (b) titanium foil from Supplier 2.

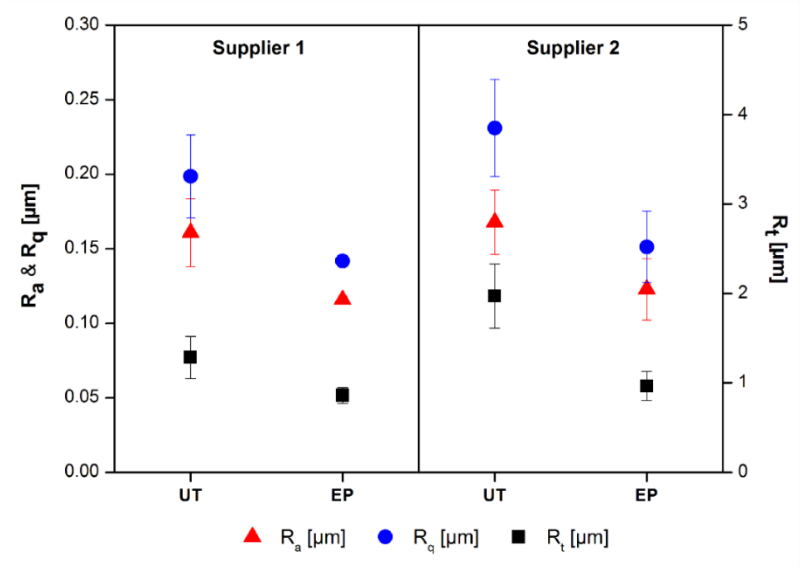

Figure S2. Measured roughness factors for both titanium foil suppliers; Ra – average arithmetical roughness, Rq – root-mean-square roughness, Rt – peak-to-valley roughness, UT – untreated, EP - electropolished.

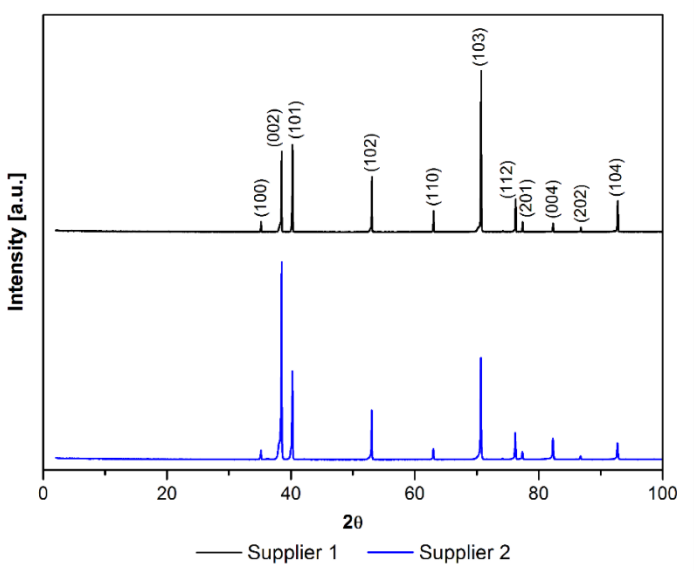

Figure S3. XRD pattern for both untreated titanium foils.

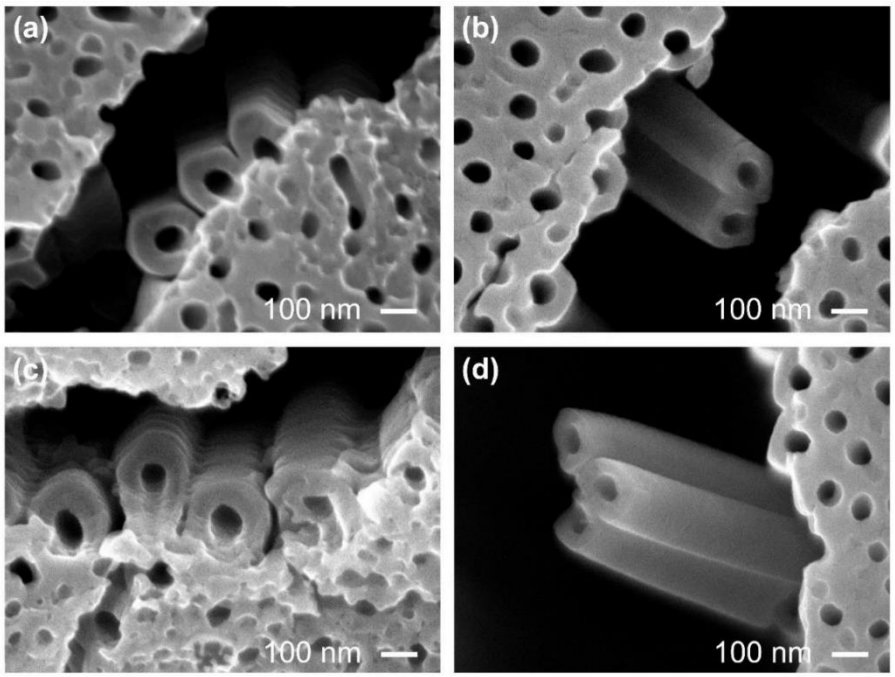

Figure S4. SEM micrographs of the anodized and annealed titanium foils showing (a) untreated and (b) electropolished titanium foil from Supplier 1. (c) Untreated and (d) electropolished titanium foil from Supplier 2.

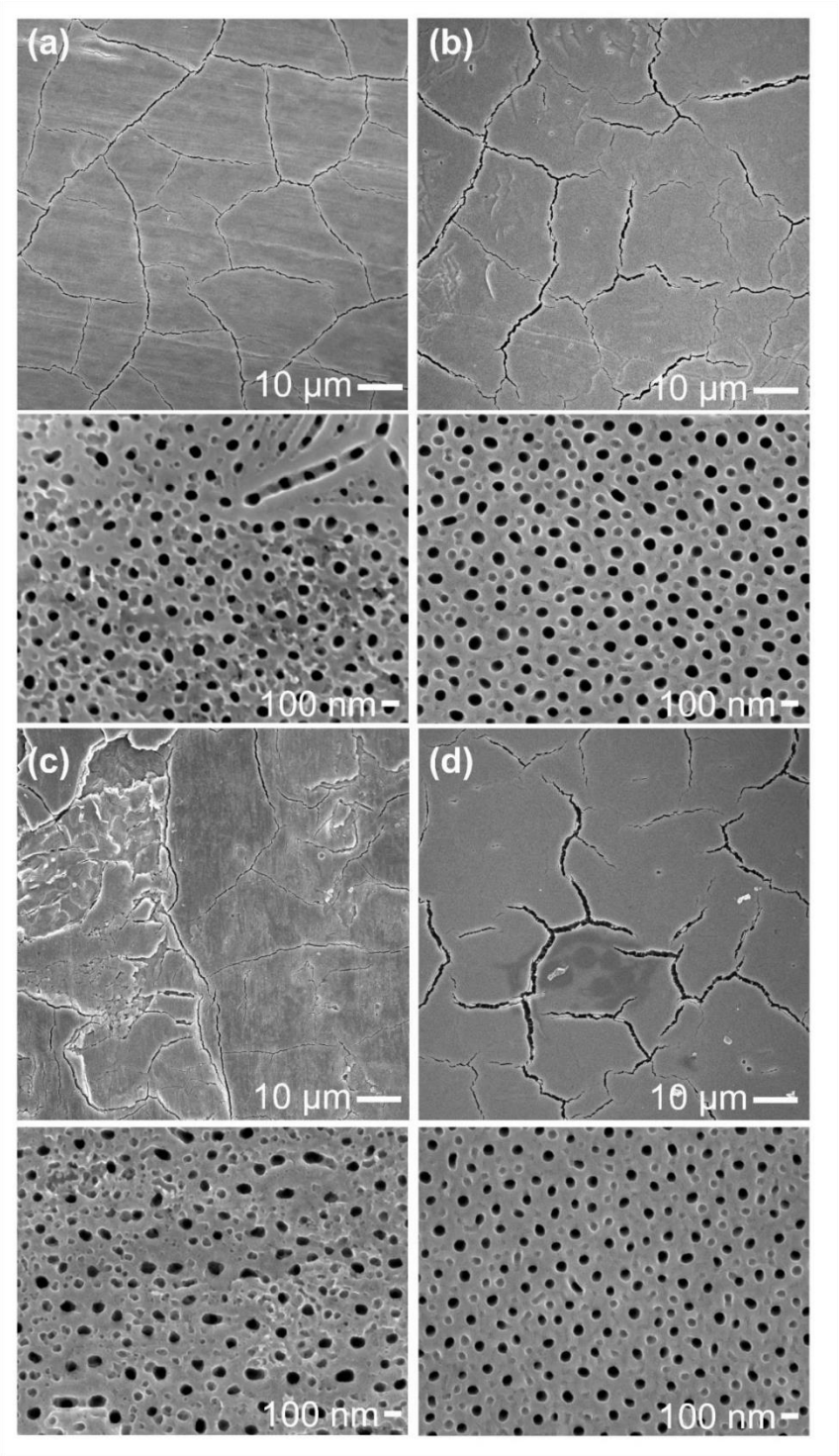

Figure S5. SEM images of the top surface of the annealed TiO_2 nanotube arrays. (a) Untreated and (b) electropolished titanium foil from Supplier 1. (c) Untreated and (d) electropolished titanium foil from Supplier 2.

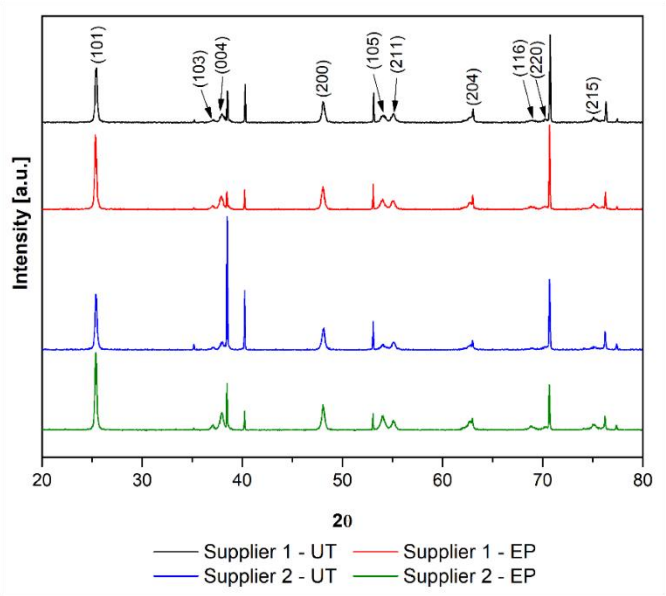

Figure S6. XRD patterns of annealed TiO_2 nanotube layers for untreated and electropolished samples of both suppliers. Unmarked peaks correspond to the titanium foil.

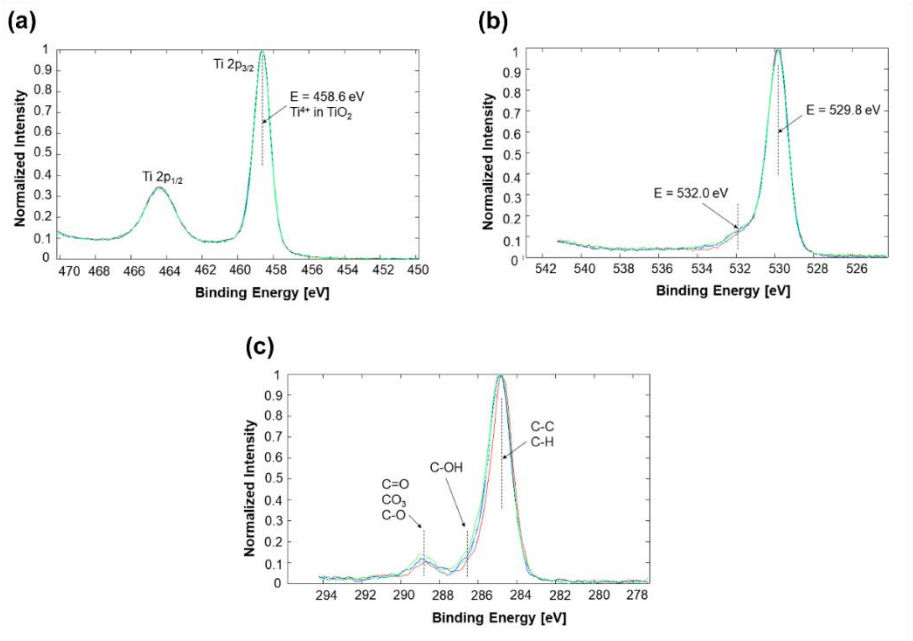

Figure S7. (a) Ti 2p, (b) O 1s and (c) C 1s spectrums from XPS measurement.

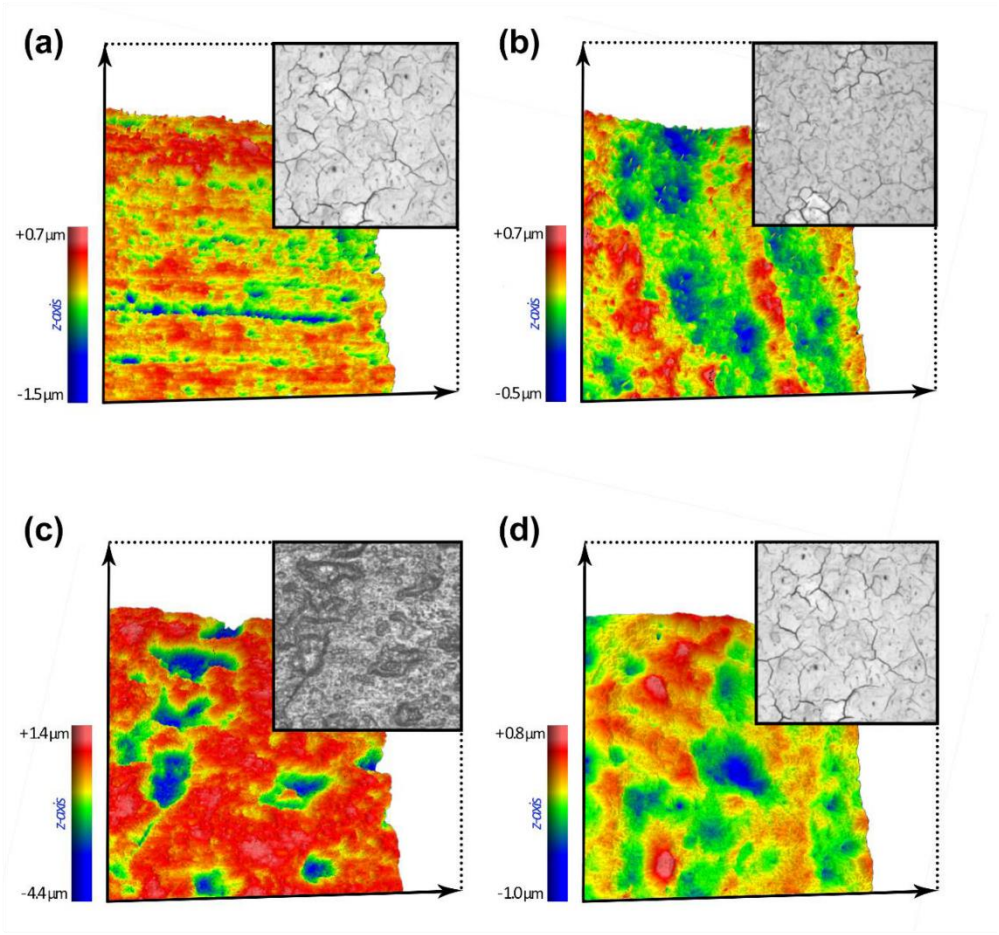

Figure S8. Average roughness evaluated over the complete 3D surface roughness of TiO_2 nanotube layers. (a) Untreated and (b) electropolished sample from Supplier 1 and (c) untreated and (d) electropolished sample from Supplier 2 are shown. Each inset is showing a captured TiO_2 nanotube layer surface as seen through camera on optical profiler.

2.1 Appendix to the Paper

2.1.1 UV-Vis Light Comparison Photocatalytic Activity

The caffeine degradation was initially measured in a UV-Vis sterilizer with a wide range of light wavelengths (*UVA from 315 to 400 nm and UVB from 280 to 315 nm*). The most appropriate wavelength for the TiO_2 anatase photocatalysis is equal to, or higher than, 387 nm (approximately 3.2 eV). Additionally, the photocatalytic efficiency of the NT samples was also tested at wavelengths of 365, 395 and 405 nm, respectively. The experimental setup for those experiments is presented in Figure 2.1, together with a setup for the experiments performed in a sterilizer (and measured in a spectrophotometer).

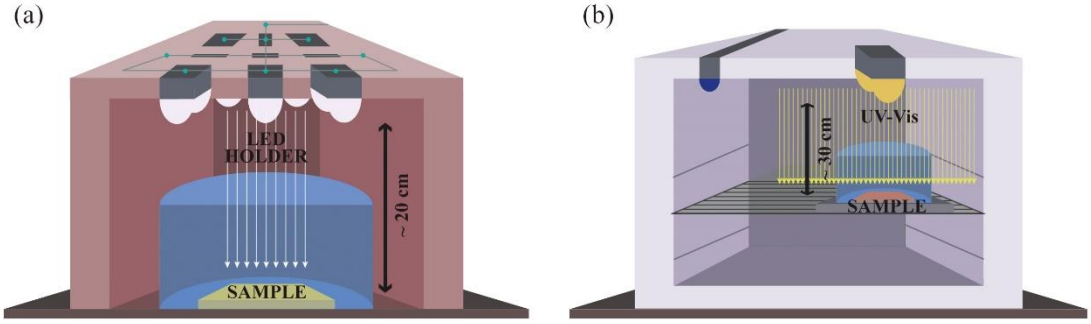

Figure 2.1: (a) Setup for catalyst-efficiency measurements at 365, 395 and 405 nm wavelengths and (b) setup for sterilizer measurements.

Caffeine was chosen as a model degradation compound since its degradation can be easily followed with a UV-VIS spectrophotometer and caffeine by-products do not absorb in the same range as caffeine. The literature shows that caffeine degradation occurs via the *in-situ* generation of free $OH^{\bullet}$ as the main reactive species [192]. Under UV illumination, $OH^{\bullet}$ radicals begin to form on the TiO_2 NT array, which decomposes the aqueous solution of caffeine [193]. Caffeine oxidation begins with the $OH^{\bullet}$ attack on C_8 and results in 1,3,7-trimethyluric acid as the final product [194]. From the literature [195], the peak in the absorption spectra of caffeine in H_2O is around 274 nm (whole spectra ranges between 243 and 302 nm, as is presented in Figure 2.2f) at room temperature [196]. The following was also confirmed in our samples (Figure 2.2a-d).

A blank sample was also used to exclude any potential light interference. The results are presented in Figure 2.2e. No degradation was measured using blank samples (Ti foil) in the 3 h experiment. The activity of the anodised samples was analysed under various light intensities. The UT sample from Supplier 1 exhibited the highest degradation among EP sample from Supplier 1 and the UT and EP samples from Supplier 2. The latter performed best when illuminated with 365 nm. The results for the EP sample from Supplier 1 are comparable under the spectrophotometer and 365 nm light. The other two wavelengths, 395 and 405 nm, yield significantly worse activity. Unfortunately, caffeine degradation is not the same as complete mineralisation, which is usually not rapid. When caffeine is consumed into persistent organic intermediates, the mineralization into CO_2, H_2O, and NH_3 is slow [192]. The degradation of caffeine is seen on the absorbance-measurements spectra as a lowering of the intensity of the measured signal between 240

and 300 nm. However, the intermediates cannot be measured in a similar way, but with more sensitive and precise methods such as HPLC.

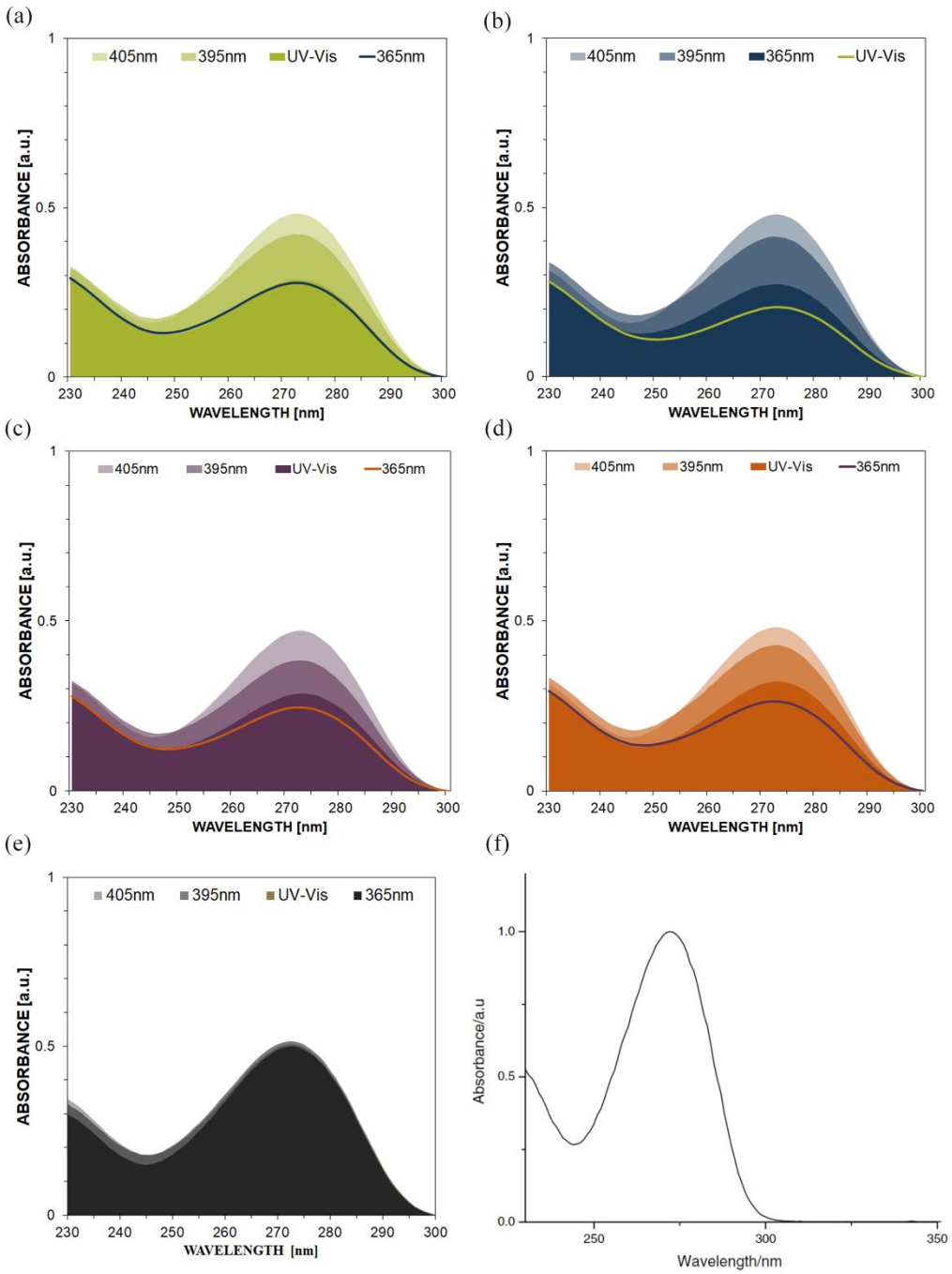

Figure 2.2: Absorbance measurements of caffeine at different wavelengths (365 nm, 395 nm, 405 nm and Vis) in 3 h measurements for (a) EP and (b) UT anodised samples from Supplier 1, (c) EP and (d) UT anodised samples from Supplier 2, (e) a blank sample of Ti foil and (f) a reference number from literature [195], Copyright © 2015 Showkat Ahmad Bhawani et al.

The NTs' morphology has an enormous impact on photocatalytic activity. Nakata and Fujishima [197] showed that a porous structure is better for photocatalytic activity. According to the authors, the NTs' formation is superior for photocatalytic degradation

since it enables the diffusion of organic pollutants into the TiO_2 NTs. Another structural characteristic is thin walls, reducing the recombination of h^+_{VB} and e^-_{CB} (due to the carrier diffusion length in TiO_2 after photo-absorption). Moreover, it was stated [198] that the nanotubular morphology showed maximum photocatalytic efficiency due to the considerable number of active sites generated by the oxygen vacancies. These vacancies then promote the generation of ROS (by O_2). Hydroxyl groups can accept photogenerated holes and thus yield more $OH^\bullet$ radicals [199].

2.1.2 ToF-SIMS analyses of Titanium Foil and TiO_2 Nanotubes Surface

ToF-SIMS depth profiling was applied to evaluate the Ti foil samples' surface composition, as seen in Figures 2.3 (Ti^+, TiO^+, Ca^+, Na^+, K^+, Al, Mg^+, Si^+, Fe^+, etc.). The analysed area was 100 × 100 µm^2, and the sputtering area was 400 × 400 µm^2. Sputtering rate was about 2 nm/s. Among investigated secondary ions, Ti^+ represents the amount of titanium (purity of titanium foil) and TiO^+ represents an amorphous oxide on top of the surface. Other identified secondary ions are indicators of chemical impurity of titanium foil. Some of those impurities were already confirmed with the XPS method. From the measured SIMS depth profiles shown in Figure 2.3a, we can observe that the EP sample from Supplier 1 contains minor impurities like Na^+, K^+, Ca^+, Al^+, and Si^+ ions. These impurities are present also in other samples, together with Mg^+. Overall, the UT samples contain higher concentration of impurities in the surface area than the EP samples. ToF-SIMS depth profiling showed that the EP sample from Supplier 1 has the thickest oxide layer; the following ones are UT from Supplier 1 and EP from Supplier 2. Interestingly, the oxide layer was the thinnest on the EP sample from Supplier 2. Those findings align with our previous XPS results, which showed that the amorphous oxide layer among samples is 4–6 nm thick.

A similar approach of the SIMS depth profile analyses was applied to TiO_2 NTs. Any possible impurities in the TiO_2 lattice could contribute to the differences in photocatalytic activity. Figure 2.4 presents the identified negative secondary ions, such as F^-, TiO^-, O_2^-, and OH^- as a function of depth.

To compare surface composition from SIMS depth profiles we integrated the SIMS signals from the surface to depth of 250 nm for all samples, what is shown in Figure 2.4e. We can observe in SIMS depth profiles in Figures 2.4 a-d that the chemical groups, such as TiO^-, OH^- and O_2^-, are related to the oxide layer and the F^- signal to the electrolyte residues in the NTs. A high F^- signal can be found in all the samples; however, the values decreased faster in the EP samples. Surprisingly, the F^- ions were not present at the surface, but beneath the oxide surface. The difference was more significant in the UT samples, which can be attributed to the thicker oxide layer (Figure 2.5).

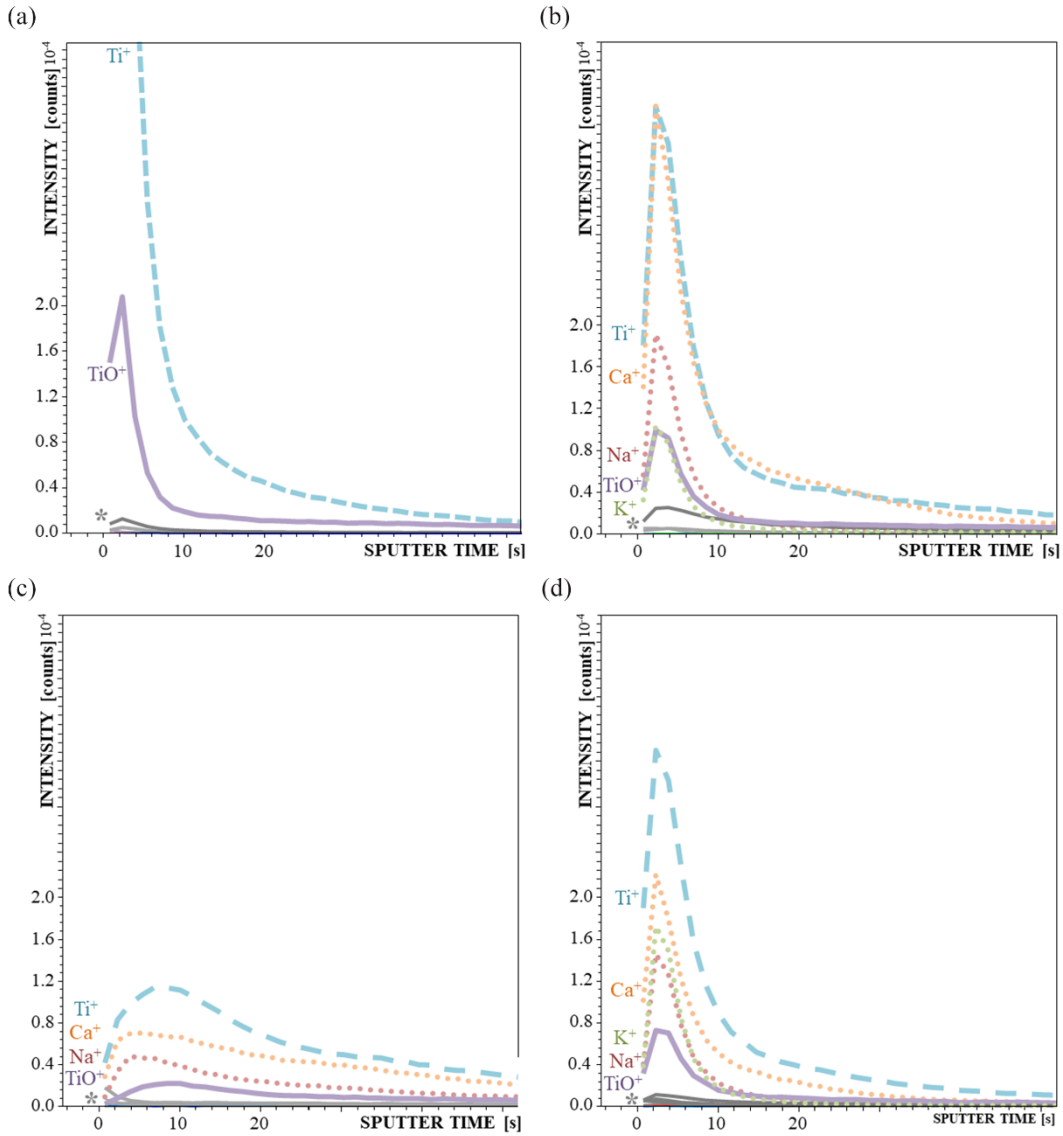

Figure 2.3: ToF-SIMS depth profiles of selected signals measured on Ti foil (a) EP and (b) UT samples from Supplier 1 and (c) EP and (d) UT samples from Supplier 2.

We confirmed that the NTs grow inwards to the Ti foil and that the surface roughness of the NTs follows the initial roughness of the Ti foil. A few nanometres (nm) at the top of the oxide layer contain no traces of the F^-, as it evaporates during the annealing. However, after those few nm, the concentration of F^- is among the largest detected, and it is constant in the case of UT samples and slowly decreasing in the EP samples. The primary function of F^- is shaping the NTs; therefore, the more F^- there is, the more precise the NTs' shape is. One theory suggests that OH^- can eliminate the fluorine ions adsorbed at the oxygen vacancies and the Ti atoms. That removal then increases the number of surface oxygen vacancies. Surface F^- and oxygen vacancies affect the terminal and bridging hydroxyl and thus influence the surface acidity [200]. If compared with F^-, the measured OH^- directly influences the photocatalytic activity.

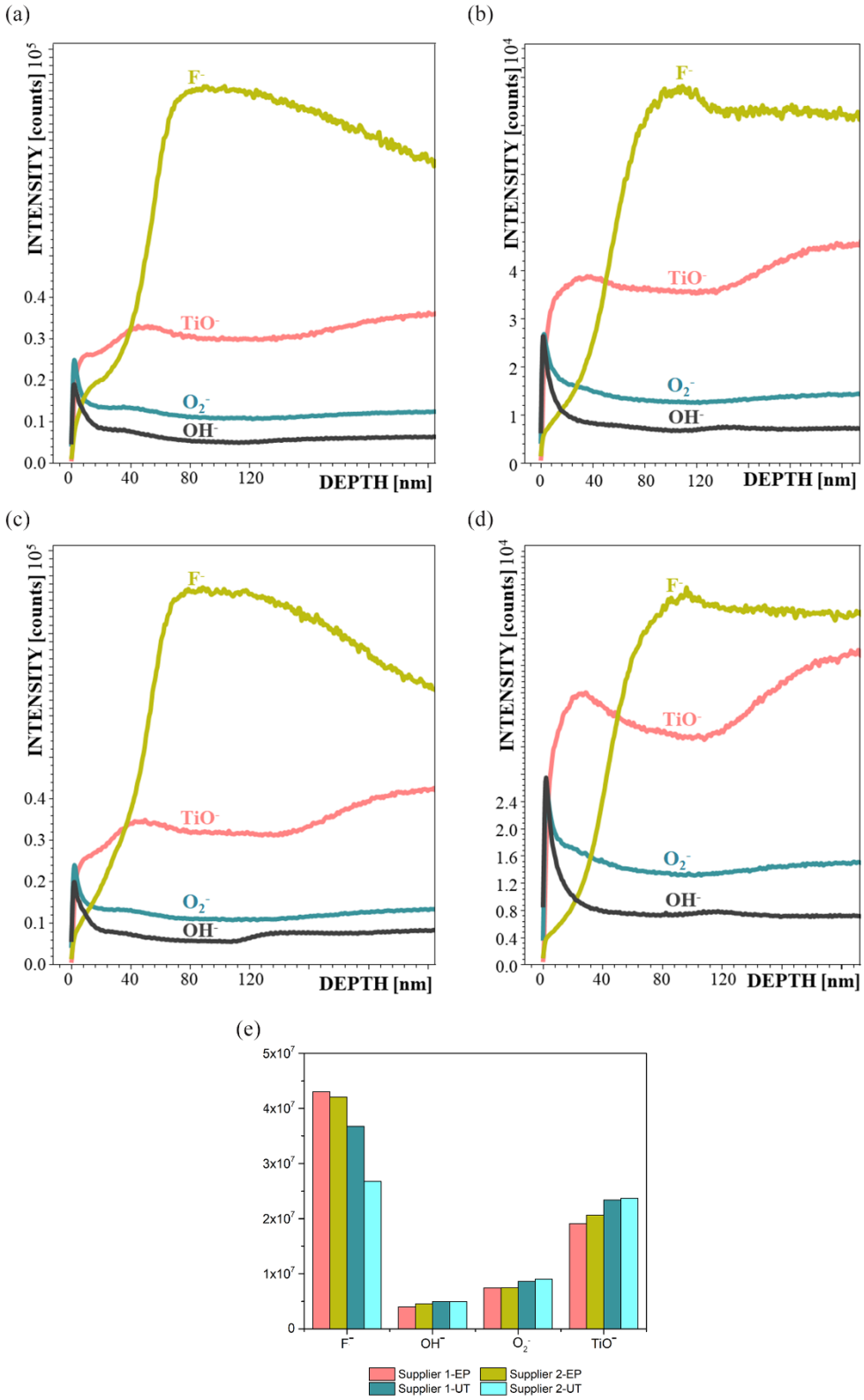

Figure 2.4: ToF-SIMS measurements of TiO_2 NTs (a) EP and (b) UT samples from Supplier 1 and (c) EP and (d) UT samples from Supplier 2, and (e) integrals of SIMS signals over a depth of 250 nm for all the samples.

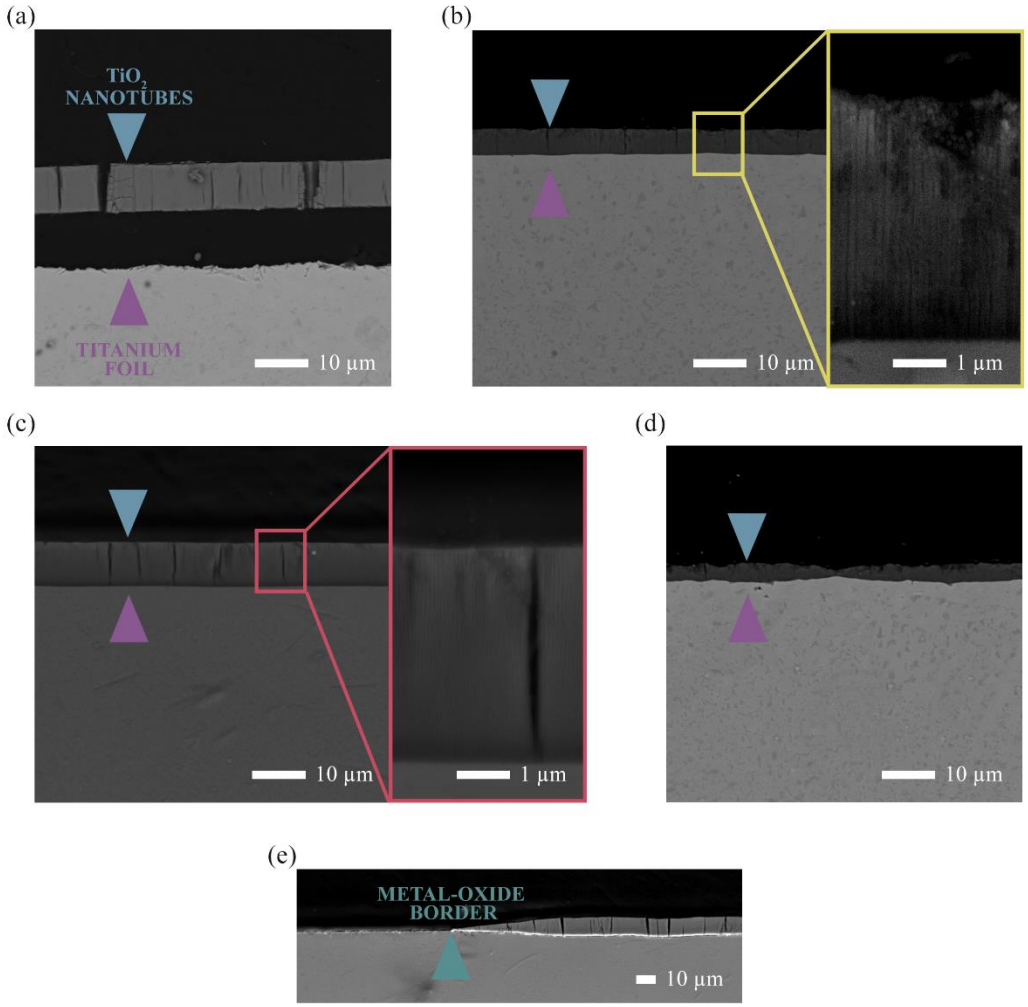

Figure 2.5: Cross-section SEM micrographs of Ti foils and TiO_2 NTs; (a) EP and (b) UT samples from Supplier 1 and (c) EP and (d) UT samples from Supplier 2. Individual NTs are shown magnified. Blue and violet arrows mark the NTs' layer thickness. (e) The metal-oxide border is marked; the NTs' layer is thinner at the edge. It is clear that the NTs grow into the substrate.

2.1.3 EBSD Analysis of Titanium Foils from Both Suppliers

Figure 2.6 shows the orientation maps (IPF-Z-colour coded), inverse pole figures and pole figure plots of the grain orientation in titanium foils from both suppliers. The EBSD data revealed a significant difference in grain size between the Ti foil provided by both suppliers. It was already mentioned that the properties of the substrate influence the physical, chemical, and electrochemical characteristics of titanium and, consequently also, the growth and uniformity of the NTs. As such, the information on the texture and grain size distribution, a preliminary guess can be made for the behaviour of grown TiO_2 NTs in the photocatalysis process. First, smaller grains equal higher grain-boundary surface density, which means more nucleation sites for NT growth, as it is not uncommon that the grain boundaries function as charge-trapping centres. That means that the active surface area of NTs will be higher and photocatalytic activity will be more prone to the degradation of organic pollutants. However, the higher density of grain boundaries means more stress was incorporated into the material during production. And that could lead to uneven growth of NTs and, consequently, to worsened electron transfer. Secondly, Leonardi et al. [150]

confirmed that the atomic density of different planes significantly influences oxide growth. It was concluded that a decreasing planar atomic density increase the growth rate and that low-packed planes are more suitable for constant oxide growth.

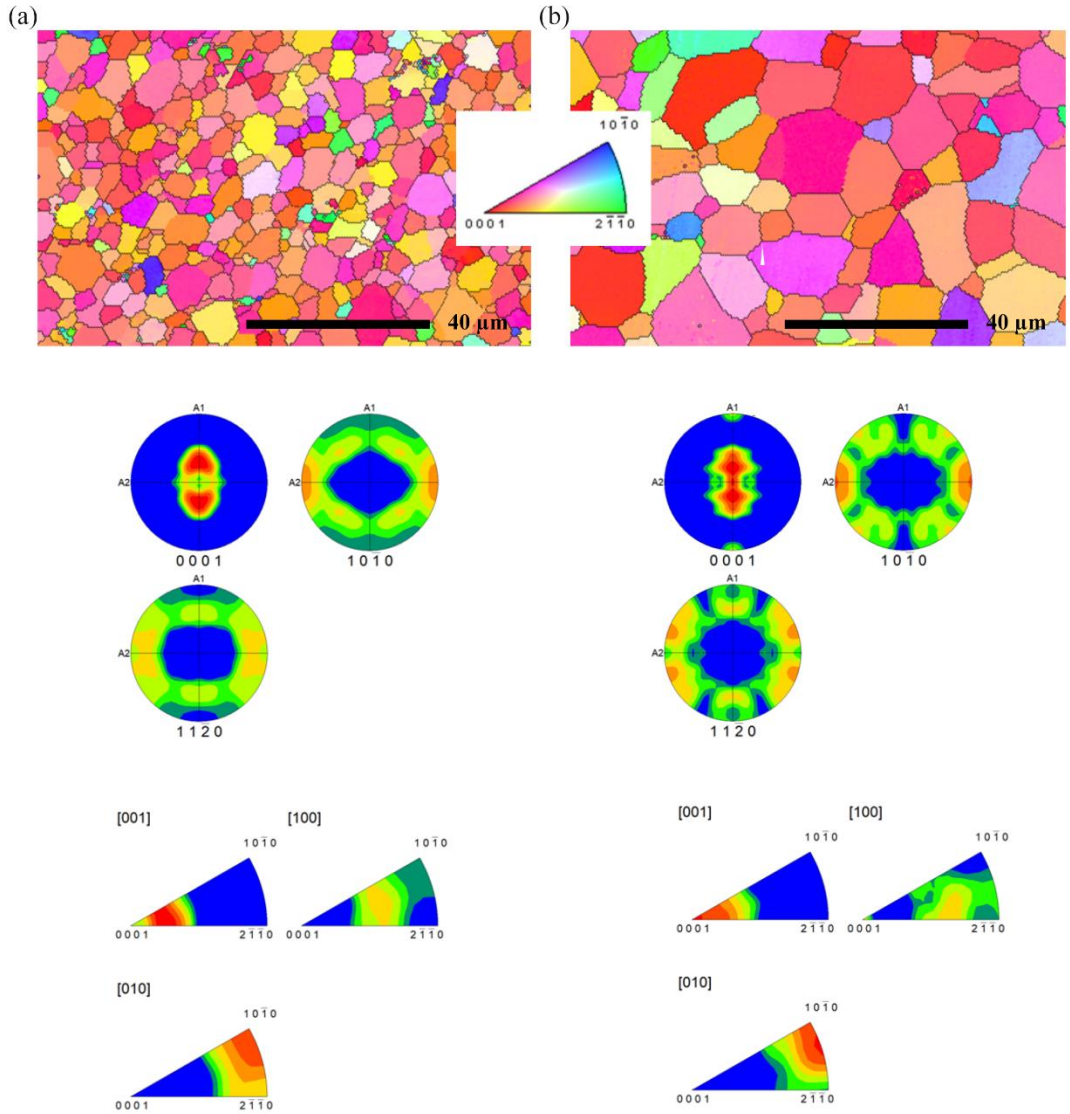

Figure 2.6: Orientation maps (IPF-Z-colour coded) and inverse pole figure (IPF) plots of grain orientation obtained from polished samples of (a) Supplier 1 (a) and Supplier 2 (b).

Chapter 3

Toward a Flexible and Efficient TiO_2 Photocatalyst Immobilized on a Titanium Foil

The previous chapter investigated Ti foils from two different suppliers in terms of the starting morphology, their chemical composition and the growth of NTs. Because the UT Ti foil from Supplier 1 yielded the most photoactive NTs, it was decided to continue experimenting with this Ti foil. Additional Ti foils with different thicknesses of 30, 50 and 100 and 200 µm were purchased in order to investigate which anodised Ti foil would withstand the bending after annealing and/or if bent Ti foils would produce photoactive NTs during the anodisation.

This chapter addresses the thesis **objective** of *how Ti foil thickness affects TiO_2 NTs' growth and the rigidity of their attachment to the Ti substrate* with the following working **hypotheses**:

3. High NTs density, shorter NTs, and fewer cracks result in better adhesion of the TiO_2 NT layer to the Ti substrate.

4. Higher grain-boundary surface density represents more nucleation sites for NT growth.

5. Higher surface roughness of TiO_2 NTs equals larger active surface area and thus higher photocatalytic activity in the degradation test.

The chapter presents an **article** with the title "*Toward a Flexible and Efficient TiO_2 Photocatalyst Immobilized on a Titanium Foil*" (**Živa Marinko**, Luka Suhadolnik, Barbara Šetina Batič, Vid Simon Šelih, Boris Majaron, Janez Kovač and Miran Čeh) that was published in the ACS Omega journal, Vol. 6 in 2021. The ACS Omega journal issue where the article was published used our proposed image for the issue's cover. The results of this work were also successfully presented at conferences listed in the Bibliography section.

This part of my research was dedicated to defining the thickness and morphology of Ti foils that would be useful as flexible and/or flat photocatalysts considering the firmness of the attachment of the NTs to the Ti substrate and the ability to degrade organic pollutants. In the Appendix of this Chapter, some additional (and not yet published) results contribute to the understanding of the already published results.

Three major demands for efficient photocatalytic reactors for purification applications are *(1)* effective photocatalyst, *(2)* maximized illumination and *(3)* smart reactor design. So far, the photocatalyst that was most used in purification reactors was in the form of nanoparticles, as it can be attached to various substrates of more complex shapes (e.g., honeycomb-shaped photocatalyst). However, purifying reactors with nanoparticulate catalysts are not upscaled in industry because of the high probability of the catalyst being released into the environment during the degradation process. In that aspect, NTs grown with anodic oxidation are a better solution because they are rigidly attached to the Ti substrate. However, they lack diversity in catalyst design (more complex shapes tend to fail due to the incorporated stress). Therefore, our idea was to overcome this obstacle and research a flexible photocatalyst grown on an otherwise flat Ti substrate.

The first step was to identify the main differences in grain size and crystallographic orientation between the foils depending on their thickness. Then, the foils were anodised and grown TiO_2 NTs annealed with the same protocol as was used in Chapter 2. The reaction-rate constants were calculated, and most importantly, the adhesion of the NTs was determined with the Scotch Tape test in order to identify the Ti foil thickness that is suitable for bending without the NTs being detached and delaminated from the Ti substrate. The efficiency was assessed by caffeine degradation and photoluminescence measurements.

After the manuscript was published, we performed additional experiments presented in the Appendix section. These included the EPR measurements in determining the hydroxy radical's concentration to clarify the differences in photocatalytic activity of the samples and anodization of the Ti foils using differently aged electrolytes. The NTs' growth was monitored during each electrolyte generation, and the photocatalytic activity was measured after each anodisation.

Regarding my contribution: I examined the Ti foil surface under FEG-SEM and measured the surface-roughness factors using stylus profilometry. Next, I anodised selected samples and annealed them. Regarding the NT characterization, I determined the NTs' length, NTs' film porosity, the area of cracks, the surface roughness of the TiO_2 NT surface layers and the adhesion of TiO_2 NTs to the Ti substrate. Finally, my contribution was to perform photocatalytic activity measurements on the anodised samples and evaluate the EPR measurements. I wrote the first draft of the paper and then finished the manuscript with the co-authors before submitting it for publication.


ACS
OMEGA
pubs.acs.org/acsomega
Volume 6, Issue 36
September 14, 2021
VOC
VOC
VOC
H_2O
CO_2
H_2O
CO_2
H_2O
ACS Publications
Most Trusted. Most Cited. Most Read.
www.acs.org

ACS OMEGA

http://pubs.acs.org/journal/acsodf

Article

Toward a Flexible and Efficient TiO_2 Photocatalyst Immobilized on a Titanium Foil

Živa Marinko,* Luka Suhadolnik, Barbara Šetina Batič, Vid Simon Šelih, Boris Majaron, Janez Kovač, and Miran Čeh

Cite This: https://doi.org/10.1021/acsomega.1c02862

Read Online

ACCESS | Metrics & More | Article Recommendations | Supporting Information

ABSTRACT: Titanium foils of different thicknesses were anodized, and the photocatalytic activity of the resulting TiO_2 nanotube (NT) layers was determined. All of the titanium foils were anodized simultaneously under identical experimental conditions to avoid the influence of the aging of the anodizing electrolyte and other anodization parameters, such as voltage, time, and temperature. To characterize the microstructures of the titanium foils, we used electron backscatter diffraction (EBSD), scanning electron microscopy (SEM), and stylus profilometry analyses. The adhesion was tested with a Scotch tape test and the morphology of the TiO_2 NTs was studied in detail using the SEM technique, while the surface areas of the TiO_2 NTs were determined using a three-dimensional (3D) optical interference profilometer. With X-ray diffraction (XRD) and X-ray photoelectron spectroscopy (XPS), the chemical composition and structure of TiO_2 oxide were established. The degradation of caffeine under UV irradiation was measured with a high-precision UV−vis−IR spectrophotometer, and the photoluminescence method was used to confirm the photocatalytic behavior of the TiO_2 NT layers. The influence of the intrinsic properties, including twinning and the grain boundaries of the starting titanium foils with similar chemical compositions, was determined and explained. Finally, we identified the main characteristics that define a highly effective and flexible photocatalyst.

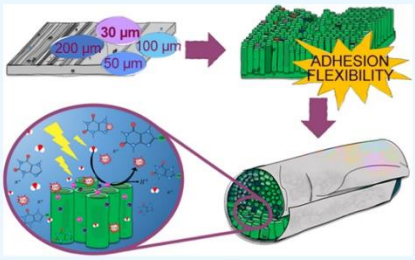

INTRODUCTION

Increasing levels of water pollution demand improved technologies for the degradation of organic pollutants in wastewaters. The photocatalytic degradation of such organic pollutants using a TiO_2 catalyst is one of the most attractive technologies to deal with this problem, as recognized by Fujishima and Honda[1] and in the pioneering work of Frank and Bard.[2] Since then, many research groups have contributed to this topic because of its immense potential and the possibility of practical use.

The technological application of TiO_2-based photocatalytic degradation of organic compounds using photocatalysis requires not only a high photocatalytic activity and a large surface area of the catalyst but also strong adhesion to a substrate or scaffold.[3−5] Flexibility of the active catalyst would also be beneficial in many applications.[6−9]

TiO_2 nanotube (NT) layers can be grown on titanium metal with the electrochemical process of anodic oxidation.[10−18] As a result of the growth mechanism, such TiO_2 NTs exhibit excellent adhesion to the titanium substrate. For this reason, they can be used directly as a platform for the degradation of organic pollutants in wastewaters.[19] Moreover, due to their connection with the substrate, they will not be released into the environment during the degradation process. Due to the many factors that influence TiO_2 NT growth, a lot of research has been done on the anodic oxidation of metal titanium in various forms. TiO_2 NT growth and photocatalytic activity are tuned with the parameters of the anodization process, like voltage, time, electrolyte composition, and pH. Additionally, the TiO_2 NTs can be modified with post-treatment processes, such as annealing or doping to move the band gap closer to visible light.[12,20−24] However, much less work has been done on the influence of the titanium substrate's properties on TiO_2 NT growth. While some earlier research was focused on the crystallographic orientation of the grains in the titanium foil and the morphology of the starting surface,[25−29] information on how the thickness of the foil influences the TiO_2 NT growth during anodization is scarce.[30]

Titanium foils, like any other metal foil, can be produced using cold or hot rolling. The titanium foils in this study were produced with cold rolling. A so-called roll coating can form

Received: June 3, 2021
Accepted: August 4, 2021

during the process, which greatly deforms the surface of titanium.[31] Moreover, the transfer of the material between the titanium sheets and the rolls often results in surface contamination and increased surface roughness.[32] However, the largest impact on the microstructure of titanium is the occurrence of plastic deformations, such as dislocation slips and twinning.[33−37] Chun et al.[35] studied twinning in commercial titanium foils and the formation of twins during the cold rolling process. The twinning was activated at a lower titanium thickness reduction, while during higher deformations, dislocation slip was the only mechanism of deformation. They also confirmed the formation of compressive twinning {11−22} <11-2-3> and tensile twinning {10−12}<10-1-1> and observed the formation of secondary and tertiary twins during the rolling process.

Of the many processes used to synthesize photoactive TiO_2 NTs, only anodic oxidation results in ordered layers of rigidly attached TiO_2 NTs on a metal titanium substrate. Any form of titanium can be anodized, meaning such catalysts can be used in a wide range of applications. We anodized titanium foils from the same supplier, but with different thicknesses. By combining various analytical techniques, we studied the influence of the chemical, structural, and morphological properties of the starting titanium foils on the growth mechanism, NT morphology, and the resulting photocatalytic activity of the anatase TiO_2 NTs. The main goal of our investigation was to synthesize a flexible photocatalyst that would withstand the stress and deformation of the otherwise flat TiO_2 NT layer. We successfully determined which foil thickness results in the most rigidly attached TiO_2 NT layer during the anodization of a flat titanium foil.

RESULTS AND DISCUSSION

Microstructure Properties of the Starting Titanium Foils. The surface morphology investigation of the as-received titanium foils using a field emission gun scanning electron microscope (FEG-SEM) revealed significant differences between the samples of different thicknesses (30, 50, 100, and 200 μm). Different rolling patterns, scratches, and other markings were the most significant features, as shown in Figure S1. It can be seen that the 30 and 100 μm samples have a similar surface with more obvious surface variations than the other two samples, where the difference in surface roughness is smaller. Meanwhile, the 200 μm sample appeared with pores on the surface and the 50 μm sample with the least surface undulations among the samples. A strong relationship between the surface roughness and the TiO_2 NT growth has been reported previously by many research groups.[38−40] To better understand the scale of the surface undulations, we three-dimensionally (3D) mapped each sample with a stylus profilometer. The results revealed the anisotropic nature of the foils' surfaces. The calculated average roughness factor (R_a) and the peak-to-valley factor (R_t), assessed over a 4 mm line across the surface, are presented in Table 1, and the roughness profiles are shown in Figure 1A. The highest surface roughness and the average peak deviation were observed for the 100 μm sample. The thinnest foil (30 μm) has a similar morphology but lower values of both factors. In contrast, the 200 μm sample has an even distribution of hills and valleys along the rolling direction, and the 50 μm sample exhibits the flattest surface among the tested foils with the lowest average roughness values. Since the thinnest titanium foil was produced by cold rolling the thickest titanium foil, we expected

Table 1. Average Roughness (R_a) and Peak-to-Valley Factor (R_t) Measurements

foil thickness (μm)	R_a (μm)	R_t (μm)
30	0.14 ± 0.01	1.23 ± 0.16
50	0.11 ± 0.02	1.42 ± 0.42
100	0.29 ± 0.01	2.52 ± 0.33
200	0.16 ± 0.01	1.24 ± 0.12

that both roughness factors would have the highest values in the 200 μm sample. However, significant undulations, in the form of individual ripples, from 0.8 μm in depth to 1.6 μm in height, were characteristic for the 100 μm sample. This resulted in higher roughness compared to the 30, 50, and 100 μm samples, where the rolling pattern (the distribution of peaks and valleys) was even and the z-axis values were significantly lower.

The chemical composition of all four samples showed that they contained more than 99.8% titanium (Figure 1B). The least pure was the 100 μm sample, with 99.8% of titanium in the foil. The main impurity detected in the titanium foil was iron.[40] The values were decreasing from 100, 200, and 30 to 50 μm sample with percentages of 0.09, 0.03 (200 and 30 μm), and 0.02%, respectively. Another chemical element that had a significantly higher concentration in the 100 μm sample was aluminum, with 0.05%. Other impurities identified in all four samples were zinc, silicon, manganese, nickel, and potassium. Although the measured concentrations are low, the impurities could influence the physicochemical properties and the NT growth through incorporation in the anodic oxide. A similar process is known for the migration of fluoride ions from the electrolyte to the oxide layer, and their influence on the NT formation and the related photocatalytic activity.[41] Moreover, higher impurity concentrations could result in surface functionalization or modulation of the photocatalytic properties of the TiO_2 NTs, as can be seen in the anodization of Ti alloys.[42]

The crystallographic orientation map of individual grains in the foils for each sample is shown in the center columns of Figure 2A. To the left of the maps are the corresponding grain size histograms, and on the right are the corresponding histograms of the grain misorientation angles between 15 and 95°. Pole figure plots obtained from the EBSD are shown in Figure 2B. Additionally, refer to Figure S2 for the inverse pole figures (IPF) for all samples. Titanium crystallizes in the hexagonal close-packed crystal system. Backscatter imaging and EBSD analyses showed only the presence of α-Ti. This system has a low lattice symmetry and few slip systems, so the texture forms easily during deformation or processing, such as rolling and annealing. The principal slip systems in Ti are prismatic {10−10} <11−20>, secondary basal {0001} <11−10>, and two pyramidal {10−11} <11−20> and {11−22} <11−23>. During the cold rolling, titanium tends to form textures with basal poles tilted at ±20 to 40° from the normal direction.[43] The occurrence of twinning depends on the surface deformation of the starting titanium foil. All of the analyzed titanium foils exhibited a strong rotated basal texture with a distinct TD split associated with rolling.[34] However, the twinning was reduced when the titanium foil was thinner.[44] The rotation was between 25 and 40°. A very strong texture associated with tensile twinning ({10−12} <−1011>) was observed in the 100 μm sample, where twins were also prominent in the microstructure. These results provide

https://doi.org/10.1021/acsomega.1c02862
ACS Omega 2021, 6, 23233−23242

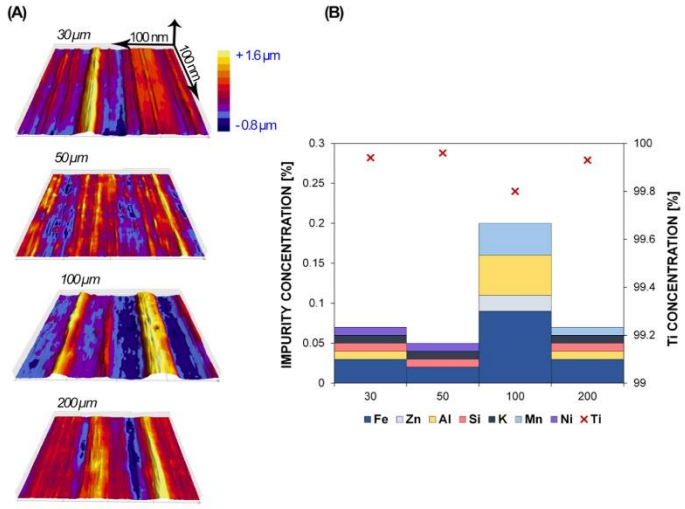

Figure 1. (A) 3D stylus profilometry mapping of the four metal titanium foils with different thicknesses. The marked *z*-axis is equal for all samples. (B) Inductively coupled plasma optical emission spectrometry (ICP-OES) analyses of all four foils. The purity of the titanium foil is marked with an "x" and the impurities indicated with color bars.

important insights into the evolution of the texture of the thinnest titanium foil.

Cold rolling additionally influences the grain size since more pronounced rolling results in smaller grains. The size of the grains can be directly linked to the material's strength; the smaller the grains, the more strength the material has.[45] The average grain size was determined for each titanium foil thickness and the grain distribution appeared specific for each sample. A Gaussian distribution of grains was specific for the 30 μm thick foil with grains averaging 2.5 μm in diameter, for the 50 μm foil with grains averaging 5.5 μm in diameter, and for the 200 μm foil with an average grain size of 4.25 μm in diameter. A significantly wider and more uniform distribution was characteristic for the 100 μm thick foil with grain diameters up to 10 μm. Interestingly, with the decreasing thickness of the titanium foil, the grains were not elongated but instead remained more or less equiaxed.[37] However, some elongation was observed due to the occurrence of slip.[35] The distribution of the grains was also observed in the polished titanium foil's cross sections (not shown here) under an optical microscope. Although the grains were evenly distributed over the foils' cross section, a notable feature was observed for the 100 μm foil. While the 30, 50, and 200 μm foils were characterized by small grains, the 100 μm sample was dominated by significantly larger grains (a smaller number of grain boundaries), which could influence the material's ductility due to reduced residual stress at the grain boundaries.

Characteristics of the Annealed TiO_2 NT Layers. The behavior of the anodization current was observed for the different thicknesses of the titanium foils. During the process, amorphous TiO_x was grown. The anodization current/time curves measured during the first 30 min of anodization with a fresh electrolyte for all foils are presented in Figure 3A. After that time, the current oscillations were not significant as the growth reached a steady state. At the beginning of the anodization of the 200 μm foil, the current was the highest, i.e., 0.023 μA, whereas, for the 100, 50, and 30 μm foils, the currents were 0.015, 0.016, and 0.015 μA, respectively. After the initial stage of anodization, the current gradually decreased with time, until it reached a steady-state value of 0.001−0.002 μA.

Figure 3B shows the TiO_2 NT layers' surfaces, measured with a 3D interference optical profilometer to determine average surface roughness. Surface regions that are higher (red) or lower (blue) than the average surface height (green) are presented. The measurements show that the thinnest foil (30 μm) exhibits the most prominent average surface roughness (0.5 μm) and average peak-to-valley (21.3 μm) profile compared to the other three samples. Analyses of the surface profile maps revealed that the TiO_2 NT layer cracks are also significantly wider than those in the other samples. Moreover, individual NTs inside the cracks were visible in the cross sections. This contributed a great deal to the larger surface area since the overall measured surface roughness is the sum of the TiO_2 NT surface and the NT wall surfaces exposed in the cracks. The second highest average surface roughness (0.4 μm) and average peak-to-valley (15.2 μm) profile were measured for the 100 μm thick anodized foil. Analyses with a stylus profilometer (see Figure 1A) showed that the key contributions to the roughness were the individual surface deviations across the NT layer (red lines in Figure 3B). Compared to the other three samples, there are not many cracks in the TiO_2 NT layer in the 100 μm sample. The anodized 200 and 50 μm thick foils have the lowest values, i.e., 0.3 and 0.2 μm, for the average surface roughness, and 13.1 and 12.1 μm, for the average peak-to-valley profile, respectively.

https://doi.org/10.1021/acsomega.1c02862
ACS Omega 2021, 6, 23233−23242

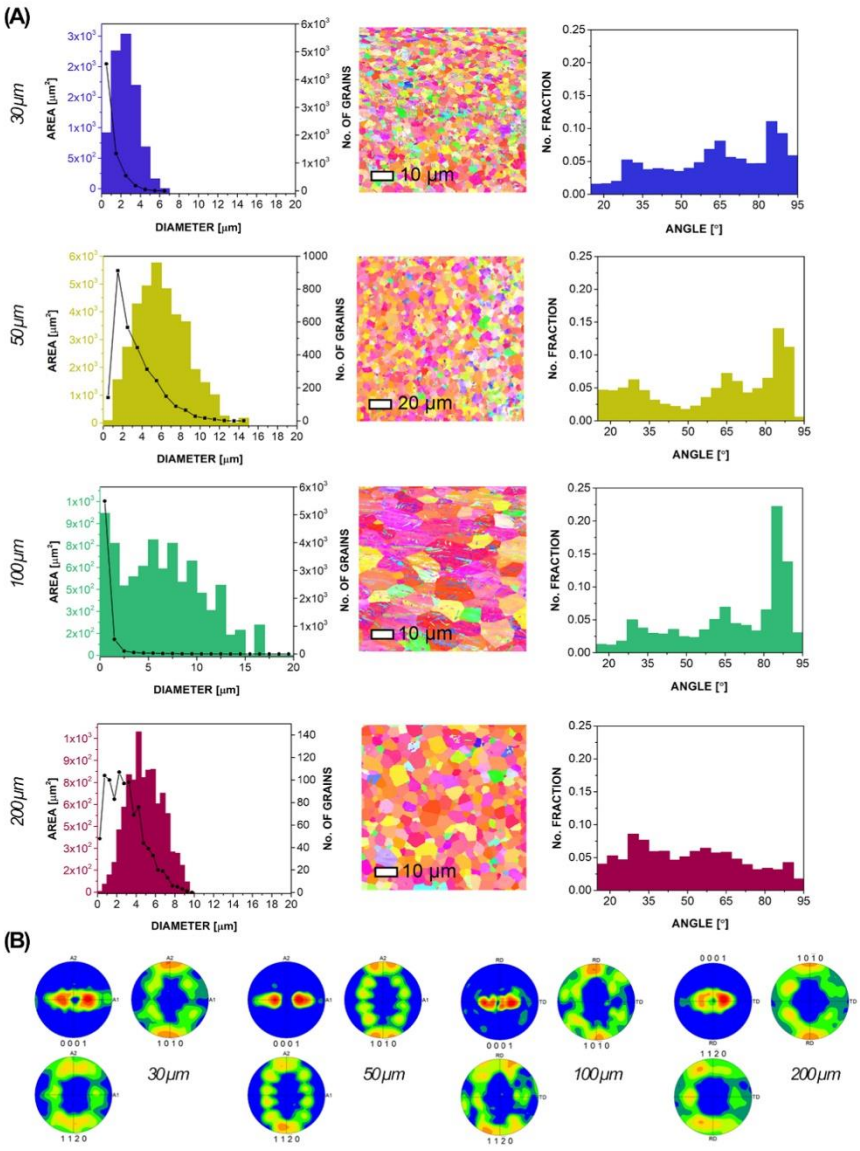

Figure 2. (A) Orientation maps (IPF-Z color coded) for titanium foils of different thicknesses are shown between two histograms. The grain size distribution on the left, where the bars represent the area of the grains and the line shows the number of grains, and the grain boundary misorientation angle distribution histograms on the right. (B) The corresponding pole figure plots of grain orientations obtained from the EBSD data.

https://doi.org/10.1021/acsomega.1c02862
ACS Omega 2021, 6, 23233−23242

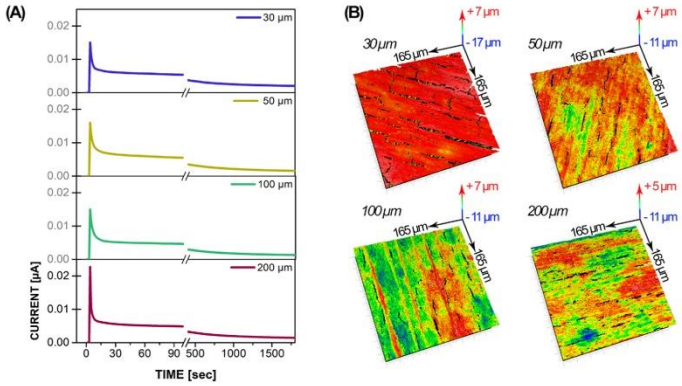

Figure 3. (A) Current/time measurements during the anodization of titanium foils with different thicknesses in the fresh electrolyte. (B) TiO_2 NTs' surface roughness as measured with a 3D interference optical profilometer.

Table 2. Analyses of TiO_2 NTs' Dimensions

		double-walled NTs			single-walled NTs
foil thickness (μm)	NT length (μm)	outer wall (nm)	inner wall (nm)	NT diameter (nm)	NT diameter (nm)
30	21.6 ± 0.7	18.6 ± 2.8	33.9 ± 4.1	148 ± 5	101 ± 16
50	21.9 ± 0.4	17.6 ± 2.7	32.7 ± 3.8	150 ± 11	94 ± 9
100	18.0 ± 0.9	18.1 ± 2.5	37.4 ± 5.2	151 ± 13	104 ± 8
200	21.2 ± 1.5	17.9 ± 2.5	36.3 ± 4.3	146 ± 9	97 ± 10

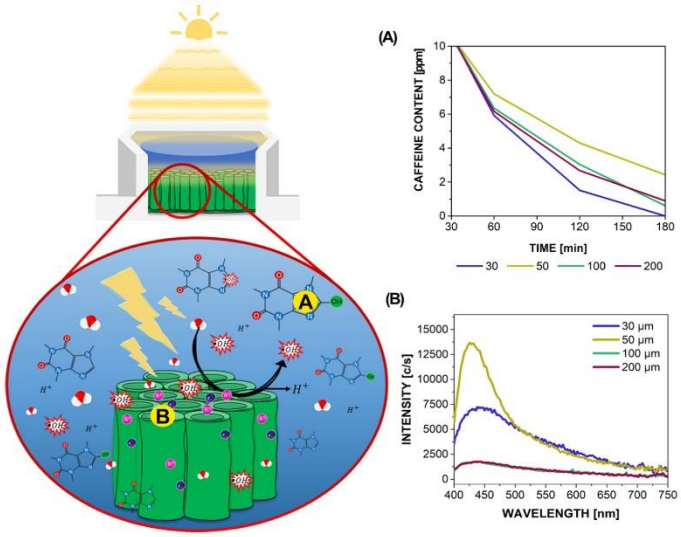

Figure 4. Photocatalytic activity of four TiO_2 NTs samples. Main aspects of this section's research are presented. (A) Caffeine degradation and (B) photoluminescence measurements.

While the morphological characterization of the annealed TiO_2 NTs resulted in interesting findings, their crystallographic structures and chemical compositions did not show significant differences (see Section S2 in the Supporting Information).

https://doi.org/10.1021/acsomega.1c02862
ACS Omega 2021, 6, 23233−23242

Analyses of the micrographs presented in Table 2 show that the NTs' average length is approximately 21 μm, except for the 100 μm sample, where the NTs are shorter (18.0 ± 0.9 μm). Analyses of the detached TiO_2 NT layer's bottom part revealed the double-walled NTs. The average thickness of the outer wall is similar for all of the samples, on average 18 nm. Meanwhile, differences in the inner wall thicknesses were more significant, but still within the measurement uncertainty. Variations in the measured values suggest that the TiO_2 NTs were not uniform. The overall diameter of the NTs (including the hollow part) was similar across the four samples (from 145 to 151 nm) and the analyses of the top surface of the TiO_2 NTs revealed that the double wall at the bottom was converted into single-walled NTs at the top during the growth/crystallization process.[46] The NTs near the top surface were, on average, 40 nm narrower in diameter than those at the bottom, which could be attributed to the prolonged etching by fluoride ions during anodization or removal of the carbon remnants on the inner wall during the annealing process.[47,48]

To investigate the adhesion of the TiO_2 NTs, we performed the Scotch tape test.[49,50] Due to the easy handling and no loss of material on the thinnest sample, it was expected that the adhesion would be the strongest, with the NT layer on the thickest foil having the poorest adhesion. However, by observing the area around the X-cut under the optical and FEG-SE microscopes, we found that almost all of the NTs peeled off the surface of the 30 μm foil easily (Figure S6). In contrast, the NTs' adhesion was the strongest to the 100 μm foil, followed by the 50 and 200 μm foils. The results are shown in Figure S6 in the Supporting Information. The adhesive properties of the NT layer are closely related to (1) the NT length, (2) the number of cracks in the TiO_2 NT layers, and (3) the surface roughness of the NTs.[51−53] Longer NTs and a larger number of cracks in the NT layer tend to weaken the adhesion. Meanwhile, uniform TiO_2 NT layers tend to strengthen it. Cao et al.[51] suggested that interfacial adhesion between the NT layer and the titanium foil is responsible for the adhesive strength, which decreases with the increase of the thickness of the TiO_2 layer. To conclude, we observed that the reason for the delamination and detachment of the TiO_2 layer is not straightforward; instead, it is a complex phenomenon influenced by the above properties.

Measurements of the Photocatalytic Degradation. The schematic presentation of our results related to photocatalysis and the photocatalytic activities of the as-synthesized TiO_2 NTs is presented in Figure 4 and is linked to the caffeine degradation results (Figure 4A) and the photoluminescence (PL) measurements (Figure 4B). Both are closely connected by providing information on some level of the photocatalytic reaction.

The caffeine degradation test, presented in Figure 4A, showed that all of the samples have the ability to degrade molecules in a 10 ppm initial aqueous solution within 3 h of UV exposure (additionally, refer to Figure S7 for the exponential curve fitting for all of the samples). The drop in caffeine concentration occurred at different rates. The corresponding initial rate constants were calculated by the following formula, assuming a first-order reaction[54]

$$K \times t = -\ln(C(t)/C_0)$$

where C is the caffeine concentration at time t and C_0 is the initial caffeine concentration.[55] The results in Table 3 revealed that the 30 μm sample exhibited the best photocatalytic activity by far, followed by the 100 and 200 μm samples, while the 50 μm sample showed the least activity. The 30 μm sample achieved the complete degradation of caffeine in less than 3 h, followed by the 100 μm sample with 99.4%, the 200 μm sample with 99.1%, and the 50 μm sample with 97.6% degradation efficiency. These results confirmed that the 30 μm foil gave the best photocatalytic result since it has the largest specific surface area (Figure 3B), which is the primary factor for degradation efficiency.[56]

Table 3. Reaction Rate Constants for Caffeine Degradation

foil thickness (μm)	reaction rate constant k ($\times 10^{-2}$ min^{-1})
30	2.12 ± 0.13
50	1.04 ± 0.06
100	1.59 ± 0.12
200	1.65 ± 0.07

Finally, the photoluminescence (PL) signal is attributed to electron−hole recombination, meaning that fewer recombinations result in a lower PL signal. These measurements provided us with additional knowledge about the presence of the TiO_2 photoactive sites. The measured PL spectra of the TiO_2 NT layers are presented in Figure 4B (lines are calculated from multiple scans). The 50 μm foil had a narrower and high-intensity peak around 430 nm. This measurement points to poor photocatalytic activity, which was already confirmed with the worst caffeine degradation measurements among the four samples. In addition, all samples possess wider bands between 400 and 540 nm. Broader photoluminescence spectra are typical for the presence of oxygen vacancies and defects on the TiO_2 surface.[57,58] With oxygen vacancies, the photoexcitation shifts slightly toward visible light, enhancing the photocatalytic activity.[59] Meanwhile, the lowest measured intensities were for the 100 and 200 μm foils, which indicated higher photocatalytic activity due to a decreased recombination rate and increased amounts of adsorbed O_2. The 50 and 200 μm samples showed a significant drop in photostability during the PL measurements. The PL measurements confirmed the influence of defect sites responsible for the signal, i.e., from the impurities and defect sites that originate from the titanium foil and can be found on the TiO_2 NT layer (Figures 1, 2, and S5) to oxygen vacancies and titanium species like Ti^{3+} in anatase TiO_2 (Figure S3). In particular, the defect sites associated with the oxygen vacancies are preferred for the adsorption of molecular oxygen onto the TiO_2 surface.[60] Please refer to Characteristics of the Annealed TiO_2 NT Layers section in the Supporting Information for more information regarding X-ray photoelectron spectroscopy (XPS) and TiO_2 NT's top surface analysis.

■ CONCLUSIONS

This paper presents thorough structural, morphological, and photocatalytic degradation studies of rigidly attached TiO_2 NT layers obtained by the anodic oxidation of titanium foils for use in flexible annular photocatalytic reactors for the degradation of organic pollutants in wastewaters. We investigated titanium foils with four different thicknesses. While many studies have noted the importance of the surface properties of the starting titanium material on the structural and morphological TiO_2 NT characteristics, only very few studies focused on a correlation with the TiO_2 NTs' photocatalytic activity.

Significant differences were observed in the surface roughness, chemical composition, grain size distribution, and

https://doi.org/10.1021/acsomega.1c02862
ACS Omega 2021, 6, 23233−23242

crystallographic orientation after the stylus profilometry, ICP-OES, and EBSD analyses were performed. It was shown that even minor differences in the titanium foil's purity could greatly improve/deteriorate the structural, morphological, and optical properties. Moreover, a titanium substrate with higher purity results in a TiO_2 NT layer with higher photocatalytic activity.[61] The least pure sample (100 μm) with a significant iron content resulted in the second best active sample. However, the chemical composition is not the only determining factor in photocatalytically active NTs. Our study confirmed the influence of the anodization parameters and the titanium properties on the formation of the passive oxide layer and the NT formation during the process of growth. It is known that ultrafine-grained metals contain more surface defects and have a higher density of grain boundaries, which means a larger number of nucleation sites for the growth of NTs. Consequently, they are less resistant to corrosion than substrates with larger grains during the anodization process, leading to faster NT growth and longer NTs. This effect was clearly seen in our experiments, where the 100 μm foil sample had the largest grains and therefore resulted in the shortest TiO_2 NTs.

Moreover, the morphological and compositional changes of the NT layer were successfully determined with various characterization techniques. Photocatalysis is a complicated process that involves morphological and optical properties. Significant morphological differences reflected in the photocatalytic activity were confirmed by measuring the optical properties and the efficiency of the caffeine degradation. Measurements of surface roughness showed that the highest surface area was available on the 30 μm foil, where complete degradation of caffeine was also measured. A considerable number and width of cracks were observed in this sample. These affect the light scattering during the production of radicals and, with that, reduce the concentrations of radicals produced. The 100 μm foil sample, which exhibits the least cracked TiO_2 NT layer surface also had the most adhesive NTs with respect to the substrate (measured with the Scotch tape test). Meanwhile, the adhesion test of TiO_2 NTs showed how poorly the TiO_2 NTs from the thinnest foil were attached to titanium. Our study showed that the main factors contributing to strong adhesion were the NT surface with fewer cracks and shorter NTs, which were the main characteristics of the 100 μm foil sample.

Our results showed that the thinnest titanium foil, although with the best caffeine degradation result, is not the most appropriate for preparing a flexible photocatalyst due to the poor adhesion of NTs to the titanium substrate. On the contrary, the 100 μm sample showed the best results. This sample showed high photocatalytic activity and the ability to bend without the risk of cracking the NTs or detaching them from the substrate.

■ EXPERIMENTAL METHODS

Characterization of the Titanium Foil. Titanium foils (99.9% purity, Baoji Lyne Metals) were processed from a titanium slab with cold rolling. We used titanium foils with starting thicknesses of 30, 50, 100, and 200 μm. The surface morphologies of the as-received titanium foils were examined using a field emission gun scanning electron microscope (FEG-SEM; JSM-7600F, JEOL), while the surface roughness, measured in a direction perpendicular to the factory rolling, was determined using a stylus profilometer (2 μm tip; DektakXT, Bruker).

The texture of the titanium foils was assessed by electron backscatter diffraction (EBSD; Hikari Super, EDAX). Before the EBSD analyses, the titanium foils were finely polished with 3 μm diamond paste, and additional OP-S (colloidal silica) polishing was applied for 5 min. Data postprocessing and analyses were performed using the OIM software package (EDAX).

The chemical composition of the titanium foils was determined by inductively coupled plasma optical emission spectrometry (ICP-OES) after the foils were digested, as follows. Accurately weighed (100 mg) pieces of the foils were digested on a hot plate using concentrated hydrochloric acid. Five milliliters of HCl (Suprapur, Merck) was added into the Ti foils and slowly heated in a covered beaker for 5 h, before being left to cool overnight. As titanium strongly resists acid attack, this procedure had to be repeated three times over several days before the Ti foils completely dissolved. The digestates were then diluted to 50 mL and measured by ICP-OES (Varian 715-ES) in a semiquantitative mode, thus revealing the chemical composition of the Ti foils.

Synthesis of TiO_2 NT Layers by Anodic Oxidation. The titanium foils were cut into 15 × 15 mm^2 samples and ultrasonically cleaned with acetone for 10 min. The samples were then rinsed with absolute ethanol and deionized water and then dried under a stream of nitrogen. The anodization electrolyte was a mixture of ethylene glycol (99.99%, Carlo Erba) and a solution of 0.3 wt % NH_4F (Sigma-Aldrich) in 2 vol % deionized water. Anodic oxidation was performed in a two-electrode electrochemical cell connected to a constant 60 V DC power supply for 3 h. A data logger (Agilent) monitored the electrical current during the entire process. The grown amorphous TiO_2 NTs on the titanium foils were rinsed with ethanol and dried under a stream of nitrogen. Afterward, these amorphous TiO_2 NTs were transformed into crystalline TiO_2 NTs with the anatase structure by annealing in a muffle furnace (Nabertherm) at 450 °C for 1 h, with heating and cooling rates of 5 °C/min.

Measurements of the Photocatalytic Degradation. The photocatalytic activity of the anodized TiO_2 NTs was measured with the degradation of a model compound, i.e., caffeine, due to its presence in wastewaters and its easy and safe handling.[62,63] Titanium foils with an anodized area of 0.8 ± 0.03 cm^2 were put in a Petri dish with 5 mL of an aqueous 10 ppm caffeine solution and placed in a sterilizer (Kambič I-265 CK UV). Under constant stirring, 200 μL of the solution was collected after 30 min in the dark. Afterward, the samples were illuminated with UV light (Ultra-Vitalux, OSRAM, UVA—from 315 to 400 nm and UVB—from 280 to 315 nm) and collected at 60, 120, and 180 min for analyses using a high-precision UV−vis−IR spectrophotometer (Lambda 950, PerkinElmer).

Characterization of the TiO_2 NT Layer. The morphologies of the anodized and annealed TiO_2 NT layers were characterized using a FEG-SEM. The average surface roughness of the TiO_2 NT layers was determined and evaluated over the surface with a 3D interference optical profilometer (ZeGage ProHR with MX Software Package, Ametek Zygo). After annealing, X-ray diffraction (XRD; X'Pert PRO, Panalytical) analysis was used to determine the crystallinity and crystal structure of TiO_2 NTs. The samples were scanned using Cu Kα radiation in a 2θ range of 20−80° for 100 s over a

https://doi.org/10.1021/acsomega.1c02862
ACS Omega 2021, 6, 23233−23242

5 mm mask. Peaks were identified with the X'Pert HighScore Plus program using the International Centre for Diffraction Data (ICDD) PDF-4+2019 database.

The photoluminescence (PL) properties of the TiO_2 NT layers were assessed using a spectrofluorometer (QuantaMaster 8000, Horiba-PTI) with a low-noise photomultiplier (Hamamatsu R2658). All of the samples were excited at 370 nm, and the emission spectra were measured between 400 and 750 nm. X-ray photoelectron spectroscopy (XPS) was used to analyze the upper 5 nm of the TiO_2 NT layers on a surface area with a diameter of 0.4 mm. The analyses were performed using a PHI-TFA XPS spectrometer (Physical Electronics Inc., Eden Prairie) with an Al monochromatic X-ray source.

Finally, the adhesion of the rigidly attached TiO_2 NTs was estimated with the Scotch tape test, following the ASTM D3359 standard. Two cuts, approximately 10 mm long and at an angle of 30−45° (X shape), were made into the TiO_2 NT layer using a clean steel blade. Just enough pressure was applied so that the blade tip penetrated the NT layer and exposed the Ti substrate. Next, a piece of Scotch tape was placed on the cut, pointing in the same direction as the smaller angles. It was pressed gently to ensure good contact with the TiO_2 layer. After the application, the tape was removed with a single quick pull. Afterward, the foils and the Scotch tape were observed under an optical microscope (Discovery V8, Carl Zeiss Microscopy). Several micrographs were stitched together and analyzed in the ImageJ program (1.53e, NIH) to determine the loss of TiO_2 NTs around the cut. Larger detached and/or delaminated areas distant from the cut were not included in the analysis. Following the analysis under the optical microscope, morphological changes on the titanium substrate and TiO_2 NT layers that occurred after the tape was pulled were inspected using the FEG-SEM (JSM-7600F, JEOL).

■ ASSOCIATED CONTENT

Supporting Information

The Supporting Information is available free of charge at https://pubs.acs.org/doi/10.1021/acsomega.1c02862.

SEM images of the metal titanium foil of different thicknesses (Figure S1); inverse pole figures (IPFs) for all samples (Figure S2); surface chemical composition in at. % and the O/Ti ratio for all samples (Table S1); high-resolution XPS spectra for (a) Ti 2p, (b) O 1s, and (c) C 1s peaks for all TiO_2 NT samples (Figure S3); XRD measurements for each sample (Figure S4); FEG-SEM micrographs of TiO_2 NTs for each foil thickness (Figure S5); adhesion of TiO_2 NTs performed with the Scotch tape test on (a) 30 μm, (b) 50 μm, (c) 100 μm, and (d) 200 μm samples (Figure S6); photocatalytic degradation of caffeine (dots) for all four samples; and exponential curve fitting (lines) for 30, 50, 100, and 200 μm samples (Figure S7) (PDF)

■ AUTHOR INFORMATION

Corresponding Author

Živa Marinko − *Department for Nanostructured Materials, Jožef Stefan Institute, 1000 Ljubljana, Slovenia; Jozef Stefan International Postgraduate School, 1000 Ljubljana, Slovenia;* orcid.org/0000-0002-6054-8137; Phone: +386-1-4773-931; Email: ziva.marinko@ijs.si

Authors

Luka Suhadolnik − *Department for Nanostructured Materials, Jožef Stefan Institute, 1000 Ljubljana, Slovenia;* orcid.org/0000-0002-9103-6687

Barbara Šetina Batič − *Vacuum Science and Optoelectronics, Institute of Metals and Technology, 1000 Ljubljana, Slovenia*

Vid Simon Šelih − *Center for Validation Tehnologies and Analytics & Department of Analytical Chemistry, National Institute of Chemistry, 1001 Ljubljana, Slovenia;* orcid.org/0000-0002-2433-5249

Boris Majaron − *Department of Complex Matter, Jožef Stefan Institute, 1000 Ljubljana, Slovenia; Faculty of Mathematics and Physics, University of Ljubljana, 1000 Ljubljana, Slovenia*

Janez Kovač − *Department of Surface Engineering, Jožef Stefan Institute, 1000 Ljubljana, Slovenia*

Miran Čeh − *Department for Nanostructured Materials, Jožef Stefan Institute, 1000 Ljubljana, Slovenia*

Complete contact information is available at: https://pubs.acs.org/10.1021/acsomega.1c02862

Author Contributions

Ž.M. and L.S.: conceptualization; Ž.M., L.S., J.K., M.Č., V.S.Š., B.M., and B.Š.: validation; Ž.M., J.K., V.S.Š., B.M., and B.Š.: investigation; Ž.M., L.S., J.K., M.Č., V.S.Š., B.M., and B.Š.: resources; Ž.M.: writing—original draft preparation; Ž.M., L.S., J.K., M.Č, V.S.Š., B.M., and B.Š.: writing—review and editing; Ž.M.: visualization; and M.Č.: supervision and project administration. All authors have read and agreed to the published version of the manuscript.

Funding

The authors would like to acknowledge the financial support from the Slovenian Research Agency (ARRS) through the following research programmes: L2-2614, P1-0034, P1-0192, P2-0056, P2-0082, and P2-0084 and funding from the European Union's Horizon 2020 research and innovation programme under grant agreement no. 823717-ESTEEM3.

Notes

The authors declare no competing financial interest.

■ ACKNOWLEDGMENTS

The authors would also like to thank Monika Koren for technical support with the photoluminescence measurements; Dr. Kristian Radan from the Electronic Ceramics Department at Jožef Stefan Institute, Ljubljana for the XRD clarification; the ULTRACOOL lab (financed by the Director's Fund 2017 from Jožef Stefan Institute, Ljubljana) for their support on working with Dektak Profilometry; and the CEMM team from Jožef Stefan Institute, Ljubljana for sharing their knowledge on electron microscopy.

■ REFERENCES

(1) Fujishima, A.; Honda, A. TiO_2 Photoelectrochemistry and Photocatalysis. *Nature* **1972**, *238*, 37−38.

(2) Frank, S. N.; Bard, A. J. Heterogeneous Photocatalytic Oxidation of Cyanide Ion in Aqueous Solutions at Titanium Dioxide Powder. *J. Am. Chem. Soc.* **1977**, *99*, 303−304.

(3) Ibhadon, A. O.; Fitzpatrick, P. Heterogeneous Photocatalysis: Recent Advances and Applications. *Catalysts* **2013**, *3*, 189−218.

(4) Dijkstra, M. F. J.; Michorius, A.; Buwalda, H.; Panneman, H. J.; Winkelman, J. G. M.; Beenackers, A. A. C. M. Comparison of the Efficiency of Immobilized and Suspended Systems in Photocatalytic Degradation. *Catal. Today* **2001**, *66*, 487−494.

(5) Bideau, M.; Claudel, B.; Dubien, C.; Faure, L.; Kazouan, H. On the "Immobilization" of Titanium Dioxide in the Photocatalytic Oxidation of Spent Waters. *J. Photochem. Photobiol., A* **1995**, *91*, 137−144.
(6) Lin, L. Y.; Yeh, M. H.; Lee, C. P.; Chen, Y. H.; Vittal, R.; Ho, K. C. Metal-Based Flexible TiO_2 Photoanode with Titanium Oxide Nanotubes as the Underlayer for Enhancement of Performance of a Dye-Sensitized Solar Cell. *Electrochim. Acta* **2011**, *57*, 270−276.
(7) Farahani, E.; Mohammadpour, R. Fabrication of Flexible Self-Powered Humidity Sensor Based on Super-Hydrophilic Titanium Oxide Nanotube Arrays. *Sci. Rep.* **2020**, *10*, No. 13032.
(8) Gulati, K.; Santos, A.; Findlay, D.; Losic, D. Optimizing Anodization Conditions for the Growth of Titania Nanotubes on Curved Surfaces. *J. Phys. Chem. C* **2015**, *119*, 16033−16045.
(9) Ghosh, J. P.; Achari, G.; Langford, C. H. Design and Evaluation of a UV LED Photocatalytic Reactor Using Anodized TiO_2 Nanotubes. *Water Environ. Res.* **2016**, *88*, 785−791.
(10) Macák, J. M.; Tsuchiya, H.; Schmuki, P. High-Aspect-Ratio TiO_2 Nanotubes by Anodization of Titanium. *Angew. Chem., Int. Ed.* **2005**, *44*, 2100−2102.
(11) Alivov, Y.; Fan, Z. Y.; Johnstone, D. Titanium Nanotubes Grown by Titanium Anodization. *J. Appl. Phys.* **2009**, *106*, No. 034314.
(12) Macak, J. M.; Tsuchiya, H.; Ghicov, A.; Yasuda, K.; Hahn, R.; Bauer, S.; Schmuki, P. TiO_2 Nanotubes: Self-Organized Electrochemical Formation, Properties and Applications. *Curr. Opin. Solid State Mater. Sci.* **2007**, *11*, 3−18.
(13) Xie, Z. B.; Blackwood, D. J. Effects of Anodization Parameters on the Formation of Titania Nanotubes in Ethylene Glycol. *Electrochim. Acta* **2010**, *56*, 905−912.
(14) Prakasam, H. E.; Shankar, K.; Paulose, M.; Varghese, O. K.; Grimes, C. A. A New Benchmark for TiO_2 Nanotube Array Growth by Anodization. *J. Phys. Chem. C* **2007**, *111*, 7235−7241.
(15) Macak, J. M.; Schmuki, P. Anodic Growth of Self-Organized Anodic TiO_2 Nanotubes in Viscous Electrolytes. *Electrochim. Acta* **2006**, *52*, 1258−1264.
(16) Ozkan, S.; Mazare, A.; Schmuki, P. Critical Parameters and Factors in the Formation of Spaced TiO_2 nanotubes by Self-Organizing Anodization. *Electrochim. Acta* **2018**, *268*, 435−447.
(17) Omidvar, H.; Goodarzi, S.; Seif, A.; Azadmehr, A. R. Influence of Anodization Parameters on the Morphology of TiO_2 nanotube Arrays. *Superlattices Microstruct.* **2011**, *50*, 26−39.
(18) Roy, P.; Berger, S.; Schmuki, P. TiO_2 nanotubes: Synthesis and Applications. *Angew. Chem., Int. Ed.* **2011**, *50*, 2904−2939.
(19) Quan, X.; Yang, S.; Ruan, X.; Zhao, H. Preparation of Titania Nanotubes and Their Environmental Applications as Electrode. *Environ. Sci. Technol.* **2005**, *39*, 3770−3775.
(20) Schmidt-Stein, F.; Thiemann, S.; Berger, S.; Hahn, R.; Schmuki, P. Mechanical Properties of Anatase and Semi-Metallic TiO_2 Nanotubes. *Acta Mater.* **2010**, *58*, 6317−6323.
(21) Macak, J. M.; Zlamal, M.; Krysa, J.; Schmuki, P. Self-Organized TiO_2 Nanotube Layers as Highly Efficient Photocatalysts. *Small* **2007**, *3*, 300−304.
(22) Ghicov, A.; Schmuki, P. Self-ordering Electrochemistry: A Review on Growth and Functionality of TiO_2 Nanotubes and Other Self-Aligned MOx Structures. *Chem. Commun.* **2009**, *20*, No. 2791.
(23) Macak, J. M.; Hildebrand, H.; Marten-Jahns, U.; Schmuki, P. Mechanistic Aspects and Growth of Large Diameter Self-Organized TiO_2 Nanotubes. *J. Electroanal. Chem.* **2008**, *621*, 254−266.
(24) Zhou, X.; Liu, N.; Schmuki, P. Photocatalysis with TiO_2 Nanotubes: "Colorful" Reactivity and Designing Site-Specific Photocatalytic Centers into TiO_2 Nanotubes. *ACS Catal.* **2017**, *7*, 3210−3235.
(25) Krbal, M.; Sopha, H.; Pohl, D.; Benes, L.; Damm, C.; Rellinghaus, B.; Kupčík, J.; Bezdička, P.; Šubrt, J.; Macak, J. M. Self-Organized TiO_2 Nanotubes Grown on Ti Substrates with Different Crystallographic Preferential Orientations: Local Structure of TiO_2 Nanotubes vs. Photo-Electrochemical Response. *Electrochim. Acta* **2018**, *264*, 393−399.
(26) Macak, J. M.; Jarosova, M.; Jäger, A.; Sopha, H.; Klementová, M. Influence of the Ti Microstructure on Anodic Self-Organized TiO_2 Nanotube Layers Produced in Ethylene Glycol Electrolytes. *Appl. Surf. Sci.* **2016**, *371*, 607−612.
(27) Leonardi, S.; Li Bassi, A.; Russo, V.; Di Fonzo, F.; Paschos, O.; Murray, T. M.; Efstathiadis, H.; Kunze, J. TiO_2 Nanotubes: Interdependence of Substrate Grain Orientation and Growth Characteristics. *J. Phys. Chem. C* **2012**, *116*, 384−392.
(28) Leonardi, S.; Russo, V.; Li Bassi, A.; Di Fonzo, F.; Murray, T. M.; Efstathiadis, H.; Agnoli, A.; Kunze-Liebhäuser, J. TiO_2 Nanotubes: Interdependence of Substrate Grain Orientation and Growth Rate. *ACS Appl. Mater. Interfaces* **2015**, *7*, 1662−1668.
(29) Sopha, H.; Tesar, K.; Knotek, P.; Jäger, A.; Hromadko, L.; Macak, J. M. TiO_2 Nanotubes Grown on Ti Substrates with Different Microstructure. *Mater. Res. Bull.* **2018**, *103*, 197−204.
(30) Hyam, R. S.; Choi, D. Effects of Titanium Foil Thickness on TiO_2 Nanostructures Synthesized by Anodization. *RSC Adv.* **2013**, *3*, 7057−7063.
(31) Utsunomiya, H.; Abe, K.; Matsumoto, R. Formation of Roll Coating in Cold Rolling of Titanium Sheets. *Procedia Eng.* **2017**, *207*, 1367−1372.
(32) Utsunomiya, H.; Kameyama, S.; Matsumoto, R. Contact Resistance between Roll and Titanium Sheet during Cold Rolling. *CIRP Ann.* **2019**, *68*, 305−308.
(33) Wang, S.; Niu, L.; Chen, C.; Pang, Y.; Liao, B.; Zhong, Z. H.; Lu, P.; Li, P.; Wu, X. D.; Coenen, J. W.; Cao, L. F.; Wu, Y. C. Size Effects on the Tensile Properties and Deformation Mechanism of Commercial Pure Titanium Foils. *Mater. Sci. Eng., A* **2018**, *730*, 244−261.
(34) Ghosh, A.; Singh, A.; Gurao, N. P. Effect of Rolling Mode and Annealing Temperature on Microstructure and Texture of Commercially Pure-Titanium. *Mater. Charact.* **2017**, *125*, 83−93.
(35) Chun, Y. B.; Yu, S. H.; Semiatin, S. L.; Hwang, S. K. Effect of Deformation Twinning on Microstructure and Texture Evolution during Cold Rolling of CP-Titanium. *Mater. Sci. Eng., A* **2005**, *398*, 209−219.
(36) Liu, N.; Wang, Y.; He, W.-j.; Li, J.; Chapuis, A.; Luan, B.-f.; Liu, Q. Microstructure and Textural Evolution during Cold Rolling and Annealing of Commercially Pure Titanium Sheet. *Trans. Nonferrous Met. Soc. China* **2018**, *28*, 1123−1131.
(37) Zherebtsov, S. V.; Dyakonov, G. S.; Salem, A. A.; Malysheva, S. P.; Salishchev, G. A.; Semiatin, S. L. Evolution of Grain and Subgrain Structure during Cold Rolling of Commercial-Purity Titanium. *Mater. Sci. Eng., A* **2011**, *528*, 3474−3479.
(38) Hu, N.; Gao, N.; Starink, M. J. The Influence of Surface Roughness and High Pressure Torsion on the Growth of Anodic Titania Nanotubes on Pure Titanium. *Appl. Surf. Sci.* **2016**, *387*, 1010−1020.
(39) Lu, K.; Tian, Z.; Geldmeier, J. A. Polishing Effect on Anodic Titania Nanotube Formation. *Electrochim. Acta* **2011**, *56*, 6014−6020.
(40) Sopha, H.; Jäger, A.; Knotek, P.; Tesař, K.; Jarosova, M.; Macak, J. M. Self-Organized Anodic TiO_2 Nanotube Layers: Influence of the Ti Substrate on Nanotube Growth and Dimensions. *Electrochim. Acta* **2016**, *190*, 744−752.
(41) Wang, X.; Li, Y.; Song, H.; Huang, Y.; Su, R.; Besenbacher, F. Fluoride Concentration Controlled TiO_2 Nanotubes: The Interplay of Microstructure and Photocatalytic Performance. *RSC Adv.* **2016**, *6*, 18333−18339.
(42) Fraoucene, H.; Sugiawati, V. A.; Hatem, D.; Belkaid, M. S.; Vacandio, F.; Eyraud, M.; Pasquinelli, M.; Djenizian, T. Optical and Electrochemical Properties of Self-Organized TiO_2 Nanotube Arrays From Anodized Ti−6Al−4V Alloy. *Front. Chem.* **2019**, *7*, No. 66.
(43) Wang, Y. N.; Huang, J. C. Texture Analysis in Hexagonal Materials. *Mater. Chem. Phys.* **2003**, *81*, 11−26.
(44) Zhong, Y.; Yin, F.; Nagai, K. Role of Deformation Twin on Texture Evolution in Cold-Rolled Commercial-Purity Ti. *J. Mater. Res.* **2008**, *23*, 2954−2966.

https://doi.org/10.1021/acsomega.1c02862
ACS Omega 2021, 6, 23233−23242

(45) Salishchev, G. A.; Mironov, S. Y. Effect of Grain Size on Mechanical Properties of Commercially Pure Titanium. *Russ. Phys. J.* **2001**, *44*, 596−601.
(46) Liu, N.; Mirabolghasemi, H.; Lee, K.; Albu, S. P.; Tighineanu, A.; Altomare, M.; Schmuki, P. Anodic TiO_2 Nanotubes: Double Walled vs. Single Walled. *Faraday Discuss.* **2013**, *164*, 107−116.
(47) Albu, S. P.; Ghicov, A.; Aldabergenova, S.; Drechsel, P.; LeClere, D.; Thompson, G. E.; Macak, J. M.; Schmuki, P. Formation of Double-Walled TiO_2 Nanotubes and Robust Anatase Membranes. *Adv. Mater.* **2008**, *20*, 4135−4139.
(48) Berger, S.; Albu, S. P.; Schmidt-Stein, F.; Hildebrand, H.; Schmuki, P.; Hammond, J. S.; Paul, D. F.; Reichlmaier, S. The Origin for Tubular Growth of TiO_2 Nanotubes: A Fluoride Rich Layer between Tube-Walls. *Surf. Sci.* **2011**, *605*, L57−L60.
(49) ASTM International Standard Test Methods for Measuring Adhesion by Tape Test D3359-09, 1−8.
(50) Mittal, K. L. Adhesion Measurement of Thin Films. *Electrocomponent Sci. Technol.* **1976**, *3*, 21−42.
(51) Cao, S.; Huang, W.; Wu, L.; Tian, M.; Song, Y. On the Interfacial Adhesion between TiO_2 Nanotube Array Layer and Ti Substrate. *Langmuir* **2018**, *34*, 13888−13896.
(52) Zou, J. P.; Wang, R. Z. Crack Initiation, Propagation and Saturation of TiO_2 Nanotube Film. *Trans. Nonferrous Met. Soc. China* **2012**, *22*, 627−633.
(53) Luo, J.; Li, B.; Ajami, S.; Ma, S.; Zhou, F.; Liu, C. Growth of TiO_2 Nanotube on Titanium Substrate to Enhance Its Biotribological Performance and Biocorrosion Resistance. *J. Bionic Eng.* **2019**, *16*, 1039−1051.
(54) Muangmora, R.; Kemacheevakul, P.; Punyapalakul, P.; Chuangchote, S. Enhanced Photocatalytic Degradation of Caffeine Using Titanium Dioxide Photocatalyst Immobilized on Circular Glass Sheets under Ultraviolet C Irradiation. *Catalysts* **2020**, *10*, No. 964.
(55) Lorenzetti, M.; Biglino, D.; Novaka, S.; Kobe, S. Photoinduced Properties of Nanocrystalline TiO_2-Anatase Coating on Ti-Based Bone Implants. *Mater. Sci. Eng., C* **2014**, *37*, 390−398.
(56) Adán, C.; Marugán, J.; Sánchez, E.; Pablos, C.; Van Grieken, R. Understanding the Effect of Morphology on the Photocatalytic Activity of TiO_2 Nanotube Array Electrodes. *Electrochim. Acta* **2016**, *191*, 521−529.
(57) Ma, L.; Zhang, Q.; Zhao, Q.; Li, Z.; Ji, C.; Bu, H.; Xu, X. J. Fabrication and Photoluminescence Properties of Ridged TiO_2 Nanotube Arrays. *J. Mater. Sci. Mater. Electron.* **2014**, *25*, 3290−3294.
(58) Lei, Y.; Zhang, L. D.; Meng, G. W.; Li, G. H.; Zhang, X. Y.; Liang, C. H.; Chen, W.; Wang, S. X. Preparation and Photoluminescence of Highly Ordered TiO_2 Nanowire Arrays. *Appl. Phys. Lett.* **2001**, *78*, 1125−1127.
(59) Etacheri, V.; Di, C.; Schneider, J.; Bahnemann, D.; Pillai, S. C. Visible-Light Activation of TiO_2 Photocatalysts: Advances in Theory and Experiments. *J. Photochem. Photobiol., C* **2015**, *25*, 1−29.
(60) Pan, X.; Yang, M. Q.; Fu, X.; Zhang, N.; Xu, Y. J. Defective TiO_2 with Oxygen Vacancies: Synthesis, Properties and Photocatalytic Applications. *Nanoscale* **2013**, *5*, 3601−3614.
(61) Taieb, S. B.; Assaker, I. B.; Bardaoui, A.; Gannouni, M.; Souissi, A.; Nowak, S.; Mouton, L.; Ammar, S.; Chtourou, R. Correlation between Titanium Foil Substrate Purity and TiO_2 NTs; Physical and Electrochemical Properties for Enhanced Photoelectrochemical Applications. *Int. J. Hydrogen Energy* **2016**, *41*, 6230−6239.
(62) Ferreira, A. P. Caffeine as an Environmental Indicator for Assessing Urban Aquatic Ecosystems. *Cad. Saude Publica* **2005**, *21*, 1884−1892.
(63) Ahmad Bhawani, S.; Fong, S. S.; Mohamad Ibrahim, M. N. Spectrophotometric Analysis of Caffeine. *Int. J. Anal. Chem.* **2015**, *2015*, 1−7.

https://doi.org/10.1021/acsomega.1c02862
ACS Omega 2021, 6, 23233−23242

Supporting Information

Toward a Flexible and Efficient TiO_2 Photocatalyst Immobilized on a Titanium Foil

Živa Marinko*[,†,‡], Luka Suhadolnik[†], Barbara Šetina Batič[§], Vid Simon Šelih[∥], Boris Majaron[⊥,#], Janez Kovač[▽], and Miran Čeh[†]

[†]Department for Nanostructured Materials, Jožef Stefan Institute, Jamova 39, 1000 Ljubljana, Slovenia; luka.suhadolnik@ijs.si (L.S.); miran.ceh@ijs.si (M.Č.)

[‡]Jozef Stefan International Postgraduate School, Jamova 39, 1000 Ljubljana, Slovenia

[§]Vacuum Science and Optoelectronics, Institute of Metals and Technology, Lepi pot 11, 1000 Ljubljana, Slovenia; barbara.setina@imt.si (B.Š.)

[∥]Center for Validation Tehnologies and Analytics & Department of Analytical Chemistry, National Institute of Chemistry, Hajdrihova 19, 1001 Ljubljana, Slovenia; vid.selih@ki.si (V.S.Š.)

[⊥]Department of Complex Matter, Jožef Stefan Institute, Jamova 39, 1000 Ljubljana, Slovenia; boris.majaron@ijs.si (B.M.)

[#]Faculty of Mathematics and Physics, University of Ljubljana, Jadranska 19, 1000 Ljubljana, Slovenia (B.M.)

[▽]Department of Surface Engineering, Jožef Stefan Institute, Jamova 39, 1000 Ljubljana, Slovenia; janez.kovac@ijs.si (J.K)

*Email: ziva.marinko@ijs.si (Ž.M.). Tel: +386-1-4773-931

Keywords

TiO_2 nanotubes; anodic oxidation; flexible photocatalyst; metal titanium foil

S1. Microstructure Properties of the Starting Titanium Foils

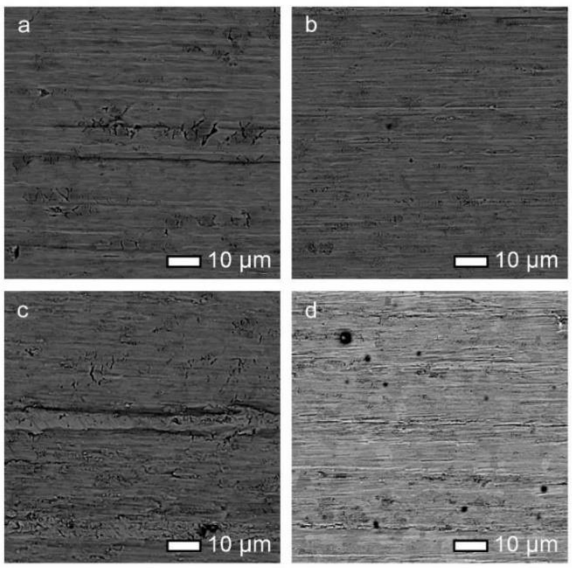

Figure S1. SEM images of metal titanium foil of different thicknesses. (a) 30 μm, (b) 50 μm, (c) 100 μm, (d) 200 μm.

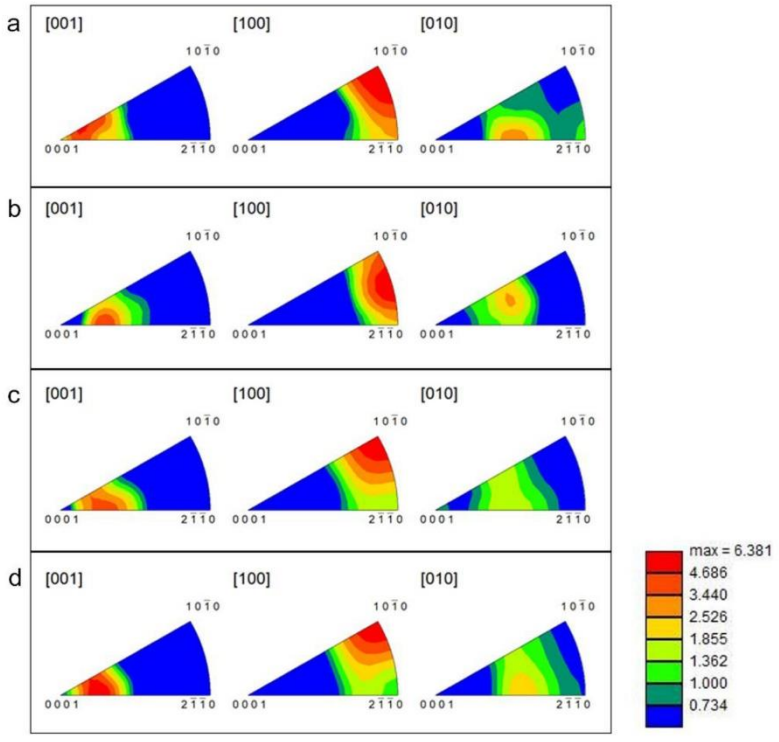

Figure S2. Inverse pole figures (IPFs) for all samples. (a) 30 μm, (b) 50 μm, (c) 100 μm, (d) 200 μm.

S2. Characteristics of the Annealed TiO_2 NT Layers

XPS analyses of all the samples were performed. The results showed that the surface's chemical composition is very comparable among the samples (Table S1). Additionally, the high-energy resolution XPS spectra Ti 2p, O 1s and C 1s are presented in Figure S3. The spectra of Ti 2p (a) from all samples are very similar. The Ti $2p_{3/2}$ peak at 458.6 eV can be assigned to Ti(4+) in TiO_2 oxide. O 1s spectra (b) are also very similar among the samples. The spectra show a large peak at 530.0 eV, which is assigned to O(2-) in the TiO_2 oxide lattice, and a small peak at 531.6 eV, which is about 15% of the total O 1s spectra and can be assigned to the OH or O vacancies in the TiO_2 oxide layer. C 1s spectra (c) are also very similar for all the samples and probably originate from the contamination or electrolyte content. Additionally, traces of nitrogen as N 1s and potassium as K 2p peaks were detected.

Table S1. Surface chemical composition in at.% and the O/Ti ratio for all samples.

Sample	Ti	O	C	O/Ti
30 µm	21.1	52.5	26.4	2.49
50 µm	20.1	47.7	32.3	2.37
100 µm	22.6	53.7	23.7	2.38
200 µm	22.7	54.1	23.2	2.38

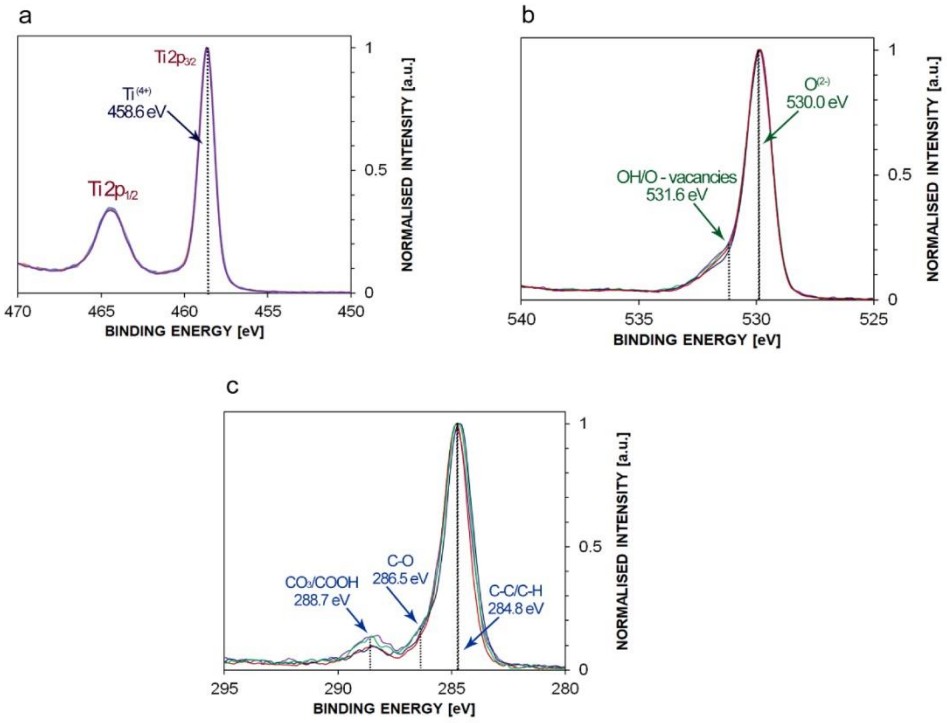

Figure S3. High-resolution XPS spectra for (a) Ti 2p, (b) O 1s and, (c) C 1s peaks for all TiO_2 NT samples.

The TiO_x NT layers grown by anodic oxidation are amorphous. Annealing at 450 °C for 1 hour transforms the amorphous NTs into the anatase phase. XRD analyses performed on all four samples

confirmed the phase transformation. At the same time, annealing significantly improves the contact between the titanium foil and the nanotubes.[1] All diffractograms in Figure S4 show distinct peaks related to the anatase phase at 2θ angles. The diffraction peaks corresponding to the titanium foil can be observed in each XRD spectra due to the relatively thin and porous TiO_2 NT layers.

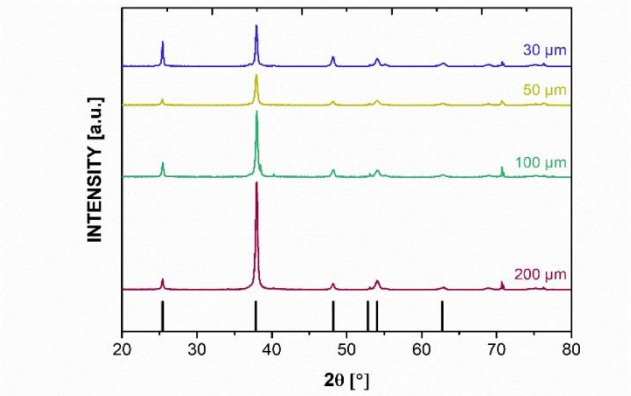

Figure S4. XRD measurements for each sample. The diffraction peaks corresponding to the titanium foil are not marked.

Analyses of the TiO_2 NTs' top surface, bottom surface, and cross-section were carried out with FEG-SEM. They show significant differences between the samples (Figure S5). Many wide, short cracks were observed on the thinnest sample's surface in the transverse and longitudinal directions. The top oxide layer was thin and, in some areas, absent. At those areas, the NT surface was etched. On the 50-µm sample, the density of the cracks decreased; they were shorter and transverse-oriented. The top oxide layer is the thinnest; NTs are seen more clearly. In contrast, was the 100 µm sample surface. Very few cracks can be observed. The TiO_2 NTs' surface is uneven with sponge-like areas of etched NTs and regularly looked like NTs with a thick oxide layer on top. Finally, the thickest foil, i.e., 200 µm, had the most even surface with the thinnest top oxide layer. Although the cracks were long and wide, they were rare, with the NTs closely packed, and the boundary between the individual NTs clearly seen.

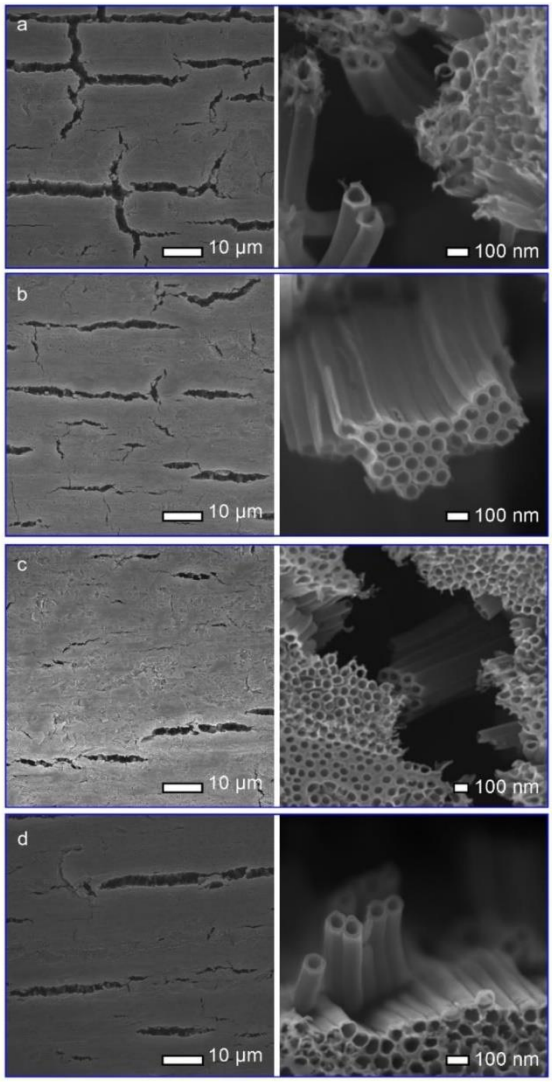

Figure S5. FEG-SEM micrographs of TiO_2 NTs for each foil thickness, (a) 30 µm, (b) 50 µm, (c) 100 µm, (d) 200 µm samples.

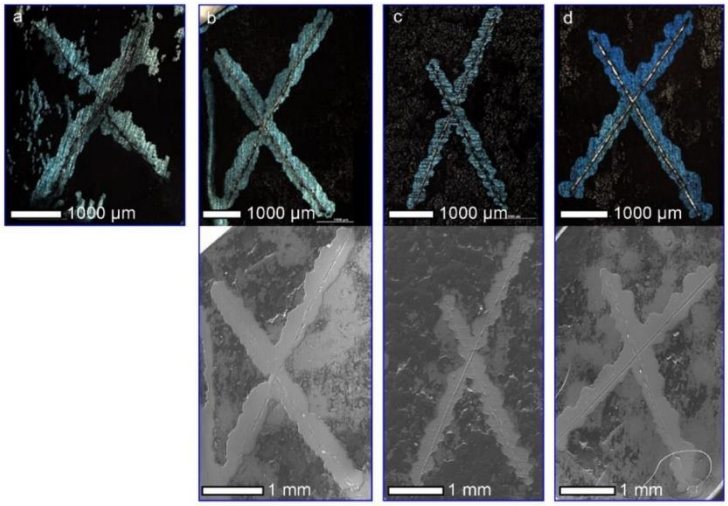

Figure S6. Adhesion of TiO_2 NTs performed with Scotch-tape test on (a) 30 µm, (b) 50 µm, (c) 100 µm, (d) 200 µm samples. Black areas on the upper micrographs are the TiO_2 NTs' remains, and blue areas are oxidised titanium foils from which the TiO_2 NTs were removed due to weak adhesion. Below are micrographs taken on FEG-SEM. Adhesion of 30 µm sample NTs was poor and did not withstand the preparation for FEG-SEM observation.

S3. Measurements of Photocatalytic Degradation

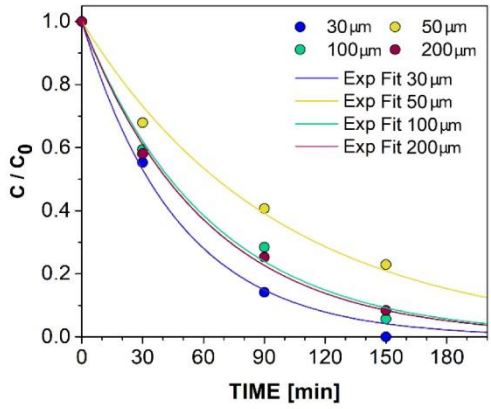

Figure S7. Photocatalytic degradation of caffeine (dots) for all four samples; and exponential curve fitting (lines) for 30, 50, 100, and 200 µm samples.

REFERENCES

(1) Xiong, J.; Wang, X.; Li, Y.; Hodgson, P. D. Interfacial Chemistry and Adhesion between Titanium Dioxide Nanotube Layers and Titanium Substrates. *J. Phys. Chem. C* **2011**, *115*, 4768–4772.

3.1 Appendix to the Paper

3.1.1 EPR Measurements

The existence of $OH^{\bullet}$ species is vital for caffeine degradation or any organic compound during the process of photocatalysis. Therefore, EPR measurements were performed to determine the presence of $OH^{\bullet}$ radicals during the photocatalytic decomposition of the caffeine by using a DEPMPO ($C_9H_{18}NO_4P$) spin-trapper in an absolute-ethanol solution. DEPMPO is a spin-trapper used in low concentrations with a high affinity to binding with $OH^{\bullet}$ radicals [201]. Following the procedure by Koklic et al. [202], the solution of spin-trapper was dissolved on the anodised Ti sheet placed in a Petri dish. At the beginning of the measurements, Tempol was used as a standard. Samples that were not irradiated were used as a control. After the designated illumination time, the solution was sucked into glass capillaries, placed into an EPR spectrometer (Bruker Elexsys) and analysed with the Xrpr programme. The measurements were performed at room temperature using a 1-Gauss modulation amplitude, 100-kHz modulation frequency, 1.28-ms time constant, 0.20-mW microwave power, and 100-G sweep width with the centre field positioned at 3320 G. A drop of 0.5-M DEPMPO (5-(Diethoxyphosphoryl)-5-methyl-1-pyrroline-N-oxide) spin trap and 30 % ethanol was formed on the TiO_2 NT surface and illuminated with a 365 nm UV light. After 3 min, the solution was drawn into a 1-mm-wide capillary, inserted into a 5-mm-wide tube (both quartz), and transferred into the EPR spectrophotometer (ELEXSYS, Bruker). The spectrum in Figure 3.1 shows the results for DEPMPO-$OH^{\bullet}$ measurements for TiO_2 NT samples with (bold lines) and without (red lines) UV illumination. Due to the binding of $OH^{\bullet}$ and spin-trapper, the signal is a quadruplet. The obtained signal is low since we used ethanol as the solvent, known as a $OH^{\bullet}$ quencher. From that data we can conclude that all the samples showed the possibility of producing radicals when illuminated with UV light. Peak-to-peak intensity analyses showed only minor differences in radical production between the samples (the signal is somewhat larger for 100 µm sample; however, the statistical significance cannot be confirmed).

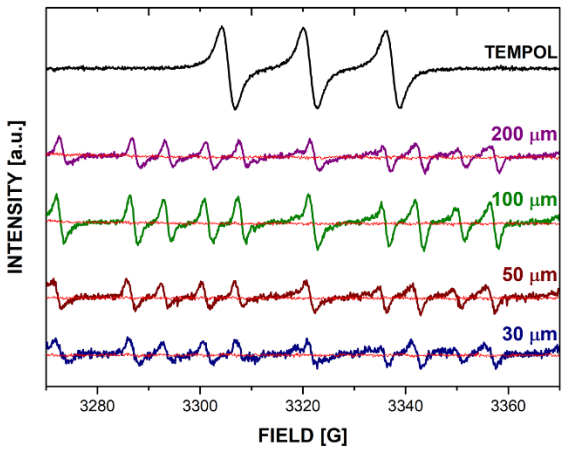

Figure 3.1: EPR spectra of $OH^{\bullet}$ concentration measurements for all four samples. At the beginning of the measures, Tempol was used as a standard. Not irradiated samples were used as a control sample (thin red lines) for UV illuminated samples (bold colour lines).

3.1.2 Ageing of Electrolyte

The age of the anodisation electrolyte significantly influences the anodisation process and the photocatalytic activity of the TiO_2 NT arrays, which will be addressed in the next chapter.

Nevertheless, as part of this work, we investigated the growth of NTs using differently aged electrolytes. Ti substrates with different thicknesses (30, 50, 100, and 200 µm) were ultrasonically cleaned to remove the processing impurities. All four samples were anodised simultaneously under identical conditions of 60 V for 3 h using the electrolyte with the composition: ethylene glycol, 2 vol % H_2O, 0.3 wt% NH_4F.

Figure 3.2 shows the measured caffeine degradation for each Ti starting thickness depends on the electrolyte age.

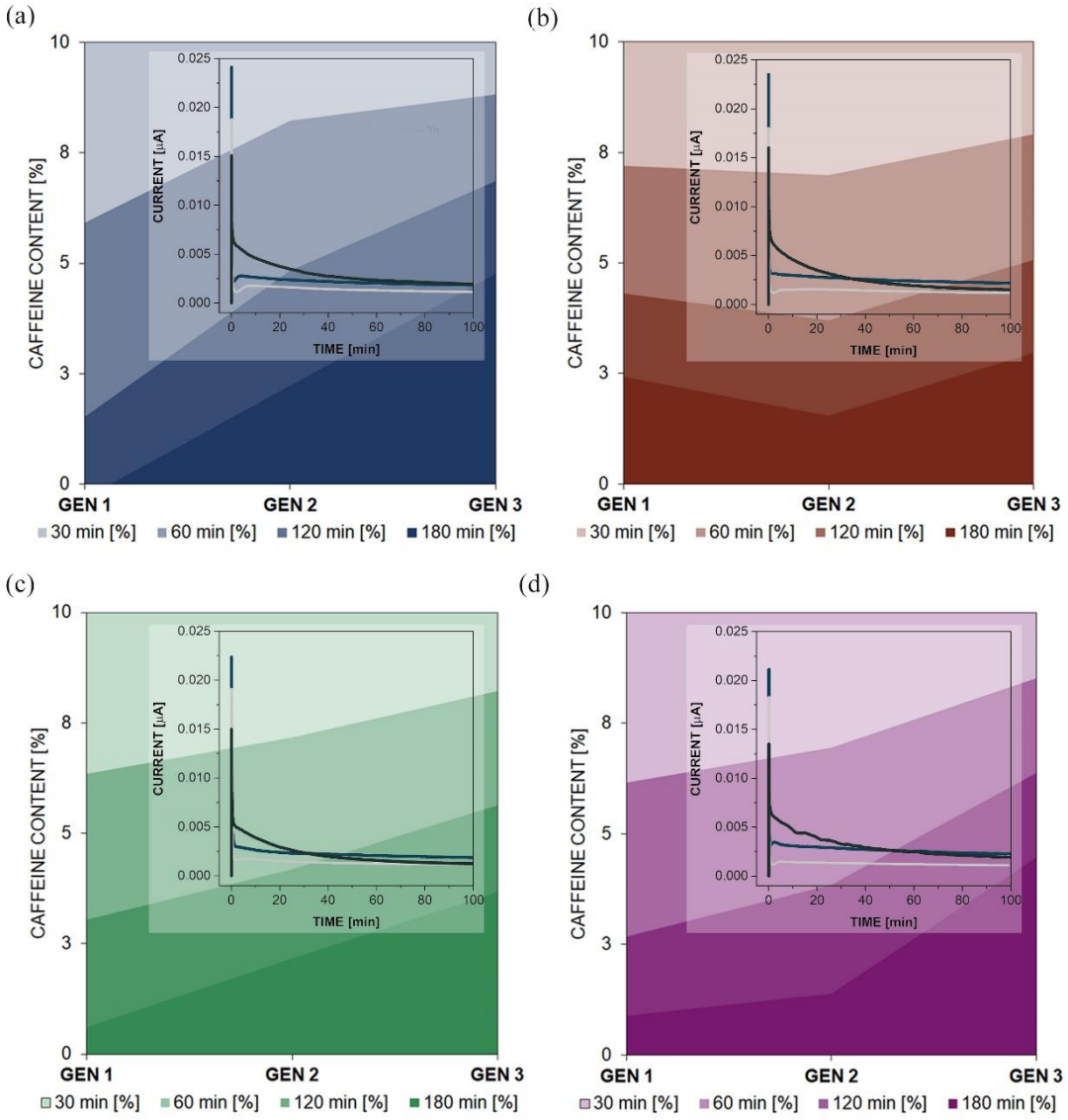

Figure 3.2: The degradation of caffeine measured with a UV-Vis-IR Spectrophotometer after 30, 60, 120 and 180 min of photocatalytical treatment. Caffeine degradation test was done for (a) 30, (b) 50, (c) 100, (d) and 200 µm samples. The inset shows a current measurement in time over 3 repetitive anodisation during preparation of the TiO_2 NT array, each performed on a new substrate. Black lines show 1st generation (GEN1), blue the 2nd (GEN2) and the light grey line the 3rd (GEN3) anodisation.

It was concluded that fresh electrolytes (e.g., GEN1 as 1st generation anodisation) for anodization resulted in more photoactive NTs. In the inset of each caffeine degradation graph, an anodization current vs time of anodization graph is shown for the first 100 min of the anodization process. At the beginning of the anodization, the starting currents were significantly higher when fresh electrolyte was used and dropped considerably with the age of the electrolyte.

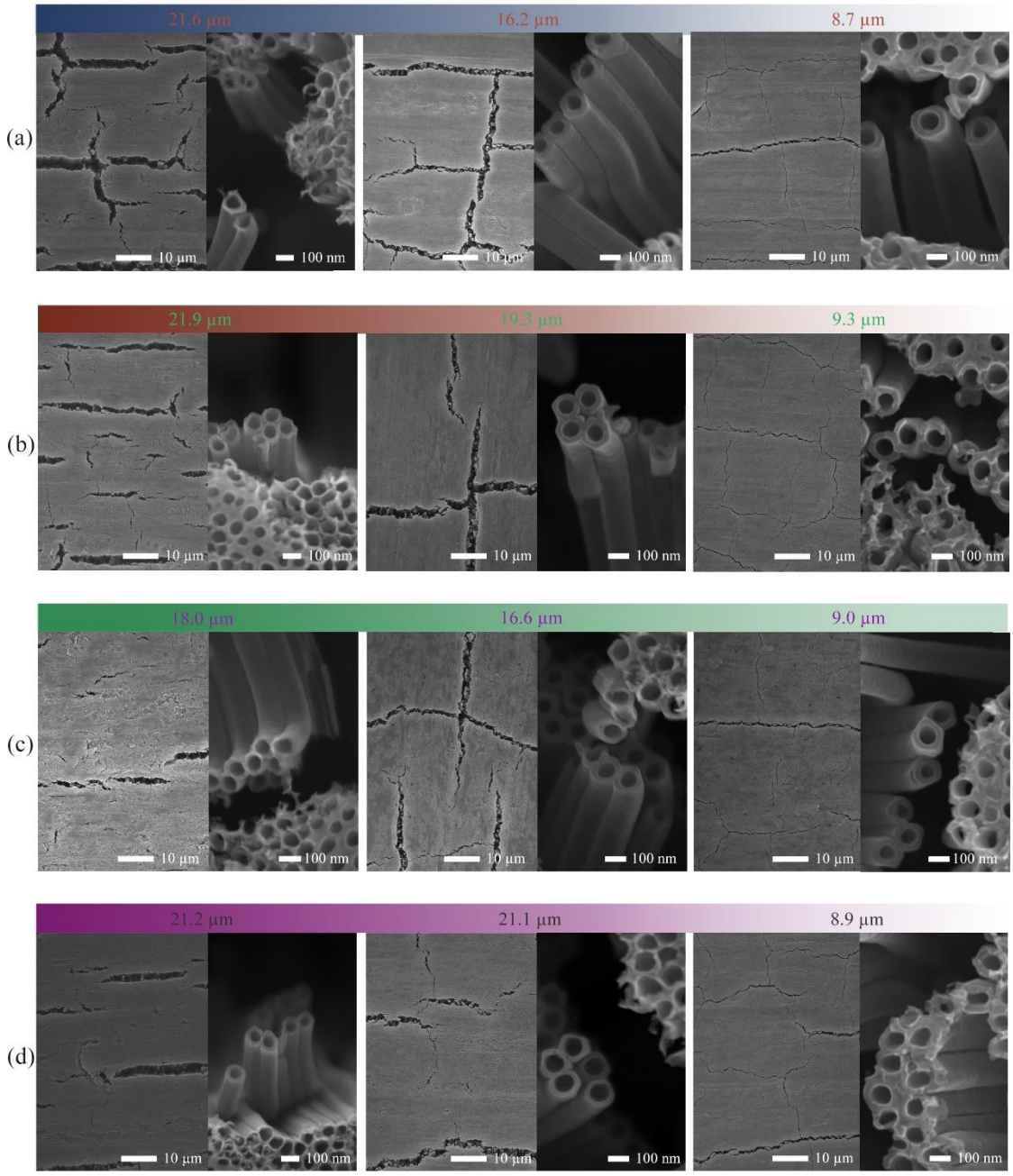

Figure 3.3: SEM imaging of crystallized TiO_2 NT layers for fresh, (a) 30, (b) 50, (c) 100, and (d) 200 µm samples. The left image shows a larger area, and the right a magnified part. The NTs thickness is measured and presented above the figures in the middle of each image.

Annealed TiO_2 NTs were investigated with SEM imaging, focusing on NTs length, porosity, and cracked area. Mentioned parameters are shown in Figure 3.3, from the thinnest, 30 µm sample (a), to the thickest, 200 µm, sample (d). The left-hand figure shows NTs grown with fresh electrolyte, the 1st generation, the middle figure in the 2nd, and the right figure where NTs are grown in the aged electrolyte (3rd anodization of electrolyte).

It was confirmed that the electrolyte's age had a significantly detrimental effect on the length of the grown NTs. The reduction was from approximately 21 µm to 9 µm. However, the NTs' length was not the only morphological change. A noticeable difference was the thickening of the nanotube wall and the amount of debris on top of the layer. With electrolyte ageing, the nanotube wall became thicker; more debris was seen on top of the NTs, meaning that the NTs were less open and with reduced uniformity. Consequently, that significantly contributed to the reduced area of active surface, which influenced the reduced photocatalytic activity in the aged electrolyte, as caffeine degradation was incomplete in all the samples. Interestingly, fresh electrolyte did not guarantee complete degradation. The results presented in Figure 3.2 show that the thinnest (30 µm) sample is the only one that completely degraded the caffeine. Following this was a 100 µm foil with 99.4 %, 200 µm with 99.1 % and 50 µm sample with 97.5 % efficiency. After the 2nd anodization, the efficiency dropped by approximately 2 % and after the 3rd anodization by roughly an additional 2 %.

Chapter 4

Influence of Anodization-Electrolyte Aging on the Photocatalytic Activity of TiO_2 Nanotube Arrays

This chapter addresses the thesis **objective** of how the electrolyte ageing influences TiO_2 NTs' growth and subsequent photocatalytic activity based on the following working **hypotheses**:

6. Repetitive anodisation changes the electrolyte's chemical composition, thus influencing the NT's growth and final photocatalytic activity.
7. Anodisation of Ti foil with fresh electrolytes results in NTs with uniform morphology.

The present chapter presents a paper with the title "*Influence of Anodization-Electrolyte Aging on the Photocatalytic Activity of TiO_2 Nanotube Arrays*" (Luka Suhadolnik, **Živa Marinko**, Maja Ponikvar-Svet, Gašper Tavčar, Janez Kovač and Miran Čeh) that was published in The Journal of Physical Chemistry C, Vol. 124 in 2020.

The importance of the electrolyte's composition has been discussed in detail in previous chapters. However, this work aimed to clarify the NTs' growth after the continuous use of the same electrolyte for many subsequent anodisation, i.e., using an ageing electrolyte. Starting Ti foil and electrolyte composition were the same as used in previous studies; however, the experiments were performed on larger substrates. The electrolyte was used in the anodization for 6 hours, thus presenting one generation of electrolyte. Each additional cycle is therefore aged by those 6 hours (e.g., *Sample 1 represents fresh electrolyte, Sample 2 is aged for 6 hours, Sample 3 for 12 hours, Sample 5 for 24 hours, Sample 20 for 114 hours, and so on*). The anodisation electrolyte was characterized by conductivity, pH and temperature. H_2O, F^- and $[TiF_6]^{2-}$ concentrations were determined periodically after the 1^{st}, 5^{th}, 13^{th} and 20^{th} cycles of anodisation with potentiometric determination, titration and spectrophotometrically. Caffeine degradation was measured using HPLC.

After many subsequent anodisation cycles, the concentration of H_2O in the electrolyte increased, while the concentration of F^- decreased. The SEM investigation of the first anodized Ti foils exhibited the usual NTs morphology and the thin NTs film formed throughout the substrate surface. However, with each additional anodised cycle, the continuous NTs thin film broke, and non-anodized areas appeared, revealing the Ti

substrate with no NTs. Finally, only the islands of anodized regions (NTs) on the substrate could be observed with clear boundaries between the NTs and the substrate surface. Moreover, on these so-called not-anodised parts (with only oxide present), individual islands of exploded oxide with observed nanotubes were identified, closely reminding of "breakdown anodisation". The decreased area of active NTs on the substrate also significantly decreased the caffeine degradation. To revitalize the electrolyte after subsequent anodisation, NH_4F was added to the aged electrolyte for its regeneration and to increase the NTs' growth.

As expected, the previously observed morphological phenomena improved. The electrolyte composition was also advanced in terms of conductivity and fluoride concentration; moreover, the caffeine degradation improved. Although the regeneration was successful, the system did not return to the old and best result of the fresher electrolytes. The results after the regeneration were not published. However, they are presented as a continuation of the already-known results. The reader should refer to the Appendix section of this chapter.

Regarding my contribution: This work was my entrance into the anodisation process of Ti, the synthesis of photoactive TiO_2 nanotubes and photocatalysis in general. With this work I started to learn about the process. With that I contributed to the anodisation of Ti foils. Furthermore, my contribution included the graphical work and part of the statistical analysis in the presented manuscript.

THE JOURNAL OF PHYSICAL CHEMISTRY C

pubs.acs.org/JPCC

Article

Influence of Anodization-Electrolyte Aging on the Photocatalytic Activity of TiO_2 Nanotube Arrays

Luka Suhadolnik,* Živa Marinko, Maja Ponikvar-Svet, Gašper Tavčar, Janez Kovač, and Miran Čeh

Cite This: J. Phys. Chem. C 2020, 124, 4073−4080

Read Online

ACCESS | Metrics & More | Article Recommendations | Supporting Information

ABSTRACT: TiO_2 nanotubular films prepared using the anodic oxidation process applied to various forms of metal titanium are promising materials for photocatalytic applications. However, during successive anodizations in batch-anodization cells, the chemical composition of the NH_4F- and water-based ethylene glycol electrolyte changes with each subsequent anodization, which greatly affects the final photocatalytic properties of the annealed TiO_2 nanotubular films. In the present study, 20 titanium discs (Φ 90 mm) were sequentially anodized in the same anodization electrolyte. The chemical composition of the electrolyte was measured after each anodization and correlated with the anodization current density, temperature, electrical conductivity, and pH of the electrolyte and with the morphology, structure, composition, and photocatalytic activity of the resulting TiO_2 nanotube films. It was found that the length of the TiO_2 nanotubes decreased with the age of the electrolyte due to its lower conductivity. The subsurface chemical composition was evaluated by time of flight secondary ion mass spectrometry (ToF SIMS) analyses, and the integrated ToF SIMS signals over a depth of 250 nm for the TiO_2 nanotube films showed that the concentration of F^- in the annealed TiO_2 film increased with each subsequent anodization due to the increased pH value of the electrolyte. As a consequence, the concentration of the OH^- and O_2^- species decreased, which is a major reason for the reduced photocatalytic activity of the TiO_2 films. It is proposed that the length of the TiO_2 nanotubes does not play a decisive role in determining the photocatalytic activity of the TiO_2 nanotube films. Finally, the best measured degradation results of 60% for caffeine were thus achieved for the first anodized titanium discs. After that the efficiency gradually decreased for each subsequent anodized disc.

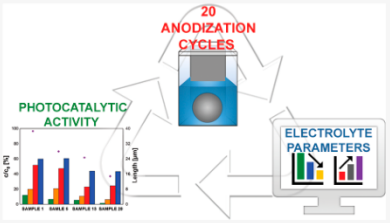

1. INTRODUCTION

Anodic oxidation is a well-known process that was first used for the protection of aluminum in the early 20th century. Its main purpose is to increase the adherent strength and the thickness of the film formed by a natural oxidation process.[1] The process is still used in industrial settings for protecting and coloring aluminum.[2] However, with the emergence of nanotechnology, researchers began to modify the anodic oxidation process to produce porous structures that can be used as a template for the synthesis of one-dimensional nanostructures[3,4] or as an immobilized nanostructured film on a metal substrate for various applications.[5,6]

Al_2O_3 is the most used template material, obtained by the anodization of aluminum,[7] while TiO_2 nanotubes, obtained by the anodization of titanium, are the most investigated materials for the direct use of anodized films. TiO_2 nanotubes have a high surface area and unique electronic, ionic, and biocompatibility properties, which lead to many different applications.[8] Among them, photocatalysis is the most studied and reported in the scientific literature.[9]

The most important characteristics of an efficient TiO_2 photocatalyst are its high activity, low cost, and good stability. Additionally, the ideal photocatalyst should be strongly adhered to a support enabling a continuous photocatalytic reaction without the need to remove and recycle the photocatalyst.[10] Immobilization can be most easily achieved with the use of an anodic oxidation process, which at the same time allows the low-cost synthesis of TiO_2 nanotube films. Moreover, anodic oxidation enables the optimization of the nanotube morphology by adjusting the anodization conditions.[11]

The influence of the most important anodization parameters (anodization voltage, time of anodization, and electrolyte composition and temperature) on the morphology of TiO_2 nanotubes has been well investigated.[12,13] At the same time, the process of nanotube growth during anodic oxidation is well-known. Water in the electrolyte oxidizes Ti to form TiO_2. In order to grow nanotubes rather than a compact TiO_2 film, fluoride must be present in the electrolyte. It participates in the TiO_2 etching process and in the complexation of titanium

Received: October 10, 2019
Revised: January 14, 2020
Published: January 21, 2020

https://dx.doi.org/10.1021/acs.jpcc.9b09522
J. Phys. Chem. C 2020, 124, 4073−4080

cations at the oxide/electrolyte interface.[14] This knowledge enables the synthesis of an immobilized TiO_2 photocatalyst with specific morphological characteristics, which can be used for various applications.[15,16] However, in order for the anodic oxidation of titanium to be used for the industrial production of TiO_2 nanotube films, a comprehensive understanding of the changes in the electrolyte's composition during the anodization process is needed.

Recently, there were a few studies pointing out the lack of reproducibility of the anodization process when titanium metal is repeatedly anodized in a fluoride-containing electrolyte solution. Lee et al. focused on the influence of the electrolyte's conductivity on the formation of TiO_2 nanotube films in a HF-based ethylene glycol electrolyte.[17] The authors tested the resulting anodic films as anodes for dye-sensitized solar cells. Two other research groups have studied the influence of electrolyte aging on the nanotube length and diameter.[18,19] The anodization electrolyte used in both studies was prepared with ethylene glycol, ammonium fluoride, and water. The study by Gulati et al.[19] focused on the anodization of curved titanium surfaces, whereas the study by Sopha et al.[18] determined the influence of electrolyte aging on the anodization of flat titanium foils. In the latter study, an adhesion analysis of the anodized nanotube film was also carried out.

Most of the studies reported in the literature focused primarily on the influence of the electrolyte's aging on the morphological changes to the TiO_2 nanotube films. It has been reported that the anodization electrolyte has to be preanodized in order to prevent the TiO_2 nanotube film's delamination from the substrate, thus improving its mechanical stability.[8] However, the range of electrolyte compositions that allows the synthesis of high-quality immobilized TiO_2 films in a reproducible way has not been yet reported and the electrolyte's aging was not linked to the application-related properties of the grown TiO_2 films.

In the present work, the influence of the anodization electrolyte's aging on its composition was studied. The aging was determined by the number of hours during which the electrolyte was used for anodization. Furthermore, the influence of the changes in the electrolyte's composition on the photocatalytic activity of annealed TiO_2 nanotubes was determined using caffeine as a model degradation molecule. During the anodization, the current−time curves and the electrolyte temperature were recorded. After the anodization, the electrolyte's conductivity was measured and the fluoride and water contents were accurately determined. To the best of our knowledge, the free-fluoride content in an anodization electrolyte that has been used for various times has not been measured and reported before. Additionally, the concentration of negative ions in an annealed TiO_2 film up to a depth of 250 nm was also measured, which is essential for explaining the photocatalytic activity of the anodized films.

2. EXPERIMENTAL SECTION

2.1. Anodic Oxidation of Titanium Discs. Highly ordered TiO_2 nanotube films were grown in a well-defined anodization setup shown in Figure 1. Titanium foils (200 μm thick, 99.8%, Baoji Lyne Metals Co., Ltd.) were first laser cut into discs with a diameter of 98.5 mm. The foils were then cleaned in acetone in an ultrasonic bath, rinsed with ethanol, and dried under a stream of nitrogen. After cleaning, the discs were anodized at a constant potential of 60 V for 6 h in an ethylene glycol electrolyte with 0.3 wt % of ammonium fluoride (99.99%, Sigma-Aldrich) and 2 vol % of deionized water. The total volume of the anodization electrolyte at the beginning of the experiments was 2 L. The area of the titanium disc exposed to the electrolyte was fixed at approximately 50 cm^2; the part of the titanium disc that was exposed to the electrolyte had a diameter of approximately 80 mm. The distance between the titanium anode and the stainless-steel cathode with a surface area of 210 cm^2 was kept constant at 90 mm. There was one anodization a day, and the total number of anodized discs was 20. During each anodization the current−time curve was measured and the electrolyte temperature was monitored throughout the entire procedure. During this time the anodization cell was covered with a lid to minimize the absorption of water from the surrounding air and sealed immediately after the anodization. The as-anodized amorphous titanium discs were washed with deionized water and ethanol and annealed at 450 °C for 1 h in air (heating and cooling at 5 °C min^{-1}).

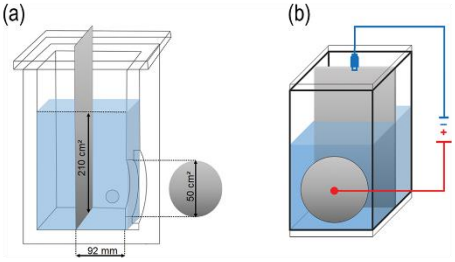

Figure 1. Anodization setup in which 20 sequential anodizations were performed. The area of the anodized titanium disc was approximately 50 cm^2, whereas the area of the stainless-steel cathode immersed into the electrolyte solution was approximately 210 cm^2. The titanium anode was connected to the positive electric potential while the cathode was connected to the negative one (b). The circle on the back of the anodization cell (a) shows the position of the temperature sensor.

2.2. Characterization of the Anodization Electrolyte. The electrolyte was characterized after each anodization in terms of conductivity and chemical composition. The electrolyte's conductivity was measured with a ProLine Plus M330 conductivity meter immediately after each anodization. The electrolyte's pH was measured before the first and after the last anodization using a benchtop pH meter (Mettler Toledo). The electrolyte samples with a volume of 1 mL were withdrawn before the start of the next anodization when the electrolyte composition reached a steady state (i.e., it was homogeneous throughout the entire volume). The fluoride, ammonia and water contents were determined in corresponding aliquots of the electrolyte sample. A Metrohm model 906 Titrando analyzer and a combined fluoride-ion selective electrode (Thermo Orion, model 9609) were used for the potentiometric determination of the fluoride using the standard addition method with the subtraction of a blank value.[20] The content of water was determined by Karl Fischer titration using a double platinum electrode (ISKRA HEP 0701) and an ISKRA voltmeter (Iskra pH−meter MA 5740).[21] The ammonia content was determined spectrophotometrically using a HACH DR/2010 spectrophotometer.

https://dx.doi.org/10.1021/acs.jpcc.9b09522
J. Phys. Chem. C 2020, 124, 4073−4080

2.3. Characterization of the Anodized Films. The morphological characterization of the anodized titanium discs was carried out in a field-emission scanning electron microscope (FSEM) (Jeol JSM-7600F). The lengths of the nanotubes were estimated from 5 cross-section cuts of the nanotubes of each sample. The structure of TiO_2 films was characterized with X-ray diffraction (D5000 Bruker AXS diffractometer with Cu−Kα radiation; λ = 1.5406 Å) and the surface composition was analyzed with X-ray photoelectron spectroscopy (XPS) on a PHI-TFA XPS spectrometer (Physical Electronics Inc.) equipped with Al-monochromatic source of X-rays. Additionally, surface composition was evaluated by time of flight secondary ion mass spectrometry (ToF SIMS). Mass spectra of positive and negative secondary ions emitted from the surface were acquired by ToF SIMS 5 instrument (ION TOF) using Bi^+ ion beam of 30 keV for spectra excitation and Cs^+ ion beam at 2 keV for ion sputtering during depth profile analyses. SIMS spectra were collected during depth profile analyses from the surface to the depth of 250 nm. Integral of specific fragments in SIMS spectra (F^-, OH^-, TiO^-, O_2^-) were calculated and compared.

2.4. Photocatalytic Degradation of Caffeine. The photocatalytic efficiency of the TiO_2 nanotube arrays was investigated by measuring the degradation of caffeine ((≥99.0% HPLC grade, Sigma-Aldrich) with an initial concentration of approximately 50 mg L^{-1}. The annealed discs were placed in a Petri dish with 50 mL of the initial caffeine solution and illuminated in a sterilizer (Kambič I-265 CK UV) for 3 h. A sample with a volume of 200 μL was collected after 30 min in the dark and then four times during the illumination time. The experimental setup was evaluated before the photocatalytic degradation tests were made. No concentration gradients were detected despite static experimental conditions being used. The results were also not influenced by the sample-collection location. All the samples were analyzed in a high-precision UV−vis-IR spectrophotometer.

3. RESULTS AND DISCUSSION

3.1. Monitoring the Anodization Process. The anodic oxidation of the titanium was monitored by measuring the electrical current density, temperature, and electrical conductivity of the electrolyte during the anodization. Additionally, the pH of the electrolyte was measured at the beginning of the anodization experiments and after the last anodization. All these parameters greatly influence the growth of the TiO_2 nanotubes, their morphology, and properties. Figure 2 shows current density vs time curves during the first 30 min of the anodization of the titanium discs in electrolytes of different ages: 0, 24, 72, and 114 h. The inset in Figure 2 shows the current−time plot for the entire 6 h anodization period together with the average electrolyte temperature during the anodizations. It is evident that the current density drops when the electrolyte is aging after subsequent anodizations. The average current density during the first anodization was more than three times higher than during the 20th (136 mA cm^{-2} compared to 42 mA cm^{-2}). The changes in the current density are the result of changes to the electrolyte's composition. The steady-state current density increases with an increasing fluoride concentration, which strongly influences the morphology of the TiO_2 nanotubes, since the higher the average current density, the thicker the TiO_2 film. In a certain range, the film thickness affects its photocatalytic activity. Like the current density, the temperature of the electrolyte during the anodization can strongly influence the morphology of the grown TiO_2 film.[17] The electrolyte's temperature increases only slightly during anodization, which can increase the current density. However, to what extent does the temperature rise depend on the anodization conditions (especially the applied voltage), the dimensions of the anodization cell (they determine the volume of the electrolyte) and the size (exposed surface area) of the electrodes. In our anodization system there was only slight change in temperature during anodization, and the average electrolyte temperature of the individual anodizations did not differ much (the lowest average temperature was 20.3 °C for the first anodization and the highest 25.7 °C in the 13th anodization), and this did not significantly affect the morphology and photocatalytic properties of the films.

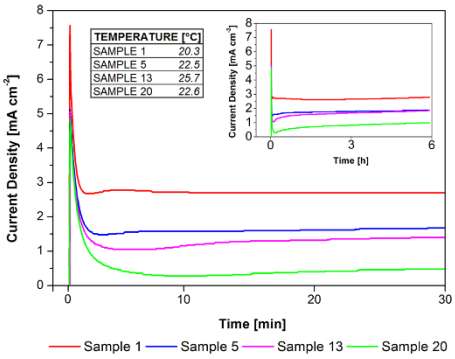

Figure 2. Current density vs time measured at the beginning of the anodization of the titanium discs in different aged electrolytes (1st, 5th, 13th, and 20th anodization). (inset) Current density vs time during the entire anodization period, together with average temperature of the anodization electrolyte.

The electrical conductivity of the electrolyte decreased with the increasing number of anodizations (Figure 3), which is due to the consumption of F^- ions and NH_4^+ ions during the

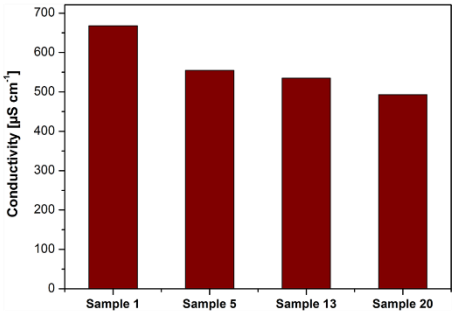

Figure 3. Conductivity of anodization electrolyte measured immediately after the anodic oxidation of samples 5, 13, and 20 and of the starting electrolyte (sample 0).

https://dx.doi.org/10.1021/acs.jpcc.9b09522
J. Phys. Chem. C 2020, 124, 4073−4080

anodization process. Fluoride ions have two main effects on the oxide-formation process. First, they form water-soluble $[TiF_6]^{2-}$ ions and prevent the formation of hydroxide. Second, they etch the formed TiO_2 so that a nanotubular layer is formed instead of a compact one.[14] Since the fluoride ions induce the chemical dissolution reaction and possess a small ionic radius, a small fraction of fluoride ions can be incorporated into the amorphous TiO_2.[22,23]

The as-grown TiO_2 nanotubes are mostly amorphous and have to be transformed to the anatase crystalline phase in order to be photocatalytically active. During annealing in air above 280 °C, most of the fluoride is removed in the form of HF from the TiO_2 film.[22] The remaining fluoride was measured with the ToF SIMS analysis of the annealed film; however, it was determined that it is almost completely removed in the case of annealing at 700 °C.[24] The concentration of ammonium ions also influences the morphology of the TiO_2 nanotubes.[25] They are consumed during the anodization process due to the formation of the $(NH_4)_2TiF_6$ salt,[26] followed by the formation of ammonia (NH_3), which is volatile under alkaline conditions (eq 2). The pH of the unused electrolyte was 5.5 ± 0.3, whereas the pH of the electrolyte used for 20 anodizations was 8.5 ± 0.4, due to the formation of ammonia and the electrolysis of the water on the cathode, according to the following equation

Reaction between the NH_4F and TiO_2 and the formation of the $(NH_4)_2TiF_6$ salt

$$6NH_4F + TiO_2 \rightarrow (NH_4)_2TiF_6 + 2H_2O + 4NH_3 \quad (1)$$

It has been reported that the pH of the electrolyte influences the structure, morphology, and photoresponse of the TiO_2 nanotube arrays.[27,28] The current density during anodization is higher when it is performed in an acidic electrolyte. This results in a thicker and denser oxide film.[29] The change in the electrical conductivity is most noticeable after the first anodization, since it decreases from 668 mS cm^{-1} (measured before the first anodization) to 561 mS cm^{-1} (measured after the second anodization), then it decreases very slowly. It was observed that the concentrations of NH_4^+ and F^- ions are not the only ones that influence the electrolyte's conductivity. The compounds that are formed during the anodization process also play an important role, since the Ti and F ions form salts. The electrolyte's conductivity influences the current density during the anodization and thus the growth rate of the TiO_2 nanotubes and their properties. Our results for the electrolyte's conductivity are in accordance with some authors;[19,30] however, not all the authors found that with an increasing number of anodizations the electrolyte's conductivity decreases.[17,18]

3.2. Analysis of the Anodization Electrolyte's Composition. The starting electrolyte that was used in the experiments consisted of ethylene glycol with 0.3 wt % ammonium fluoride and 2 vol % deionized water. The measurements of the electrolyte's composition after the anodizations showed that F^- ions and NH_4^+ ions were consumed during each anodization (Figure 4, Table 1). The water content increased over time, since ethylene glycol is relatively hygroscopic and tends to take up water from the surrounding air.[10] The concentration of water increased by about 35%, despite the fact that the anodization cell was covered during every anodization and sealed in between the individual anodizations. The increase in water content in the electrolyte causes the formation of an initial thick compact oxide layer that also reduces the growth rate of the TiO_2 nanotubes.[31]

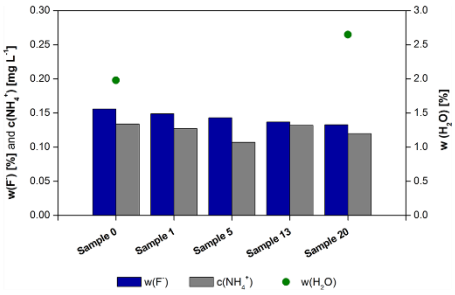

Figure 4. Water content and concentration of ammonium and fluoride ions in the anodization electrolyte used for the anodization of an increasing number of samples. Sample 0 represents the starting electrolyte.

Table 1. Concentration of Ammonium and Fluoride Ions, Together with the Water Content, in the Anodization Electrolyte Used for an Increasing Number of Samples

sample	0	1	5	13	20
$w(F^-)$ [%]	0.156	0.149	0.143	0.137	0.133
$c(NH_4^+)$ [mg L^{-1}]	0.134	0.127	0.107	0.132	0.120
$w(H_2O)$ [%]	1.98	no data	no data	no data	2.65

As shown in Table 1, the concentration of F^- decreases with the increasing number of anodizations. A similar trend is observed for the concentration of NH_4^+, except that the measured values fluctuate considerably. Nevertheless, it can be concluded that NH_4^+ is also consumed during the anodization process, most probably as the volatile, gaseous ammonia evaporates from the anodizing electrolyte. Lim et. al found that uniform nanotubes can be formed at a NH_4F content of 0.25−1.0 wt %.[32] However, our results show that changes in NH_4F concentration result in noticeable morphological changes to the TiO_2 film, although the NH_4F concentration did not fall below 0.25 wt %. The reason for this is the changes in the electrolyte's pH. At higher pH, the formation of the $(NH_4)_2TiF_6$ salt is reduced, and the nanotubes' morphologies (surface structure, pore diameter, wall thickness, length) are altered.[29] The most noticeable changes in the film's general appearance began with the 17th anodization, as two different morphologies were easily distinguished, even at very low magnifications (Figure S1). The reason for this could be the presence of dissolved titanium salts that disrupt the anodization process when their concentration is too high.

3.3. Structure, Composition, and Morphology of the TiO_2 Nanotube Films. The XRD analysis of the annealed nanotubes films showed that the films are polycrystalline in nature and that all the peaks corresponding to the TiO_2 anatase crystal structure are clearly resolved (Figure S2). The additional XRD peaks in all the spectra correspond to the metal titanium substrate. The visibility of the Ti peaks depends on the thickness of the TiO_2 film. The comparison of the highest intensity peaks for the TiO_2 and Ti ratios and also the absolute TiO_2 peak intensities (all the XRD spectra were recorded under same conditions) confirm that the TiO_2 film

https://dx.doi.org/10.1021/acs.jpcc.9b09522
J. Phys. Chem. C 2020, 124, 4073−4080

(sample 1) is the thickest and that each subsequent anatase TiO_2 film is thinner.

The XPS spectra acquired from the surface of the TiO_2 films (samples 1 and 20) did not show any major differences. Signals of Ti 2p, O 1s, and C 1s are present in all spectra and composition of the surfaces between these TiO_2 films does not differ significantly (Figure S3). The XPS valence band spectra are also similar (Figure S4). The estimated valence band maxima are approximately 2.9 eV for all samples. However, the ToF SIMS analysis which is much more sensitive than XPS analysis (analyzing the region from the surface to depth of 250 nm) of the F^- content showed that sample 1 contained much less F^- than sample 20 (Figure S5). This could be due to the acidic pH of 5.5 ± 0.3 during the first anodization and the basic pH of 8.5 ± 0.4 during the last anodizations. This is because the acidic pH mainly causes the formation of TiF_6^{2-} ions, while different oxofluorides are formed at the basic pH. The TiF_6^{2-} ions are soluble in the anodization electrolyte in comparison with the less soluble oxofluorides, which to a greater extent remain in the TiO_2 film.

Figures 5 and 6 show the top surfaces of the anodized titanium discs annealed at 450 °C. SEM micrographs of one

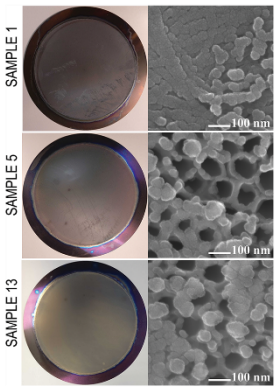

Figure 5. Top surface of anodized titanium discs (samples 1, 5, 13): photographs (left column) and high-magnification SEM images (right column).

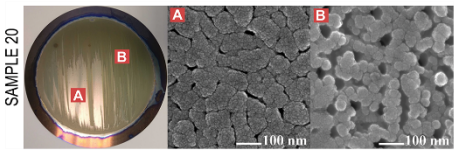

Figure 6. Top surface of anodized sample 20: photograph (left-hand side) and high-magnification SEM images (right-hand side). Two distinctive areas are observed: one with the formed TiO_2 nanotubes (B) and areas where only a compact TiO_2 film is present (A).

unannealed sample are shown in Figure S6. Since unannealed samples are amorphous, the surface does not show any distinct features as compared to annealed samples. The photographs of the discs in Figures 5 and 6 show the macroscopic appearance of the films, while the SEM images reveal the morphological characteristics of their surfaces. Four samples are shown. The results indicate that the top surfaces of the TiO_2 films vary greatly. The anodization of the first sample resulted in nanotubes with an almost completely closed top surface, due to the excessive etching and the "nanograss" formation on the top surface of the sample (Figure S7). The top surface of the first sample does not show any visible irregularities. These only appeared during and after the 17th anodization, when there were regions that appeared polished and free of any oxide film. These regions became more pronounced with each subsequent anodization and are shown for sample 20. In Figure 6, regions A and B are clearly distinguished even at low magnifications. The SEM micrographs of these regions reveal that the entire sample is anodized, but the morphology in region A differs from that in B. The morphology of the top surface of the TiO_2 film in region B is very similar to that of sample 1. The top surface of the nanotube film is almost completely closed. The morphology of the film in region A is not typical for anodized titanium, as a compact spongelike oxide was formed instead of the nanotubes. The top surfaces of samples 5 and 13 consist of very open nanotubes with a diameter of approximately 100 nm. We found that the anodization electrolyte's pH has an important influence on the morphology of the nanotube film, and it slowly increased during the experiments. It is known from the literature that morphologically the most uniform and consistent nanotubes are grown in a neutral electrolyte medium,[28] which is consistent with our results. A slightly acidic or alkaline electrolyte caused a structural disorder of the top surface of the nanotubes, which were relatively closed. When the pH of the electrolyte was in the neutral region, the top surface of the nanotubes was more regular and open. This occurred in the case of the fifth anodization.

3.4. Caffeine Degradation. The photocatalytic activity of the TiO_2 nanotube arrays was determined by measuring the degradation of caffeine. Figure 7 shows the degradation of caffeine using four different samples after different reaction times. The same figure also shows the length of the TiO_2 nanotubes for all four samples. The length of nanotubes was measured from cross-sectional SEM images (Figure S8).

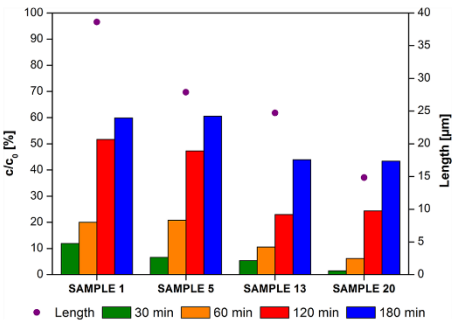

Figure 7. Photocatalytic degradation of caffeine using anodized titanium discs (samples 1, 5, 13, and 20). The average TiO_2 nanotube film thickness (dots and the legend on the right-hand *y*-axis) is also shown for these samples.

https://dx.doi.org/10.1021/acs.jpcc.9b09522
J. Phys. Chem. C 2020, 124, 4073−4080

Samples 1 and 5 show similar activity, i.e., a degradation of approximately 60% of the initial caffeine during a UV illumination period of 3 h. Samples 13 and 20 have a poorer photocatalytic performance. Both samples achieved a degradation of approximately 44% of the caffeine after the longest reaction time. In order to better describe the achieved caffeine conversions, the photonic efficiencies (ξ) and initial reaction rates (R_i) were calculated using the equations described by Krivec et al.[10] Photonic efficiency is defined as the number of transformed reactant molecules divided by the number of incident photons of monochromatic light. It was calculated with eq 2, while the initial reaction rate was calculated from eq 3.

$$\zeta = \frac{\Delta cV}{I_0 \Delta t A}, \quad \text{where } I_0 = \frac{I\lambda}{N_a h c} \tag{2}$$

$$R_i = \frac{\Delta c}{N_a \Delta t} \tag{3}$$

Δc is the difference in caffeine concentration in reaction time Δt. V is the volume of the caffeine solution, A is the geometric surface area, and I_0 is photon flux. It is calculated from UV light intensity I (1.097 mW cm^{-1} during our experiments), wavelength of UV light λ, Avogadros constant N_a, Planck constant h, and the speed of light c. The best photonic efficiency was approximately 0.43%, achieved with sample 5. The largest number of incident photons was lost during the photocatalytic reaction on the surface of sample 20, whose photonic efficiency was approximately 0.31%. The initial reaction rates followed the same order. The best achieved R_i was approximately 0.014×10^{-6} mol L^{-1} s^{-1}. The photonic efficiencies and the initial reaction rates of samples 1, 5, 13, and 20 are shown in the Supporting Information (Figure S9). It is known from the literature that the photocatalytic activity is influenced by the morphology and the length of the TiO_2 nanotubes, whereby the photodegradation efficiency is improved with increasing lengths of the nanotubes, due to higher surface area and the increased light absorption.[33] However, the photocatalytic activity is enhanced only to a certain extent, since there exists a limited penetration depth of UV light.[34] The longer nanotubes have thinner walls and greater volumes in the upper part of the tubes, meaning that the UV light has to travel on a longer pathway before absorption and the production of electron−hole pairs.[35] According to the data in the literature, many authors observed that the best photocatalytic results were obtained with TiO_2 nanotubes of different lengths. The following optimum nanotube lengths were reported: 2.2,[34] 4.8,[33] and 7 μm.[35] Irrespective of all the literature data, our results show that the length of the nanotubes, when comparing samples that were anodized with different ages of electrolytes, is not the decisive parameter in determining the photocatalytic activity of the TiO_2 films. The reason why the thickness of the TiO_2 film does not significantly influence its photocatalytic activity is that our thinnest film (measured for sample 20) already has had a thickness of approximately 15 μm, which is more than the most often reported optimum thickness for the nanotube films. The longest TiO_2 nanotubes were grown during the first anodization, when the electrolyte was still fresh and its conductivity was the highest. The length of the nanotubes after 6 h of anodization was approximately 40 μm. Our findings regarding the effect of the nanotubes' morphology and length on their photocatalytic activity are in accordance with a study conducted by Mabiala Masiala et al. using H_2SO_4- and NaOH-based anodization electrolytes. Those authors reported that anodization in acid electrolytes results in stable oxide films with improved adhesion to the titanium metal substrate and an improved photoresponse.[27] Our results show a gradual decrease in the photocatalytic efficiency with the aging of the electrolyte due to an increase of the electrolyte's pH. Furthermore, the differences in the intensities of the OH^-, O_2^-, and TiO^- signals observed from the ToF SIMS analyses of samples 1 and 20 (Figure 8) also explain the differences in the photocatalytic activities of all the samples. The signal intensities of all three negative ionic fragments follow the same trend as the photocatalytic efficiencies of the samples. The intensities observed for sample 1 are higher than for sample 20. The obtained results are in accordance with the literature data. Since the photocatalytic oxidation of caffeine proceeds via hydroxyl radicals,[36] the concentration of the surface OH^- greatly influences the activity of the catalyst. In sample 20, the concentration of the surface OH^- is reduced due to the fluoride-exchange. It can be seen in Figure S3 that the amount of F^- in the nanotube films increases after the first anodization. The difference in the intensity of the TiO^- and O_2^- species does not play a role in the photocatalytic reactions. Due to the bombardment of the primary ion beam of bismuth during the ToF SIMS analysis, there is a desorption of TiO^- and O_2^- species originating from the TiO_2 structure. However, some of the oxygen (O_2^-) could also represent the oxygen adsorbed as superoxo which plays an important role in the catalytic oxidation reactions.[37]

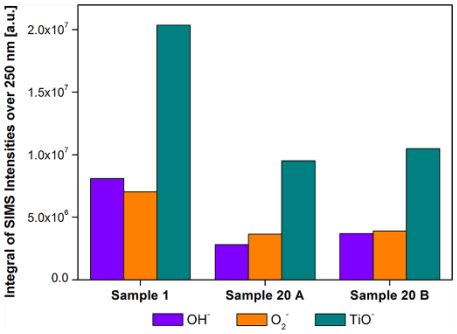

Figure 8. Integrals of SIMS signals of OH^-, O_2^-, and TiO^- ions over a depth of 250 nm for samples 1 and 20. Regions A and B of sample 20 were analyzed.

Figure 9 summarizes the results and correlates the changes in the electrolyte composition due to repeated anodizations with the growth of the TiO_2 nanotubes and their photocatalytic activity. It can be concluded that changes in the electrolyte's composition negatively affect the growth rate of the nanotubes and their photocatalytic properties. The electrolyte's pH is gradually increasing, which plays a very important role.

https://dx.doi.org/10.1021/acs.jpcc.9b09522
J. Phys. Chem. C 2020, 124, 4073−4080

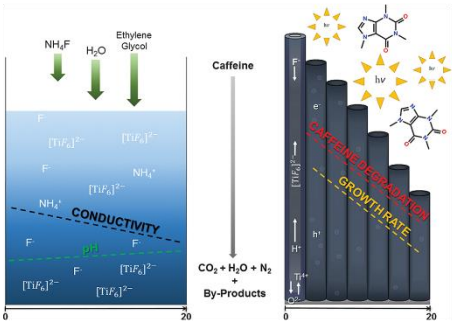

Figure 9. Effect of repeated anodic oxidations in the same electrolyte on the anodization electrolyte's composition and conductivity, as well as on the growth rate and photocatalytic activity of the grown TiO_2 nanotubes.

5. CONCLUSIONS

We studied the influence of an anodization electrolyte's aging after sequential anodizations with respect to the morphology, structure, composition, and photocatalytic activity of TiO_2 nanotube films. Twenty titanium foils were anodized in the same electrolyte to grow rigidly attached TiO_2 nanotube films. The samples were then annealed to transform the amorphous TiO_2 to the anatase structure. As a general rule, it was found that with each subsequent anodization the length of the TiO_2 nanotubes gradually decreased, as did the corresponding photocatalytic activities of the formed TiO_2 films. A microstructural characterization further revealed that the last anodized discs, apart from the areas of formed TiO_2 nanotubes, also contained areas where only a compact TiO_2 film was present. The electrolyte's aging was monitored by analyzing its chemical composition after each anodization and by measuring the current density and the temperature during the anodization, as well as the conductivity and pH of the electrolyte. It was determined that the conductivity of the electrolyte was decreasing with each anodization, while the pH value was increasing. Although the concentration of F^- in the electrolyte after each subsequent anodization did not change significantly, an integrated ToF SIMS signal over a depth of 250 nm showed that the F^- ions did incorporate into the TiO_2 films and that the concentration of F^- in the last anodized disc was approximately three times higher than for the first disc (Figure S3). On the other hand, the concentration of OH^- and O_2^- in the annealed TiO_2 films showed the opposite trend. It was concluded that a reduced concentration of OH^- and O_2^- species at the TiO_2 surface was the main factor responsible for the reduced photocatalytic activity of the TiO_2 films after successive anodizations and that the decreased length of the TiO_2 nanotubes after each anodization does not have a significant effect on the photocatalytic activity of the TiO_2 films. Moreover, the length of the TiO_2 nanotubes is primarily governed by the current density, which is a consequence of the electrolyte's conductivity. Our results also suggest that batch-type anodization cells cannot yield reproducible TiO_2 nanotube films due to aging of the anodization electrolyte and that a continuous regeneration of the anodization electrolyte is needed to obtain TiO_2 films with comparable photocatalytic activities.

■ ASSOCIATED CONTENT

Supporting Information

The Supporting Information is available free of charge at https://pubs.acs.org/doi/10.1021/acs.jpcc.9b09522.

Additional figures showing photograph of annealed anodized film, XRD and XPS spectra of anodized films, amount of F^- in annealed nanotubes and anodization electrolyte, SEM image of unannealed sample, top surface of sample 1, and cross-section of the TiO_2 films (PDF)

■ AUTHOR INFORMATION

Corresponding Author

Luka Suhadolnik − *Department for Nanostructured Materials, Jožef Stefan Institute, SI-1000 Ljubljana, Slovenia;* orcid.org/0000-0002-9103-6687; Phone: +386 1 477 3931; Email: luka.suhadolnik@ijs.si

Authors

Živa Marinko − *Department for Nanostructured Materials, Jožef Stefan Institute, SI-1000 Ljubljana, Slovenia; Jožef Stefan International Postgraduate School, SI-1000 Ljubljana, Slovenia*

Maja Ponikvar-Svet − *Department of Inorganic Chemistry and Technology, Jožef Stefan Institute, SI-1000 Ljubljana, Slovenia*

Gašper Tavčar − *Department of Inorganic Chemistry and Technology, Jožef Stefan Institute, SI-1000 Ljubljana, Slovenia;* orcid.org/0000-0001-9891-6153

Janez Kovač − *Department of Surface Engineering and Optoelectronics, Jožef Stefan Institute, SI-1000 Ljubljana, Slovenia*

Miran Čeh − *Department for Nanostructured Materials, Jožef Stefan Institute, SI-1000 Ljubljana, Slovenia*

Complete contact information is available at: https://pubs.acs.org/10.1021/acs.jpcc.9b09522

Notes

The authors declare no competing financial interest.

■ ACKNOWLEDGMENTS

The provision of financial support for the research and the preparation of the manuscript by the Slovenian Research Agency (ARRS) within the research programs P2-0084, P1-0045, and P2-0082 is gratefully acknowledged. This project has also received funding from the European Union's Horizon 2020 research and innovation programme under grant agreement No 823717-ESTEEM3.

■ REFERENCES

(1) Donaldson Craig, J. Anodic Oxidation of Aluminium and Its Alloys. *J. R. Aeronaut. Soc.* **1938**, *42* (331), 603−612.

(2) Donahue, C. J.; Exline, J. A. Anodizing and Coloring Aluminum Alloys. *J. Chem. Educ.* **2014**, *91* (5), 711−715.

(3) O'Sullivan, J. P.; Wood, G. C. The Morphology and Mechanism of Formation of Porous Anodic Films on Aluminium. *Proc. R. Soc. London, Ser. A* **1970**, *317* (1531), 511.

(4) Furneaux, R. C.; Rigby, W. R.; Davidson, A. P. The Formation of Controlled-Porosity Membranes from Anodically Oxidized Aluminium. *Nature* **1989**, *337*, 147.

(5) Macak, J. M.; Tsuchiya, H.; Schmuki, P. High-Aspect-Ratio TiO_2 Nanotubes by Anodization of Titanium. *Angew. Chem., Int. Ed.* **2005**, *44* (14), 2100−2102.

(6) Kim, S. J.; Choi, J. Self-Assembled Arrays of ZnO Stripes by Anodization. *Electrochem. Commun.* **2008**, *10* (1), 175−179.

https://dx.doi.org/10.1021/acs.jpcc.9b09522
J. Phys. Chem. C 2020, 124, 4073−4080

(7) Chen, Y.-Y.; Yu, B.-Y.; Wang, J.-H.; Cochran, R. E.; Shyue, J.-J. Template-Based Fabrication of SrTiO3 and BaTiO3 Nanotubes. *Inorg. Chem.* **2009**, *48* (2), 681−686.
(8) Roy, P.; Berger, S.; Schmuki, P. TiO_2 Nanotubes: Synthesis and Applications. *Angew. Chem., Int. Ed.* **2011**, *50* (13), 2904−2939.
(9) Zhou, X.; Liu, N.; Schmuki, P. Photocatalysis with TiO_2 Nanotubes: "Colorful" Reactivity and Designing Site-Specific Photocatalytic Centers into TiO_2 Nanotubes. *ACS Catal.* **2017**, *7* (5), 3210−3235.
(10) Krivec, M.; Žagar, K.; Suhadolnik, L.; Čeh, M.; Dražić, G. Highly Efficient TiO_2-Based Microreactor for Photocatalytic Applications. *ACS Appl. Mater. Interfaces* **2013**, *5* (18), 9088.
(11) Haring, A.; Morris, A.; Hu, M. Controlling Morphological Parameters of Anodized Titania Nanotubes for Optimized Solar Energy Applications. *Materials* **2012**, *5* (10), 1890−1909.
(12) Nischk, M.; Mazierski, P.; Gazda, M.; Zaleska, A. Ordered TiO_2 Nanotubes: The Effect of Preparation Parameters on the Photocatalytic Activity in Air Purification Process. *Appl. Catal., B* **2014**, *144*, 674−685.
(13) Qin, L.; Chen, Q.; Lan, R.; Jiang, R.; Quan, X.; Xu, B.; Zhang, F.; Jia, Y. Effect of Anodization Parameters on Morphology and Photocatalysis Properties of TiO_2 Nanotube Arrays. *J. Mater. Sci. Technol.* **2015**, *31* (10), 1059−1064.
(14) Macak, J. M.; Tsuchiya, H.; Ghicov, A.; Yasuda, K.; Hahn, R.; Bauer, S.; Schmuki, P. TiO_2 Nanotubes: Self-Organized Electrochemical Formation, Properties and Applications. *Curr. Opin. Solid State Mater. Sci.* **2007**, *11* (1), 3−18.
(15) Sreekantan, S.; Saharudin, K. A.; Wei, L. C. Formation of TiO_2 Nanotubes via Anodization and Potential Applications for Photocatalysts, Biomedical Materials, and Photoelectrochemical Cell. *IOP Conf. Ser.: Mater. Sci. Eng.* **2011**, *21* (1), 012002.
(16) Lv, H.; Li, N.; Zhang, H.; Tian, Y.; Zhang, H.; Zhang, X.; Qu, H.; Liu, C.; Jia, C.; Zhao, J.; et al. Transferable TiO_2 Nanotubes Membranes Formed via Anodization and Their Application in Transparent Electrochromism. *Sol. Energy Mater. Sol. Cells* **2016**, *150*, 57−64.
(17) Lee, K.; Kim, J.; Kim, H.; Lee, Y.; Tak, Y.; Kim, D.; Schmuki, P. Effect of Electrolyte Conductivity on the Formation of a Nanotubular TiO_2 Photoanode for a Dye-Sensitized Solar Cell. *J. Korean Phys. Soc.* **2009**, *54* (3), 1027−1031.
(18) Sopha, H.; Hromadko, L.; Nechvilova, K.; Macak, J. M. Effect of Electrolyte Age and Potential Changes on the Morphology of TiO_2 Nanotubes. *J. Electroanal. Chem.* **2015**, *759*, 122−128.
(19) Gulati, K.; Santos, A.; Findlay, D.; Losic, D. Optimizing Anodization Conditions for the Growth of Titania Nanotubes on Curved Surfaces. *J. Phys. Chem. C* **2015**, *119* (28), 16033−16045.
(20) Ponikvar, M.; Stibilj, V.; Zemva, B. Daily Dietary Intake of Fluoride by Slovenian Military Based on Analysis of Total Fluorine in Total Diet Samples Using Fluoride Ion Selective Electrode. *Food Chem.* **2007**, *103* (2), 369−374.
(21) Vogel, A. I.; Bassett, J. *Vogel's Textbook of Quantitative Inorganic Analysis : Including Elementary Instrumental Analysis*; Longman, 1978.
(22) Indira, K.; Mudali, U. K.; Nishimura, T.; Rajendran, N. A Review on TiO_2 Nanotubes: Influence of Anodization Parameters, Formation Mechanism, Properties, Corrosion Behavior, and Biomedical Applications. *J. Bio- Tribo-Corrosion* **2015**, *1* (4), 28.
(23) Peng, Z.; Ni, J. Surface Properties and Bioactivity of TiO_2 Nanotube Array Prepared by Two-Step Anodic Oxidation for Biomedical Applications. *R. Soc. Open Sci.* **2019**, *6* (4), 181948.
(24) Chung, E. H.; Baek, S. R.; Yu, S. M.; Kim, J. P.; Hong, T. E.; Kim, H. G.; Bae, J.-S.; Jeong, E. D.; Khan, F. N.; Jung, O. Self-Organized TiO_2 Nanotube Arrays in the Photocatalytic Degradation of Methylene Blue under UV Light Irradiation. *J. Korean Phys. Soc.* **2015**, *66* (7), 1135−1139.
(25) Shankar, K.; Mor, G. K.; Fitzgerald, A.; Grimes, C. A. Cation Effect on the Electrochemical Formation of Very High Aspect Ratio TiO2 Nanotube Arrays in Formamide−Water Mixtures. *J. Phys. Chem. C* **2007**, *111*, 21.
(26) Raja, K. S.; Gandhi, T.; Misra, M. Effect of Water Content of Ethylene Glycol as Electrolyte for Synthesis of Ordered Titania Nanotubes. *Electrochem. Commun.* **2007**, *9* (5), 1069−1076.
(27) Mabiala Masiala, T.; Bantu, A. K. M.; Bakambo, G. E.; Lunguya, J. M.; Kanza, J. L. K.; Muamba, O. M. Influence of PH Preparation on the Photo-Response of Electrodeposited Titanium Dioxide TiO_2 Thin Films. *Int. J. Mater. Sci. Appl.* **2016**, *5* (5), 207.
(28) Joseph, S.; David, T. M.; Ramesh, C.; Sagayaraj, P. The Role of Electrolyte PH in Enhancing the Surface Morphology of TiO_2 Nanotube Arrays Grown on Ti Substrate. *Int. J. Sci. Eng. Res.* **2014**, *5*, 85−91.
(29) Sreekantan, S.; Lockman, Z.; Hazan, R.; Tasbihi, M.; Tong, L. K.; Mohamed, A. R. Influence of Electrolyte PH on TiO2 Nanotube Formation by Ti Anodization. *J. Alloys Compd.* **2009**, *485* (1−2), 478−483.
(30) Jarosz, M.; Pawlik, A.; Kapusta-Kołodziej, J.; Jaskuła, M.; Sulka, G. D. Effect of the Previous Usage of Electrolyte on Growth of Anodic Titanium Dioxide (ATO) in a Glycerol-Based Electrolyte. *Electrochim. Acta* **2014**, *136*, 412−421.
(31) Li, H.; Ding, M.; Jin, J.; Sun, D.; Zhang, S.; Jia, C.; Sun, L. Effect of Electrolyte Pretreatment on the Formation of TiO_2 Nanotubes: An Ignored yet Non-Negligible Factor. *ChemElectroChem* **2018**, *5* (7), 1006−1012.
(32) Ying Chin, L.; Zainal, Z.; Khusaimi, Z.; Sarah Ismail, S. *Electrochemical Synthesis of Ordered Titania Nanotubes in Mixture of Ethylene Glycol and Glycerol Electrolyte*; 2016; Vol. *20*.
(33) Adán, C.; Marugán, J.; Sánchez, E.; Pablos, C.; van Grieken, R. Understanding the Effect of Morphology on the Photocatalytic Activity of TiO_2 Nanotube Array Electrodes. *Electrochim. Acta* **2016**, *191*, 521−529.
(34) Wang, W.-Y.; Chen, B.-R. Characterization and Photocatalytic Activity of TiO_2 Nanotube Films Prepared by Anodization. *Int. J. Photoenergy* **2013**, *2013*, 1−12.
(35) Marien, C. B. D.; Cottineau, T.; Robert, D.; Drogui, P. TiO_2 Nanotube Arrays: Influence of Tube Length on the Photocatalytic Degradation of Paraquat. *Appl. Catal., B* **2016**, *194*, 1−6.
(36) Dalmazio, I.; Santos, L. S.; Lopes, R. P.; Eberlin, M. N.; Augusti, R. *Environ. Sci. Technol.* **2005**, *39*, 5982.
(37) Setvín, M.; Aschauer, U.; Scheiber, P.; Li, Y.-F.; Hou, W.; Schmid, M.; Selloni, A.; Diebold, U. Reaction of O_2 with Subsurface Oxygen Vacancies on TiO_2 Anatase. *Science* **2013**, *341* (6149), 988−991.

https://dx.doi.org/10.1021/acs.jpcc.9b09522
J. Phys. Chem. C 2020, 124, 4073−4080

Supporting Information

Influence of Anodization-Electrolyte Aging on the Photocatalytic Activity of TiO_2 Nanotube Arrays

Luka Suhadolnik,[1,*] Živa Marinko,[1,3] Maja Ponikvar-Svet,[2] Gašper Tavčar,[2] Janez Kovač,[4] Miran Čeh[1]

[1] Department for Nanostructured Materials, Jožef Stefan Institute, Jamova 39, SI-1000 Ljubljana, Slovenia

[2] Department of Inorganic Chemistry and Technology, Jožef Stefan Institute, Jamova 39, SI-1000 Ljubljana, Slovenia

[3] Jožef Stefan International Postgraduate School, Jamova 39, SI-1000 Ljubljana, Slovenia

[4] Department of Surface Engineering and Optoelectronics, Jožef Stefan Institute, Jamova 39, SI-1000 Ljubljana, Slovenia

* Corresponding author: Dr. Luka Suhadolnik, email: luka.suhadolnik@ijs.si, phone: +386 1 477 3931

102

Film general appearance

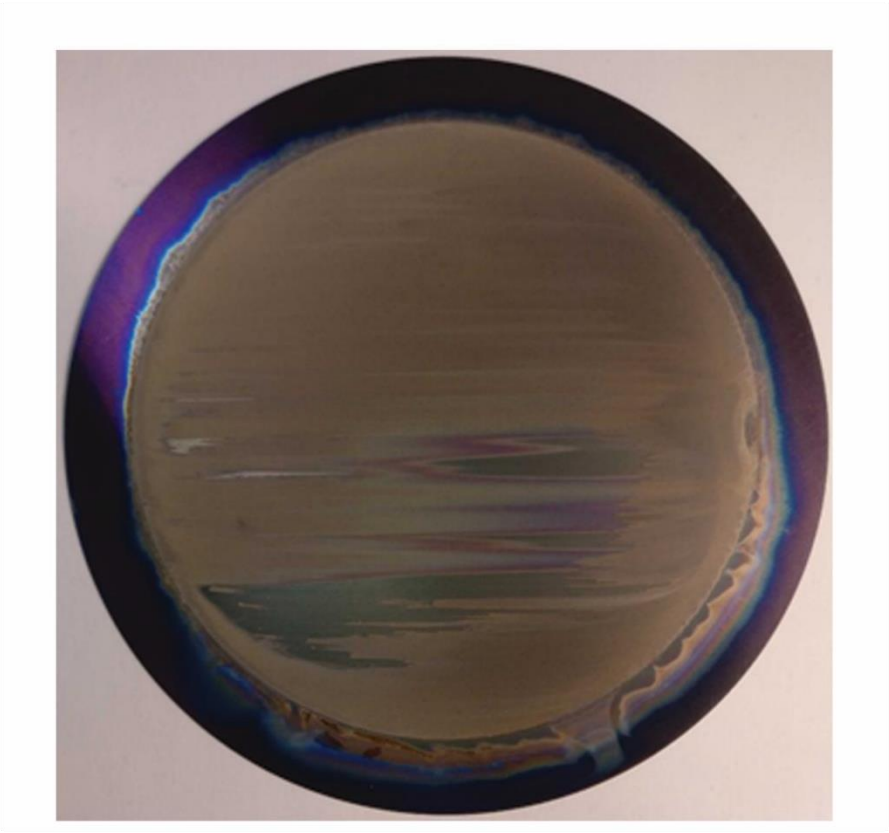

Figure S1. A photograph of the annealed anodized film prepared in the 18th anodization.

XRD spectra of anodized films

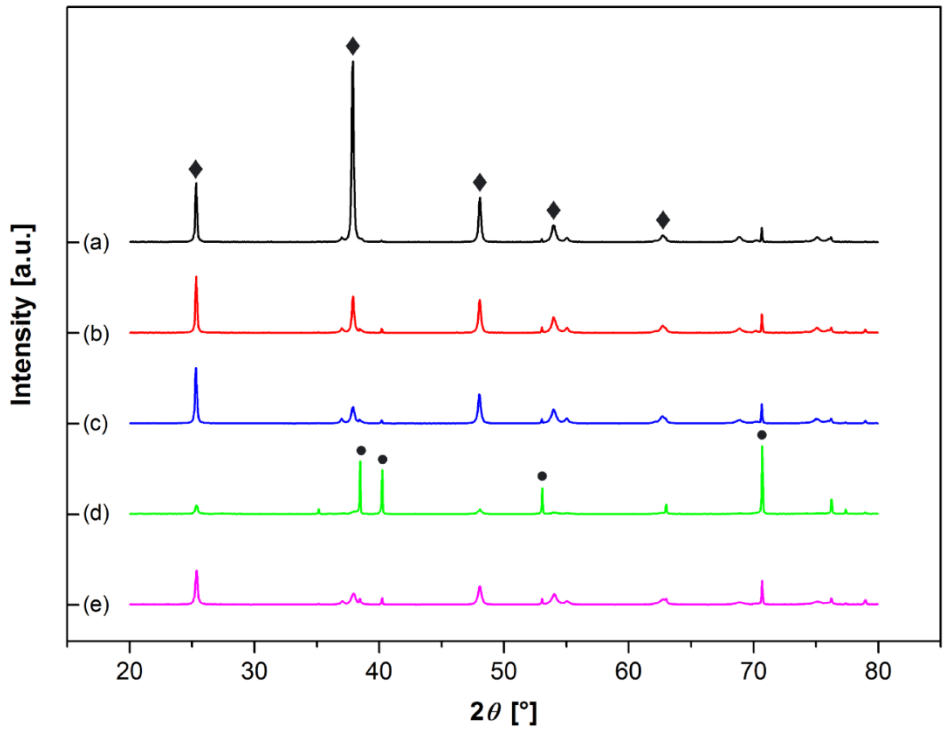

Figure S2. XRD spectra of (a) sample 1, (b) sample 5, (c) sample 13, (d) region A of sample 20 and (e) region B of sample 20. Peaks marked with ♦ correspond to the tetragonal anatase TiO_2 (PDF 01-071-1166) while the peaks marked with • correspond to the hexagonal titanium substrate (PDF 00-005-0682).

XPS spectra of anodized films

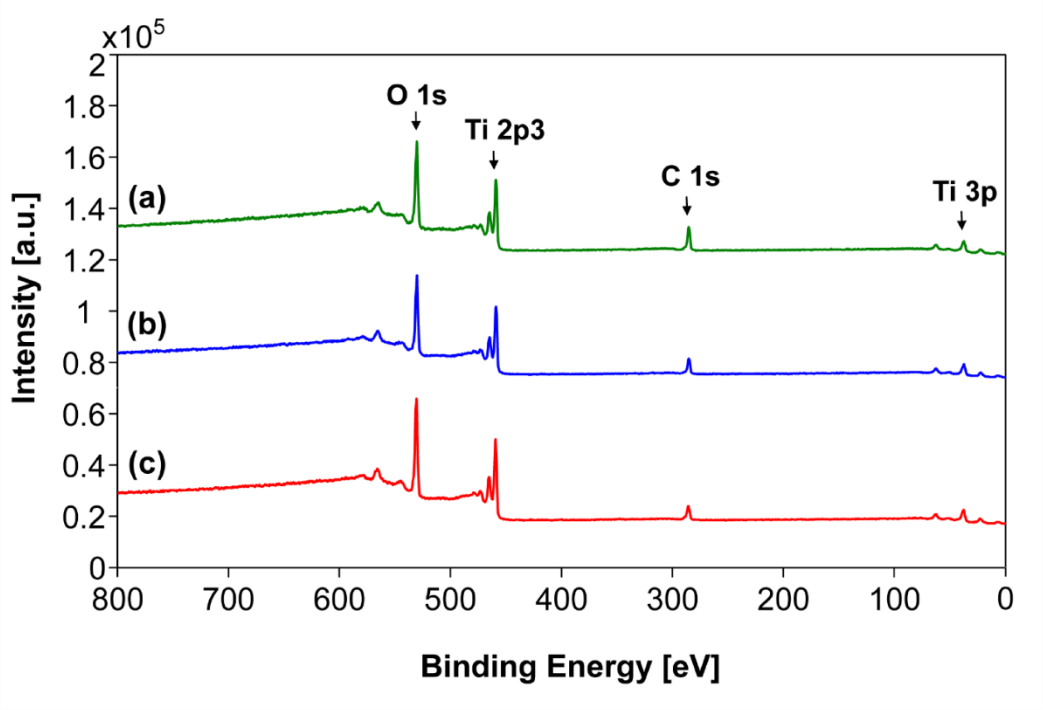

Figure S3. XPS spectra of (a) region A of sample 20, (b) region B of sample 20 and (c) sample 1. O1s, Ti 2p3, Ti 3p and C 1s peaks are marked.

XPS valence band spectra of anodized films

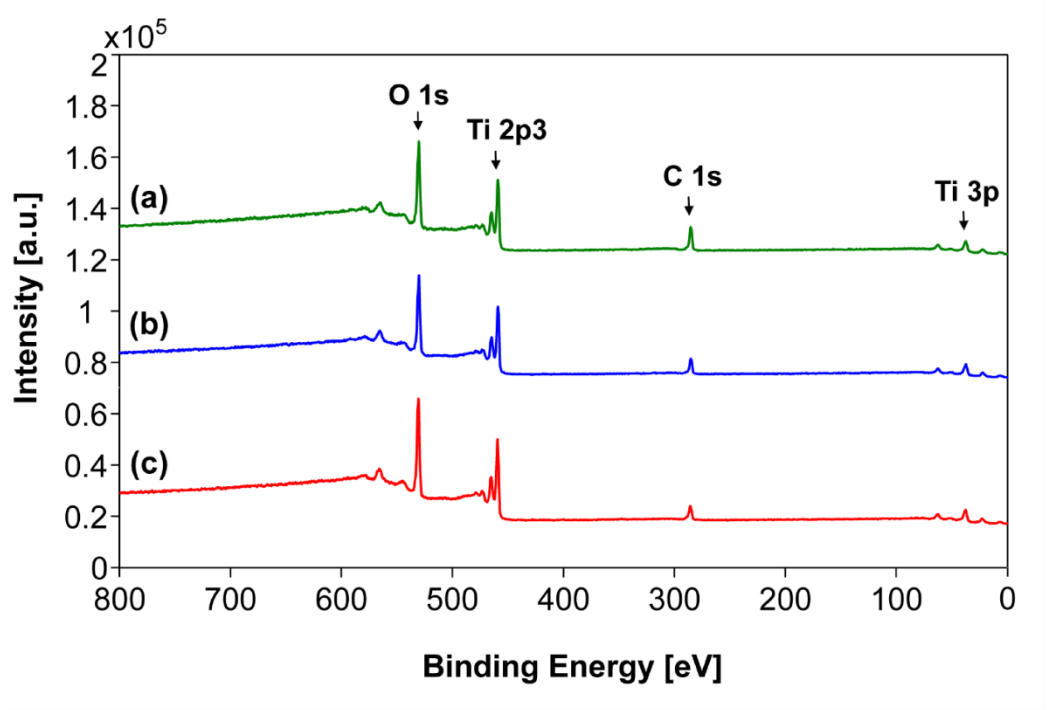

Figure S4. The XPS valence band spectra of sample 1 (red), region A of sample 20 (green) and region B of sample 20 (blue).

Amount of F^- in annealed nanotubes and concentration of F^- in the anodization electrolyte

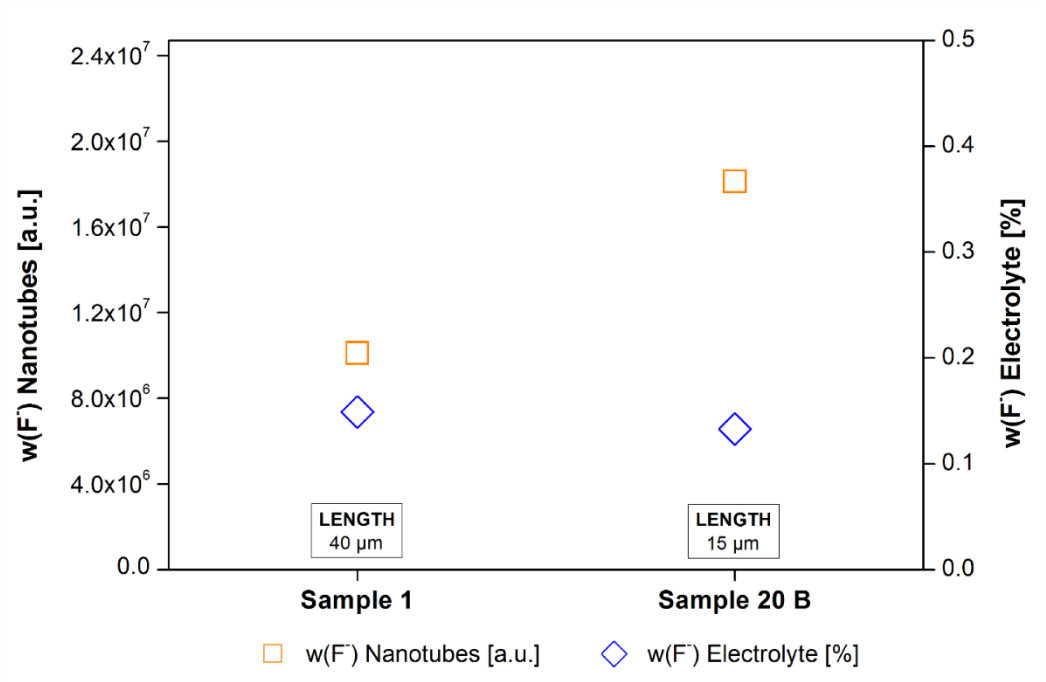

Figure S5. Amount of F^- inside TiO_2 nanotubes (□) as calculated from SIMS signals over depth of 250 nm of anodized annealed samples. Concentration of F^- (◊) in the anodization electrolyte. Additionally, the lengths of TiO_2 nanotubes are shown.

SEM image of unannealed sample

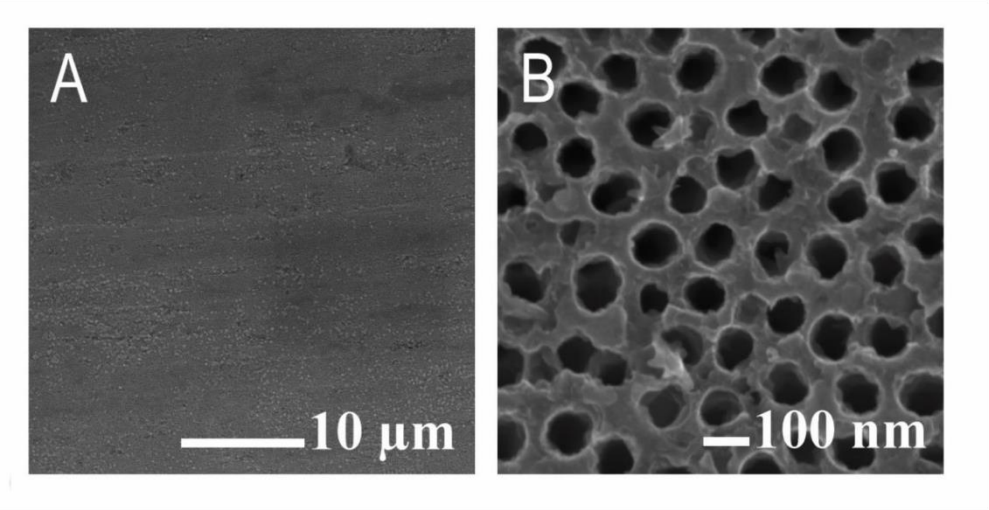

Figure S6. SEM image of top surface of unannealed anodized sample at lower (a) and higher (b) magnification.

Low-magnification SEM image of sample 1

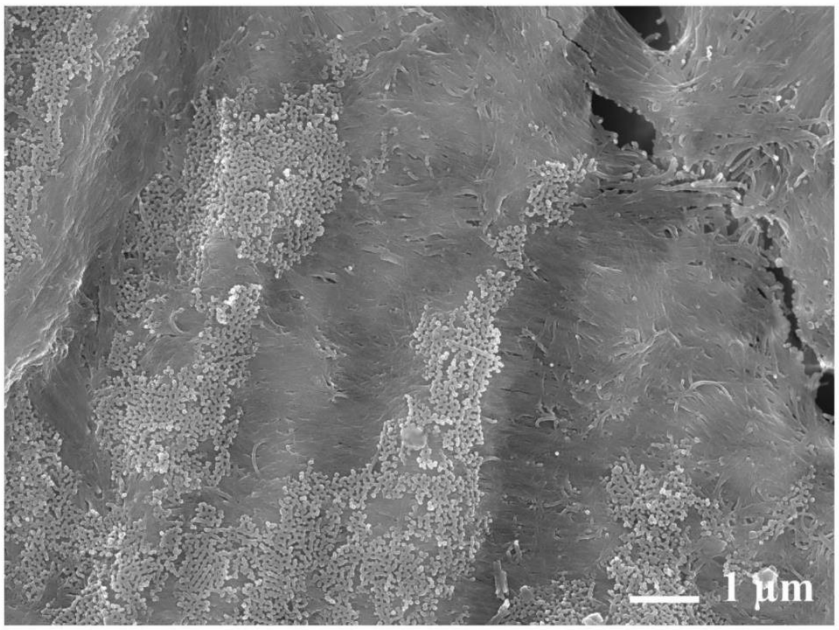

Figure S7. Low-magnification SEM image of top surface of anodized sample 1.

Cross-sectional SEM images

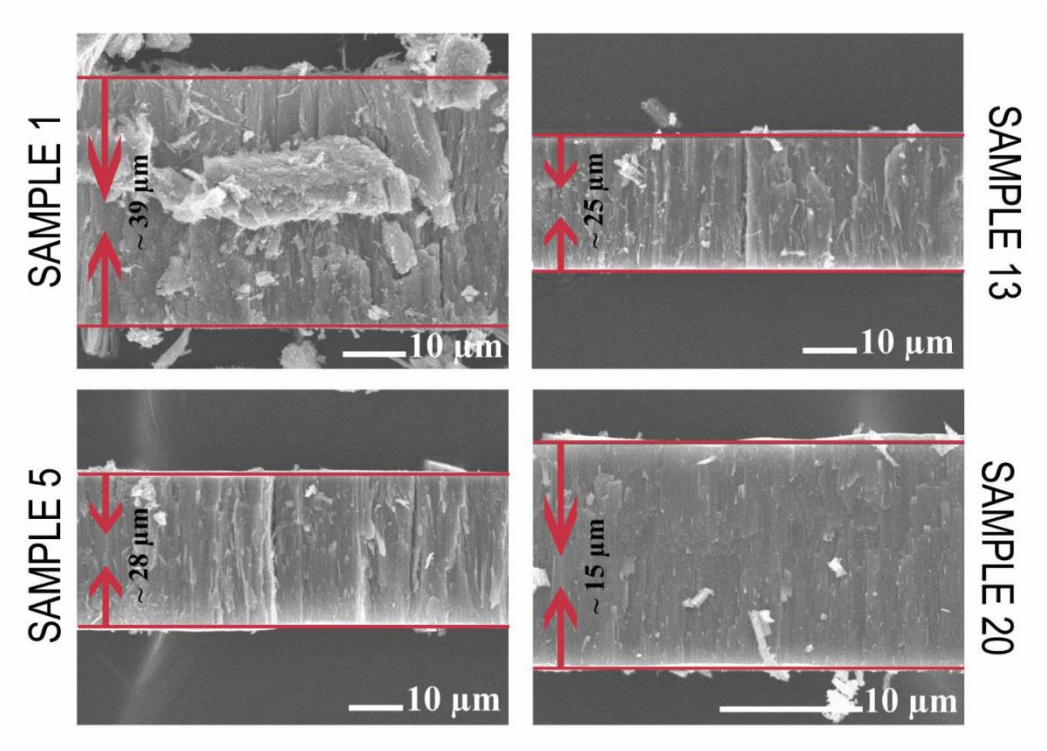

Figure S8. SEM cross-section view of the TiO_2 films prepared in 1st, 5th, 13th and 20th anodization. Average nanotubes length is shown in each micrograph.

110

Photonic efficiency and initial reaction rate

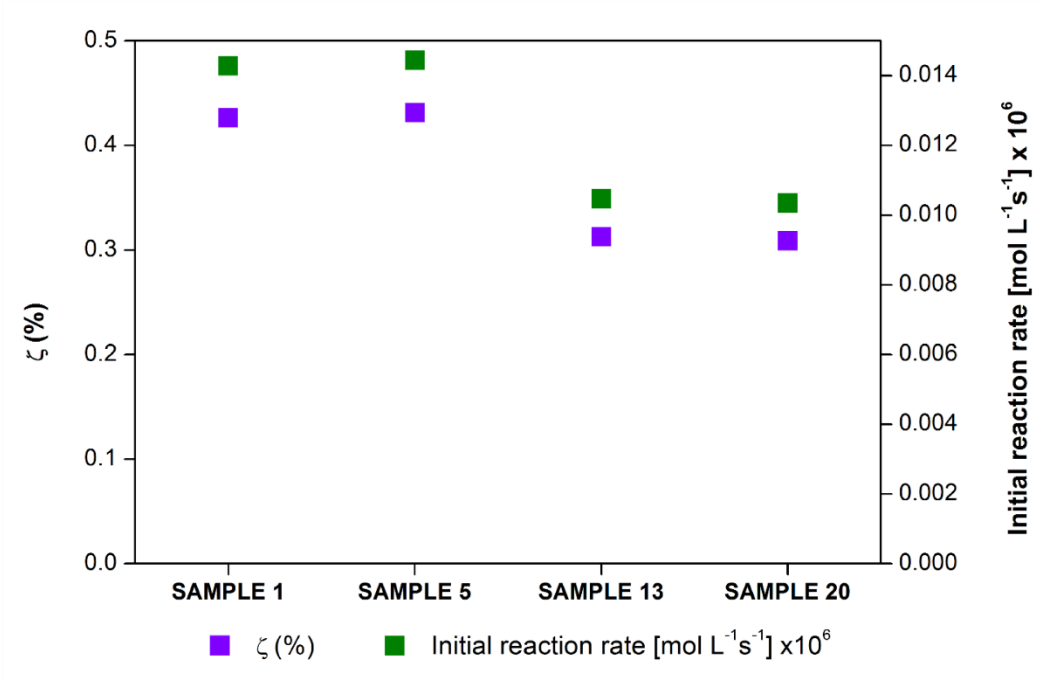

Figure S9. Photonic efficiencies and initial reaction rates of samples 1, 5, 13 and 20.

4.1 Appendix to the Paper

The anodic oxidation of Ti foil is an electrochemical process that results in self-organized TiO_2 NT layers. Under optimized experimental conditions, an ordered TiO_2 nanotube layer is formed on the Ti substrate. However, after several anodisations using the same electrolyte, the ratio between the F^-, H_2O and NH_4^+ concentrations are altered since the composition of the electrolyte changes due to the NTs' growth mechanism. As a result, a disordered and disconnected nanotubular layer is formed on the substrate, sometimes only a porous oxide without the NTs (Figure 4.1.).

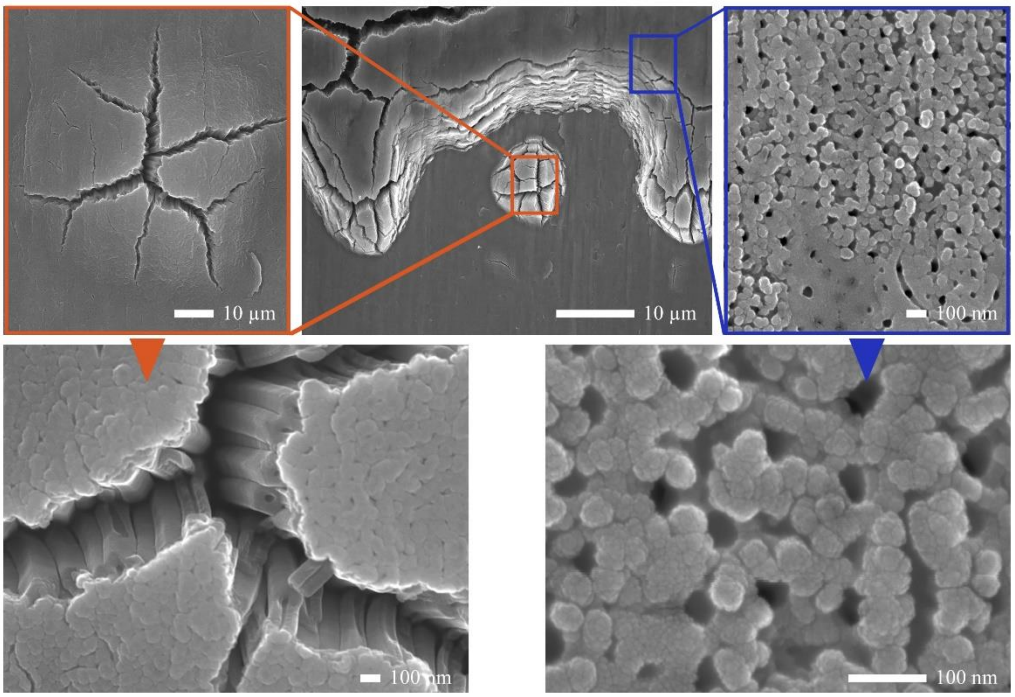

Figure 4.1: SEM imaging of the annealed anodised film was prepared in the 20th anodisation. A central image shows the anodised titanium foil's magnified part after the electrolyte regeneration. Blue marking (right) is dedicated to the individual anodised burst over the titanium foil, dedicated only to the oxide, and orange marking (left) is dedicated to the anodised film. Below each image, a magnified view is shown.

The electrolyte regeneration was achieved by adding the consumed amount of NH_4F into the aged electrolyte. The addition of NH_4F somewhat improved the growth of NTs; however, the NT growth was still retarded, and the caffeine degradation worse compared to the NTs grown in a fresh electrolyte.

The concentrations of the major electrolyte constituents after performing 23 anodisations are shown in Table 4.1. Additionally, also results of electrolyte composition and characterization of grown TiO_2 NTs of Sample 1 (*fresh electrolyte*) and Sample 23 (*regenerated electrolyte*) are presented.

Table 4.1: Regeneration of the electrolyte data.

		SAMPLE 1	SAMPLE 23
		Electrolyte	
Composition	**F^-** [%]	*0.149 ± 0.001*	*0.153 ± 0.001*
	NH_4^+ [mg L^{-1}]	*0.127 ± 0.003*	*0.128 ± N/D*
	H_2O [%]	*1.98 ± 0.06**	*2.82 ± 0.06*
Conductivity [µS cm^{-1}]		*~ 670*	*~ 560*
AO current density [mA cm^{-2}]		*~ 125*	*~ 70*
		TiO_2 NTs	
Length [µm]		*~ 40*	*~ 19*
Ti/O ratio (XPS)		*2.31*	*2.40*
Integral intensites over 250 nm [a.u.] (ToF-SIMS)	**OH^-**	*0.8 × 10^7*	*0.3 × 10^7*
	O_2^-	*0.7 × 10^7*	*0.3 × 10^7*
	TiO^-	*2.0 × 10^7*	*0.9 × 10^7*
	F^-	*1.0*	*1.5*
		Photocatalysis	
Photonic efficiency [%]		*0.43*	*0.18*
Initial reaction rate [mol L^{-1} s^{-1}]		*0.014 × 10^6*	*0.006 × 10^6*
Caffeine degradation efficiency		*~ 60 %*	*~ 25 %*

**fresh electrolyte*

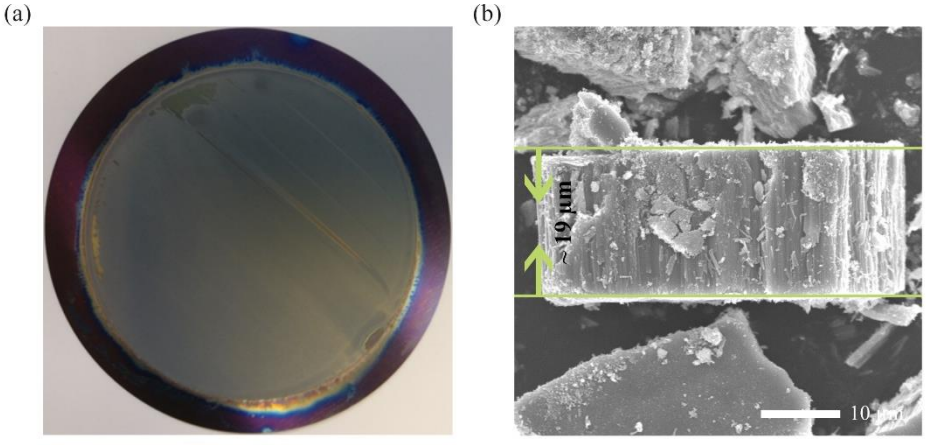

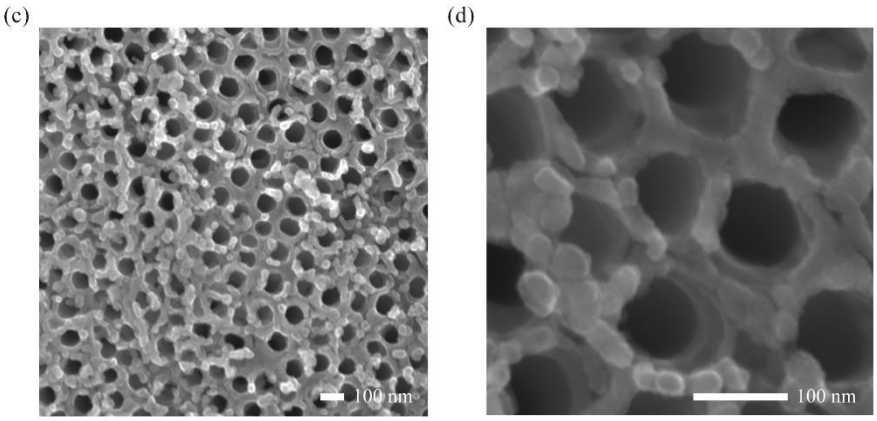

Figure 4.2: SEM images of the annealed anodised layer that was prepared during the 23rd anodisation. Presented is a (a) whole anodised disk, (b) length of the NT film in the cross-section and (c and d) magnified view of the nanotubular surface. The Figure shows the surface of anodised Ti after the 23rd anodisation and added NH_4F. The NT growth improved significantly, but the non-anodised surface area decreased.

We observed that the electrolyte regeneration was not as successful as expected, despite the fact that the measured F^- concentration in the aged electrolyte was comparable to the starting concentration in the fresh electrolyte. High F^- concentration within the NTs also decreased their length which resulted in poor photocatalytic activity. Furthermore, adding the NH_4F salt for regeneration of the electrolyte increased the H_2O concentration to almost 1.5-times higher value compared to the initial concentration of H_2O in starting electrolyte. The results presented in this chapter suggest that the addition of NH_4F salt is not appropriate for electrolyte regeneration.

Chapter 5

Conclusions

5.1 The Influence of a Surface Treatment of Metallic Titanium on the Photocatalytic Properties of TiO_2 Nanotubes Grown by Anodic Oxidation

The experimental work investigated the morphological and structural parameters as well as the chemical composition of the starting Ti metal foil prior to the anodic oxidation process. The work focused on investigating two different titanium foils with different chemical compositions and surface roughnesses. The working hypotheses were *(1) substrate pre-treatment influences the TiO_2 NT growth and their photocatalytic activity, and (2) substrate surface roughness significantly impacts the final surface area of the photocatalytically active TiO_2 NT layers.*

The main takeaway message from this work confirmed our hypotheses, shown by the original experimental work in the published manuscript. We reduced the surface roughness of the starting foils by electropolishing them. Nevertheless, the differences in the properties between the titanium foils of the two suppliers remained substantial. By performing the anodic oxidation on all the selected samples, the differences were observed in the nanotube growth as well as in their morphology. The main finding was that the flatter surfaces result in a thicker TiO_2 nanotube array with a more ordered structure. The additional analysis confirmed the primary speculations that titanium purity is essential.

The published results additionally show that all the NT samples could form reactive species and contribute to the degradation mechanism. With the additional results, we confirmed that the photocatalytic activity was the best when 365-nm light illumination or a broad spectrum from the Sterilizer was used as an illumination source.

We concluded from the results that the best photoactive NTs grew on the titanium foil from Supplier 1 (UT). Despite the thinnest NT array, the active surface area was the largest due to the high measured surface roughness. We proposed that the surface roughness of the NTs' film is a deciding factor for the high photocatalytic activity for the complete degradation of the model compound caffeine.

5.2 Toward a Flexible and Efficient TiO_2 Photocatalyst Immobilized on a Titanium Foil

This work aimed to study the effect of Ti foil thickness on TiO_2 NTs growth and their adhesion to the titanium substrate. For this study, we selected titanium foils from Supplier 1 with thicknesses of 30, 50, 100 and 200 µm. These thicknesses of titanium foils can also

be easily bent into a flexible photocatalyst. The hypotheses for this work were *(1) high NT density, shorter NTs, and fewer cracks result in better adhesion of the TiO_2 NT layer to the Ti substrate, (2) higher grain-boundary surface density represents more nucleation sites for NT growth and (3) higher surface roughness of TiO_2 NTs equals larger active surface area and thus in higher photocatalytic activity in the degradation test.*

The experimental work confirmed our hypotheses. After anodization and thermal treatment of the initial titanium foils with different thicknesses, we found that the most rigidly attached NTs were the ones on the 100-µm-thick titanium foil. The same sample exhibited the most prominent surface roughness and the thinnest layer of grown NTs nanotubes. It was concluded that the thinner NTs' layer and smaller nanotubes contribute significantly to the layer adhesion in this foil.

The 100-µm sample showed promising results for further exploitation as a flexible photocatalyst grown on an otherwise flat Ti substrate due to the excellent adhesion of the NTs with the titanium substrate. Using bent photocatalysts with a large active area is a significant advantage, since it enables the design of light reactors with better illumination of the active surfaces.

5.3 Influence of Anodization-Electrolyte Aging on the Photocatalytic Activity of TiO_2 Nanotube Arrays

This work was focused on the influence of electrolyte ageing on the NTs' growth and their subsequent photocatalytic activity. The work hypotheses were *(1) repetitive anodisation changes the electrolyte's chemical composition, thus influencing the NT growth and final photocatalytic activity, and (2) anodisation of Ti foil with fresh electrolytes results in NTs with uniform morphology.*

The experiments on electrolyte ageing were performed on surface-untreated titanium foils from Supplier 1. However, the surfaces of the used titanium substrates and the electrolyte volume were significantly larger (up to 20 times). The observed changes in the NTs' growth after each anodisation using the same electrolyte were the following:

- The water content in the electrolyte increased after each anodisation.
- The concentration of F^- decreased after each anodisation, resulting in a reduced conductivity of the electrolyte.

Other changes were the observed slower nanotube growth and the decreased photocatalytic activity after each anodisation. Consequently, the electrolyte regeneration was performed by adding excess NH_4F to the electrolyte. With the addition of F^- to the electrolyte, the nanotube growth improved; however, it was still worse than when using the fresh electrolyte.

This work confirmed our hypotheses, shown by the experimental work in the published manuscript and additional testing after the publication.

Chapter 6

Dissemination and Future Exploitation

The conclusions and findings, specified in the previous chapters, can be implemented directly into applications when designing reactors to degrade organic pollutants in wastewater and/or air. The design of purification reactors has some crucial requirements that must be fulfilled, as already mentioned in the thesis. These are *(1)* an effective photocatalyst, *(2)* maximised illumination and *(3)* a smart reactor design. Within the scope of the thesis, we provided an insight into effective photocatalysts.

1. We learned the basics and pivot points regarding titanium-substrate purity and surface roughness (Chapter 2). Moreover, we explored the flexibility of titanium foil to produce a stable and flexible photocatalyst based on TiO_2 NTs (Chapter 3). Last, we studied the electrolyte ageing after multiple anodisations using the same electrolyte in the batch experiments (Chapter 4).
2. It is vital to successfully implement the illumination, because the photocatalyst must receive as many photons as possible. With the technology we know, a considerable percentage of e^-/h^+ pairs are recombined, i.e., lost in the generation of reactive oxygen species.
3. Smart and innovative reactor design can either enhance the degradation of pollutants or reduce them. Simple trial and error can improve the design. Better yet, those data can upgrade the kinetics modelling and help implement artificial intelligence into the design process.

Since there are numerous possibilities for reactor design, we propose to use 3D technology for printing titanium electrodes. In this way, we could avoid the most crucial obstacle, the loss of a poorly adhered catalyst during the catalytic reaction. One could also innovate a reactor of various shapes and practically any size. Next, different elements could be added to the 3D-printing powder to adjust the bandgap of the catalyst and make it useful in visible light. Once anodised and annealed, 3D electrodes could be used in any proposed reactor design. With such a photocatalyst, it would be possible to attain optimum illumination of active surface area.

Secondly, to overcome the recombination of e^-/h^+ pairs during photocatalysis, the electrocatalysis component could be added to the process. Because it retains the recombination of the e^-/h^+ pair, the degradation process would be increased.

Finally, in the following Appendix, the abstracts of three manuscripts are shown, to which I have contributed as a co-author. I invite the reader to take time and read them.

Appendix

In the following sub-sections, additional published manuscripts are shown with my contribution. They are not explained in detail because the content of the manuscripts is not directly related to the aim of this thesis. However, due to their high impact and novelty, I believe they show the broad spectrum of possibilities that TiO_2 NTs exhibit in the photo-electro-catalytic area.

A.1 Increasing the Oxygen-Evolution Reaction Performance of Nanotubular Titanium Oxynitride-Supported Ir Nanoparticles by a Strong Metal–Support Interaction

ACS Catalysis

pubs.acs.org/acscatalysis Research Article

Increasing the Oxygen-Evolution Reaction Performance of Nanotubular Titanium Oxynitride-Supported Ir Nanoparticles by a Strong Metal–Support Interaction

Marjan Bele, Primož Jovanovič,* Živa Marinko, Sandra Drev, Vid Simon Šelih, Janez Kovač, Miran Gaberšček,* Gorazd Koderman Podboršek, Goran Dražić, Nejc Hodnik, Anton Kokalj, and Luka Suhadolnik*

Cite This: ACS Catal. 2020, 10, 13688–13700 Read Online

ACCESS | Metrics & More | Article Recommendations | Supporting Information

ABSTRACT: This study targets one of the grand challenges of electrochemical hydrogen production: a durable and cost-effective oxygen-evolution catalyst. We present a thin-film composite electrode with a unique morphology and an ultralow loading of iridium that has extraordinary electrocatalytic properties. This is accomplished by the electrochemical growth of a defined, high-surface-area titanium oxide nanotubular film, followed by the nitridation and effective immobilization of iridium nanoparticles. The applicative relevance of this production process is justified by a high oxygen-evolution reaction (OER) activity and high stability. Enhanced OER performance is due to the strong metal–support interaction (SMSI). The high durability is achieved by self-passivation of the titanium oxynitride (TiON) surface layer with TiO_2, which in addition also effectively embeds the Ir nanoparticles while still keeping them electrically wired. An additional contribution to the enhanced durability comes from the nitrogen atoms, which according to our density functional theory (DFT) calculations reduce the tendency of the Ir nanoparticles to grow. Materials are analyzed by advanced electrochemical characterization techniques. Namely, the entire process of the TiON–Ir electrode's preparation and the electrochemical evaluation can be tracked with scanning electron microscopy, X-ray diffraction (XRD), and X-ray photoelectron spectroscopy (XPS) at identical locations. In general, the experimental approach allows for the unique morphological, structural, and compositional insights into the preparation and electrocatalytic performance of thin films, making it useful also outside electrocatalysis applications.

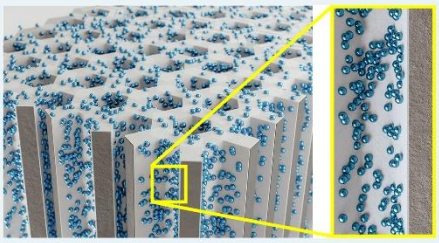

KEYWORDS: *electrocatalysis, oxygen-evolution reaction, TiON–Ir-nanotube catalyst, thin-film electrode, titanium oxynitride nanotubular support, TiON–Ir catalyst, iridium nanoparticles, IL-SEM*

1. INTRODUCTION

In the field of electrocatalysis, catalytic materials are utilized in the form of a high-surface-area, highly conductive thin film. The benefits of such materials are the good accessibility of the reactants and the assurance of good electrical contacts with the supporting material. However, the design of such materials is often challenging due to the harsh electrochemical environment that leads to degradation of the thin-film catalyst.[1] This is especially true for the oxygen-evolution reaction (OER), where electrochemical conditions are more severe in comparison to other reactions of the energy-conversion sector. Ruthenium and iridium oxides are the material of choice for OER.[2−6] Especially, iridium, due to its high price, must be dispersed on a substrate with a high surface area to increase the utilization of the catalyst layer.[7−10] Among OER thin-film approaches, the state of the art are still dimensionally stable anodes (DSAs) that are synthesized by the co-precipitation of RuO_2 and IrO_2 oxides supported by a titanium substrate with a thickness of a few micrometers.[11−15] This results in a high crystallinity as well as mechanical and electrochemical stability, both of which meet industrial demands for long-term operation. Although these electrodes are very stable, they require high noble-metal loadings. As iridium is one of the scarcest metals on earth as well as being geologically unevenly distributed (it is predominantly concentrated in the Republic of South Africa), it is of the highest importance to utilize it as effectively as possible if the technology of electrochemical hydrogen

Received: August 24, 2020
Revised: October 29, 2020
Published: November 10, 2020

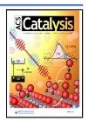

https://dx.doi.org/10.1021/acscatal.0c03688
ACS Catal. 2020, 10, 13688–13700

A.2 Effect of the Morphology of the High-Surface-Area Support on the Performance of the Oxygen-Evolution Reaction for Iridium Nanoparticles

ACS Catalysis

pubs.acs.org/acscatalysis Research Article

Effect of the Morphology of the High-Surface-Area Support on the Performance of the Oxygen-Evolution Reaction for Iridium Nanoparticles

Leonard Moriau, Marjan Bele, Živa Marinko, Francisco Ruiz-Zepeda, Gorazd Koderman Podboršek, Martin Šala, Angelja Kjara Šurca, Janez Kovač, Iztok Arčon, Primož Jovanovič,* Nejc Hodnik,* and Luka Suhadolnik*

Cite This: *ACS Catal.* 2021, 11, 670−681 Read Online

ACCESS | Metrics & More | Article Recommendations | Supporting Information

ABSTRACT: The development of affordable, low-iridium-loading, scalable, active, and stable catalysts for the oxygen-evolution reaction (OER) is a requirement for the commercialization of proton-exchange membrane water electrolyzers (PEMWEs). However, the synthesis of high-performance OER catalysts with minimal use of the rare and expensive element Ir is very challenging and requires the identification of electrically conductive and stable high-surface-area support materials. We developed a synthesis procedure for the production of large quantities of a nanocomposite powder containing titanium oxynitride ($TiON_x$) and Ir. The catalysts were synthesized with an anodic oxidation process followed by detachment, milling, thermal treatment, and the deposition of Ir nanoparticles. The anodization time was varied to grow three different types of nanotubular structures exhibiting different lengths and wall thicknesses and thus a variety of properties. A comparison of milled samples with different degrees of nanotubular clustering and morphology retention, but with identical chemical compositions and Ir nanoparticle size distributions and dispersions, revealed that the nanotubular support morphology is the determining factor governing the catalyst's OER activity and stability. Our study is supported by various state-of-the-art materials' characterization techniques, like X-ray photoelectron spectroscopy, scanning and transmission electron microscopies, X-ray powder diffraction and absorption spectroscopy, and electrochemical cyclic voltammetry. Anodic oxidation proved to be a very suitable way to produce high-surface-area powder-type catalysts as the produced material greatly outperformed the IrO_2 benchmarks as well as the Ir-supported samples on morphologically different $TiON_x$ from previous studies. The highest activity was achieved for the sample prepared with 3 h of anodization, which had the most appropriate morphology for the effective removal of oxygen bubbles.

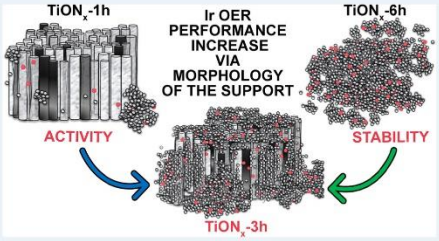

KEYWORDS: *electrocatalysis, oxygen-evolution reaction, $TiON_x$-Ir powder catalyst, iridium nanoparticles, anodic oxidation, morphology−activity correlation*

1. INTRODUCTION

The hydrogen cycle is a promising way to store energy from renewable sources, like solar and wind, through the splitting of water in an electrolyzer. This energy can subsequently be made available on-demand using a fuel cell that combines the hydrogen and the oxygen.[1] However, the efficiency of the water-splitting reaction is limited by the slow kinetics of the oxygen-evolution reaction (OER).[2] Indeed, even with a state-of-the-art catalyst in acidic media, i.e., IrO_2, an overpotential of around 0.3 V is usually required to achieve proper current densities.[3] Moreover, iridium is a precious and scarce metal, which hinders the commercialization of this technology. One way to decrease the cost of the device is to improve the utilization of the iridium. An example of this is the deposition of iridium in the form of nanoparticles on a suitable support.[4] This makes it possible to lower the cost as well as to potentially improve the catalyst's performance, which, together with the properties of the catalytically active sites, strongly depends on the interactions with the support. The so-called strong metal−support interaction (SMSI), mostly known from heterogeneous catalysis, was shown to also affect the structural and

Received: October 31, 2020
Revised: December 16, 2020
Published: December 30, 2020

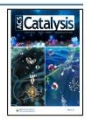

https://dx.doi.org/10.1021/acscatal.0c04741
ACS Catal. 2021, 11, 670−681

A.3 Photocatalytic, Electrocatalytic and Photoelectrocatalytic Degradation of Pharmaceuticals in Aqueous Media: Analytical Methods, Mechanisms, Simulations, Catalysts and Reactors

Journal of Cleaner Production 343 (2022) 131061

Contents lists available at ScienceDirect

Journal of Cleaner Production

journal homepage: www.elsevier.com/locate/jclepro

Photocatalytic, electrocatalytic and photoelectrocatalytic degradation of pharmaceuticals in aqueous media: Analytical methods, mechanisms, simulations, catalysts and reactors

Belisa A. Marinho [a,*], Luka Suhadolnik [a], Blaž Likozar [b], Matej Huš [b,c], Živa Marinko [a,d], Miran Čeh [a]

[a] Department for Nanostructured Materials, Jožef Stefan Institute, Jamova 39, 1000, Ljubljana, Slovenia
[b] Department of Catalysis and Chemical Reaction Engineering, National Institute of Chemistry, Hajdrihova 19, SI 1000, Ljubljana, Slovenia
[c] Association for Technical Culture of Slovenia (ZOTKS), Zaloška 65, 1000, Ljubljana, Slovenia
[d] Jožef Stefan International Postgraduate School, Jamova 39, 1000, Ljubljana, Slovenia

ARTICLE INFO

Handling Editor: Zhen Leng

Keywords:
Advanced oxidation process
Persistent organic compounds
Pharmaceutical by products
Degradation mechanism
Reactor design
Analytical methods

ABSTRACT

Pharmaceuticals are used every day in most parts of the world and great proportions of these substances are excreted unaltered or as active sub-products, posing a threat of pollution. To protect the aquatic ecosystems, innovative solutions such as photocatalysis, electrocatalysis and photoelectrocatalysis are required. In this article we provide a comprehensive review of photo- and electrocatalytic techniques for the removal of pharmaceuticals from water and wastewaters. The analytical and toxicity methods commonly used to study the degradation of pharmaceuticals are presented, and it is pointed high performance liquid chromatography analysis as the most common analytical method to evaluate the efficiency in the pharmaceutical's degradation. However, it is also highlighted that the evaluation of the toxicity is fundamental to ensure adequate treatment. The determination of the reactive species and the mechanistic evaluation of pharmaceuticals degradation are essential to understanding and enhancing the degradation process. A deep discussion of photocatalysis, electrocatalysis and photoelectrocatalysis principles and practical examples of their application in pharmaceuticals treatment is presented. The catalytic materials and the reactors used in these processes for the removal of pollutants are reviewed focusing on some representative examples. The reusability of catalysts is still restricted to a few reuse cycles. It was observed very limited results in the treatment of larger amounts of effluent and a lack of information about process costs, which were correlated to the difficulty of application of these techniques on real scale. Finally, the main advantages of photocatalysis, electrocatalysis and photoelectrocatalysis as high efficiency on pharmaceuticals degradation, and the main drawbacks, as the low quantum efficiency and/or high energetic consume are pointed out along with alternatives to overcome these limitations.

1. Introduction

Pharmaceuticals are an important class of substances used for healing and preventing diseases as well as improving the quality of life. Nevertheless, they are also emerging as environmental pollutants that can adversely affect the aquatic environment and so have long-term consequences for human health (Zhou et al., 2020). They reach the natural environment in its development stage as raw materials, during the production, transportation and storage, as well as through domestic sewage, hospitals and industrial wastewater, livestock farming, and solid-waste leachate, among other daily human activities (Rodriguez-Mozaz et al., 2020). The situation is worsened by their indiscriminate use (without medical planning) coupled with improper disposal (de Oliveira et al., 2020). Several classes of pharmaceuticals used in human medicine are only partially metabolized by the organism, and are excreted unaltered or in active forms. For example, more than 75% of the antibiotics from the tetracyclines family are excreted as active metabolites (Xu et al., 2021).

Numerous pharmaceuticals were already found in surface, ground and drinking water in concentrations from parts-per-trillion (ng/L) to

* Corresponding author.
E-mail address: belisa.alcantara.marinho@ijs.si (B.A. Marinho).

https://doi.org/10.1016/j.jclepro.2022.131061
Received 7 September 2021; Received in revised form 16 February 2022; Accepted 19 February 2022
Available online 23 February 2022

References

[1] Oil and Colour Chemists' Association, "Titanium dioxide pigments," in *Surface Coatings*, Oil and Colour Chemists' Association, Australia: Springer, 1983, pp. 305-312. doi: 10.1007/978-94-011-6940-0_26.

[2] B. A. van Driel, P. J. Kooyman, K. J. van den Berg, A. Schmidt-Ott, and J. Dik, "A quick assessment of the photocatalytic activity of TiO_2 pigments - From lab to conservation studio!," *Microchemical Journal*, vol. 126, pp. 162–171, 2016, doi: 10.1016/j.microc.2015.11.048.

[3] A. Turgeon and E. Morse. "Sun." National Geographic Society. [Online]. Available: https://www.nationalgeographic.org/encyclopedia/sun.

[4] E. G. Chipman, D. L. De Vincenzi, B. M. French, D. Gilman, S. P. Maran, and P. C. Rambaut, "The sun and earth in space: The sun and us," in A Meeting with the universe, NASA. [Online]. Available: https://history.nasa.gov/EP-177/ch3-1.

[5] D. H. Sliney, "What is light? The visible spectrum and beyond," *Eye*, vol. 30, pp. 222–229, Feb. 2016, doi: 10.1038/eye.2015.252.

[6] K. W. Böer, "The photovoltaic effect," in *Introduction to Space Charge Effects in Semiconductors, Springer Series in Solid-State Sciences (vol. 160)*, Springer, Berlin, Germany, 2009, pp. 201–218. doi: 10.1007/978-3-642-02236-4_8.

[7] A. V. Emeline, V. N. Kuznetsov, V. K. Ryabchuk, and N. Serpone, "Heterogeneous photocatalysis: Basic approaches and terminology," in *New and Future Developments in Catalysis*, S. L. Suib, Elsevier, 2013, pp. 1–47. doi: 10.1016/B978-0-444-53872-7.00001-7.

[8] N. Serpone, A. v. Emeline, S. Horikoshi, V. N. Kuznetsov, and V. K. Ryabchuk, "On the genesis of heterogeneous photocatalysis: A brief historical perspective in the period 1910 to the mid-1980s," *Photochemical and Photobiological Sciences*, vol. 11, no. 7, pp. 1121–1150, 2012, doi: 10.1039/c2pp25026h.

[9] K. Hashimoto, H. Irie, and A. Fujishima, "TiO_2 photocatalysis: A historical overview and future prospects," *Japanese Journal of Applied Physics*, vol. 44, no. 12, pp. 8269–8285, 2005, doi: 10.1143/JJAP.44.8269.

[10] C. F. Goodeve and J. A. Kitchener, "The mechanism of photosensitisation by solids," *Transactions of the Faraday Society*, vol. 34, pp. 902–908, 1938, doi: 10.1039/TF9383400902.

[11] J. M. Coronado, F. Fresno, M. D. Hernández-Alonso, and R. Portela, *Design of Advanced Photocatalytic Materials for Energy and Environmental Applications*, London: Springer London, 2013, pp. 348. doi: 10.1007/978-1-4471-5061-9.

[12] A. Navrotsky and O. J. Kleppa, "Enthalpy of the anatase-rutile transformation," *Journal of the American Ceramic Society*, vol. 50, no. 11, p. 626, 1967, doi: 10.1111/j.1151-2916.1967.tb15013.x.

[13] E. H. Taylor, "The effects of ionizing radiation on solid catalysts," *Advances in Catalysis*, vol. 18, pp. 111–258, 1968, doi: 10.1016/S0360-0564(08)60429-0.

[14] J. H. Lunsford, "Electron Spin Resonance in Catalysis," *Advances in Catalysis*, vol. 22, pp. 265–344, 1972, doi: 10.1016/S0360-0564(08)60249-7.

[15] R. F. Baddour and C. W. Selvidge, "Physical and Chemical Properties of Semiconductor Surfaces," *Progress in Solid State Chemistry*, vol. 3, pp. 45–82, 1967, doi: 10.1016/0079-6786(67)90032-5.

[16]] M. Che and C. Naccache, "Nature of paramagnetic species produced by oxygen treatment of titanium dioxide," *Chemical Physics Letters*, vol. 8, no. 1, pp. 45–48, 1971, doi: 10.1016/0009-2614(71)80571-7.

[17] H. K. Livingston, "The cross-sectional areas of molecules adsorbed on solid surfaces," *Journal of Colloid Science*, vol. 4, no. 5, pp. 447–458, 1949, doi: 10.1016/0095-8522(49)90043-4.

[18] P. Tarte, "Infra-red spectroscopic evidence of four-fold co-ordination of titanium in barium orthotitanate," *Nature*, vol. 191, pp. 1002–1003, 1961, doi: 10.1038/1911002a0.

[19] H.-P. Boehm, "Functional groups on the surfaces of solids," *Angewandte Chemie International Edition*, vol. 5, no. 6, pp. 533–544, 1966, doi: 10.1002/anie.196605331.

[20] G.-M. Schwab, "Conductivity and Surface Chemistry of Crystals," *Angewandte Chemie International Edition*, vol. 2, no. 2, pp. 59–66, 1963, doi: 10.1002/anie.196300591.

[21] G. H. Jonker and S. van Houten, "Semiconducting properties of transition metal oxides," in *Halbleiterprobleme. Advances in Solid State Physics (vol HP6)*, Springer, Berlin, Germany, 1961, pp. 118–151. doi: 10.1007/BFb0119537.

[22] L. H. Princen and M. J. DeVena, "Reactivity of zinc oxide and titanium dioxide in the presence of dispersing agents," *Journal of the American Oil Chemists Society*, vol. 40, pp. 131–135, 1963, doi: 10.1007/BF02640718.

[23] G. C. Bond, "Catalysis in the context of chemistry," *Royal Institute of Chemistry, Reviews*, vol. 3, pp. 1–26, 1970, doi: 10.1039/RR9700300001.

[24] P. F. Cornaz, J. H. C. van Hooff, F. J. Pluijm, and G. C. A. Schuit, "Surface co-ordination of oxygen on oxygen-deficient TiO_2 and MoO_3 as revealed by e.s.r.-measurements," *Discussions of the Faraday Society*, vol. 41, pp. 290–304, 1966, doi: 10.1039/DF9664100290.

[25] R. A. Marcus, "On the theory of electrochemical and chemical electron transfer processes," *Canadian Journal of Chemistry*, vol. 37, no. 1, pp. 155–163, 1959, doi: 10.1139/v59-022.

[26] W. O. Williamson, "Photo-sensitive titanium dioxide," *Nature*, vol. 143, pp. 279, 1939, doi: 10.1038/143279a0.

[27] R. F. Moore, "The photochemical degradation of polyamides and related model N-alkylamides," *Polymer*, vol. 4, pp. 493–513, 1963, doi: 10.1016/0032-3861(63)90062-4.

[28] O. Cicchetti and F. Gratani, "The effect of titanium compounds on photo-oxidation of 2, 4, 6, 8-tetramethylnonane (a liquid model of polypropylene)," *European Polymer Journal*, vol. 8, no. 4, pp. 561–573, 1972.

[29] G. Munuera, "A study of the mechanisms of formic acid dehydration on TiO_2," *Journal of Catalysis*, vol. 18, no. 1, pp. 19–29, 1970, doi: 10.1016/0021-9517(70)90306-4.

[30] O. V. Krylov, "Reactions of Oxidation and Decomposition of Oxygen-Containing Compounds," in *Catalysis by Nonmetals*, E. M. Loebl, Ed. Academic Press, 1970, pp. 168–197. doi: 10.1016/b978-0-12-427250-7.50013-3.

[31] O. V. Krylov, "Decomposition of Alcohols and Acids," in *Catalysis by Nonmetals*, E. M. Loebl, Ed. Academic Press, 1970, pp. 115–139. doi: 10.1016/b978-0-12-427250-7.50010-8.

[32] F. Solymosi, L. Gera, and S. Börcsök, "Catalytic pyrolysis of HClO4 and its relation to the decomposition and combustion of NH_4ClO_4," *Symposium (International) on Combustion*, vol. 13, no. 1, pp. 1009–1017, 1971, doi: 10.1016/S0082-0784(71)80100-5.

[33] S. Carrà, R. Ugo, and L. Zanderighi, "Aspects of Olein catalysis by transition metal oxides," *Inorganica Chimica Acta Reviews*, vol. 3, pp. 55–74, 1969, doi: 10.1016/0073-8085(69)80013-6.

[34] N. R. Dhar and S. K. Mukherjee, "Photosynthesis of amino acids *in vitro*," *Nature*, vol. 134, p. 499, 1934, doi: 10.1038/134499a0.

[35] K. V. Giri, G. D. Kalyankar, C. S. Vaidyanathan, "Photolysis of amino acids in sunlight in presence of the photosensitizer titanium dioxide," *Naturwissenschaften*, vol. 40, pp. 440–441, 1953, doi: 10.1007/BF00590359.

[36] I. N. Nazarov, N. A. Kravchenko, and E. I. Klabunovskii, "Catalytic synthesis of isoprene from hydrocarbon gases," *Bulletin of the Academy of Sciences of the USSR, Division of chemical science*, vol. 8, pp. 2067–2072, 1959, doi: 10.1007/BF00909054.

[37] M. A. Popov and N. I. Shuikin, "Catalytic synthesis of nitriles," *Bulletin of the Academy of Sciences of the USSR, Division of chemical science*, vol. 10, pp. 1729–1731, 1961, doi: 10.1007/BF00911450.

[38] N. I. Shuikin and V. V. An, "Catalytic decomposition of epoxides," *Bulletin of the Academy of Sciences of the USSR, Division of chemical science*, vol. 12, pp. 1343–1347, 1963, doi: 10.1007/BF00847807.

[39] A. A. Tolstopyatova, T. N. Filatova, and A. A. Balandin, "Investigation of the properties of mixed catalysts based on TiO_2 and Nd_2O_3 in the conversion of alcohols," *Bulletin of the Academy of Sciences of the USSR, Division of chemical science*, vol. 18, pp. 1339–1342, 1969, doi: 10.1007/BF00908727.

[40] E. R. S. Winter, "Exchange reactions of oxides. Part VIII. The homomolecular exchange of carbon monoxide," *Journal of the Chemical Society*, pp. 5781–5799, 1964, doi: 10.1039/JR9640005781.

[41] Z. Long, Q. Li, T. Wei, G. Zhang, and Z. Ren, "Historical development and prospects of photocatalysts for pollutant removal in water," *Journal of Hazardous Materials*, vol. 395, pp. 122599, 2020, doi: 10.1016/j.jhazmat.2020.122599.

[42] Università di Bologna, Dipartimento di Chimica "Giacomo Ciamician". "History of the Department, Short history of the Department and its founder, Prof. Giacomo Ciamician." Unibo.it. [Online]. Available: https://chemistry.unibo.it/en/department/presentation/history-of-the-department.

[43] A. Fujishima and K. Honda, "Electrochemical photolysis of water at a semiconductor electrode," *Nature*, vol. 238, pp. 37–38, 1972.

[44] J. Schneider, M. Matsuoka, M. Takeuchi, J. Zhang, Y. Horiuchi, M. Anpo, and D. W. Bahnemann, "Understanding TiO_2 photocatalysis: Mechanisms and materials," *Chemical Reviews*, vol. 114, no. 19, pp. 9919–9986, 2014, doi: 10.1021/cr5001892.

[45] S. N. Frank and A. J. Bard, "Heterogeneous photocatalytic oxidation of cyanide ion in aqueous solutions at titanium dioxide powder," *Journal of the American Chemical Society*, vol. 99, no. 1, pp. 303–304, 1977, [Online]. Available: https://pubs.acs.org/doi/10.1021/ja00443a081.

[46] M. Ge, C. Cao, J. Huang, S. Li, Z. Chen, K.-Q. Zhang, S. S. Al-Deyabd, and Y. Lai, "A review of one-dimensional TiO_2 nanostructured materials for environmental and energy applications," *Journal of Materials Chemistry A*, vol. 4, pp. 6772–6801, 2016, doi: 10.1039/c5ta09323f.

[47] W. Zhang, Y. Tian, H. He, L. Xu, W. Li, and D. Zhao, "Recent advances in the synthesis of hierarchically mesoporous TiO_2 materials for energy and environmental applications," *National Science Review*, vol. 7, no. 11, pp. 1702–1725, 2020, doi: 10.1093/nsr/nwaa021.

[48] B. Li, S. Wu, and X. Gao, "Theoretical calculation of a TiO_2-based photocatalyst in the field of water splitting: A review," *Nanotechnology Reviews*, vol. 9, no. 1, pp. 1080–1103, 2020, doi: 10.1515/ntrev-2020-0085.

[49] Y. Paz, "Application of TiO_2 photocatalysis for air treatment: Patents' overview," *Applied Catalysis B: Environmental*, vol. 99, no. 3-4, pp. 448–460, 2010, doi: 10.1016/j.apcatb.2010.05.011.

[50] Y. Boyjoo, H. Sun, J. Liu, V. K. Pareek, and S. Wang, "A review on photocatalysis for air treatment: From catalyst development to reactor design," *Chemical Engineering Journal*, vol. 310, pp. 537–559, 2017, doi: 10.1016/j.cej.2016.06.090.

[51] H. Dong, G. Zeng, L. Tang, C. Fan, C. Zhang, X. He, and Y. He, "An overview on limitations of TiO_2-based particles for photocatalytic degradation of organic pollutants and the corresponding countermeasures," *Water Research*, vol. 79, pp. 128–146, 2015, doi: 10.1016/j.watres.2015.04.038.

[52] V. Etacheri, C. di Valentin, J. Schneider, D. Bahnemann, and S. C. Pillai, "Visible-light activation of TiO_2 photocatalysts: Advances in theory and experiments," *Journal of Photochemistry and Photobiology C: Photochemistry Reviews*, vol. 25, pp. 1–29, 2015, doi: 10.1016/j.jphotochemrev.2015.08.003.

[53] J. Chen, F. Qiu, W. Xu, S. Cao, and H. Zhu, "Recent progress in enhancing photocatalytic efficiency of TiO_2-based materials," *Applied Catalysis A: General*, vol. 495, pp. 131–140, 2015, doi: 10.1016/j.apcata.2015.02.013.

[54] J. Chen and C. Poon, "Photocatalytic construction and building materials: From fundamentals to applications," *Building and Environment*, vol. 44, no. 9, pp. 1899–1906, 2009, doi: 10.1016/j.buildenv.2009.01.002.

[55] H. A. Foster, I. B. Ditta, S. Varghese, and A. Steele, "Photocatalytic disinfection using titanium dioxide: Spectrum and mechanism of antimicrobial activity," *Applied Microbiology and Biotechnology*, vol. 90, pp. 1847–1868, 2011, doi: 10.1007/s00253-011-3213-7.

[56] H. Schneider, N. Niegisch, M. Mennig, and H. Schmidt, "Hydrophilic Coating Materials," in *Sol-Gel Technologies for Glass Producers and Users*, Springer, Boston, MA, 2004, pp. 187–194. doi: 10.1007/978-0-387-88953-5_26.

[57] T. A. Egerton, "UV-Absorption-The primary process in photocatalysis and some practical consequences," *Molecules*, vol. 19, no. 11, pp. 18192–18214, 2014, doi: 10.3390/molecules191118192.

[58] A. Fujishima, N. T. Rao, and A. D. Tryk, "Titanium dioxide photocatalysis," *Journal of Photochemistry and Photobiology C: Photochemistry Reviews*, vol. 1, no. 1, pp. 1–21, 2000, doi: 10.1016/S1389-5567(00)00002-2.

[59] T. Matsunaga, R. Tomoda, T. Nakajima, and H. Wake, "Photoelectrochemical sterilization of microbial cells by semiconductor powders," *FEMS Microbiology Letters*, vol. 29, no. 1-2, pp. 211–214, 1985, doi: 10.1111/j.1574-6968.1985.tb00864.x.

[60] K. Sunada, Y. Kikuchi, K. Hashimoto, and A. Fujishima, "Bactericidal and detoxification effects of TiO_2 thin film photocatalysts," *Environmental Science and Technology*, vol. 32, no. 5, pp. 726–728, 1998, doi: 10.1021/es970860o.

[61] Y. Kikuchi, K. Sunada, T. Iyoda, K. Hashimoto, and A. Fujishima, "Photocatalytic bactericidal effect of TiO_2 thin films: Dynamic view of the active oxygen species responsible for the effect," *Journal of Photochemistry and Photobiology A: Chemistry*, vol. 106, no. 1–3, pp. 51–56, 1997, doi: 10.1016/S1010-6030(97)00038-5.

[62] S. Zhu and D. Wang, "Photocatalysis: Basic principles, diverse forms of implementations and emerging scientific opportunities," *Advanced Energy Materials*, vol. 7, no. 23, pp. 1–24, 2017, doi: 10.1002/aenm.201700841.

[63] J. Schneider, M. Matsuoka, M. Takeuchi, J. Zhang, Y. Horiuchi, M. Anpo, and D. W. Bahnemann, "Understanding TiO_2 photocatalysis: Mechanisms and materials," *Chemical Reviews*, vol. 114, no. 19, pp. 9919–9986, 2014, doi: 10.1021/cr5001892.

[64] M. Kulkarni, A. Mazare, E. Gongadze, Š. Perutkova, V. Kralj-Iglič, I. Milošev, P. Schmuki, A. Iglič, and M. Mozetič, "Titanium nanostructures for biomedical applications," *Nanotechnology*, vol. 26, no. 6, pp. 1–18, 2015, doi: 10.1088/0957-4484/26/6/062002.

[65] M. Hasanzadeh Kafshgari and W. H. Goldmann, "Insights into theranostic properties of titanium dioxide for nanomedicine," *Nano-Micro Letters*, vol. 12, no. 22, 2020. doi: 10.1007/s40820-019-0362-1.

[66] S. Jafari, B. Mahyad, H. Hashemzadeh, S. Janfaza, T. Gholikhani, and L. Tayebi, "Biomedical Applications of TiO_2 Nanostructures: Recent Advances," *International Journal of Nanomedicine*, vol. 15, pp. 3447–3470, 2020, doi: 10.2147/IJN.S249441.

[67] G. F. Nordberg and O. Andersen, "Metal interactions in carcinogenesis: Enhancement, inhibition," *Environmental Health Perspectives*, vol. 40, pp. 65–81, 1981, doi: 10.1289/ehp.814065.

[68] D. Ziental, B. Czarczynska-Goslinska, D. T. Mlynarczyk, A. Glowacka-Sobotta, B. Stanisz, T. Goslinski, and L. Sobotta, "Titanium dioxide nanoparticles: Prospects

and applications in medicine," *Nanomaterials*, vol. 10, no.2, pp. 387, 2020, doi: 10.3390/nano10020387.

[69] N. Vlachopoulos, P. Liska, J. Augustynski, and M. Grätzel, "Very efficient visible light energy harvesting and conversion by spectral sensitization of high surface area polycrystalline titanium dioxide films," *Journal of the American Chemical Society*, vol. 110, no. 4, pp. 1216–1220, 1988, doi: 10.1021/ja00212a033.

[70] N. Vlachopoulos, P. Liska, A. J. McEvoy, and M. Grätzel, "Efficient sensitisation of TiO_2 electrodes using transition metal charge transfer complexes," *Advances In Solar Energy Technology*, pp. 3003–3009, 1988, doi: 10.1016/B978-0-08-034315-0.50554-1.

[71] M. Grätzel and P. Liska, "Photo-Electrochemical Cell," U.S. Patent 4,927,721, 22 May, 1990. [Online]. Available: https://patentimages.storage.googleapis.com/0d/31/68/56ebba9cfa5c70/US4927721.pdf

[72] B. O'Regan and M. Grätzel, "A low-cost, high-efficiency solar cell based on dye-sensitized colloidal TiO_2 films," *Nature*, vol. 353, pp. 737–740, 1991, doi: 10.1038/353737a0.

[73] Y. Fu and A. Mo, "A review on the electrochemically self-organized titania nanotube arrays: Synthesis, modifications, and biomedical applications," *Nanoscale Research Letters*, vol. 13, no. 187, 2018, doi: 10.1186/s11671-018-2597-z.

[74] J. S. Khaw, M. Curioni, P. Skeldon, C. R. Bowen, and S. H. Cartmell, "A novel methodology for economical scale-up of TiO_2 nanotubes fabricated on Ti and Ti alloys," *Journal of Nanotechnology*, vol. 2019, pp. 1–13, 2019, doi: 10.1155/2019/5902346.

[75] L. Aïnouche, L. Hamadou, A. Kadri, N. Benbrahim, and D. Bradai, "Interfacial barrier layer properties of three generations of TiO_2 nanotube arrays," *Electrochimica Acta*, vol. 133, pp. 597–609, 2014, doi: 10.1016/j.electacta.2014.04.086.

[76] J. M. Macak, H. Tsuchiya, L. Taveira, S. Aldabergerova, and P. Schmuki, "Smooth anodic TiO_2 nanotubes," *Angewandte Chemie - International Edition*, vol. 44, no. 45, pp. 7463–7465, 2005, doi: 10.1002/anie.200502781.

[77] M. Paulose, K. Shankar, S. Yoriya, H. E. Prakasam, O. K. Varghese, G. K. Mor, T. J. LaTempa, A. Fitzgerald, and C. Grimes, "Anodic growth of highly ordered TiO_2 nanotube arrays to 134 μm in length," *Journal of Physical Chemistry B*, vol. 112, no. 47, pp. 15261, 2008, doi: 10.1021/jp809312r.

[78] J. Wan, X. Yan, J. Ding, M. Wang, and K. Hu, "Self-organized highly ordered TiO_2 nanotubes in organic aqueous system," *Materials Characterization*, vol. 60, no. 12, pp. 1534–1540, 2009, doi: 10.1016/j.matchar.2009.09.002.

[79] R. P. Nogueira, J. D. Uchoa, F. Hilario, G. de Fátima Santana-Melo, L. Marotta Reis de Vasconcellos, F. R. Marciano, V. Roche, A. M. Jorge Junior, and A. O. Lobo, "Characterization of optimized TiO_2 nanotubes morphology for medical implants: Biological activity and corrosion resistance," *International Journal of Nanomedicine*, vol. 16, pp. 667–682, 2021, doi: 10.2147/IJN.S285805.

[80] B. Ohtani, O. O. Prieto-Mahaney, D. Li, and R. Abe, "What is Degussa (Evonik) P25? Crystalline composition analysis, reconstruction from isolated pure particles and photocatalytic activity test," *Journal of Photochemistry and Photobiology A: Chemistry*, vol. 216, no. 2–3, pp. 179–182, 2010, doi: 10.1016/j.jphotochem.2010.07.024.

[81] T. Ohno, K. Sarukawa, K. Tokieda, and M. Matsumura, "Morphology of a TiO_2 photocatalyst (Degussa, P-25) consisting of anatase and rutile crystalline phases," *Journal of Catalysis*, vol. 203, no. 1, pp. 82–86, 2001, doi: 10.1006/jcat.2001.3316.

[82] B. Y. Xia, P. Yang, Y. Sun, Y. Wu, B. Mayers, B. Gates, Y. Yin, F. Kim, and H. Yan, "One-Dimensional Nanostructures: Synthesis, Characterization, and Applications," vol. 15, no. 5, pp. 353–389, 2003, doi: 10.1002/adma.200390087.

[83] J. Jeevanandam, A. Sundaramurthy, V. Sharma, C. Murugan, K. Pal, M. H. A. Kodous, and M. K. Danquah, "Sustainability of One-Dimensional Nanostructures," in *Sustainable Nanoscale Engineering*, *From Materials Design to Chemical Processing*, Elsevier, 2020, pp. 83–113. doi: 10.1016/B978-0-12-814681-1.00004-7.

[84] A. Kumar and G. Pandey, "Different methods used for the synthesis of TiO_2 based nanomaterials: A review," *American Journal of Nano Research and Applications*, vol. 6, no. 1, pp. 1-10, 2018, doi: 10.11648/j.nano.20180601.11.

[85] J. Krýsa, G. Waldner, H. Měšťánková, J. Jirkovský, and G. Grabner, "Photocatalytic degradation of model organic pollutants on an immobilized particulate TiO_2 layer: Roles of adsorption processes and mechanistic complexity," *Applied Catalysis B: Environmental*, vol. 64, no. 3–4, pp. 290–301, 2006, doi: 10.1016/j.apcatb.2005.11.007.

[86] R. Beranek, H. Tsuchiya, T. Sugishima, J. M. Macak, L. Taveira, S. Fujimoto, H. Kisch, and P. Schmuki, "Enhancement and limits of the photoelectrochemical response from anodic TiO_2 nanotubes," *Applied Physics Letters*, vol. 87, no. 24, pp. 1–3, 2005, doi: 10.1063/1.2140085.

[87] S. -Z. Chu, S. Inoue, K. Wada, S. Hishita, and K. Kumshima, "Self-organized nanoporous anodic titania films and ordered titania nanodots/nanorods on glass," *Advanced Functional Materials*, vol. 15, no. 8, pp. 1343–1349, 2005, doi: 10.1002/adfm.200400253.

[88] M. A. Henderson, "A surface science perspective on TiO_2 photocatalysis," *Surface Science Reports*, vol. 66, no. 6–7, pp. 185–297, 2011, doi: 10.1016/j.surfrep.2011.01.001.

[89] A. di Paola, M. Bellardita, and L. Palmisano, "Brookite, the least known TiO_2 photocatalyst," *Catalysts*, vol. 3, no. 1, pp. 36–73, 2013, doi: 10.3390/catal3010036.

[90] T. Zhu and S.-P. Gao, "The stability, electronic structure, and optical property of TiO_2 polymorphs," *The Journal of Physical Chemistry C*, vol. 118, no. 21, pp. 11385–11396, 2014, doi: 10.1021/jp412462m.

[91] M. Landmann, E. Rauls, and W. G. Schmidt, "The electronic structure and optical response of rutile, anatase and brookite TiO_2," *Journal of Physics: Condensed Matter*, vol. 24, no. 19, p. 195503, 2012, doi: 10.1088/0953-8984/24/19/195503.

[92] A. Pimentel, D. Nunes, S. Pereira, R. Martins, and E. Fortunato, "Photocatalytic Activity of TiO_2 Nanostructured Arrays Prepared by Microwave-Assisted

Solvothermal Method," in *Semiconductor Photocatalysis - Materials, Mechanisms and Applications*, Wenbin Cao, IntechOpen, 2016. doi: 10.5772/63237.

[93] O. Carp, C. L. Huisman, and A. Reller, "Photoinduced reactivity of titanium dioxide," *Progress in Solid State Chemistry*, vol. 32, no. 1–2, pp. 33–177, 2004, doi: 10.1016/j.progsolidstchem.2004.08.001.

[94] B. Prasai, B. Cai, M. K. Underwood, J. P. Lewis, and D. A. Drabold, "Properties of amorphous and crystalline titanium dioxide from first principles," *Journal of Materials Science*, vol. 47, pp. 7515–7521, 2012, doi: 10.1007/s10853-012-6439-6.

[95] L. Kavan, M. Grätzel, S. E. Gilbert, C. Klemenz, and H. J. Scheel, "Electrochemical and Photoelectrochemical Investigation of Single-Crystal Anatase," *Journal of the American Chemical Society*, vol. 118, no. 28, pp. 6716–6723, 1996, doi: 10.1021/ja954172l.

[96] T. Luttrell, S. Halpegamage, J. Tao, A. Kramer, E. Sutter, and M. Batzill, "Why is anatase a better photocatalyst than rutile? - Model studies on epitaxial TiO_2 films," *Scientific Reports*, vol. 4, pp. 1–8, 2014, doi: 10.1038/srep04043.

[97] S.-D. Mo and W. Y. Ching, "Electronic and optical properties of three phases of titanium dioxide: Rutile, anatase, and brookite," *Physical Review B*, vol. 51, no. 19, pp. 13023–13032, 1995, doi: 10.1103/PhysRevB.51.13023.

[98] R. Zallen and M. P. Moret, "The optical absorption edge of brookite TiO_2," *Solid State Communications*, vol. 137, no. 3, pp. 154–157, 2006, doi: 10.1016/j.ssc.2005.10.024.

[99] V. Etacheri, C. Di Valentin, J. Schneider, D. Bahnemann, and S. C. Pillai, "Visible-light activation of TiO_2 photocatalysts : Advances in theory and experiments," *Journal of Photochemistry and Photobiology C: Photochemistry Reviews*, vol. 25, pp. 1–29, 2015, doi: 10.1016/j.jphotochemrev.2015.08.003.

[100] Hudson Institute of Mineralogy, "TiO_2." Mindat.org. [Online]. Available: https://www.mindat.org

[101] J. M. Macak, S. Aldabergerova, A. Ghicov, and P. Schmuki, "Smooth anodic TiO_2 nanotubes: Annealing and structure," *Physica Status Solidi (A)*, vol. 203, no. 10, pp. R67-R69, 2006, doi: 10.1002/pssa.200622214.

[102] W.-J. Lee, M. Alhoshan, and W. H. Smyrl, "Titanium dioxide nanotube arrays fabricated by anodizing processes," *Journal of The Electrochemical Society*, vol. 153, pp. B499, 2006, doi: 10.1149/1.2347098.

[103] C-c. Chen, J-h. Chen, C-g. Chao, and W. C. Say, "Electrochemical characteristics of surface of titanium formed by electrolytic polishing and anodizing," *Journal of Materials Science*, vol. 40, pp. 4053–4059, 2005, doi: 10.1007/s10853-005-2802-1.

[104] H. Masuda and K. Fukuda, "Ordered metal nanohole arrays made by a two-step replication of honeycomb structures of anodic alumina," *Science*, vol. 268, no. 5216, pp. 1466–8, 1995, doi: 10.1126/science.268.5216.1466.

[105] H. Masuda, H. Yamada, M. Satoh, and H. Asoh, "Highly ordered nanochannel-array architecture in anodic alumina," *Applied Physics Letters*, vol. 71, no. 19, pp. 2770–2772, 1997, doi: 10.1063/1.120128.

[106] Z. Wei-ya, L. Yu-bao, L. Zu-qin, T. Dong-sheng, Z. Xiao-ping, and W. Gang, "Self-organized formation of hexagonal nanopore arrays in anodic alumina," *Chinese Physics*, vol. 10, no. 3, pp. 218–222, 2001, doi: 10.1088/1009-1963/10/3/309.

[107] P. Skeldon, G. E. Thompson, S. J. Garcia-Vergara, L. Iglesias-Rubianes, and C. E. Blanco-Pinzon, "A tracer study of porous anodic alumina," *Electrochemical and Solid-State Letters*, vol. 9, no. 11, pp. B47, 2006, doi: 10.1149/1.2335938.

[108] V. Zwilling, E. Darque-Ceretti, A. Boutry-Forveille, D. David, M. Y. Perrin, and M. Aucouturier, "Structure and physicochemistry of anodic oxide films on titanium and TA6V alloy," *Surface and Interface Analysis*, vol. 27, no. 7, pp. 629–637, 1999, doi: 10.1002/(SICI)1096-9918(199907)27:7<629::AID-SIA551>3.0.CO;2-0.

[109] P. Roy, S. Berger, and P. Schmuki, "TiO_2 nanotubes: Synthesis and applications," *Angewandte Chemie - International Edition*, vol. 50, no. 13, pp. 2904–2939, 2011, doi: 10.1002/anie.201001374.

[110] J. M. Macak, H. Tsuchiya, A. Ghicov, K. Yasuda, R. Hahn, S. Bauer, and P. Schmuki, "TiO_2 nanotubes: Self-organized electrochemical formation, properties and applications," *Current Opinion in Solid State and Materials Science*, vol. 11, no. 1–2, pp. 3–18, 2007, doi: 10.1016/j.cossms.2007.08.004.

[111] Q. Cai, M. Paulose, C. A. Grimes, and O. K. Varghese, "The effect of electrolyte composition on the fabrication of self-organized titanium oxide nanotube arrays by anodic oxidation," *Journal of Materials Research*, vol. 20, pp. 230–236, 2005, doi: 10.1557/JMR.2005.0020.

[112] Z. B. Xie and D. J. Blackwood, "Effects of anodization parameters on the formation of titania nanotubes in ethylene glycol," *Electrochimica Acta*, vol. 56, no. 2, pp. 905–912, 2010, doi: 10.1016/j.electacta.2010.10.004.

[113] D. Regonini, C. R. Bowen, A. Jaroenworaluck, and R. Stevens, "A review of growth mechanism, structure and crystallinity of anodized TiO_2 nanotubes," *Materials Science and Engineering R: Reports*, vol. 74, no. 12, pp. 377–406, 2013, doi: 10.1016/j.mser.2013.10.001.

[114] G. D. Sulka, J. Kapusta-Kołodziej, A. Brzózka, and M. Jaskuła, "Anodic growth of TiO_2 nanopore arrays at various temperatures," *Electrochimica Acta*, vol. 104, pp. 526–535, 2013, doi: 10.1016/j.electacta.2012.12.121.

[115] K. Lu, Z. Tian, and J. A. Geldmeier, "Polishing effect on anodic titania nanotube formation," *Electrochimica Acta*, vol. 56, no. 17, pp. 6014–6020, 2011, doi: 10.1016/j.electacta.2011.04.098.

[116] D. Prando, A. Brenna, M. V. Diamanti, S. Beretta, F. Bolzoni, M. Ormellese, MP. Pedeferri, "Corrosion of titanium: Part 2: Effects of surface treatments," *Journal of Applied Biomaterials and Functional Materials*, vol. 16, no. 1, pp. 3–13, 2017, doi: 10.5301/jabfm.5000396.

[117] W. M. Seong, D. H. Kim, I. J. Park, G. D. Park, K. Kang, S. Lee, and K. S. Hong, "Roughness of Ti substrates for control of the preferred orientation of TiO_2 nanotube arrays as a new orientation factor," *Journal of Physical Chemistry C*, vol. 119, no. 23, pp. 13297–13305, 2015, doi: 10.1021/acs.jpcc.5b02371.

[118] J. M. Macak, H. Hildebrand, U. Marten-Jahns, and P. Schmuki, "Mechanistic aspects and growth of large diameter self-organized TiO_2 nanotubes," *Journal of*

Electroanalytical Chemistry, vol. 621, no. 2, pp. 254–266, 2008, doi: 10.1016/j.jelechem.2008.01.005.

[119] J. M. Macák, H. Tsuchiya, and P. Schmuki, "High-aspect-ratio TiO_2 nanotubes by anodization of titanium," *Angewandte Chemie - International Edition*, vol. 44, no. 14, pp. 2100–2102, 2005, doi: 10.1002/anie.200462459.

[120] S. Durdu, G. Cihan, E. Yalcin, and A. Altinkok, "Characterization and mechanical properties of TiO_2 nanotubes formed on titanium by anodic oxidation," *Ceramics International*, vol. 47, no. 8, pp. 10972–10979, 2021, doi: 10.1016/j.ceramint.2020.12.218.

[121] K. Yasuda, J. M. Macak, S. Berger, A. Ghicov, and P. Schmuki, "Mechanistic Aspects of the Self-Organization Process for Oxide Nanotube Formation on Valve Metals," *Journal of The Electrochemical Society*, vol. 154, no. 9, p. C472, 2007, doi: 10.1149/1.2749091.

[122] H. Habazaki, K. Fushimi, K. Shimizu, P. Skeldon, and G. E. Thompson, "Fast migration of fluoride ions in growing anodic titanium oxide," *Electrochemistry Communications*, vol. 9, no. 5, pp. 1222–1227, 2007, doi: 10.1016/j.elecom.2006.12.023.

[123] J. M. Macák, H. Tsuchiya, and P. Schmuki, "High-aspect-ratio TiO_2 nanotubes by anodization of titanium," *Angewandte Chemie International Edition*, vol. 44, no. 14, pp. 2100–2102, 2005, doi: 10.1002/anie.200462459.

[124] F. Yang, X. Fenga, F. Gea, T. Zhang, J. Qi, D. Li, X. Zhu, "Rapid growth of titanium oxide nanotubes under the critical breakdown voltage: Evidence against the dissolution reaction of fluoride ions," *Electrochemistry Communications*, vol. 103, pp. 17–21, 2019, doi: 10.1016/j.elecom.2019.04.010.

[125] Q. Dou, P. Shrotriya, W. Li, and K. R. Hebert, "Stress-generating electrochemical reactions during the initial growth of anodic titanium dioxide nanotube layers," *Electrochimica Acta*, vol. 295, pp. 418–426, 2019, doi: 10.1016/j.electacta.2018.10.094.

[126] S. P. Albu and P. Schmuki, "Influence of anodization parameters on the expansion factor of TiO_2 nanotubes," *Electrochimica Acta*, vol. 91, pp. 90–95, 2013, doi: 10.1016/j.electacta.2012.12.094.

[127] Z. Zhang, Q. Wang, H. Xu, W. Zhang, Q. Zhou, H. Zeng, J. Yang, J. Zhu, X. Zhu, "TiO_2 nanotube arrays with a volume expansion factor greater than 2.0: Evidence against the field-assisted ejection theory," *Electrochemistry Communications*, vol. 114, pp. 106717, 2020, doi: 10.1016/j.elecom.2020.106717.

[128] J. M. Macak and P. Schmuki, "Anodic growth of self-organized anodic TiO_2 nanotubes in viscous electrolytes," *Electrochimica Acta*, vol. 52, no. 3, pp. 1258–1264, 2006, doi: 10.1016/j.electacta.2006.07.021.

[129] A. Ghicov, S. P. Albu, R. Hahn, D. Kim, T. Stergiopoulos, J. Kunze, C.-A. Schiller, P.Falaras, P. Schmuki, "TiO_2 nanotubes in dye-sensitized solar cells: critical factors for the conversion efficiency," *Chemistry – An Asian Journal*, vol. 4, no. 4, pp. 520–525, 2009, doi: 10.1002/asia.200800441.

[130] S. P. Albu, A. Ghicov, S. Aldabergenova, P. Drechsel, D. LeClere, G. E. Thompson, J. M. Macak, P. Schmuki, "Formation of double-walled TiO_2 nanotubes and robust

anatase membranes," *Advanced Materials*, vol. 20, no. 21, pp. 4135–4139, 2008, doi: 10.1002/adma.200801189.

[131] A. Valota, D. J. LeClere, P. Skeldon, M. Curioni, T. Hashimoto, S. Berger, J. Kunze, P. Schmuki, G. E. Thompson, "Influence of water content on nanotubular anodic titania formed in fluoride/glycerol electrolytes," *Electrochimica Acta*, vol. 54, no. 18, pp. 4321–4327, 2009, doi: 10.1016/j.electacta.2009.02.098.

[132] M. Krivec, K. Žagar, L. Suhadolnik, M. Čeh, and G. Dražić, "Highly efficient TiO_2-based microreactor for photocatalytic applications," *ACS Applied Materials and Interfaces*, vol. 5, no. 18, pp. 9088–9094, 2013, doi: 10.1021/am402389t.

[133] B. Chong, D-l. Yu, M.-q Gao, H.-w Fan, C.-y Yang, W.-h Ma, S.-y Zhang, and X.-f Zhu, "Formation mechanism of gaps and ribs around anodic TiO_2 nanotubes and method to avoid formation of ribs," *Journal of The Electrochemical Society*, vol. 162, pp. H244–H250, 2015, doi: 10.1149/2.0721504jes.

[134] W. Huang, H. Xu, Z. Ying, Y. Dan, Q. Zhou, J. Zhang, X. Zhu, "Split TiO_2 nanotubes − Evidence of oxygen evolution during Ti anodization," *Electrochemistry Communications*, vol. 106, pp. 106532, 2019, doi: 10.1016/j.elecom.2019.106532.

[135] G. Lütjering and J. C. Williams, *Titanium*, 2 Edition. Berlin, Heidelberg: Springer Berlin Heidelberg, 2007. [Online]. doi: 10.1007/978-3-540-73036-1.

[136] H. Sopha, A. Jäger, P. Knotek, K. Tesař, M. Jarosova, and J. M. Macak, "Self-organized Anodic TiO_2 Nanotube Layers: Influence of the Ti substrate on Nanotube Growth and Dimensions," *Electrochimica Acta*, vol. 190, pp. 744–752, 2016, doi: 10.1016/j.electacta.2015.12.121.

[137] G. A. Crawford and N. Chawla, "Tailoring TiO_2 nanotube growth during anodic oxidation by crystallographic orientation of Ti," *Scripta Materialia*, vol. 60, no. 10, pp. 874–877, 2009, doi: 10.1016/j.scriptamat.2009.01.043.

[138] U. König and B. Davepon, "Microstructure of polycrystalline Ti and its microelectrochemical properties by means of electron-backscattering diffraction (EBSD)," *Electrochimica Acta*, vol. 47, no. 1–2, pp. 149–160, 2001, doi: 10.1016/S0013-4686(01)00572-2.

[139] V. Asgari, M. Noormohammadi, A. Ramazani, and M. A. Kashi, "A new approach to electropolishing of pure Ti foil in acidic solution at room temperature for the formation of ordered and long TiO_2 nanotube arrays," *Corrosion Science*, vol. 136, pp. 38–46, 2018, doi: 10.1016/j.corsci.2018.02.040.

[140] M. Ziomek-Moroz, "Electropolishing," in *ASM Handbook, Corrosion: Fundamentals, testing, and protection*, vol. 13a, S. D. Cramer and B. S. Covino, Jr., ASM International, 2003.

[141] N.-S. Peighambardoust and F. Nasirpouri, "Electropolishing behaviour of pure titanium in perchloric acid–methanol–ethylene glycol mixed solution," *The International Journal of Surface Engineering and Coatings*, vol. 92, no. 3, pp. 132–139, 2014, doi: 10.1179/0020296713Z.000000000135.

[142] P. Schmuki, "From Bacon to barriers: A review on the passivity of metals and alloys," *Journal of Solid State Electrochemistry*, vol. 6, pp. 145–164, 2002, doi: 10.1007/s100080100219.

[143] B. G. Lee, S.-Y. Hong, J. E. Yoo, and J. Choi, "Electropolishing for the formation of anodic nanotubular TiO_2 with uniform length and density," *Applied Surface Science*, vol. 257, no. 16, pp. 7190–7194, 2011, doi: 10.1016/j.apsusc.2011.03.089.

[144] J. M. Macak, S. P. Albu, and P. Schmuki, "Towards ideal hexagonal self-ordering of TiO_2 nanotubes," *Physica Status Solidi - Rapid Research Letters*, vol. 1, no. 5, pp. 181–183, 2007, doi: 10.1002/pssr.200701148.

[145] J. Macak, H. Sopha, and P. Knotek, "Self-organized titanium dioxide nanotube layers: Influence of repetitive anodizations," *Conference Proceedings: NANOCON 2015 - 7th International Conference on Nanomaterials - Research and Application*, pp. 33–38, 2015.

[146] G. Zhang, H. Huang, Y. Zhang, H. L. W. Chan, and L. Zhou, "Highly ordered nanoporous TiO_2 and its photocatalytic properties," *Electrochemistry Communications*, vol. 9, no. 12, pp. 2854–2858, 2007, doi: 10.1016/j.elecom.2007.10.014.

[147] J. M. Macak, M. Jarosova, A. Jäger, H. Sopha, and M. Klementová, "Influence of the Ti microstructure on anodic self-organized TiO_2 nanotube layers produced in ethylene glycol electrolytes," *Applied Surface Science*, vol. 371, pp. 607–612, 2016, doi: 10.1016/j.apsusc.2016.03.012.

[148] B. Davepon, J. W. Schultze, U. König, and C. Rosenkranz, "Crystallographic orientation of single grains of polycrystalline titanium and their influence on electrochemical processes," *Surface and Coatings Technology*, vol. 169–170, pp. 85–90, 2003, doi: 10.1016/S0257-8972(03)00163-4.

[149] S. Leonardi, A. Li Bassi, V. Russo, F. Di Fonzo, O. Paschos, T. M. Murray, H. Efstathiadis, and J. Kunze, "TiO_2 nanotubes: Interdependence of substrate grain orientation and growth characteristics," *Journal of Physical Chemistry C*, vol. 116, no. 1, pp. 384–392, 2011, doi: 10.1021/jp209418n.

[150] S. Leonardi, V. Russo, A. Li Bassi, F. Di Fonzo, T. M. Murray, H. Efstathiadis, A. Agnoli, and J. Kunze-Liebhäuser, "TiO_2 nanotubes: Interdependence of substrate grain orientation and growth rate," *ACS Applied Materials and Interfaces*, vol. 7, no. 3, pp. 1662–1668, 2015, doi: 10.1021/am507181p.

[151] H. Sopha, L. Hromadko, K. Nechvilova, and J. M. Macak, "Effect of electrolyte age and potential changes on the morphology of TiO_2 nanotubes," *Journal of Electroanalytical Chemistry*, vol. 759, pp. 122–128, 2015, doi: 10.1016/j.jelechem.2015.11.002.

[152] K. S. Raja, T. Gandhi, and M. Misra, "Effect of water content of ethylene glycol as electrolyte for synthesis of ordered titania nanotubes," *Electrochemistry Communications*, vol. 9, no. 5, pp. 1069–1076, 2007, doi: 10.1016/j.elecom.2006.12.024.

[153] S. P. Albu, A. Ghicov, J. M. Macak, and P. Schmuki, "250 μm long anodic TiO_2 nanotubes with hexagonal self-ordering," *physica status solidi (RRL) – Rapid* Research Letters, vol. 1, no. 2, pp. R65–R67, 2006, doi: 10.1002/pssr.200600069.

[154] G. K. Mor, O. K. Varghese, M. Paulose, N. Mukherjee, and C. A. Grimes, "Fabrication of tapered, conical-shaped titania nanotubes," *Journal of Materials Research*, vol. 18, pp. 2588–2593, 2003, doi: 10.1557/JMR.2003.0362.

[155] O. K. Varghese, D. Gong, M. Paulose, K. G. Ong, E. C. Dickey, and C. A. Grimes, "Extreme changes in the electrical resistance of titania nanotubes with hydrogen exposure," *Advanced Materials*, vol. 15, no. 7-8, pp. 624–627, 2003, doi: 10.1002/adma.200304586.

[156] D. Gong, C. A. Grimes, O. K. Varghese, W. Hu, R. S. Singh, Z. Chen, and E. C. Dickey, "Titanium oxide nanotube arrays prepared by anodic oxidation," *Journal of Materials Research*, vol. 16, pp. 3331–3334, 2001, doi: 10.1557/JMR.2001.0457.

[157] J. M. Macak, K. Sirotna, and P. Schmuki, "Self-organized porous titanium oxide prepared in Na_2SO_4/NaF electrolytes," *Electrochimica Acta*, vol. 50, no. 18, pp. 3679–3684, 2005, doi: 10.1016/j.electacta.2005.01.014.

[158] K. Shankar, G. K. Mor, A. Fitzgerald, and C. A. Grimes, "Cation effect on the electrochemical formation of very high aspect ratio TiO_2 nanotube arrays in formamide−water mixtures," *The Journal of Physical Chemistry C*, vol. 111, no. 1, pp. 21–26, 2006, doi: 10.1021/jp066352v.

[159] S. Yoriya, G. K. Mor, S. Sharma, and C. A. Grimes, "Synthesis of ordered arrays of discrete, partially crystalline titania nanotubes by Ti anodization using diethylene glycol electrolytes," *Journal of Materials Chemistry*, vol. 18, no. 28, pp. 3332–3336, 2008, doi: 10.1039/B802463D.

[160] B. Wieland, J. P. Lancaster, C. S. Hoaglund, P. Holota, and W. J. Tornquist, "Electrochemical and infrared spectroscopic quantitative determination of the platinum-catalyzed ethylene glycol oxidation mechanism at CO adsorption potentials," *Langmuir*, vol. 12, no. 10, pp. 2594–2601, 1996, doi: 10.1021/la9506943.

[161] J. M. Macak, L. v. Taveira, H. Tsuchiya, K. Sirotna, J. Macak, and P. Schmuki, "Influence of different fluoride containing electrolytes on the formation of self-organized titania nanotubes by Ti anodization," *Journal of Electroceramics volume*, vol. 16, pp. 29–34, 2006, doi: 10.1007/s10832-006-3904-0.

[162] B.-G. Lee, J.-W. Choi, S.-E. Lee, Y.-S. Jeong, H.-J. Oh, and C.-S. Chi, "Formation behavior of anodic TiO_2 nanotubes in fluoride containing electrolytes," *Transactions of Nonferrous Metals Society of China*, vol. 19, no. 4, pp. 842–845, 2009, doi: 10.1016/S1003-6326(08)60361-1.

[163] J. Han, L. Kiss, H. Mei, A. M. Remete, M. Ponikvar-Svet, D. M. Sedgwick, R. Roman, S. Fustero, H. Moriwaki, and V. A. Soloshonok, "Chemical Aspects of Human and Environmental Overload with Fluorine," *Chemical Reviews*, vol. 121, no. 8, pp. 4678–4742, 2021, doi: 10.1021/acs.chemrev.0c01263.

[164] C. Richter, E. Panaitescu, R. Willey, and L. Menon, "Titania nanotubes prepared by anodization in fluorine-free acids," *Journal of Materials Research*, vol. 22, pp. 1624–1631, 2007, doi: 10.1557/JMR.2007.0203.

[165] N. K. Allam and C. A. Grimes, "Formation of Vertically Oriented TiO_2 Nanotube Arrays using a Fluoride Free HCl Aqueous Electrolyte," *The Journal of Physical Chemistry C*, vol. 111, no. 35, pp. 13028–13032, 2007, doi: 10.1021/jp073924i.

[166] N. K. Allam, K. Shankar, and C. A. Grimes, "Photoelectrochemical and water photoelectrolysis properties of ordered TiO_2 nanotubes fabricated by Ti anodization in fluoride-free HCl electrolytes," *Journal of Materials Chemistry*, vol. 18, no. 20, pp. 2341–2348, 2008, doi: 10.1039/b718580d.

[167] C. Richter, Z. Wu, E. Panaitescu, R. J. Willey, and L. Menon, "Ultrahigh-aspect-ratio titania nanotubes," *Advanced Materials*, vol. 19, no. 7, pp. 946–948, 2007, doi: 10.1002/adma.200602389.

[168] Y. L. Cheong, F. K. Yam, S. W. Ng, Z. Hassan, S. S. Ng, and I. M. Low, "Fabrication of titanium dioxide nanotubes in fluoride-free electrolyte via rapid breakdown anodization," *Journal of Porous Materials*, vol. 22, no. 6, pp. 1437–1444, Dec. 2015, doi: 10.1007/s10934-015-0024-8.

[169] V. Loddo, M. Bellardita, G. Camera-Roda, F. Parrino, and L. Palmisano, "Chapter 1 - Heterogeneous Photocatalysis: A Promising Advanced Oxidation Process," in *Current Trends and Future Developments on (Bio-) Membranes*, Elsevier, 2018, pp. 1–43. doi: 10.1016/B978-0-12-813549-5.00001-3.

[170] N. Serpone, "Photocatalysis," in *Kirk-Othmer Encyclopedia of Chemical Technology*, Hoboken, NJ, USA: John Wiley & Sons, Inc., 2000, pp. 1–17, doi: 10.1002/0471238961.1608152019051816.a01.

[171] H. Kisch, "Semiconductor photocatalysis - Mechanistic and synthetic aspects," *Angewandte Chemie - International Edition*, vol. 52, no. 3, pp. 812–847, 2012, doi: 10.1002/anie.201201200.

[172] R. Qian, H. Zong, J. Schneider, G. Zhou, T. Zhao, Y. Li, J. Yang, D. W. Bahnemann, J. Hong Pan, "Charge carrier trapping, recombination and transfer during TiO_2 photocatalysis: An overview," *Catalysis Today*, vol. 335, pp. 78–90, Sep. 2019, doi: 10.1016/j.cattod.2018.10.053.

[173] M. Curti, D. W. Bahnemann, and C. B. Mendive, "Mechanisms in heterogeneous photocatalysis: Titania under UV and visible light illumination," in *Reference Module in Materials Science and Materials Engineering*, Elsevier, 2016, pp. 1–6, doi: 10.1016/B978-0-12-803581-8.03800-5.

[174] Y. Huang, Y. Yu, Y. Yu, and B. Zhang, "Oxygen Vacancy Engineering in Photocatalysis," *Solar RRL*, vol. 4, no. 8, pp. 1–14, 2020, doi: 10.1002/solr.202000037.

[175] Y.-F. Li, U. Aschauer, J. Chen, and A. Selloni, "Adsorption and reactions of O2 on anatase TiO_2," *Accounts of Chemical Research*, vol. 47, no. 11, pp. 3361–3368, 2014, doi: 10.1021/ar400312t.

[176] Y. Tamaki, A. Furube, M. Murai, K. Hara, R. Katoh, and M. Tachiya, "Dynamics of efficient electron–hole separation in TiO_2 nanoparticles revealed by femtosecond transient absorption spectroscopy under the weak-excitation condition," *Physical Chemistry Chemical Physsics*, vol. 9, no. 12, pp. 1453–1460, 2007, doi: 10.1039/B617552J.

[177] S. H. Szczepankiewicz, A. J. Colussi, and M. R. Hoffmann, "Infrared spectra of photoinduced species on hydroxylated titania surfaces," *Journal of Physical Chemistry B*, vol. 104, no. 42, pp. 9842–9850, 2000, doi: 10.1021/jp0007890.

[178] S. H. Szczepankiewicz, J. A. Moss, and M. R. Hoffmann, "Electron traps and the stark effect on hydroxylated titania photocatalysts," *Journal of Physical Chemistry B*, vol. 106, no. 31, pp. 7654–7658, 2002, doi: 10.1021/jp020472v.

[179] L. Xiong and J. Tang, "Strategies and challenges on selectivity of photocatalytic oxidation of organic substances," *Advanced Energy Materials*, vol. 11, no. 8, p. 2003216, 2021, doi: 10.1002/aenm.202003216.

[180] Y. Nosaka and A. Nosaka, "Understanding Hydroxyl Radical (•OH) Generation Processes in Photocatalysis," *ACS Energy Letters*, vol. 1, no. 2, pp. 356–359, 2016, doi: 10.1021/acsenergylett.6b0017410.1021/acsenergylett.6b00174.

[181] M. Melchionna and P. Fornasiero, "Updates on the roadmap for photocatalysis," *ACS Catalalysis*, vol. 10, no. 10, pp. 5493–5501, 2020, doi: 10.1021/acscatal.0c01204.

[182] J. M. Macak, M. Zlamal, J. Krysa, and P. Schmuki, "Self-Organized TiO_2 Nanotube Layers as Highly Efficient Photocatalysts," *Small*, vol. 3, no. 2, pp. 300–304, 2007, doi: 10.1002/smll.200600426.

[183] J. Liu and P. M. Hosseinpour, "TiO_2 nanotube arrays for photocatalysis: Effects of crystallinity, local order, and electronic structure," *Journal of Vacuum Science & Technology A*, vol. 33, no. 2, p. 021202, 2015, doi: 10.1116/1.4902350.

[184] B. Ohtani, "Photocatalysis A to Z—What we know and what we do not know in a scientific sense," *Journal of Photochemistry and Photobiology C: Photochemistry Reviews*, vol. 11, no. 4, pp. 157–178, 2010, doi: 10.1016/j.jphotochemrev.2011.02.001.

[185] K.-H. Choo, "Chapter 10:Modeling Photocatalytic Membrane Reactors," in *Current Trends and Future Developments on (Bio-) Membranes*, Elsevier, 2018, pp. 297–316, doi: 10.1016/B978-0-12-813549-5.00010-4.

[186] J.-M. Herrmann, "Heterogeneous photocatalysis: Fundamentals and applications to the removal of various types of aqueous pollutants," *Catalysis Today*, vol. 53, no. 1, pp. 115–129, 1999, doi: 10.1016/S0920-5861(99)00107-8.

[187] A. O. Ibhadon and P. Fitzpatrick, "Heterogeneous photocatalysis: Recent advances and applications," *Catalysts*, vol. 3, no. 1, pp. 189–218, 2013, doi: 10.3390/catal3010189.

[188] X. Zhou, N. Liu, and P. Schmuki, "Photocatalysis with TiO_2 nanotubes: 'Colorful' reactivity and designing site-specific photocatalytic centers into TiO_2 nanotubes," *ACS Catalysis*, vol. 7, no. 5, pp. 3210–3235, 2017, doi: 10.1021/acscatal.6b03709.

[189] U. Diebold, "The surface science of titanium dioxide," *Surface Science Reports*, vol. 48, no. 5–8, pp. 53–229, 2003, doi: 10.1016/S0167-5729(02)00100-0.

[190] N. Hu, N. Gao, and M. J. Starink, "The influence of surface roughness and high pressure torsion on the growth of anodic titania nanotubes on pure titanium," *Applied Surface Science*, vol. 387, pp. 1010–1020, 2016, doi: 10.1016/j.apsusc.2016.07.036.

[191] J. Pouilleau, D. Devilliers, F. Garrido, S. Durand-Vidal, and E. Mahé, "Structure and composition of passive titanium oxide films," *Materials Science and Engineering B*, vol. 47, no. 3, pp. 235–243, 1997.

[192] I. Dalmázio, L. S. Santos, R. P. Lopes, M. N. Eberlin, and R. Augusti, "Advanced oxidation of caffeine in water: On-line and real-time monitoring by electrospray Ionization mass spectrometry," *Environmental Science and Technology*, vol. 39, no. 16, pp. 5982–5988, 2005, doi: 10.1021/es047985v.

[193] J. Zhang and Y. Nosaka, "Mechanism of the OH radical generation in photocatalysis with TiO_2 of different crystalline types," *The Journal of Physical Chemistry C*, vol. 118, no. 20, pp. 10824–10832, 2014, doi: 10.1021/jp501214m.

[194] J. P. Telo and A. J. S. C. Vieira, "Mechanism of free radical oxidation of caffeine in aqueous solution," *Journal of the Chemical Society, Perkin Transactions 2*, vol. 2, no. 9, pp. 1755–1758, 1997, doi: 10.1039/a700944e.

[195] S. Ahmad Bhawani, S. S. Fong, and M. N. Mohamad Ibrahim, "Spectrophotometric Analysis of Caffeine," *International Journal of Analytical Chemistry*, vol. 2015, pp. 7, 2015, doi: 10.1155/2015/170239.

[196] A. Belay, K. Ture, M. Redi, and A. Asfaw, "Measurement of caffeine in coffee beans with UV/vis spectrometer," *Food Chemistry*, vol. 108, no. 1, pp. 310–315, 2008, doi: 10.1016/j.foodchem.2007.10.024.

[197] K. Nakata and A. Fujishima, "TiO_2 photocatalysis: Design and applications," *Journal of Photochemistry and Photobiology C: Photochemistry Reviews*, vol. 13, no. 3, pp. 169–189, 2012, doi: 10.1016/j.jphotochemrev.2012.06.001.

[198] M. Rosales, T. Zoltan, C. Yadarola, E. Mosquera, F. Gracia, and A. García, "The influence of the morphology of 1D TiO_2 nanostructures on photogeneration of reactive oxygen species and enhanced photocatalytic activity," *Journal of Molecular Liquids*, vol. 281, pp. 59–69, 2019, doi: 10.1016/j.molliq.2019.02.070.

[199] N. Wang, J. Li, L. Zhu, Y. Dong, and H. Tang, "Highly photocatalytic activity of metallic hydroxide/titanium dioxide nanoparticles prepared via a modified wet precipitation process," *Journal of Photochemistry and Photobiology A: Chemistry*, vol. 198, no. 2–3, pp. 282–287, 2008, doi: 10.1016/j.jphotochem.2008.03.021.

[200] G. Gao, X. Wang, Q. Chen, C. Xie, J. Zheng, H. Fan, L. Ma, R. Guan, Y. Fang, and X. Hua, "Synergy of surface fluorine and oxygen vacancy of TiO2 nanosheets for O_2 activation in selective photocatalytic organic transformations," *Journal of Materials Chemistry C*, vol. 9, no. 5, pp. 1593–1603, 2021, doi: 10.1039/d0tc04874g.

[201] C. J. Rhodes, "Electron spin resonance (some chemical applications)," *Annual Reports Section "C" (Physical Chemistry)*, vol. 102, pp. 166-202, 2006, doi: 10.1039/b417213m.

[202] T. Koklic, I. Urbančič, I. Zdovc, M. Golob, P. Umek, Z. Arsov, G. Dražić, Š. Pintarič, M. Dobeic, J. Štrancar, "Surface deposited one-dimensional copper-doped TiO_2 nanomaterials for prevention of health care acquired infections," *PLoS One*, vol. 13, pp:1-20, 2018, doi: 10.1371/journal.pone.0201490.

Bibliography

Publications Related to the Thesis

Journal Articles

[1] Ž. Marinko, L. Suhadolnik, Z. Samardžija, J. Kovač, and M. Čeh, "The influence of a surface treatment of metallic titanium on the photocatalytic properties of TiO_2 Nanotubes grown by anodic oxidation," *Catalysts*, vol. 10, no. 7, pp. 803-1-803-16, 2020.

[2] Ž. Marinko, L. Suhadolnik, B. Šetina, V. S. Šelih, B. Majaron, J. Kovač, and M. Čeh, "Toward a flexible and efficient TiO_2 photocatalyst immobilized on a titanium foil", *ACS omega*, vol. 6, no. 36, pp. 23233-23242, 2021.

[3] L. Suhadolnik, Ž. Marinko, M. Ponikvar-Svet, G. Tavčar, J. Kovač, and M. Čeh, "Influence of anodization-electrolyte aging on the photocatalytic activity of TiO_2 nanotube arrays", *The journal of physical chemistry. C, Nanomaterials and interfaces*, pp. 35, 2020.

Conference Papers

[1] Ž. Marinko, L. Suhadolnik, and M. Čeh, Miran, "The influence of metal titanium surface treatment on the properties of TiO_2 nanotubes grown by anodic oxidation," in 26th International Conference on Materials and Technology, Portorož, Slovenia, 2018, pp. 92. Available: http://mit.imt.si/Revija/izvodi/mit184/BookOfAbstracts_26ICM&T.pdf.

[2] Ž. Marinko, L. Suhadolnik, Z. Samardžija, J. Kovač, and M. Čeh, "Connecting metal titanium surface properties and TiO_2 nanotube photocatalytic activity : top-down approach," *in* EAAOP-6: 6th European Conference on Environmental Applications of Advanced Oxidation Processes, Portorož - Portorose, Slovenia, 2019, pp. 649-650.
Reward for the Živa Marinko for the third place at the student paper contest.

[3] L. Suhadolnik, and Ž. Marinko, "Synthesis of 2D arrays of TiO_2 nanotubes by anodic oxidation for photocatalytic and photoelectrocatalytic applications," in 33° Latin-American Congress of Chemistry (33-CLAQ) and X. Congress of chemical Sciencses, Technology and Innovation (Quimicuba'2018), La Habana, Cuba, 2018.

[4] Ž. Marinko, L. Suhadolnik, and M. Čeh, "Substrate thickness and electrolyte aging as main factors influencing photocatalytic activity of TiO_2 nanotube," *in* 11th Jožef Stefan International Postgraduate School Students' Conference and 13th Young Researchers' Day, Planica, Slovenia, 15th and 16th May 2019, pp. 79. Available: http://ipssc.mps.si/Proceedings/Proceedings2019.pdf.

[5] Ž. Marinko, L. Suhadolnik, B. Šetina, and M. Čeh, "Towards highly efficient flexible heterogenous photocatalysts for removal of persistent organic compounds," in EFCATS Summer School 2020, Portorož - Portorose, Slovenia, 15-19 September 2020, pp. 18.

[6] Ž. Marinko, L. Suhadolnik, and M. Čeh, "Anodized titanium foils for a flexible TiO_2 photocatalyst" in 1st Crossnano Crossborder Workshop in Nanoscience and Nanotechnology, Trieste, Italy, 23-25 February 2021, pp. 9. Available: http://web.units.it/dottorato/nanotecnologie/sites/nanotecnologie/files/CrossNano%20Workshop%202021%20Abstract%20Book.pdf.

[7] M. Čeh, L. Suhadolnik, and Ž. Marinko, "Photocatalytic and photoelectrocatalytic degradation of organic compounds in TiO_2-nanotubes-based reactor," in Twenty-second Annual Conference YUCOMAT 2019, Herceg Novi, Montenegro, August 30 - September, 3, 2019, pp. 39.

[8] M. Čeh, L. Suhadolnik, and Ž. Marinko, "TiO_2-nanotubes-based reactors for highly efficient photocatalytic and photoelectrocatalytic degradation of organic compound," in International Conference on Oxide Materials for Electronic Engineering - fabrication, properties and applications, OMEE-2021, Lviv, Ukraine, September 28 - October 2, 2021, pp. 79. Available: http://science.lpnu.ua/sites/default/files/attachments/2021/sep/24928/omee-2021-abstracts-and-title.pdf.

[9] Ž. Marinko, L. Suhadolnik, and M. Čeh, "*Anodic TiO_2 nanotubes for photocatalytic application*," in 56th International Conference on Microelectronics, Devices and Materials & the Workshop on Personal Sensor for Remote Health Care Monitoring, MIDEM - Society for Microelectronics, Electronic Components and Materials, Ljubljana, Slovenia, September 22 - September 24, 2021, pp. 29-30.

Other Publications Related to the TiO_2 Nanotubes

Journal Articles

[1] M. Bele, P. Jovanovič, Ž. Marinko, S. Drev, V. S. Šelih, J. Kovač, M. Gaberšček, G. Koderman Podboršek, G. Dražić, N. Hodnik, A. Kokalj, and L. Suhadolnik, "Increasing the oxygen-evolution reaction performance of nanotubular titanium oxynitride-supported Ir nanoparticles by a strong metal - support Interaction," *ACS catalysis*, vol. 10, iss. 22, pp. 13688-13700, 2020.

[2] L. Moriau, M. Bele, Ž. Marinko, F. Ruiz-Zepeda, G. Koderman Podboršek, M. Šala, A. K. Surca, J. Kovač, I. Arčon, P. Jovanovič, N. Hodnik, and L. Suhadolnik, "Effect of the morphology of the high-surface-area support on the performance of the oxygen-evolution reaction for iridium nanoparticles," *ACS catalysis*, vol. 11, iss. 2, pp. 670-681, 2021.

[3] B. Alcantara Marinho, L. Suhadolnik, B. Likozar, M. Huš, Ž. Marinko, and M. Čeh, "Photocatalytic, electrocatalytic and photoelectrocatalytic degradation of pharmaceuticals in aqueous media : analytical methods, mechanisms, simulations, catalysts and reactors," *Journal of cleaner production*, vol. 343, pp. 1-38, 2022.

Conference Papers

[1] L. Suhadolnik, M. Bele, P. Jovanovič, L. Moriau, Ž. Marinko, N. Hodnik, G. Koderman Podboršek, and M. Čeh, "Synthesis and characterization of novel TiONIr electrocatalyst for oxygen evolution reaction," in 7th Baltic Electrochemistry Conference: Finding New Inspiration (BEChem 2018), Tartu, Estonia. November 4-7, 2018. Available: https://sisu.ut.ee/sites/default/files/webform/Suhadolnik_Luka.pdf.

[2] M. Podlogar, T. Radošević, A. Černoša, Ž. Marinko, M. Kovač Viršek, D. Vengust, L. Suhadolnik, M. Čeh, N. Gunde-Cimerman, and S. Šturm, "Photo- and biodegradation of polypropylene microplastic," in 5th Green and Sustainable Chemistry online Conference. Available: https://www.elsevier.com/events/conferences/green-and-sustainable-chemistry-conference/programme.

[3] B. Ljubec, B. Alcantara Marinho, Ž. Marinko, and M. Čeh, "Comparison of photo-, electro- and photoelectrocatalytic processes in degradation of tetracycline by titanium-based nanotube layers," in 5th International Conference on Applied Surface Science, Palma, Mallorca, Spain, 25-28 April 2022. Available: https://www.elsevier.com/events/conferences/international-conference-on-applied-surface-science#:~:text=The%205th%20International%20Conference%20on,science%20to%20present%20their%20work.

[4] L. Moriau, M. Bele, Ž. Marinko, F. Ruiz-Zepeda, G. Koderman Podboršek, M. Šala, P. Jovanovič, N. Hodnik, and L. Suhadolnik, "Influence of the morphology of high surface area $TiON_x$ support on the performance of the oxygen," in 12th International Scientific Conference on Hydrogen Technologies, Prague, Czech Republic, March 23th – 25th, 2022, pp. 64.

[5] M. Čeh, B. Ljubec, Ž. Marinko, B. Alcantara Marinho, M. Bele, and L. Suhadolnik, "Photo-, electro- and photoelectrocatalytic degradation of persistent organic pollutants (POPs) using TiO_2-based nanotube arrays," in The 6th International Conference on New Photocatalytic Materials for Environment, Energy and Sustainability (NPM-6) and the 7th International Conference on Photocatalytic and Advanced Oxidation Technologies for the Treatment of Water, Air, Soil and Surface (PAOT-7), Ljubljana, Slovenia, April 4-6, 2022, pp. 25.

Other Work

[1] L. Suhadolnik, K. Žagar, M. Bele, Ž. Marinko, M. Kocen, M. Čeh, "Method for functionalization of nanostructured films during crystallization," European Patent Office. EP20202274.5. [S. l.], 16. 10. 2020.

[2] L. Suhadolnik, M. Bele, and Ž. Marinko, "An apparatus for anodic oxidation of very small metal grids," München, European Patent Office. DE EP21163572.7, 19. 3. 2021.

[3] "Science of the future how to stay up-to-date with your research!" in Book of abstracts, M. Topole, T. Turk Dermastia, M. Dežman, B. Škrlj, A. Jurov, K. Bačnik, J. Masten, Ž. Marinko, P. Jovičević Klug, R. Pahič, I. Rybkin, J. Černilogar, A. Kikaj, 11th Jožef Stefan International Postgraduate School Students' Conference and 13th Young Researchers' Day, Jožef Stefan International Postgraduate School: Jožef Stefan Institute, 2019, pp. 99. Available: http://ipssc.mps.si/2019/Proceedings/Proceedings2019.pdf.

[4] Book of abstracts, P. Jovičević Klug, M. Dežman, K. Bačnik, R. Novak, T. Turk Dermastia, Ž. Marinko, A. Kikaj, A. Jurov, M. Topole, 12th Jožef Stefan International Postgraduate School Students' Conference and 14th Young Researchers' Day [Online], Jožef Stefan International Postgraduate School: Jožef Stefan Institute, 2020, pp. 71. Available: http://ipssc.mps.si/2020/BookOfAbstracts.pdf.

Biography

The author of this work, Živa Marinko, graduated from Biotechnology at the Biotechnical Faculty (University of Ljubljana), Slovenia in 2010. During the graduate study, she was an active member of study bodies and organising committees (*e.g., 10th anniversary of programme Biotechnology, Biotechnical Faculty, University of Ljubljana*). Moreover, she has enrolled in multiple research projects, the most important one being "Hair *in vitro*". There she collaborated with numerous authors (Dr. Polona Tratnik, Dr. Ajda Marič, Asst. Prof. Miomir Knežević, Prof. Dr. Primož Rožman, Aleš Leskovšek, Dr. Med., Doc. Mag. Robert Černelč and Jože Baša). Apart from various multimedia presentations, the project led her towards the research for her B.Sc thesis, entitled "Hair growth *in vitro*", under the supervision of Asst. Prof. Miomir Knežević.

She continued her master's degree in Molecular Biology at the Biotechnical Faculty (University of Ljubljana), Slovenia, with the M.Sc thesis entitled "Correlation between bacteria that produce cyanide and are resistant to mercury and are isolated from biofilm of Idrijca River stones" under the supervision of Prof. Dr. Romana Marinšek Logar and co-supervision of Dr. Tomaž Rijavec.

After her master's degree, the author spent some fruitful years in the industry and crowdfunding/coworking environment until she started working at the Jožef Stefan Institute as a young researcher in 2017. In the same year, she enrolled in her doctoral studies at the Jožef Stefan International Postgraduate School in Ljubljana, Slovenia. There too, she was an active member of student bodies; moreover, as a committee member, she co-organised the 11th and 12th Jožef Stefan International Postgraduate School Students' Conference and the 13th and 14th CMBE day.

During her employment at the Jožef Stefan Institute, her research focus was anodic oxidation, photocatalysis and surface examination of titanium foil. She successfully collaborated with other departments at the Institute and various industry partners. Moreover, her work brought joint publications with the National Institute of Chemistry and Institute for Materials and Technology.

Živa Marinko successfully presented her work at several recognised conferences and a summer school on materials, nanoscience, etc. In addition, she was awarded 3rd place in the student paper contest at the EAAOP-6: 6th European Conference on Environmental Applications of Advanced Oxidation Processes in 2019.

Lastly, her work can also be found outside the academic ground, where she is involved in more humanistic projects, which helps her think "outside the box" in her academic endeavours.